



The
University
Of
Sheffield.

Development of novel chemical probes
to image penicillin binding proteins in
Staphylococcus aureus

A thesis submitted for partial fulfilment of the requirements for the degree of
Doctor of Philosophy

Haneesh Gangotra

The University of Sheffield
Faculty of Science
Department of Chemistry

September 2020

Abstract

The shortage of new antibiotics has given rise to unprecedented levels of antimicrobial resistance and demands research into the complex mechanisms utilised by bacteria to adapt, grow and evolve as a species. One of these mechanisms is the dynamicity that bacteria possess to grow and divide whilst maintaining a flexible but rigid structure. The key determinant for these attributes is the unique polymer, peptidoglycan, a major component of eubacterial cell walls responsible for cellular shape and size. Penicillin binding proteins (PBPs) are a group of enzymes that mediate the construction of peptidoglycan and are therefore crucial for cellular viability. They are the target of some of the most clinically effective antibiotics, β -lactams, which operate by inhibiting PBP function, causing cell apoptosis. Despite the function of PBPs being known, certain strains of bacteria such as Methicillin-resistant *Staphylococcus aureus* (MRSA) express PBPs which resist such antibiotics. The reasons behind this are not understood. In addition, the precise roles of PBPs in peptidoglycan assembly and mechanisms which follow their inhibition remain elusive. To help elucidate this, a series of chemical probes were developed to bind to PBPs for imaging in fluorescence microscopy.

Novel cephalosporin scaffolds demonstrated good antibacterial activity against *Staphylococcus aureus* and were subsequently ligated to various fluorescent dyes *via* click chemistry. Each of the five functionalised chemical probes retained antibacterial activity and successfully imaged PBPs in *Staphylococcus aureus* using widefield microscopy. The chemical probes displayed specificity for PBPs which was hypothesised to be a result of the size or charge exhibited by each compound. Chemical probe Ceph-1 Cy5 **55** imaged PBPs in stochastic optical reconstruction microscopy and gave the highest resolution fluorescent images of PBPs in any organism to date. A potential PBP2a binder was also synthesised for biological testing against MRSA and subsequent ligation to fluorophores. A moenomycin based fluorescent probe to bind to a subset of PBPs and transglycosylase enzymes in *Staphylococcus aureus* was prepared and demonstrated localised fluorescence in widefield microscopy. A novel oxetanyl dipeptide scaffold was synthesised but did not induce any antibacterial activity. Finally, the chemical methodology for a series oxetanyl phosphonates as potential β -lactamase inhibitors was established.

Acknowledgements

I would like to begin by saying a thank you to Prof. Simon Jones and The Florey Institute for giving me the opportunity to carry out this research. A special thank you to Simon for his continued support and guidance throughout my PhD studies. Thank you to my second supervisor, Prof. Simon Foster, along with Dr. Victoria Lund and Dr. Kasia Wacnik for mentoring me in all the microbiological work that was carried out in this project. I would also like to say thanks to the technical staff who contributed to this work through advice and training. A separate mention for Rob Hanson who helped in HPLC purification as well as being a terrific friend.

To the people I became friends with in the Department of Chemistry: Thank you to Dan Cox and Jenna for welcoming me into the Jones group all those years ago and their continued friendship throughout. Thanks to all other members of the Jones group past and present, notably Al, Matt, Joe, Huda, Shuwen, Najwa and Sian. To Will and Sam, the MChem students I supervised, who were a pleasure to mentor and made lab life so much more entertaining (I'll leave it at that!). Thanks to all those I knew outside the Jones group, not least Anthony who I became a fellow lab buddy with mid-way through my PhD and compatriot for fortnightly trips to the infamous Jezza's (John's) Van. Also to Nick from stores who always helped out with items at short notice and for all things football related!

Finally, to my two sisters and parents who have never wavered in their support throughout my studies and PhD. I'll never forget what you've done for me. Thank you for everything.

Mum and Dad. This is for you.

Declaration

I hereby declare that all work contained herein is of my own unless otherwise referenced.

Abbreviations

Ac	acetyl
ABPP	activity-based protein profiling
ADMET	absorption, distribution, metabolism, excretion, transport
Ar	aryl
7-ACA	7-aminocephalosporanic acid
6-APA	6-aminopenicillanic acid
AMR	antimicrobial resistance
AFM	atomic force microscopy
Ala	alanine
app	apparent
ATR	attenuated total reflectance
b.p.	boiling point
Bn	benzyl
Boc	tert-butoxycarbonyl
<i>n</i>-Bu	<i>n</i> -butyl
c	concentration
cm	centimetre
CuAAC	copper-catalysed azide–alkyne cycloaddition
d	doublet
dd	double doublet
dba	dibenzylideneacetone
DCI	deuterium chloride
DCM	dichloromethane
deg	degree
DDQ	2,3-dichloro-5,6-dicyano-1,4-benzoquinone
dH₂O	distilled water
DIAD	diisopropyl azodicarboxylate
DIPEA	<i>N,N</i> -diisopropylethylamine
DMAP	4-dimethylamino pyridine
DMF	dimethyl formamide
DMSO	dimethyl sulfoxide
dr	diastereomeric ratio
dSTORM	direct STORM
ee	enantiomeric excess
EDCI	1-ethyl-3-(3-dimethylaminopropyl)carbodiimide
EI	electron impact
ES	electrospray
Et	ethyl
FDAA	fluorescent D-amino acid
FT-IR	fourier transformed infrared spectroscopy
GFP	green fluorescent protein
Glu	glutamic acid
h	hour
HATU	1-[bis(dimethylamino)methylene]-1H-1,2,3-triazolo[4,5-b]pyridinium 3-oxide hexafluorophosphate
HPLC	high performance liquid chromatography

Hz	hertz
HMW	high molecular weight
iPr	iso-propyl
J	coupling constant
kDa	kilodalton
Lac	lactic acid
LC-MS	liquid chromatography mass spectrometry
LDA	lithium diisopropylamide
LMW	low molecular weight
Lys	lysine
m	multiplet
m.p.	melting point
MDR	multi-drug resistant
Me	methyl
MGE	mobile genetic element
MIC	minimum inhibitory concentration
mins	minutes
MoeA	moenomycin A
MRSA	methicillin resistant <i>Staphylococcus aureus</i>
Ms	methanesulfonyl
MS	molecular sieves
NAG	<i>N</i> -acetyl glucosamine
NAM	<i>N</i> -acetyl muramic acid
NHS	<i>N</i> -hydroxysuccinimide
NMR	nuclear magnetic resonance
Nu	nucleophile
PALM	photoactivated localisation microscopy
PBP	penicillin binding protein
PEG	poly(ethylene glycol)
PGT	peptidoglycan glycosyltransferase
Ph	phenyl
PMB	4-methoxybenzyl
PPL	porcine pancreatic lipase
pTs	p-toluenesulfonyl
o/n	overnight
OD600	optical density (at 600 nm)
q	quadruplet
R-BINAP	(<i>R</i>)-(+)-(1,1'-binaphthalene-2,2'-diyl)bis(diphenylphosphine),
rt	room temperature
s	singlet
SDS-PAGE	sodium dodecyl sulfate-polyacrylamide gel electrophoresis
SEDS	shape, elongation, division & sporulation
SIM	structured illumination microscopy
SM	starting material
STED	stimulated emission depleted microscopy
STORM	stochastic optical reconstruction microscopy
t	triplet
TBS	tert-butyldimethyl silyl
tert	tertiary
Tf	trifluoromethanesulfonyl

TGase	transglycosylase
TFA	trifluoroacetic acid
THF	tetrahydrofuran
TLC	thin layer chromatography
TMS	trimethyl silyl
TOF	time of flight
TSB	tryptic soy broth
UV	ultra-violet
VRSA	vancomycin resistant <i>Staphylococcus aureus</i>
WHO	World Health Organisation

Contents

Abstract.....	i
Acknowledgements.....	ii
Declaration.....	iii
Abbreviations.....	iv
1 Introduction.....	1
1.1 Context.....	1
1.2 <i>Staphylococcus aureus</i>	2
1.3 Bacterial cell wall.....	2
1.3.1 Cell division.....	3
1.3.2 Peptidoglycan in <i>Staphylococcus aureus</i>	4
1.3.3 Penicillin binding proteins.....	6
1.3.4 Inhibition of PBPs.....	8
1.3.5 β -Lactam resistance in <i>Staphylococcus aureus</i>	9
1.3.5.1 PBP2a resistance.....	10
1.3.5.2 Emerging resistance pathways.....	11
1.4 Penicillin binding protein visualisation.....	12
1.4.1 Fluorescence microscopy.....	13
1.4.2 Previous studies.....	13
1.5 Structure-activity relationships of β -lactam antibiotics.....	16
1.6 Aims of this study.....	20
2 Antibiotic probe scaffold.....	21
2.1 Background.....	21
2.2 Synthesis of cephalosporin probes.....	24
2.2.1 Synthesis of Ceph-1 23	24
2.2.2 Synthesis of Ceph-2 39	27

2.2.3	Synthesis of Ceph-3 and Ceph-4.....	31
2.3	Biological imaging and evaluation of Ceph-1 23 and Ceph-2 39	36
2.3.1	Biological activity of Ceph-1 23 and Ceph-2 39	36
2.3.2	Investigation of labelling PBPs using a post click strategy.....	38
2.3.3	Synthesis of fluorescent derivatives of Ceph-1 23 and Ceph-2 39	41
2.3.4	Biological activity of fluorescent derivatives.....	43
2.3.5	Labelling of PBPs in <i>S. aureus</i> using a pre-click strategy.....	44
2.3.6	Profiling of selectivity for PBPs in <i>S. aureus</i>	50
2.3.7	Visualisation of PBPs in <i>S. aureus</i> using STORM.....	52
2.4	Future work.....	57
3	Moenomycin scaffold.....	58
3.1	Background.....	58
3.2	Synthesis of MoeA analogues.....	59
3.2.1	Synthesis of MoeA-NH ₂ 62 and MoeA-N ₃ 63	59
3.2.2	Fluorescent derivatisation of MoeA 61	63
3.3	Biological and imaging of moenomycin derivatives.....	64
3.3.1	Biological activity of moenomycin derivatives.....	64
3.3.2	Labelling and imaging of PGTs in <i>S. aureus</i>	65
3.4	Future work.....	66
4	Oxetanyl dipeptide scaffold.....	68
4.1	Background.....	68
4.2	Development of an oxetanyl dipeptide.....	70
4.2.1	Synthesis of an oxetanyl dipeptide.....	70
4.2.2	Biological evaluation of oxetanyl dipeptide.....	75
4.2.3	Synthetic approaches towards acylating an oxetanyl dipeptide.....	75
4.3	Future work.....	78
5	Oxetanyl phosphonates as β -lactamase inhibitors.....	79

5.1	Background	79
5.2	Synthesis of ketophosphonate diesters 115 and 116	80
5.3	Synthesis of an oxetanyl phosphonate	82
5.4	Approaches towards the hydrolysis of ketophosphonate diesters 115 and 116	84
5.5	Future work	85
6	Summary and conclusion	86
7	Methods and materials	88
7.1	Growth media	88
7.2	Buffers and solutions	88
7.2.1	Phosphate buffered saline (PBS)	88
7.2.2	Fixative preparation	88
7.2.2.1	Preparation of 16% (w/v) paraformaldehyde	88
7.2.2.2	Fixative	89
7.2.3	Click-iT® reaction buffer mix	89
7.3	<i>Staphylococcus aureus</i> strain and growth conditions	89
7.4	Chemicals used for microbiological work	89
7.5	Centrifugation	89
7.6	Determination of bacterial cell density	90
7.7	Determination of minimum inhibitory concentration (MIC)	90
7.8	Cell labelling	90
7.8.1	Fixed cell labelling	90
7.8.2	Live cell labelling	90
7.8.3	Click-iT® reaction for post clicking	91
7.9	Microscopy imaging	91
7.9.1	Preparation of samples for widefield microscopy	91
7.9.2	Widefield fluorescence microscopy	91
7.9.3	N-STORM microscopy	92

7.10	PBP analysis by SDS-PAGE	92
8	Chemical experimental	93
9	References.....	144
10	Appendix.....	158

1 Introduction

1.1 Context

Antibiotic resistance is becoming an ever-increasing danger worldwide that has the potential to cause alarmingly high mortality in the future. Indeed, “*The Review on Antimicrobial Resistance (AMR)*” published in 2016 forecast 10 million deaths per year attributable to AMR by 2050 – 1.8 million more than cancer.¹

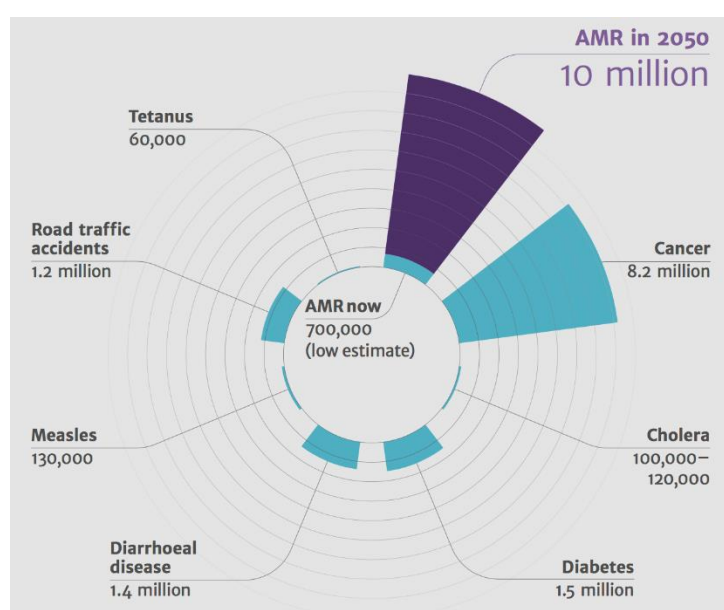


Figure 1-1: Major causes of deaths predicted in 2050. Adapted from The Review on Antibacterial Resistance.¹

Antibiotic resistance is seen as a high priority by the World Health Organisation (WHO) that have endorsed a global action plan to tackle resistance based on 5 key factors: (i) Improve awareness and understanding of AMR, (ii) strengthen research, (iii) reduce incidence of infection, (iv) optimise use of antibiotics and (v) ensure sustainable investment for countering AMR.² Whilst points (ii) and (iv) have been the prime suspects for escalated AMR, it is point (i) which demands acceleration for the search of new cures. A considerable amount of research is, and has been, focused towards structure-based design and enhancing existing molecules – *à la* the traditional medicinal chemistry approach. Other studies have recently outlined the validity of using platforms such as culturing soil bacteria, citing the “golden era” of antibiotics between 1940 to 1960 as inspiration.³⁻⁵ Both approaches are invaluable towards finding a new

class of antibacterial drug; however, they fail to address the inevitable occurrence of new resistant pathogens. It is therefore vital we learn intrinsic mechanistic information of how these pathogens develop and operate to better understand this, especially with the boom of multidrug-resistant (MDR) superbugs.

1.2 *Staphylococcus aureus*

Staphylococcus aureus (*S. aureus*) is a Gram positive, non-motile, spheroid bacterium approximately 1 µm in size. It is both a commensal organism and opportunistic pathogen and typically resides in the anterior nares of humans.⁶ Approximately 20% of the population are permanent carriers of *S. aureus* whilst 60% are transiently associated as asymptomatic nasal carriers whereby the bacteria are part of normal flora.⁷ It is a leading cause of community and nosocomial infection, being only second to *Clostridium difficile* for hospitalised patients in the USA and UK.^{8,9} Figures published by Public Health England for the period 2018/2019 show a total of 12,878 *S. aureus* cases reported, a 30.3% increase from 2011/2012, indicating its ongoing prevalence to human health.¹⁰ *S. aureus* is commonly associated with mild skin conditions but is also responsible for deeper, invasive illnesses due to the repertoire of virulence factors it expresses. Most noteworthy is the secretion of surface proteins that promote adhesion to host cells, form biofilms to evade host defences and penetrate tissue to spread infection and gain access to the blood.¹¹ The result of these can lead to fatal conditions such as endocarditis, toxic shock syndrome, septic shock and pneumonia.¹² The pathogenesis of *S. aureus* is exacerbated as most disease cases cannot be explained by a single virulence determinant and are a combinatorial effect as a consequence of multiple virulent factors.¹³ Many of these factors have been acquired through horizontal gene transfer via mobile genetic elements (MGE's) and contribute towards highly resistant strains.¹⁴ In turn, *S. aureus* has gained a proficient ability to adapt to host systems and conferred resistance to many antibiotics has led to highly resistant strains such as Methicillin-resistant *Staphylococcus aureus* (MRSA).¹⁵

1.3 Bacterial cell wall

Bacterial cells are faced with unpredictable and hostile environments and require flexibility in order to survive as well as grow as a species. To meet these demands, bacteria have evolved a dynamic cell wall to protect themselves whilst allowing cellular processes and interactions

with the environment for proper function.¹⁶ As such, the cell wall is an essential element for viability and has become a prominent area of biological science for the development of new medicines.

S. aureus is a Gram-positive bacterium due to the retention of the Gram stain. Contained in the cell envelope is a major constituent called peptidoglycan (murién), an exoskeleton composed of sugars unique to almost all bacteria and a determinant for the rigid shape of the cell and protection against lysis.¹⁶ It comprises 50% of the total cell wall weight in staphylococcal bacteria, with the other structural features being teichoic acids that span across the peptidoglycan and lipoteichoic acids, which are anchored to the cell membrane by diacylglycerol.^{17,18} This is contrary to Gram negative bacteria for which peptidoglycan accounts for only <10% of the total cell wall.¹⁹ The presence of a unique outer membrane composed of lipids and polysaccharides compensates the thinner layer of peptidoglycan, acting as an additional barrier for protection and facilitating selective transport in and out of the cell.¹⁶

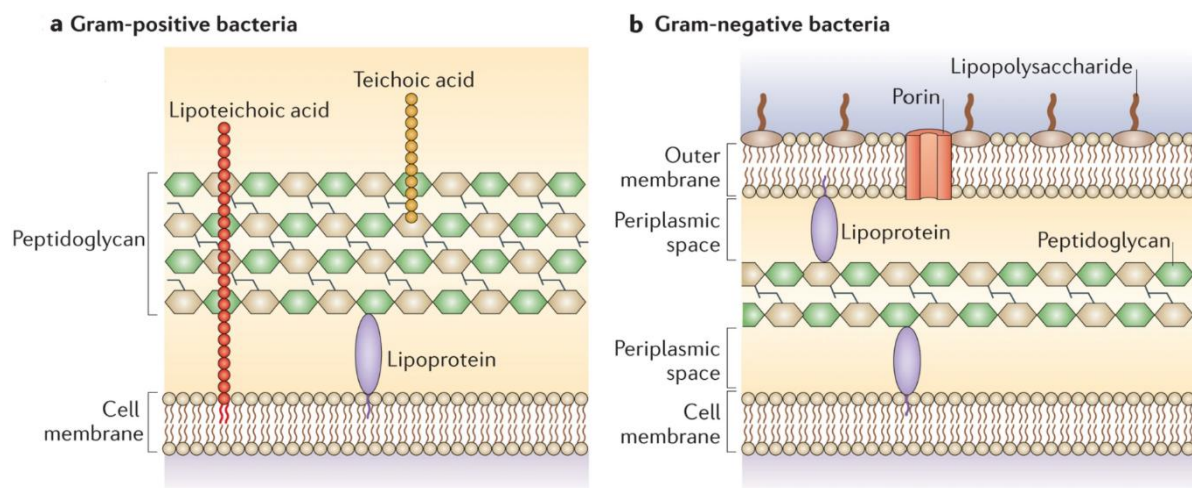


Figure 1-2: General structure of Gram-negative and Gram-positive cell envelopes. a) Gram positive have a thick layer of peptidoglycan with no outer membrane. b) Gram negative bacteria consists of 3 layers; the outer membrane, peptidoglycan and the cell membrane. Adapted from Brown et al.¹⁸

1.3.1 Cell division

Cell division is a fundamental process required by bacteria to grow and divide. It is conducted by a set of proteins, known as the divisome, which coordinate in a timely manner to regulate the division of parental cells into two daughter cells.²⁰ Central to its function is the insertion of peptidoglycan, the major structural component in the cell wall, which is required for cell integrity. The chief orchestrator in the divisome is FtsZ, a eukaryotic tubulin homologue, that

localizes at the site of septation and directs subsequent proteins (**Figure 1-3**) to form a ring (“Z-ring”) on the interior of the cell.²¹ In *S. aureus*, FtsZ is regulated by EzrA which also interacts with other divisome components to mediate their assembly.²² Septation is then initiated, driving late stage cell division proteins such as penicillin binding proteins (PBPs) for peptidoglycan insertion and degradation.^{21,23} Division is completed by peptidoglycans hydrolases, termed autolysins, which are recruited to the septum and allow daughter cell separation.²⁴

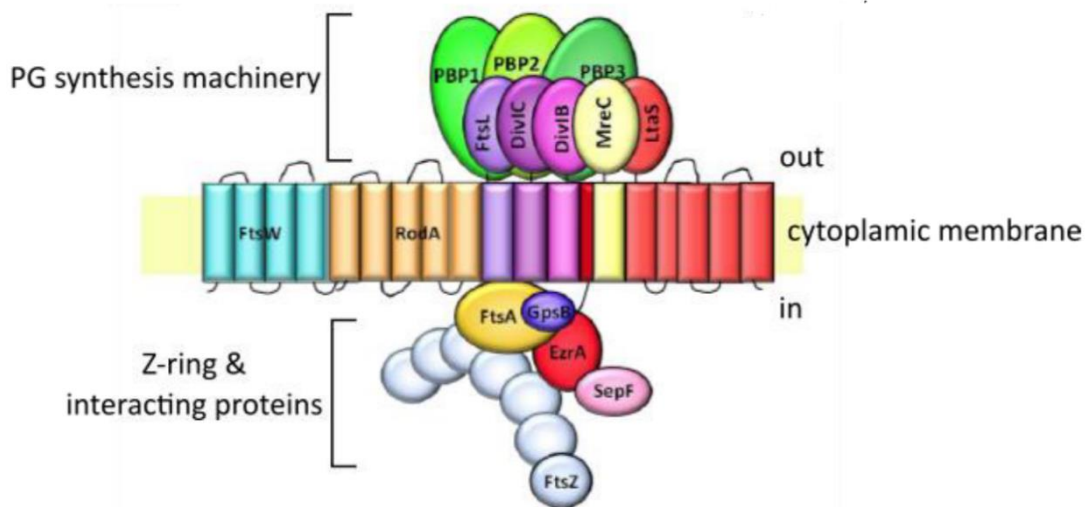


Figure 1-3: Schematic illustrating the cell division machinery (divisome) in S. aureus. Adapted from Bottomley and Lund.^{25,26}

1.3.2 Peptidoglycan in *Staphylococcus aureus*

The fundamental core of peptidoglycan consists of a layered disaccharide of alternating *N*-acetyl glucosamine (NAG) and *N*-acetyl muramic acid (NAM) residues linked by a β -1,4 glycosidic bond which are cross-linked with peptide chains. This structural motif is broadly conserved in the bacterial kingdom however variations of glycan length and peptide composition exist between different species.²⁷ In *S. aureus*, the glycan chains are predominantly 3-6 disaccharide units in length.²⁸ Branching off each NAM residue is a pentapeptide chain consisting of L-Ala, D-Glu, L-Lys and two D-Ala amino acids.¹⁹ Crosslinking occurs by formation of a covalent bond between the fourth D-Ala residue and third L-Lys of the neighbouring pentapeptide via a pentaglycine bridge. Unique to *S. aureus* peptidoglycan is the of high degree of cross-linkage present, which enables cells to withstand extensive osmotic pressure of up to 25 atmospheres, providing significant protection against external influences and maintaining internal processes.²⁸

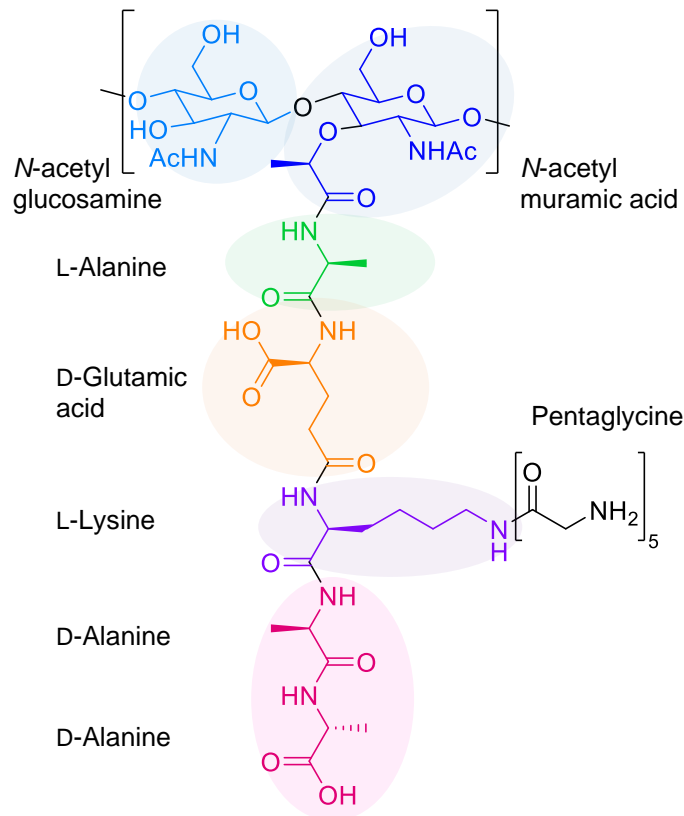


Figure 1-4: Chemical structure of *S. aureus* peptidoglycan. A monomer of peptidoglycan consisting of NAG and NAM sugars which are covalently bonded with a pentapeptide chain. The terminal D-ala residue is expelled during the cross-linking process.

The biosynthesis of peptidoglycan is a highly coordinated process that involves circa. 20 reactions and take places in three different locations in the cell.²⁹ Numerous enzymes which participate in its assembly are essential and are not found in mammalian cells, thus representing excellent targets for the discovery of new antibiotics.²⁹ The first stage of synthesis occurs in the cytoplasm where NAG is synthesised from fructose-6-phosphate and NAM is subsequently synthesised from NAG. Construction of the pentapeptide chain is next performed by a series of Mur ligases which successively add each amino acid. Then, the resulting NAM-pentapeptide precursor is linked to the transport lipid, undecaprenyl pyrophosphate, on the inner leaf off the cytoplasm which generates lipid I. Addition of NAG to lipid I forms lipid II, to which the pentaglycine chain is subsequently added to the third amino acid in the peptide chain, L-Lys, by a series of FemABX peptidyl transferases. The disaccharide is then flipped across the membrane to the outer leaflet where it is incorporated into nascent peptidoglycan by penicillin binding proteins (PBPs).

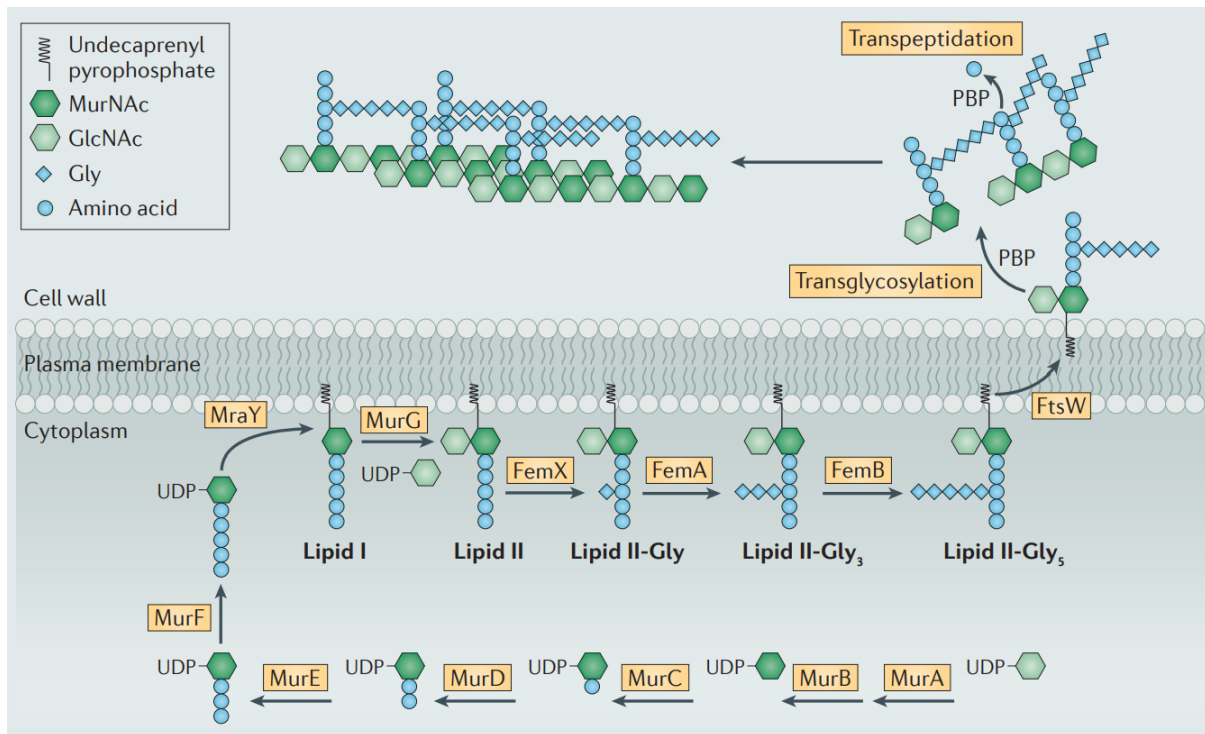


Figure 1-5: The biosynthetic pathway of peptidoglycan in *S. aureus*. Synthesis occurs in three key stages and locations: The precursors are formed in the cytoplasm, followed by disaccharide assembly in the cytoplasm membrane and polymerisation on the outer leaflet mediate by PBPs. Adapted from Pinho et al.³⁰

1.3.3 Penicillin binding proteins

Penicillin binding proteins (PBPs) are a group of enzymes which catalyse the polymerisation (transglycosylation) and cross-linking (transpeptidation) of peptidoglycan.³¹ They are crucial for cell wall integrity and disruption to their activities can cause irregularities to cell morphology and eventual apoptosis.³² PBPs are classified into two main groups based on their molecular weight; high molecular weight (HWM) and low molecular weight (LMW). HWM-PBPs have two domains and conduct the late stages of peptidoglycan synthesis whilst also being responsible for insertion into the pre-existing cell wall.³¹ They can be further divided by the number of reactions a single enzyme is able to catalyse.³³ In Class A HWM-PBP's, the N-terminal domain participate in transglycosylation whilst the membrane-associated C-terminal domain catalyses transpeptidation.³¹ Class B HWM-PBP's bear the same transpeptidation activity at the C-terminal however the function of their N-terminal is ambiguous and believed to play a part in cell morphogenesis with the interaction of other proteins.^{31,34} LWM-PBPs on the other hand have only one domain and possess either carboxypeptidase or endopeptidase activities. They are therefore key instigators in the maintenance, remodelling and recycling of peptidoglycan.³⁵ Indeed, the level of cross-linking in peptidoglycan is mediated by LWM-

PBPs.³³ Bacteria also contain monofunctional transglycosylases (TGase) and SEDS proteins, capable of catalysing the glycan chain assembly but do not contain a transpeptidase domain and so are not referred as PBPs.^{36,37}

The number and types of PBPs possessed varies amongst bacterial species. For example, *Escherichia coli* contains 12 native PBPs whereas *Bacillus subtilis* has 16.³¹ Not all of these are required for bacterial survival, however, and generally bacteria only require two HMW-PBPs to survive, one being class A and the other class B.³⁵ This is the case in *S. aureus*, which produces only 4 native PBPs and therefore provides a minimalist model for studying cell wall regulation (**Table 1-1**). Additionally, *S. aureus* contains 2 monofunctional transglycosylases, MGT and SgtA, and recruits SEDS proteins, FtsW and RodA, to mediate peptidoglycan assembly.^{38,39}

PBP	Classification	Function
1	Class B HMW	Essential for cell growth and survival ⁴⁰
2	Class A HMW	Essential for cell growth and survival ⁴¹
3	Class B HMW	Maintains cell morphology ⁴²
4	LMW	Required for highly crosslinked peptidoglycan ⁴³
MGT ^a	TGase	Involved in glycan polymerisation ³⁸
SgtA ^a	TGase	Involved in glycan polymerisation ³⁸

Table 1-1: The classification of native PBPs present in S. aureus. ^aMonofunctional transglycosylase.

Two Class B HWM-PBP's, PBP1 and PBP3, are responsible for transpeptidase activity whilst the bifunctional Class A PBP2 localises at the septum to catalyse both transpeptidase and transglycosylase reactions.^{31,44} Methicillin resistant *S. aureus* (MRSA) strains possess a non-native, unique class B HMW called PBP2a, which supports transpeptidase activity when it is inhibited by β -lactam drugs in the other four native PBPs.³⁴ Finally, PBP4 is the only LWM-PBP present and is responsible for the high degree of cross-linkage found in *S. aureus* peptidoglycan by having additional transpeptidase activity.⁴³

Only PBP1 and PBP2 are essential for the *S. aureus* growth and survival; depletion of either leads to complete peptidoglycan disruption and results in apoptosis.⁴⁵ However, non-essential enzymes are required for normal growth in complex habitats such as in the presence of antibiotics.

1.3.4 Inhibition of PBPs

PBPs are named as such due to their affinity for penicillin and similar β -lactam containing molecules. This stems from the structural resemblance that is displayed between β -lactam antibiotics and the terminal D-Ala-D-Ala dipeptide in the peptidoglycan side chain.

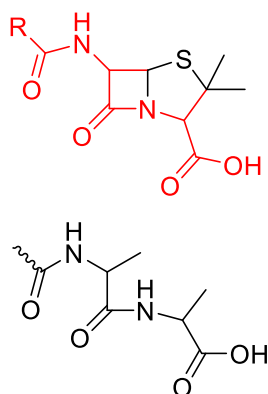


Figure 1-6: Structural similarity between the penicillin core (top) and D-Ala-D-Ala portion of peptidoglycan.

PBPs are required to catalyse the cross-linking (transpeptidation) of peptidoglycan to maintain cell wall integrity. β -Lactam antibiotics inhibit this process by mimicking the D-Ala-D-Ala dipeptide, causing acylation of the active site serine of the PBP by the β -lactam ring to form a covalent acyl-enzyme complex.⁴⁶ This complex is hydrolysed at a very slow rate which essentially renders the enzyme inactive.³⁴ Thereby, the amount of peptidoglycan cross-linking is reduced which leads to an increase in cell turgor pressure and eventual cell wall breakage.⁴⁷

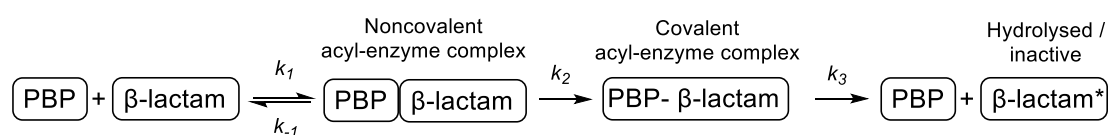


Figure 1-7: A kinetic representation of the reaction between a PBP and β -lactam antibiotic. A slow deacetylation (k_3) effectively renders β -lactam antibiotics as suicide inhibitors.

PBPs can also be inhibited via their transglycosylase domain, however very little success has been achieved in this approach due to the limited structural information of TGase binding sites. It is only recently that crystal structures of some transglycosylase domains have been determined which has significantly hampered progress for *de novo* drug design, compared to the efforts directed towards transpeptidase binders in years previous.⁴⁸⁻⁵⁰ Moenomycin is the only well studied example which directly inhibits TGase activity by binding to the glycosyl

donor site and mimicking lipid II.⁴⁸ Despite its high affinity for the TGase domain in Gram-positive organisms and no resistance being reported in animals, moenomycin has poor pharmacokinetic properties, which makes it unavailable for human use.⁵¹ In contrast, the *indirect* inhibition of transglycosylation has been attained by glycopeptides. Vancomycin is the most prominent example, binding to the D-Ala-D-Ala terminus of lipid II by forming hydrogen bonds with the peptide chain, which prevents transglycosylation from occurring through steric hindrance.^{52,53} Resistant strains incorporate an altered terminus, such as D-Ala-D-Lac in vancomycin resistant *Staphylococcus aureus* (VRSA), which significantly lowers the glycopeptide's affinity.⁵⁴ Despite this, Ge *et al.* demonstrated that Vancomycin can still exhibit antibacterial activity even when the ability to bind to lipid II is lost, owing to secondary mechanisms of action being present.²⁰ Sieber *et al.* later proved it bound to Atl, the major autolysin in *S. aureus* responsible for peptidoglycan degradation.⁵⁵

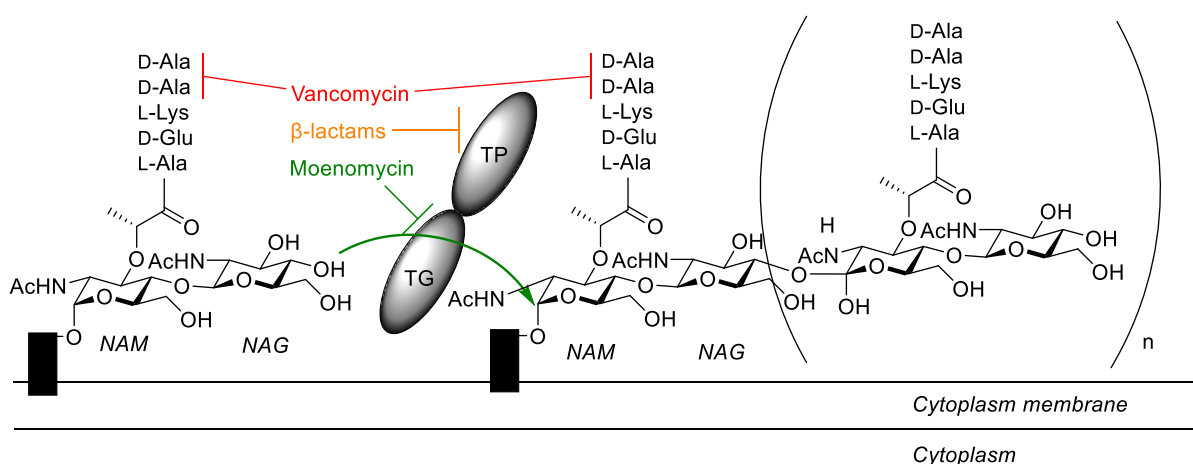


Figure 1-8: Inhibition sites in peptidoglycan by antibiotics. Green arrow indicates the transglycosylase reaction. Black rectangles represent the transport lipid, undecaprenyl pyrophosphate. TP = Transpeptidation. TG = Transglycosylation. Adapted from Ostash and Walker.⁵⁶

1.3.5 β -Lactam resistance in *Staphylococcus aureus*

The first case of β -lactam resistance was found shortly after the introduction of penicillin in 1940.⁵⁷ Bacterial penicillinases, known more broadly as β -lactamases, were observed to hydrolyse the β -lactam ring, thus deactivating it and allowing transpeptidase enzymes to catalyse pentapeptide cross linking of peptidoglycan. This led to the discovery and administration of numerous “semi-synthetic” penicillins, which by chemical modification of the *N*-acyl substituent, were able to withstand acidic hydrolysis.⁵⁸ Despite proving successful

initially, it was only 3 years before the appearance of highly resistant bacterial strains. Methicillin resistant *Staphylococcus aureus* (MRSA) is arguably the most prominent example due its prevalence in hospitals. A third of the population is colonised with MRSA much like *Mycobacterium tuberculosis*, and whilst it is not responsible for as many infections or deaths, it is still regarded as “superbug” due to its comprehensive resistance to antibiotics.⁵⁹

1.3.5.1 PBP2a resistance

The resistance of MRSA is founded by the presence of a unique 78-kDa transpeptidase called penicillin binding protein 2a (PBP2a).⁶⁰ It is encoded by the gene *MecA* and has very low affinity for β -lactam antibiotics compared to the 4 PBPs (PBP1-4) present in native *S. aureus*. It has long been hypothesised that PBP2a takes over the functions of these PBPs and continues to catalyse cell wall biosynthesis - exactly how it does this is not known; however, significant progress has been made over the last 15 years. Mobashery *et al.* proved that PBP2a was significantly less prone to acylation by antibiotics via kinetic measurements.⁶¹ More interestingly, they indicated the enzyme contained a hindered active site which opened upon forming the acylated species *in vitro*. This conformation change was later illustrated by Otero *et al.* who co-crystallised PBP2a with the recently approved anti-MRSA drug Ceftaroline.⁶² X-ray crystallographic analysis showed this change as a result of the drug binding non covalently to an allosteric site, causing a twist in shape and allowing access to the now open active site. Further co-crystallisation with other antibiotics, along with extensive computational study by the Mobashery group, offered an in-depth explanation on the effects of this allosteric domain to PBP2a resistance.⁶³

The allosteric site is observed to be 60 Å from the active site. Despite this distance, its occupancy causes a significant change in conformation of PBP2a by realigning “gatekeeper” residues outside of the active site and enabling access.⁶²⁻⁶⁴ This site-to-site communication has been proven to occur through a series of salt-bridge interactions. The allostery in PBP2a is such that the change in conformation is directly dependent on the occupant of the allosteric site. During un-inhibited catalysis, the site is occupied by nascent peptidoglycan which allows stepwise access to the active site for the acyl donor and acyl acceptor portions of the pentapeptide to crosslink. When PBP2a is dosed with Ceftaroline, the drug can effectively compete with peptidoglycan and bind to the allosteric site, causing a specific conformation change. Ceftazidime, Cefepime and Oxacillin, in comparison, only weakly bind to the allosteric

site and do not trigger the same salt-bridge interactions required for the conformation change.⁶² Ceftaroline's effectiveness is due to its high similarity in size and conformation pose to nascent peptidoglycan when bound to the allosteric site. It therefore appears exact peptidoglycan mimicry is required for optimal transpeptidase inhibition, such is the exclusive attributes required for allosteric access.

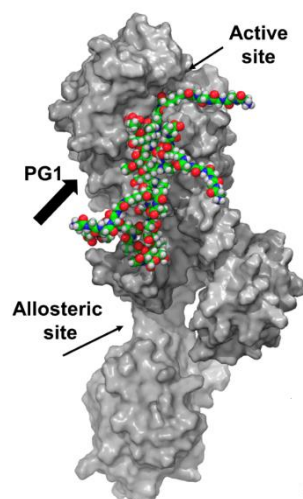


Figure 1-9: A 3D model of PBP2a showing the location of both sites. Adapted from Mahasenan et al.⁶²

1.3.5.2 Emerging resistance pathways

Allosteric regulation of PBP2a represents a significant discovery in the understanding of anti-MRSA drug design. Indeed, cases of Ceftaroline resistance point towards mutations with altered salt-bridge amino acid residues.⁶⁵ This highlights the importance of its allostery to the bacterium's defence mechanism. However new studies are emerging which disprove the long held assumption that PBP2a is the sole contributor towards significant β -lactam resistance.

By using a strain of MRSA lacking the *MecA* gene, i.e., without PBP2a, it has been shown high level resistance to Ceftaroline still arises.⁶⁶ More specifically, multiple gene knockout experiments have indicated PBP4 as the key participant for this resistance. This is not the first time PBP4 has been flagged as a possible target, with Memmi *et al.* demonstrating a 16-fold reduction of the MIC of Oxacillin in a PBP4 knockout MRSA strain.⁶⁷ It has also been known that PBP4 is the only PBP, apart from PBP2a, to mutate when dosed with Ceftobiprole, but its effect has been considered negligible to MRSA until only recently.⁶⁸ We are now learning that PBP4 could in fact provide an alternative transpeptidase mediator for bacteria when PBP2a is inhibited.⁶⁹

MecA negative MRSA strains with high beta lactam resistance have also revealed mutations in two non-PBP species: (i) GdpP, a protein which regulates the cyclic diadenosine monophosphate (c-di-AMP) cell messenger, and (ii) AcrB, a drug efflux transporter.^{66,69} Efflux pumps have been well documented as an antibiotic resistance pathway however little is known about GdpP. It has been reported that c-di-AMP levels increase in GdpP deleted strains, which result in a reduction of cell size; the reasoning behind this and wider relevance to bacterial resistance is yet to be understood.⁷⁰

Additional bacterial defence mechanisms are likely to be discovered, such is the evolving nature of bacteria, however PBPs remain the prime focus for resolving the ambiguity surrounding antibiotic resistance. PBP2a has been heavily investigated, and quite rightly so, however a renaissance into general PBP understanding is required after the finding of high level β -lactam resistance due to PBP4. The cooperative workings of PBP2, PBP2a and PBP4 in cell wall biosynthesis has been known for some time and further warrants the need to understand the dynamics of these proteins on both a micro and a macro level.⁷¹

1.4 Penicillin binding protein visualisation

Much of the exploration into bacterial systems thus far has been conducted through assay or computational design. Both have been invaluable tools in our current understanding of AMR however they rely heavily on *in vitro* testing and mathematical predictions. Advances in microscopy have given rise to image-based techniques for visualisation of targets, offering new insights into biological structure and critically extending the models that have been universally accepted previously. For example, it has long been known that minor differences in the composition of peptidoglycan exist between bacterial species, such as in the peptide cross linking bridge.²⁷ However the implementation of imaging techniques is now revealing that this fundamental structure is in fact assembled in various shapes and sizes yielding unexpected tertiary architectures. Atomic force microscopy (AFM) has shown that peptidoglycan in *S. aureus* is arranged in “rings and knobbls” compared to “cables” found in *B. subtilis*, whilst in *E. coli*, the thickness and porosity vary in different regions.⁷² This increased complexity opens up the potential for new understanding into how peptidoglycan maintains cell integrity.

Key to peptidoglycan biosynthesis is of course PBPs and whilst their biochemical function is known, the mechanistic understanding that leads to cell death is poorly understood. Moreover, the specific role of each PBP remains elusive given the redundancy of some PBPs for cellular

survival as well as localisation patterns displayed by cell divisome components as discussed previously. The necessity to probe their interactions is therefore vital to further understand the dynamicity of peptidoglycan and cellular growth.

1.4.1 Fluorescence microscopy

The advent of fluorescent microscopy has given the ability to investigate biomolecules in their native environments by non-invasive means. It has revealed the high degree of intracellular organisation bacteria possess whereby proteins are deployed in a specific manner as a function of the demands they respond to.⁷³ The growing application of fluorescent microscopy in microbiology, by virtue of green fluorescent protein (GFP) fusions for example, has led to advanced microscopy techniques being utilised in order to study the nanoscale framework of bacteria.⁷⁴ Conventional techniques such as widefield fluorescence microscopy illuminate the entire sample of interest and are thus restricted to the Abbe diffraction limit of 200 nm.⁷³ These can be useful to assess if a protein has been bound, however they fail to offer the in-depth analysis required for elucidating the complex processes' that occur within each cell. Consequently, super resolution microscopy techniques, which overcome the diffraction limit have become vital for discerning protein localisation. Methods such as stimulated emission depletion (STED) and structured illumination microscopy (SIM) work by depleted and patterned illumination to modulate the fluorescence of a sample within a diffraction limited region, such that emission occurs at different times and thereby attaining a sub-diffraction limit resolution.⁷⁵ Stochastic optical reconstruction (STORM) or photoactivated localization (PALM) microscopy on the other hand, rely on the emission of a single molecule or small group of molecules at a time through a controlled manner. The process is repeated through numerous cycles before the images are reconstructed to form one high resolution image. Whilst compatible fluorophores are required, these techniques have been shown to offer lateral resolution of up to 20 nm and are therefore excellent for visualising targets such as PBPs.⁷⁶

1.4.2 Previous studies

The first labelling of PBPs was conducted by Livermore in 1987 who used radioactive ¹⁴C benzylpenicillin to bind to PBPs in *Pseudomonas aeruginosa*.⁷⁷ Different rates of saturation were observed for each PBP which suggested varying levels of affinity for the antibiotic.

Further radioactive penicillin derivatives were developed for PBP assays however limitations of being invasive and unsafe proved a stumbling block for extensive studies.⁷⁸

More recent studies have employed fluorophores for analysis by microscopy. Pinho and Errington constructed a GFP-PBP2 fusion to reveal the localisation patterns of PBP2 around the future division site in *S. aureus* cells.⁴⁴ Moreover, Strauss and co-workers partnered this construct with a GFP-FtsZ fusion and demonstrated similar localisations of PBP2 and FtsZ, suggesting the co-operative functions of both proteins in cell division.⁷⁵

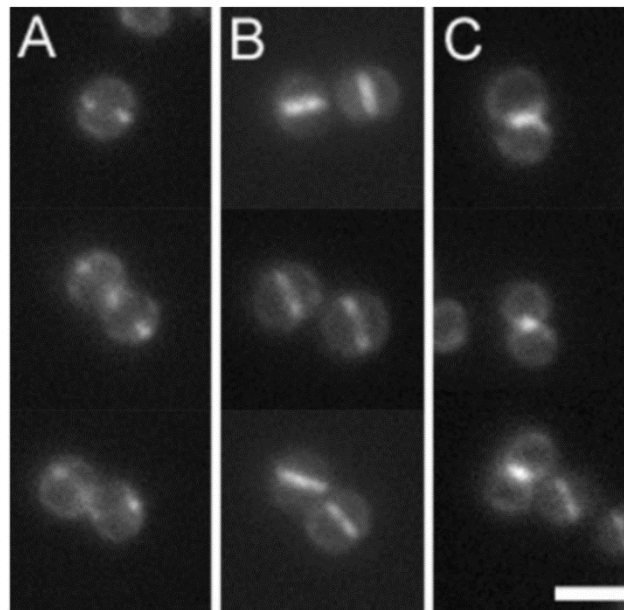


Figure 1-10: Localisation of PBP2 during the cell cycle in S. aureus. A) PBP2 is seen as two spots corresponding to ring formation. B) The pattern is now a line across the cell indicating disk colocalization across the septum. C) The pattern persists as the cells separate. Adapted from Pinho and Errington.⁴⁴

Despite the success of using GFP for PBP visualisation and other biomolecules in general, it has been recently shown that the GFP fusion component can affect protein localisation. Initial studies on MreB, a protein that mediates cell elongation in rod-shaped bacteria, was observed to form helical patterns during cellular growth using a GFP fusion but was later evidenced that this was in fact an artefact of the protein tag.^{79,80} As such, an activity-based protein profiling (ABPP) like approach by which small molecular probes are designed to covalently bind to the protein target are at a considerable advantage due to their unambiguity surrounding nonspecific interference.^{81,82}

Bocillin-FL **1** represented the first fluorescent small molecule probe to “tag” PBPs whereby Gee *et al.* labelled global PBP activity in *E.coli*.⁸³

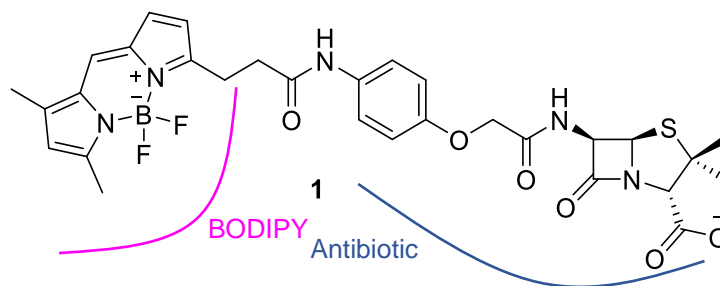


Figure 1-11: The structure of Bocillin-FL, 1

Their success of harnessing an antibiotic as the scaffold for probe design inspired the fundamental strategy for subsequent studies. Staub and Steiber developed a set of natural and synthetic β -lactams attached to an alkyne moiety.⁸⁴ Bacterial cells were treated with the probes, lysed, and then a fluorophore dye bearing an azide handle was introduced. This enabled conjugation of the dye and labelled proteins via the Huisgen 1,3-dipolar cycloaddition (“click chemistry”). Analysis by gel electrophoresis and mass spectrometry showed a preference of certain probes binding to specific PBPs, as well as binding to non-PBP enzymes associated with cell wall virulence.

The first imaging of PBPs via fluorescent microscopy was conducted by Kocaoglu *et al.*⁸⁵ They synthesised a probe based on cephalosporin C and a rhodamine to enable imaging with 3D structured illumination microscopy (SIM). The probe selectively labelled PBP1a/b, PBP2a/b/c and PBP4 in *B. subtilis* and showed their distribution was not uniform but in fact localised at the division site of the bacteria. Later, Sharifzadeh and coworkers established a series of β -lactone probes which bound selectively to PBPs in *S. pneumoniae*.⁸⁶ Through the use of PBP mutant strains and dual labelling experiments, it was found that PBP2b and PBP2x colocalise as a ring during the early part of cell division but as it progresses, only the latter has activity at the central septal site whilst the former remains at the outer ring. These findings proved that PBP activity was functional-specific, and much like peptidoglycan, more complex than the “textbook” definitions long accepted.

1.5 Structure-activity relationships of β -lactam antibiotics

β -Lactams have remained a mainstay for antibiotic drug design since the discovery of penicillin. The detailed understanding of their mechanism of action, together with high potency and specificity for targeting the bacterial cell wall, has given rise to numerous drugs based on the β -lactam scaffold.

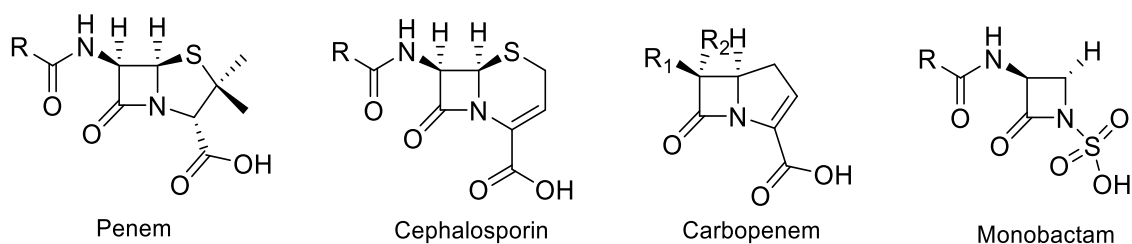


Figure 1-12: The four classes of beta lactam antibiotics

Central to the activity is the ring strain induced by the four-membered ring which gives a highly electrophilic site for nucleophilic attack to occur by the serine-OH residue of PBPs. Bicyclic systems induce further strain causing the lone pair of the nitrogen to be out of the plane with the ring for resonance to occur and thus, the carbonyl exhibits ketone rather than inert amide character. The carboxylic acid aids in recognition within the active site via electrostatic interactions with a lysine NH_3^+ , whilst the amide N-H allows hydrogen bonding with the carbonyl of a valine.⁸⁷ Modification of either of these factors results in a significant decrease in biological activity. In addition, all β -lactam antibiotics are chiral, and in the case of bicyclic structures, relative configuration of the two bridged protons (**Figure 1-123**) is imperative for any activity.⁸⁸

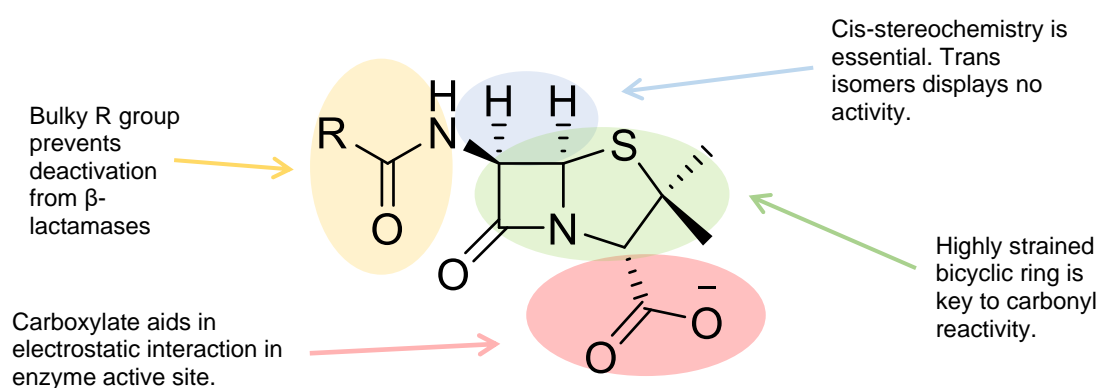


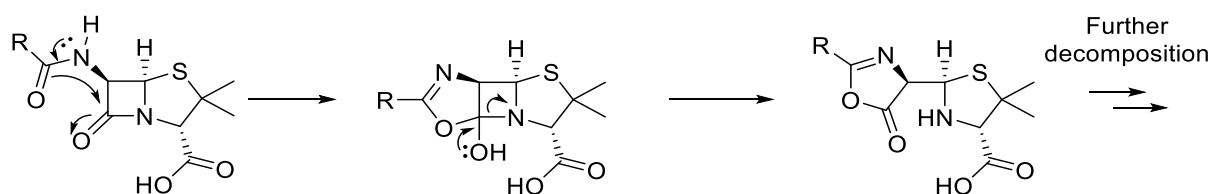
Figure 1-13: SAR of penem derivatives

The degree of carbonyl reactivity, and in turn potency, is reflected in the strength of the C-N amide bond which can be quantified by the Woodward parameter (h). This measures the trigonal pyramidal distance between the nitrogen and its 3 adjacent carbons.

PBP	Penem	Cephem	Carbopenem	Monobactam
Woodward parameter, h (Å)	0.40 – 0.50	0.20 – 0.25	0.50 – 0.60	0.05 – 0.10

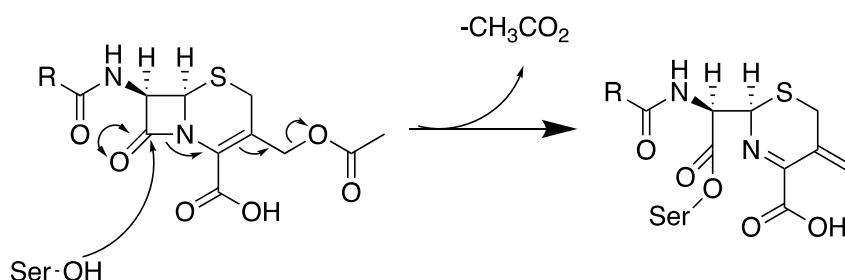
Table 1-2: The Woodward parameters of four beta lactam classes.⁸⁷

Monobactams exhibit the strongest C-N bond as the monocyclic structure allows amide resonance to occur which mirrors their lower potency. Carbopenems have the weakest C-N bond and are therefore the most reactive and potent. However, a more reactive site also causes higher susceptibility to hydrolysis and acid mediated degradation. These pathways have been well documented in the deactivation of penicillins.⁸⁹



Scheme 1-1: The intramolecular decomposition pathway of penicillin derivatives

Cephalosporins (Cephems), on the other hand, have enhanced stability in acidic environments and are therefore very attractive for drug design despite their lower potency compared to other β -lactam scaffolds.



Scheme 1-2: The mechanism of action of cephalosporin derivatives

The acyl R group and leaving group alpha to the carboxylic acid allow two points of derivatisation. This has led to five generations of synthetic cephalosporins, each with improved

pharmacokinetics and pharmacodynamics, as well as spectrum of activity against both Gram positive and Gram-negative bacteria. Early-generation cephalosporins are still used in some applications, however the third and subsequent generations represent the biggest improvement for antibiotic administration.⁹⁰ Chemically, these differ by the presence of an oxime which provides resistance against β -lactamases and improves cell penetration. This must be in the *syn* configuration for optimal fit in the enzyme active site – the *anti* isomer is 10-50 times less potent.⁹¹ The leaving groups of later generations trend towards aromatic substituents. Simple substituents such as a chlorine atom or methyl group show significantly less activity against *S. aureus* than larger nitrogen-containing heterocyclic rings.⁹¹ Furthermore, fifth-generation cephalosporins, which are highly effective against MRSA, have extended cationic nitrogen heterocycles incurring zwitterionic nature.

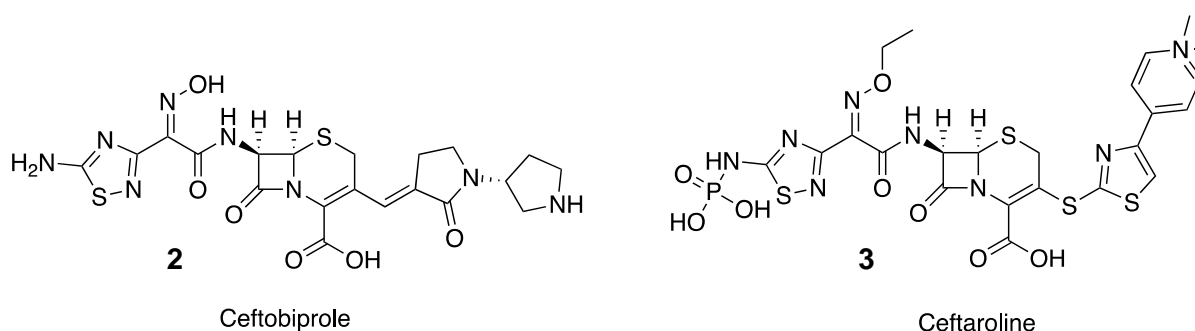


Figure 1-14: Chemical structures of two fifth-generation cephalosporins

Ceftobiprole **2** and Ceftaroline **3** display similar binding modes within the enzyme active site.⁹² The extended linkers both contain polar moieties and are of comparable size, enabling additional interactions that are key to improved anti-MRSA activity. This, in addition to the thiadiazole ring that replaces the thiazole ring, offer a preliminary pharmacophore for PBP2a binding. Cephalosporins also encompass the widest β -lactam class to have a higher affinity for specific PBPs. This makes them ideal tools for examining biological processes.

Antibiotic	Structure	PBP1	PBP2	PBP3	PBP4
Ceftriaxone ⁹³	<p>4</p>		✓		
Cefotaxime ⁹³	<p>5</p>		✓		
Cefaclor ⁹³	<p>6</p>			✓	
Cefoxitin ⁹³	<p>7</p>				✓
Ceftizoxime ⁷¹	<p>8</p>		✓		
Ceftaroline ⁹⁴	<p>3</p>	✓	✓	✓	
Oxacillin ⁹⁴	<p>9</p>	✓	✓	✓	
Meropenem ⁹³	<p>10</p>	✓			
Imipenem ⁹⁵	<p>11</p>	✓			

Table 1-3: PBP affinity of several β -lactams antibiotics

1.6 Aims of this study

The investigation into PBPs is required to further the understanding of essential bacterial components, such as peptidoglycan, and gain a better comprehension of antibiotic resistance mechanisms. PBPs are not simply cell wall biosynthesis mediators; bacteria employ them as a major pathway for resistance against potent drugs. They act to “modify” or “inactivate” or “destroy” β -lactam antibiotics. Their distribution across the cell wall is not known, nor is it known which PBPs are involved or the biological processes occurring upon drug uptake. Answers to these questions are essential for designing next generation antibiotic drugs.

The labelling and visualisation of PBPs via fluorescent β -lactam based probes has been a successful approach in identifying key attributes towards their function in cellular growth and division.⁸³⁻⁸⁶ The most recent of these studies represents the imaging of PBPs via super resolution of microscopy and shows individual localisation of PBPs, indicating the possibility of determining specific function. However, the imaging of PBPs from *S. aureus* is yet to be conducted – understanding the dynamics of PBP2a is of course a chief target of interest due to MRSA. In addition, a superior method of high-resolution imaging such as Stochastic Optical Reconstruction Microscopy (STORM) has yet to be applied. This project sets out to develop a toolbox of probes that can selectively label individual PBPs in *S. aureus* and be functionalised with various fluorophores to enable interpretation by methods such as STORM.

2 Antibiotic probe scaffold

2.1 Background

The development of probes based on penicillin and cephalosporin derivatives has been the primary strategy of choice thus far.^{83–85} β -Lactam antibiotics are natural substrates for PBPs, making them ideal scaffolds for developing effective and specifically binding probes. As described previously, Bocillin-FL is a β -lactam fluorophore conjugate which is commercially available, however is non selective, targeting a broad range of PBPs. It is also not compatible in single molecule localisation microscopy and hence only images with limited resolution can be obtained. Cephalosporin C derivatives prepared by Kocaoglu *et al.* do target PBPs selectively, but their rigid design does not offer the flexibility for *in situ* conjugation with different fluorophore dyes.

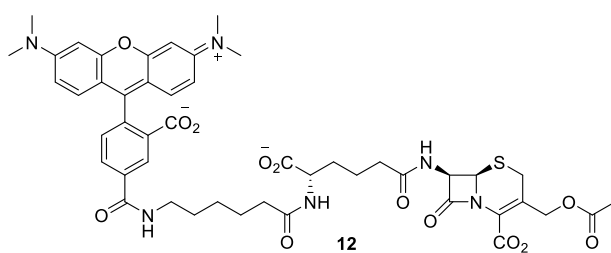


Figure 2-1: A cephalosporin C derivative bound to a rhodamine⁸⁵

To address these limitations, probes were targeted which could allow such flexibility and be synthesised from readily available starting materials. The scaffold was based on the premise of having an antibiotic coupled to a linker bearing an azide, which could in turn be reacted with an alkyne functionality of a fluorescent dye via “click chemistry” for conjugation prior to, or preceding, cell incubation.⁹⁶



Figure 2-2: Basis of the antibiotic probe scaffold

This “click kit” methodology had been shown to be successful in the imaging of a variety of other targets, including newly synthesised proteins in mammalian cells, nucleic acids and

unnatural D-amino acid incorporation in bacteria.⁹⁷⁻⁹⁹

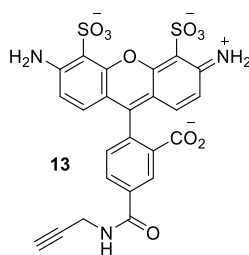


Figure 2-3: Structure of Alexa Fluor 488[®] azide 13, a STORM-compatible dye

Such an approach was seen to be beneficial in a practical sense too, as the antibiotic-linker portion could be synthesised in isolation of the dye. Fluorophores compatible with high resolution microscopy are often large, complex structures and hence installing in the last stage of synthesis would allow for easier and more definite probe characterisation.

The precise size and characteristics required of the linker for optimum labelling would not be established until biological analysis was conducted for several compounds bearing different linkers. In light of this, a polyethylene glycol (PEG) backbone was chosen for simplicity. PEG chains are widely used in drug discovery to improve the pharmacokinetic profiles of compounds. They are also typically biologically inert, making them ideal to use as labelling tags and crosslinkers.¹⁰⁰ Straight-chain carbon linkers offer an alternative however the increased lipophilicity is likely to hinder aqueous solubility compared to analogous PEG chains.

The incorporation of penicillin derivatives as the antibiotic ‘recognition element’ were initially chosen for synthesising preliminary chemical probes and validating the scaffold approach. However, following their unsuccessful manipulation by previous members of the research group, and confirmation of their instability in acidic environments, cephalosporins were chosen instead as the β -lactam component. These were expected to be more stable compared to penicillins, as per their Woodward parameter, and would also fulfil the requirement of being selective for specific PBPs.

Two targets were initially chosen: (i) a simple cephalosporin probe, Ceph-1, to ascertain practical issues of synthesis, tolerability in bacteria and imaging of PBPs and (ii) a more PBP-selective cephalosporin, Ceph-2.

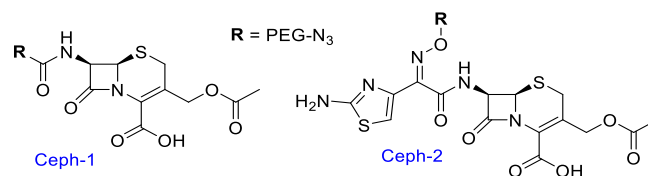


Figure 2-4: Structural basis of the first cephalosporin targets

The second target was designed upon the basic pharmacophore found in late-generation cephalosporin antibiotics, that is, the inclusion of an aminothiazole and oxime moiety. Both functionalities have been found to be key to increasing the antibacterial profile of the drug.⁹¹ More crucially, some antibiotics have a higher affinity for certain PBPs such as cefotaxime **5**, which is a strong PBP2 binder.⁹³ It was therefore reasoned this would be an excellent recognition tag for specific PBP visualisation. The PEG linker was positioned as such to minimise any steric influence on biological activity.

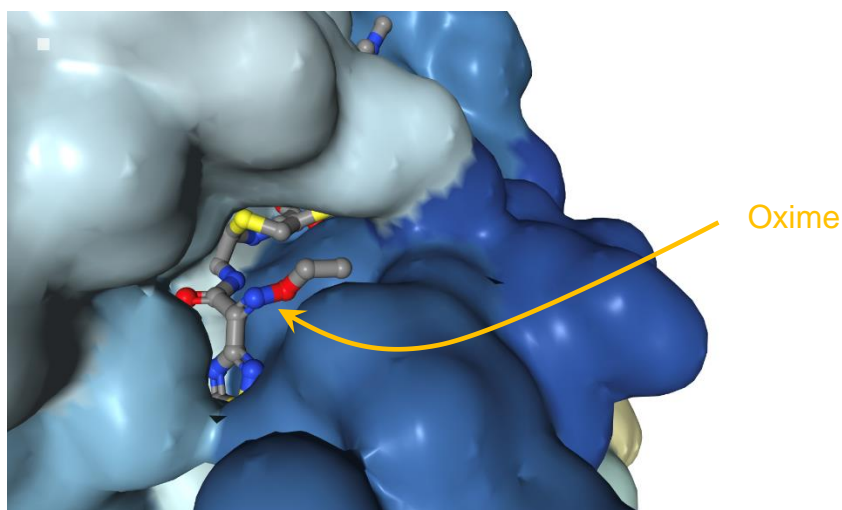


Figure 2-5: Ceftaroline non-covalently bound to the active site of PBP2a¹⁰¹

A survey of crystal structures of cephalosporins bound to PBPs in *S. aureus* indicated the oxime as the ideal branch point.^{101–103} In all cases, it was observed to point away from the enzyme pocket, and hence offered the perfect location for non-participating groups, such as the PEG-N₃ chain and subsequent fluorescent dye, to be linked through.

Following success of the first two probes, a third set was then rationally designed to bind PBP2a. These were based on the anti-MRSA drug, ceftaroline **3**, and contained the important 1,3-thiazole motif required for key interactions and binding within the enzyme site.¹⁰⁴ The

acylamino side chains on carbon 7 were not changed to allow for use of previously made intermediates and translation of reaction methodology from the synthesis of Ceph-1 and Ceph-2. Additionally, this successive approach would be advantageous for the logical design of future PBP selective probes.

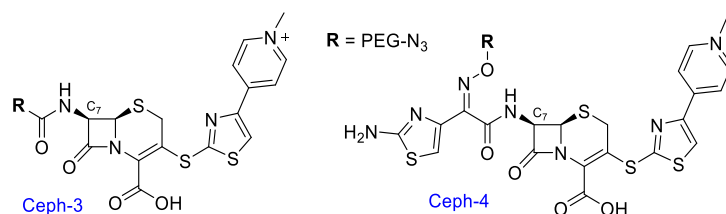
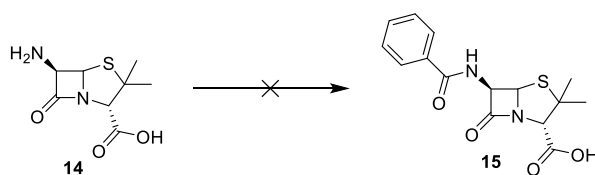


Figure 2-6: Targets designed to bind PBP2a

2.2 Synthesis of cephalosporin probes

2.2.1 Synthesis of Ceph-1 **23**

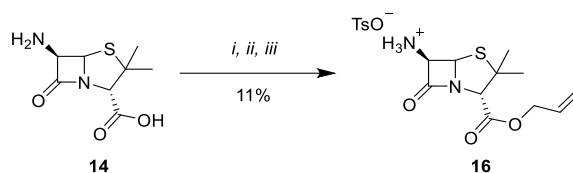
Initially, efforts looked at a chemical probe based on a penicillin ring. This appeared to be the most efficient approach in synthesising a simple molecule due to the widely available precursor, 6-aminopenicillanic acid (6-APA) **14**. A literature review pointed towards direct acylation of 6-APA **14** using an acid chloride under Schotten-Baumann conditions.^{58,105,106} Despite reservations of using acid chlorides in aqueous media, the conditions were attempted and yielded crude material shown to contain the desired product by mass spectrometry. Closer inspection by LC-MS showed numerous peaks present, whilst ¹H NMR spectroscopy indicated several undetermined products. Subsequently, direct acylation was not continued and instead protection of the acid pursued following similar efforts of previous group members.



Scheme 2-1: PhCOCl, 10% aq. sol. NaHCO₃, acetone, 0 °C - RT, o/n

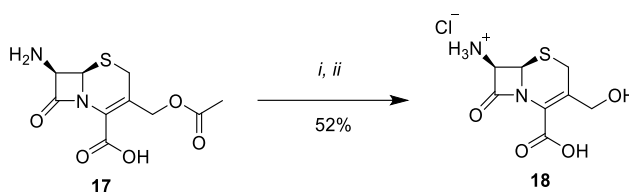
An allyl protecting group was chosen to allow orthogonal deprotection in the presence of an azide. The poor yield was owed to inefficient *in situ* enamine deprotection and salt formation by pTsOH. Camphorsulfonic acid, methanesulfonic acid, trifluoroacetic acid and conc. hydrochloric acid were tried as alternatives but all gave negligible solid upon induced precipitation. It was speculated that acidic media may be causing degradation of the penicillin

ring. Indeed, an acidic workup was also attempted on the trial acylation of 6-APA **14** (**Scheme 2-1**), which further suggested that penem derivatives were sensitive to acidic environments.¹⁰⁷



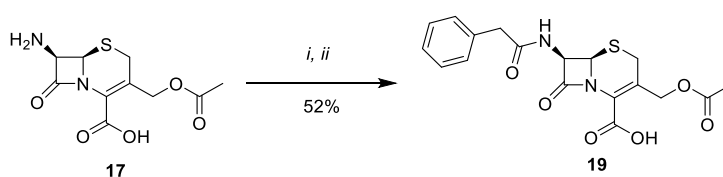
Scheme 2-2: i) methyl acetoacetate, Et₃N, CH₂Cl₂, RT, 3 h. ii) allyl bromide, DMF, RT, o/n. iii) pTsOH.H₂O, Et₂O, 1 h

Efforts then switched to manipulating the analogous cephalosporin of 6-APA, 7-aminocephalosporanic acid (7-ACA) **17**. Protection of the carboxylic acid was well documented in the literature, with diphenyl and *tert*-butyl esters being the protecting groups of choice.^{108,109} However, successful deacetylation indicated stability towards acidic workup, leading to attempt a Schotten-Baumann type acylation of 7-ACA.



Scheme 2-3: i) 3 M aq. NaOH, -20 °C - RT, 30 min. ii) conc. hydrochloric acid

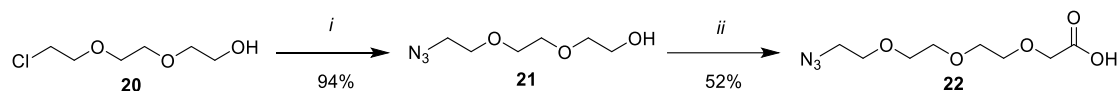
Efficient conversion was obtained with the expected hydrolysed acid chloride as the only byproduct. This methodology provided the fundamental strategy for synthesising cephalosporin probe, Ceph-1.



Scheme 2-4: i) phenylacetyl chloride, sat. aq. NaHCO₃, acetone, 0 °C - RT, 17 h. ii) 2 M hydrochloric acid

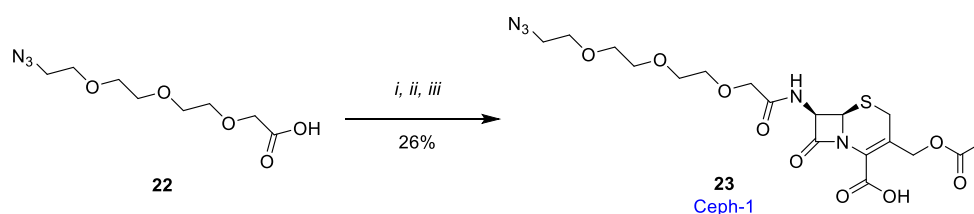
2-[2-(2-Chloroethoxy)ethoxy]ethanol **20** was chosen as the PEG linker backbone due to its readily availability. The azide displacement required 2 days for completion and was monitored by ¹H NMR spectroscopy due to identical R_f values of the starting material and product on

TLC. Alkylation of azide **21** with bromoacetic acid provided the carboxylic acid linker **22** for coupling to 7-ACA.



Scheme 2-5: i) NaN₃, NaI, H₂O, 80 °C, 2 days. ii) bromoacetic acid, NaH, THF, 0 °C - RT, o/n

The linker was first converted to an acid chloride under Vilsmeier-Haack conditions, prior to reacting with 7-ACA **17** using the acylation conditions previously validated. Much like the validation reaction, the only byproduct formed was hydrolysed acid chloride. This could not be removed by simple trituration with Et₂O and required purification by preparative HPLC that likely contributed to the poor yield. Nonetheless, Ceph-1 **23** was successfully synthesised via an efficient route needing no protection and deprotection steps.



Scheme 2-6: i) oxalyl chloride, cat. DMF, CH₂Cl₂, 0 °C - RT, 17 h. ii) 7-ACA, sat. aq. NaHCO₃, acetone, 0 °C - RT, 22 h. iii) 2 M hydrochloric acid

Degradation of Ceph-1 **23** was observed upon storage at room temperature which was unsurprising given the temperature sensitivity of precursor, 7-ACA **17**. A stability study by leaving the substrate at room temperature was conducted over several days and monitored by ¹H NMR spectroscopy, using CDCl₃ as solvent, and LC-MS – both analysis methods indicated impurities being formed. A brief analysis into the identity of these impurities based on common degradation adducts of penicillin resulted in no matches (**Figure 2-7**).¹⁰⁷ This was not investigated further. Storing Ceph-1 **23** at -20 °C circumvented any degradation issues, both when kept neat or as a solution in DMSO.

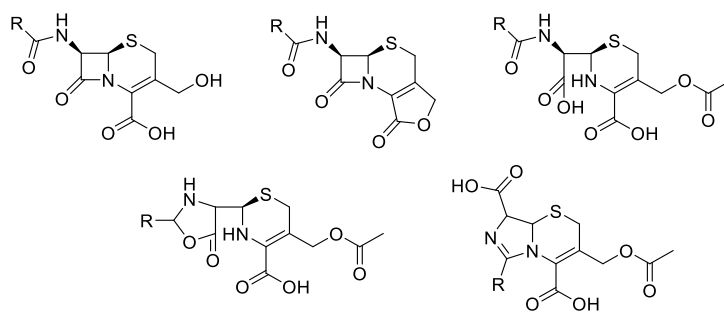
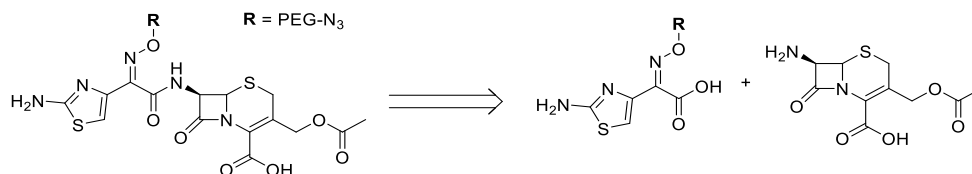


Figure 2-7: Possible degradation adducts of Ceph-1 23

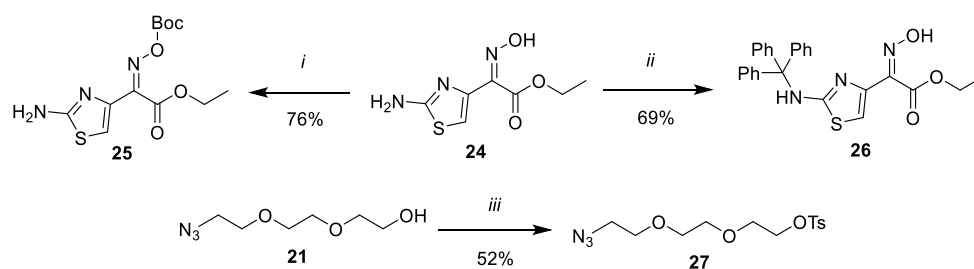
2.2.2 Synthesis of Ceph-2 39

With the success of acylating 7-ACA **17** directly as found in the synthesis of Ceph-1 **23**, the same approach was theorised for the construction the Ceph-2.



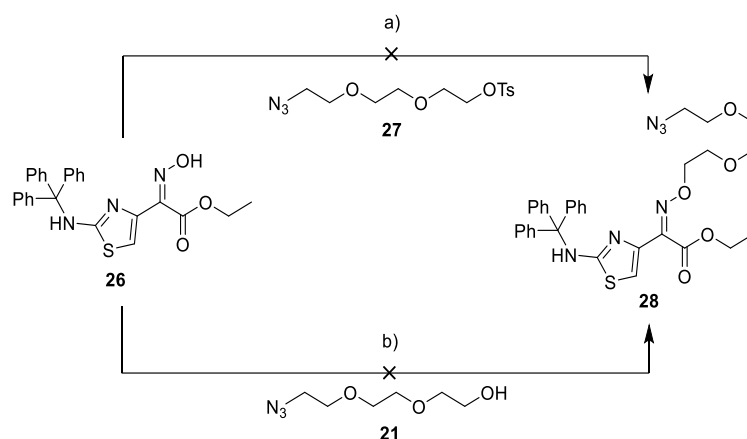
Scheme 2-7: Retrosynthetic analysis of the second cephalosporin target

The first challenge was synthesising the aminothiazole ring, with the coupling of the PEG chain to the oxime assumed to be the most problematic step. Literature precedence of a similar transformation suggested alkylation of the oxime as a feasible route.¹¹⁰ The amine of commercially available *Z* configured oxime ester **24** required protection prior to subsequent steps. This was initially attempted using a Boc group, however analysis of the resulting product by ¹H NMR spectroscopy showed the presence of a broad singlet integrated to two protons, which likely corresponded to the amine and indicated protection of the oxime had occurred instead. Comparison to the starting material confirmed the undesired carbamate **25** had formed; the oxime proton at 11.6 ppm was no longer observed. It was hypothesised that the electron withdrawing thiazole ring reduced nucleophilicity of the amine and thus the oxime reacted chemoselectively. Successful protection was, however, achieved using trityl chloride to give protected amine **26**. The linker substrate for the coupling **27** was synthesised by tosylation of the alcohol **21** made in the synthesis of Ceph-1 **23**.



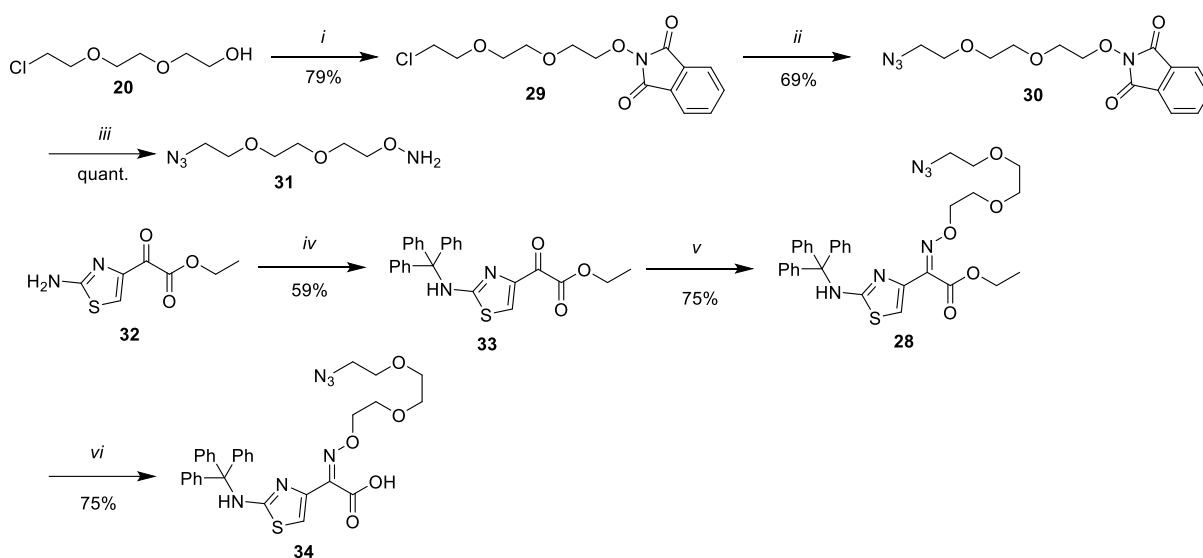
Scheme 2-8: i) *Boc*₂*O*, 1M aq. *NaOH*, THF, RT, o/n ii) trityl chloride, *Et*₃*N*, DMF, RT, o/n. iii) *p*-*TsCl*, *Et*₃*N*, DCM, 0 °C – RT, o/n

Different bases were then tested for validation of the alkylation of the oxime **26** (Scheme 2-9, route a). Triethylamine and potassium *tert*-butoxide both resulted in no consumption of starting materials and it therefore appeared formal deprotonation was required. Sodium hydride was employed which provided evidence of product formation. THF proved to be the better reaction solvent than DMF due to the ease of workup and formation of fewer impurities. The conditions were subsequently used in a scaled-up reaction however the target ester could not be isolated in sufficient purity despite numerous attempts to purify by flash column chromatography. The impurity appeared to be a tosyl-related species according to ¹H NMR spectroscopy and therefore it was anticipated that an acid/base workup in the subsequent hydrolysis step could still yield a usable precursor for coupling to 7-ACA. This unfortunately proved unsuccessful as both ¹H NMR spectroscopy and LC-MS indicated a mixture of desired product, the unknown tosyl species and a small amount of hydrolysed target. To avoid the presence of a tosyl containing reactant, a Mitsunobu alkylation was attempted using the alcohol **21** (Scheme 2-9, route b). TLC suggested a new product was formed; however, purification by flash chromatography showed this to be the reduced DIAD by-product. The starting materials were recovered in good mass return which signified the oxime hydroxyl was not acidic enough for deprotonation. Following the failed attempts to alkylate the oxime, the polarities of both substrates were switched to proceed via a condensation of the analogous keto ester starting material.



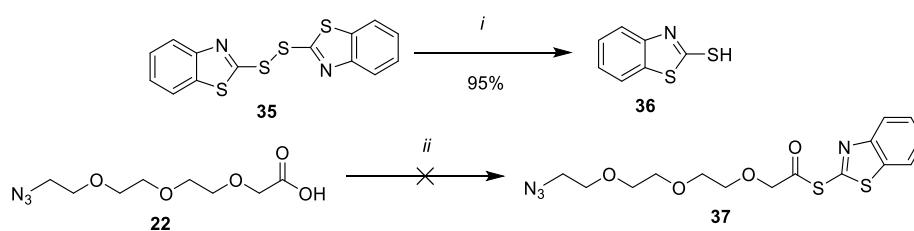
Scheme 2-9: a) **27**, NaH, THF, 0 °C – RT, o/n. b) **21**, PPh₃, DIAD, THF, 0 °C – RT, o/n

Facile preparation of hydroxylamine containing PEG linker **31** and trityl protection of the keto ester was achieved as expected. The condensation of both proceeded in good yield and the product proved easy to purify by flash column chromatography giving ester **28**. Subsequent saponification required heating in MeOH to afford the carboxylic acid **34**. A moderate yield was likely accounted by a large quantity of aqueous acid used to acidify the reaction and the product not sufficiently extracted with organic solvent. With the key aminothiazole **34** now in hand, coupling to 7-ACA **17** was attempted using the Vilsmeier-Haack and Schotten -Baumann conditions established in the synthesis of Ceph-1 **23**. However, no product was formed and only starting materials were recovered after an aqueous workup. PCl₅ was then used for acid chloride formation prior to adding amine 7-ACA **17**, however again only starting materials were recovered. Activation of the carboxylic acid **34** by a mixed anhydride approach using isobutyl chloroformate also resulted in no reaction.



Scheme 2-10: i) *N*-hydroxyphthalimide, PPh_3 , DIAD, THF, $0\text{ }^\circ\text{C} - RT$, *o/n*. ii) NaN_3 , KI, DMF, $80\text{ }^\circ\text{C}$, 19 h. iii) $N_2H_4 \cdot H_2O$, CH_2Cl_2 , $0\text{ }^\circ\text{C} - RT$, 2 h. iv) trityl chloride, Et_3N , DMF, RT, 2 h. v) **31**, cat. AcOH, MeOH, $60\text{ }^\circ\text{C}$, *o/n*. vi) 2 M aq. NaOH, THF: H_2O (1:1), RT, *o/n*

A patent review of the synthesis of MRSA drug Cefotibiprole indicated the use of mercaptobenzothiazole **36** as an activating group for the carboxylic acid.¹¹¹ The resulting thioester **37** could be isolated before coupling of the amine and therefore giving a synthetic advantage over *in situ* methods. Mercaptobenzothiazole was first synthesised by reducing the readily available bis precursor **35**. Reacting this with carboxylic acid **34** under triphenylphosphine-mediated conditions resulted in no reaction. To confirm if this was substrate-dependent, the conditions were attempted on the carboxylic acid **22**. This also yielded no reaction, both in the use of the mono thiazole adduct (**Scheme 2-11**) and bis precursor.

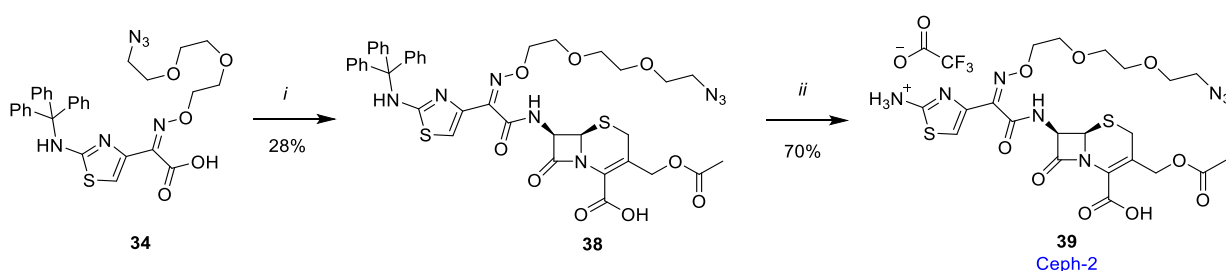


Scheme 2-11: i) $NaBH_4$, $CH_2Cl_2/MeOH$, RT, 30 min. ii) **22**, PPh_3 , Et_3N , CH_2Cl_2 , RT, *o/n*

Attention was then switched to using traditional “amide coupling” reagents. It was interesting to note that these were not typically used for similar transformations in the literature, potentially due to the byproducts of these reagents often being notoriously difficult to remove. With that in mind, EDCI was attempted first due to the water soluble nature of the urea by-product. Unfortunately, LC-MS analysis of the crude material indicated negligible amount of desired

product and was undetermined by ^1H NMR spectroscopy. Valeur's and Bradley's extensive review of amide couplings suggested the use of HATU due to its superior reactivity and efficiency compared to other reagents.¹¹²

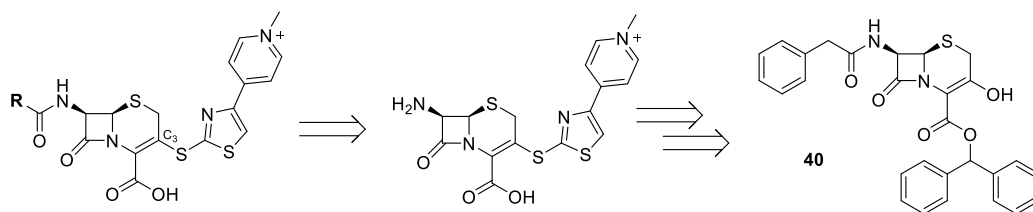
Using DMF as solvent for solubility purposes, treating carboxylic acid **34** with HATU prior to adding 7-ACA **17**, gave the expected amide product in moderate yield following purification by preparative HPLC. Synthesis of Ceph-2 **39** was furnished by trityl deprotection of key intermediate **38** using TFA in DCM.



Scheme 2-12: i) HATU, DIPEA, DMF, RT, 15 min, then 7-ACA, RT, o/n. ii) TFA, CH_2Cl_2 , RT, 1 h.

2.2.3 Synthesis of Ceph-3 and Ceph-4

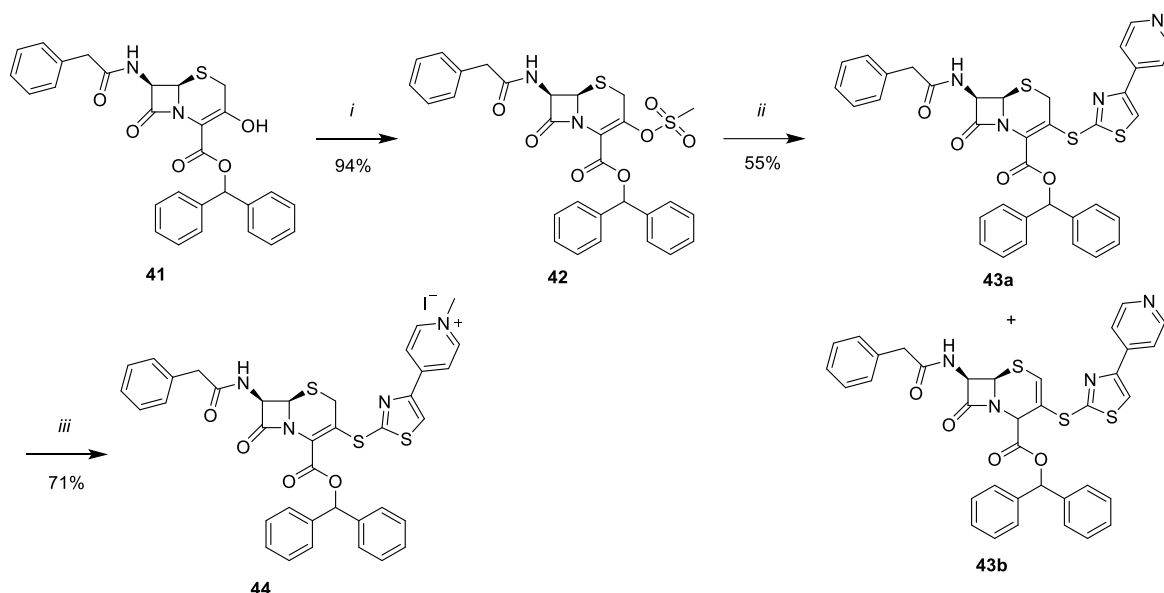
The structures of Ceph-3 and Ceph-4 were based upon the PBP2a binding drug, ceftaroline **3**, and thus unlike Ceph-1 **23** and Ceph-2 **39**, required installation of a heteroatom to carbon 3 of the cephem skeleton. Whilst this could have been feasible from 7-ACA **17**, it was reasoned the commercially available enol **40** be used as the starting material given the precedence and efficiency demonstrated in the process route to ceftaroline **3** reported by Ishikawa *et al.*¹¹³ The thiol bearing the key 1,3 thiazole was also found to be widely available and provided further economical validity for utilising this synthetic route.



Scheme 2-13: Retrosynthetic analysis of Ceph-3 and Ceph-4

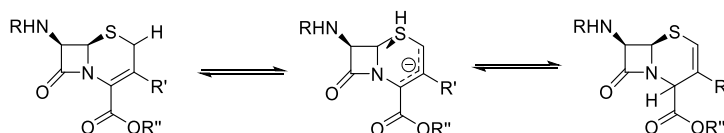
Synthesis began with transforming alcohol **41** into mesylate **42**. Under conditions described in the patent literature which used triethylamine as base, no reaction was observed.¹¹⁴ Changing to potassium carbonate proved successful however, and gave the desired intermediate required

for a Michael addition-elimination sequence to install the thiol side chain. This was first validated using sodium methoxide as base and provided target thiol **43a** in reasonable purity. However, attempts in scaling the reaction to gram scale were plagued with significant formation of the inseparable Δ^2 cephem isomer **43b** in up to 30% w/w as judged by ^1H NMR spectroscopy.



Scheme 2-14: i) MsCl , K_2CO_3 , DMF , -40°C , 2 h. ii) 4-(4-pyridinyl)thiazole-2-thiol, 30% NaOMe in MeOH , THF , -5°C – RT , o/n. iii) MeI , DMF , RT , o/n.

The $\Delta^3 \rightarrow \Delta^2$ isomerisation is a well-documented obstacle in the chemistry of cephalosporins and has been shown to exacerbate in high pH environments, particularly in the case of cephalosporin esters.^{115–118} The amount of isomerisation varies considerably on the substituents of the cephem ring, indicating that electronic influences are of huge importance.¹¹⁹

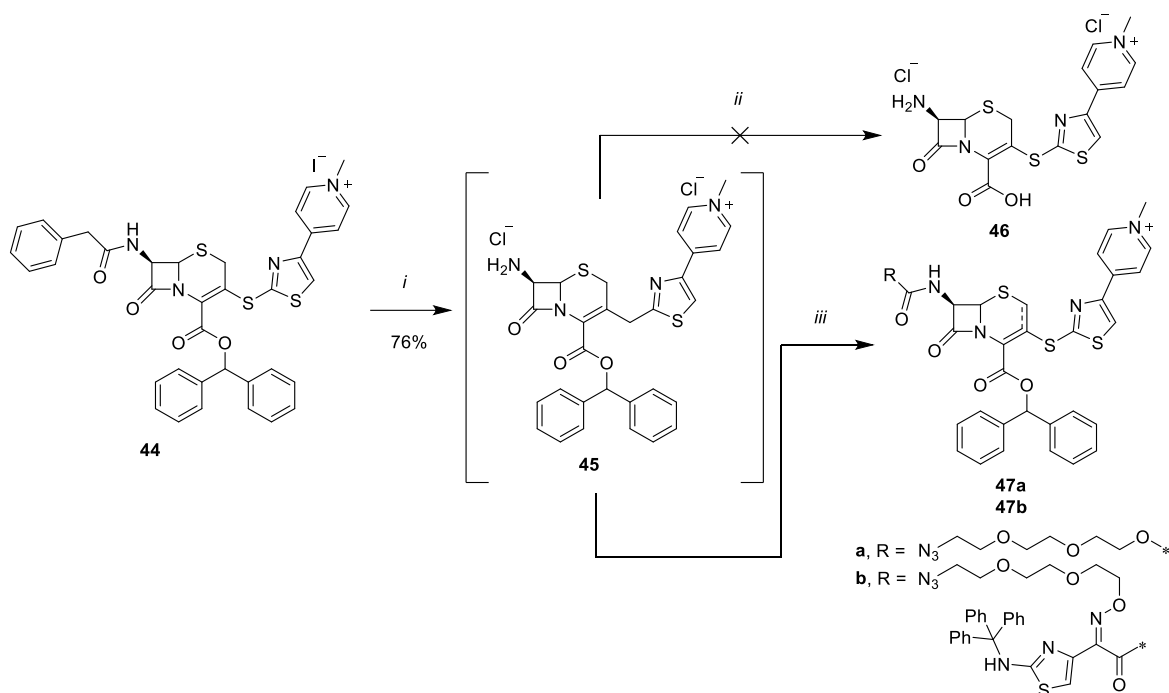


Scheme 2-15: The Δ^3/Δ^2 isomerisation of cephalosporins

In addition, the presence of a leaving group at carbon 3, such as in mesylate **42**, likely augments the possibility of isomerisation by direct displacement. Indeed, poorer leaving groups such as halogens have been shown to increase this effect compared to stronger leaving groups such as organosulfonates, which favour the desired addition-elimination reaction.¹²⁰

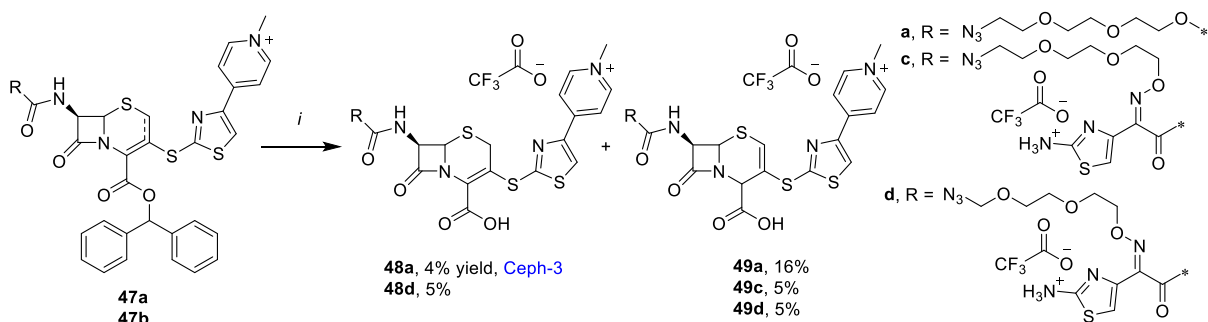
Ishikawa *et al.* did not indicate the amount of Δ^2 isomer formed in their synthesis of ceftaroline and its thiol heterocycle analogues, either when employing sodium methoxide or sodium hydride as base.¹¹³ Their yields, however, suggest the extent was not as substantial, particularly in the case of sodium hydride, which resulted in a 1:1 mixture of the isomers when attempted here. It was decided to proceed by using sodium methoxide with the hope of removing the unwanted Δ^2 isomer at a later stage of the synthesis. This was partially achieved upon precipitation of the crude iodide salt **44** with diethyl ether and acetonitrile, following methylation of the pyridine with methyl iodide. It should be noted that the yield was determined from the desired isomer **43a** only, i.e. taking 70% purity into account. Isomerisation could have occurred *in situ* due to the unknown equilibria between the Δ^2 and Δ^3 isomers when subjected to different conditions, however it was not considered in this or any following reactions for simplicity.

Deprotection of the phenyl acetyl group was achieved using established literature conditions to give the amine salt **45** and, as per the literature precedent, was used without purification.¹¹³ Following a protocol to deprotect the diphenyl ester, however, was unsuccessful despite formation of carboxylic acid **46** as judged by LC-MS. Ishikawa *et al.* utilised SP-207 resin for isolation, however its lack of availability required the need for preparative HPLC, of which carboxylic acid **46** was highly sensitive to both basic and acidic conditions. In light of this, the synthetic route was altered and acylation of the amine attempted first. Schotten-Baumann conditions with carboxylic acid **22**, as used in the synthesis of Ceph-1 **23**, offered no reaction and only the Δ^2 isomer of the starting material **45** was isolated, confirmed by 2D NMR spectroscopy. Switching to HATU mediated conditions *did* afford precursor **47a**, although in a 1:1 mixture of Δ^2 : Δ^3 isomers. Separation was attempted by preparative HPLC however the required acidic conditions gave partial deprotection of the diphenyl ester. As such, the mixture was prosecuted to the final deprotection step as a concentrated reaction mixture, which successfully furnished Ceph-3 **48a** as a pure TFA salt following purification. Interestingly, a 5:1 mass return in favour of the Δ^2 isomer **49a** was isolated, again illustrating the capricious nature of cephalosporin chemistry. Yields were calculated from crude amine **45**.



Scheme 2-16: i) PCl_3 , pyridine, CH_2Cl_2 , RT, 1 h, then MeOH, 0 °C – 5 °C o/n. ii) conc. HCl, MeCN, RT, 30 min. iii) **22** or **34**, HATU, DIPEA, DMF, RT, o/n.

The thiazole-oxime motif was installed to amine **45** via the same conditions using the carboxylic acid **34** synthesised previously for Ceph-2 **39**. Much like analogue **47a**, oxime **47b** was highly unstable to HPLC conditions due to the acid labile diphenyl and trityl groups. These were subsequently removed via TFA but disappointingly the proposed structure for Ceph-4, “**48c**”, was not isolated in adequate purity following attempts via preparative HPLC. The competing Δ^2 isomer **49c** made purification convoluted, but this was worsened by the unforeseen formation of *E*-oxime isomers **48d** and **49d**. Both these and Δ^2 isomer **49c** were successfully isolated in sufficient amounts for characterisation by ^1H NMR spectroscopy and mass spectrometry.



Scheme 2-17: i) TFA, anisole, CH_2Cl_2 , RT, 15min - 2 h

The *E* configuration of some oxime containing cephalosporin antibiotics have been reported to be impurities in their synthesis as well as degradation products when under U.V. light or varied pH conditions.^{121–123} Their biological activity is considerably lower than that of their *Z*-isomer counterparts, as mentioned previously, and are negated in synthesis via the use of *Z* configured oxime-carboxylic acids, such as acid **34** used here.

Surprisingly, no *E* isomer was observed in the synthesis of Ceph-2 **39** despite largely the same acylation, deprotection and subsequent purification conditions being employed, meaning the isomerisation was likely substrate-dependent. The relative *E* / *Z* (*anti* / *syn*) assignment was determined by ¹H NMR spectroscopy using the chemical shift value of the thiazole proton.



Figure 2-8: Hydrogen bonding between the thiazole proton and oxime oxygen

It was hypothesised the chemical shift value of this proton would be higher for the *E* isomer due to the possibility of hydrogen bonding to the oxygen of the oxime. It had been previously reported a difference of approximately 0.7 ppm between both isomers following the explicit assignment for a range of cephalosporin antibiotics and their isomerised counterparts.^{121,123} Indeed, this trend corroborated with assigned Δ^2 *Z* isomer **49c** and *E* isomer **49d** having chemical shifts of 7.3 ppm and 7.7 ppm, respectively, and thus X-ray crystallography was not deemed necessary.

Notwithstanding the low overall yield, it was pleasing to have obtained Ceph-3 **48a** as a potential PBP2a binder despite issues encountered in its synthesis and purification. In addition, the Δ^2 and *E* isomer derivatives of Ceph-4 could still be suitable depending on their biological profile.

2.3 Biological imaging and evaluation of Ceph-1 **23** and Ceph-2 **39**

2.3.1 Biological activity of Ceph-1 **23** and Ceph-2 **39**

The feasibility of Ceph-1 **23** and Ceph-2 **39** for PBP labelling studies commenced with their minimum inhibitory concentrations (MIC) being evaluated against a wild-type strain of *S. aureus*, SH1000. Antibiotics cefaloram **50** and cefotaxime **51** (see appendix for synthesis) were used as reference markers and sans-acyl cephalosporin 7-ACA **17** as a control. Ceph-1 **23** readily dissolved in water at a concentration of 1 mg/mL whilst Ceph-2 **39** required DMSO for complete solubility.

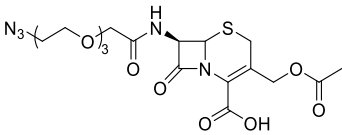
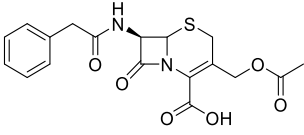
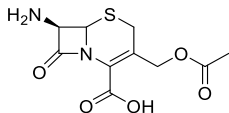
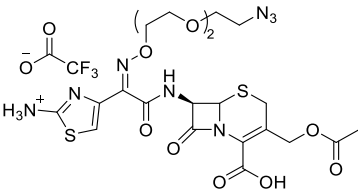
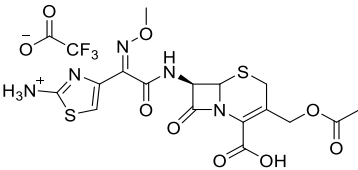
Entry	Compound	Structure	MIC ($\mu\text{g/mL}$)
1	Ceph-1 23		5
2	Cefaloram 50		<1
3	7-ACA 17		>50
4	Ceph-2 39		5 – 10
5	Cefotaxime ^a 51		2 – 5

Table 2-1: MICs of cephalosporins against SH1000. Assays were conducted by broth dilution procedure. Inoculation was conducted at 37 °C for 24 hours. The MIC was determined to be the lowest concentration at which no bacterial growth occurred as measured by optical density (OD_{600}).
^a Synthesis scheme is shown in the appendix.

Ceph-1 **23** was estimated to be 5 \times less potent than reference antibiotic **50**. Encouragingly, it did show *some* activity unlike the precursor 7-ACA **17** which alleviated any fears the PEG

chain was being cleaved. It also displayed stability at the elevated temperature required for microbial growth and eased the concerns of temperature sensitivity found upon its isolation. Ceph-2 **39**, in contrast, had a similar MIC to parent antibiotic cefotaxime **51**, illustrating that the PEG chain was not having a significant effect on its activity. It had an identical activity to Ceph-1 **23** which was unsurprising given the variability of activity across the cephalosporin antibiotic classes. Indeed, the trend between reference compounds cefaloram **50** and cefotaxime **51** was consistent with that of first-generation cephalosporin antibiotics being more potent than their newer third generation counterparts against *S. aureus*.^{124–126}

A direct comparison to previously reported chemical probes could not be made; either their antibacterial activity had not been assessed or they had not been tested against *S. aureus*. Using the available data as a guide however, it was clear that a wide range of MICs still allowed for PBP analysis in other bacterial strains, particularly in the case of the β -lactone probes developed by Sharifzadeh *et al.* (Table 2-2, Entry 3), which enabled selective PBP visualisation in *S. pneumoniae* using SIM microscopy. Notwithstanding, a MIC of 5 $\mu\text{g/ml}$ achieved by Ceph-1 **23** and Ceph-2 **39** indicated significant PBP inhibition, making the chemical probes ideal for fluorescent labelling purposes without the attendant worry of non-specific binding.

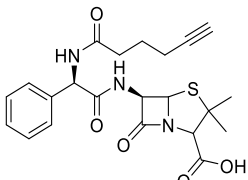
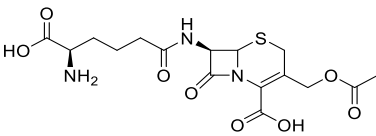
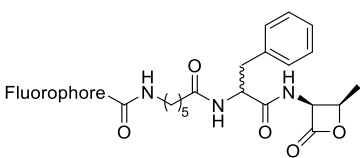
Entry	Chemical probe	Bacterial strain	MIC ($\mu\text{g/mL}$)
1		<i>B. licheniformis</i> <i>L. welshimeri</i>	8 1
2		<i>B. subtilis</i>	3 – 10
3		<i>S. pneumoniae</i>	80

Table 2-2: MICs of chemical probes used for PBP labelling. Entry 1⁸⁴, Entry 2⁸⁵, Entry 3⁸⁶

2.3.2 Investigation of labelling PBPs using a post click strategy

The labelling of PBPs in *S. aureus* was envisaged via two different methodologies: (i) A pre-click strategy, that is ligating the probe to a fluorescent dye via a copper-catalysed azide–alkyne cycloaddition (CuAAC) prior to incorporating into cells, or (ii) by post-clicking, i.e., treating cells with the probe first before conducting the ligation *in situ*. The second strategy was considerably more attractive, namely in a practical sense but also a versatility perspective, by which the chemical probes could be used as a universal tool and allow easy conjugation to different fluorescent dyes. Furthermore, it was the only strategy deemed suitable for FDAA incorporation. Attempting to pre-click FDAAs with STORM compatible dyes, chiefly Alexa Fluor™ 647, yielded no specific fluorescence in the bacteria; it was reasoned the dyes were too large or too charged to cross the cytoplasmic membrane of live *S. aureus*.¹²⁷

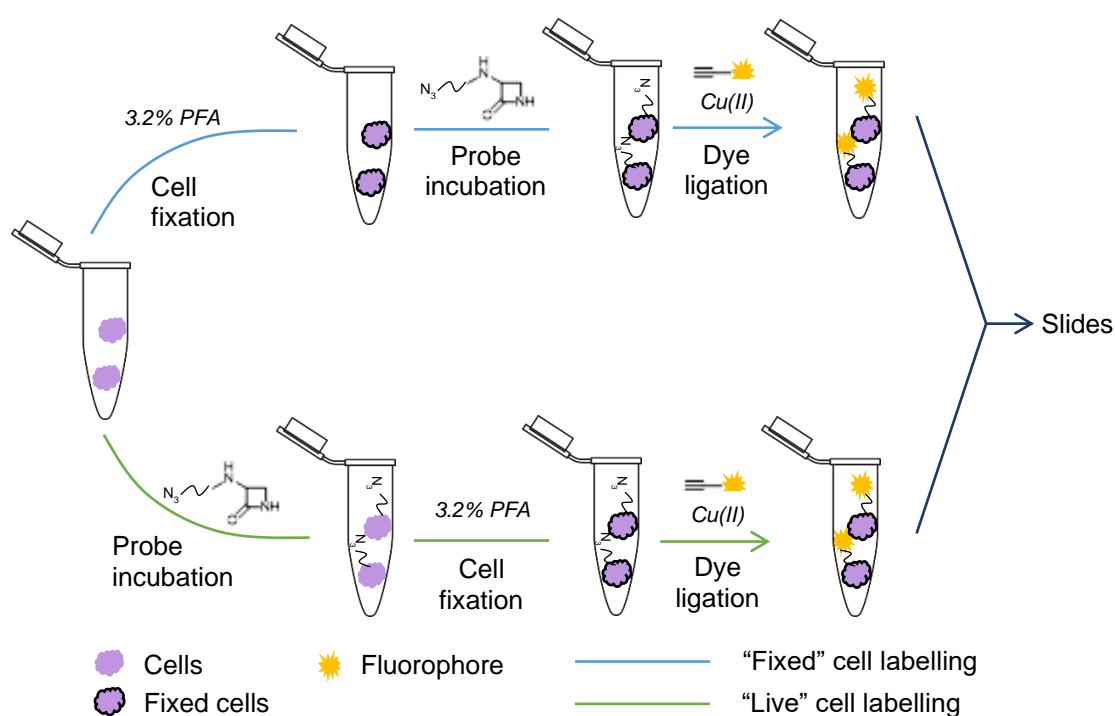


Figure 2-9: Post-click labelling strategy. Two possible labelling routes prior to dye ligation; fixation of cells prior to probe incorporation represented by the blue line and vice-versa as represented by the green line.

Thus, a post-click labelling protocol was attempted using Ceph-1 **23** in the first instance and visualised by conventional widefield microscopy for preliminary assessment. Incubation was undertaken at the MIC of Ceph-1 **23** to avoid significant disturbance of cellular structure. Exponential phase cells were fixed before and after incorporation of the probe to assess if live imaging was feasible (**Figure 2-9**). Alkyne-functionalised ATTO 488 and BDP-FL were

chosen as fluorescent dye partners. These would allow easy translation to STORM microscopy if successful and a comparison point to Bocillin-FL **1**. The *in situ* ligation was conducted with a commercially available “Click-iT® cell reaction kit”, which contained a buffer, CuSO₄ solution and an unknown additive, presumed to be a reducing agent for copper(I) to form and the cycloaddition to proceed.¹²⁸

Ceph-1 **23** ligated to ATTO 488 showed some cell wall incorporation, as indicated by the yellow arrow, but this was largely irregular and much of the fluorescence signal came from whole-cell labelling. This indicated the entire probe was getting into the cell, rather than binding to PBPs specifically. Treating stationary phase cells with Ceph-1 **23**, i.e. fixed cells (images not shown) did not yield any improvement and indicated a similar pattern. Ligation to BDP-FL showed no incorporation at all, with the cells appearing to be stained by the dye itself. This was confirmed by treating cells with the dye, des-probe; an identical image was obtained (see appendix). The FDAA, ADA, was used as a control for both experiments and clearly showed the desired cell wall and septum labelling as expected.

Following unsuccessful attempts to utilise the post click strategy, it was reasoned that the ligation of a fluorophore, prior to incorporation, was crucial for non-intrusive PBP labelling. Indeed, previously reported antibiotic chemical probes, Bocillin-FL **1** and a Cephalosporin C derivative **12** developed by Kocaoglu *et al.*, had a fluorophore already in place. It was therefore proposed a similar approach be taken here.

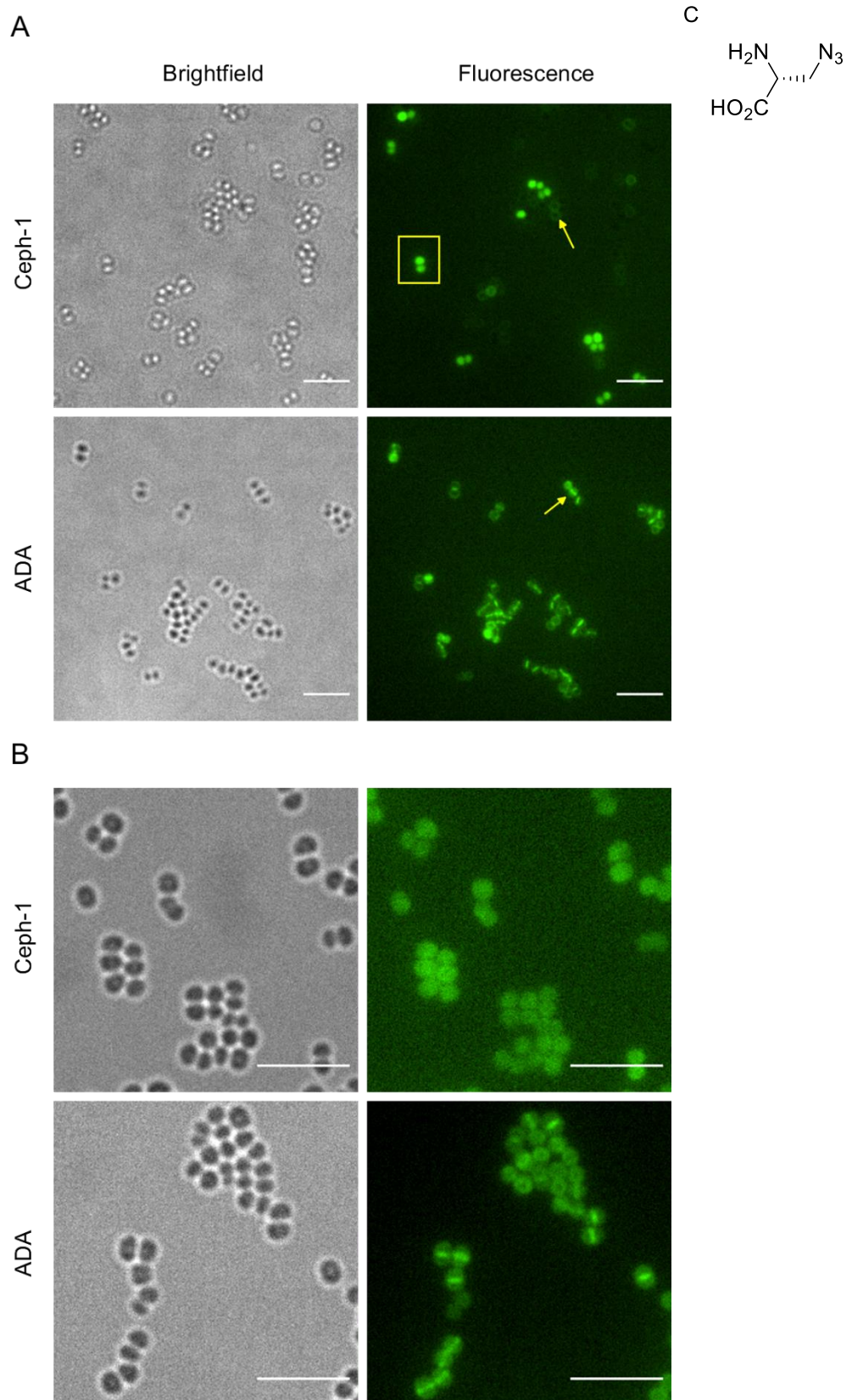
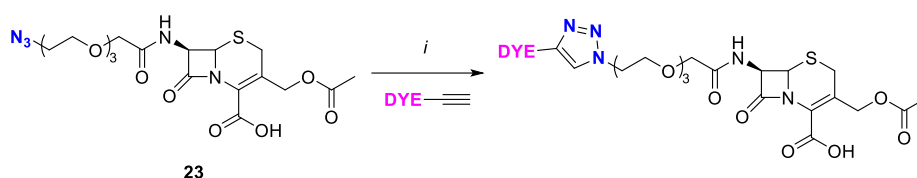


Figure 2-10: Ceph-1 23 and ADA incorporation via a post-click strategy. *S. aureus* SH1000 exponential phase cells were treated with Ceph-1 23 (5 $\mu\text{g}/\text{mL}$) or ADA for 5 min, fixed and click-labelled. A) ATTO 488. The box indicates entire cell labelling and the arrows cell wall and septum incorporation. B) BDP-FL. C) Structure of ADA. Images are of the middle stack. Scale bars 5 μm . Microscope setup was carried out by Kasia Wacnik.

2.3.3 Synthesis of fluorescent derivatives of Ceph-1 **23** and Ceph-2 **39**

To allow for more accurate and thorough characterisation, the fluorescent derivatisation of Ceph-1 **23** and Ceph-2 **39** was conducted by a formal synthesis procedure with the isolation of each analogue prior to incorporating into cells. As per the post-click strategy, the conjugation of the chemical probes to the fluorophores was attempted by the well-established copper catalysed Huisgen 1,3-dipolar cycloaddition.



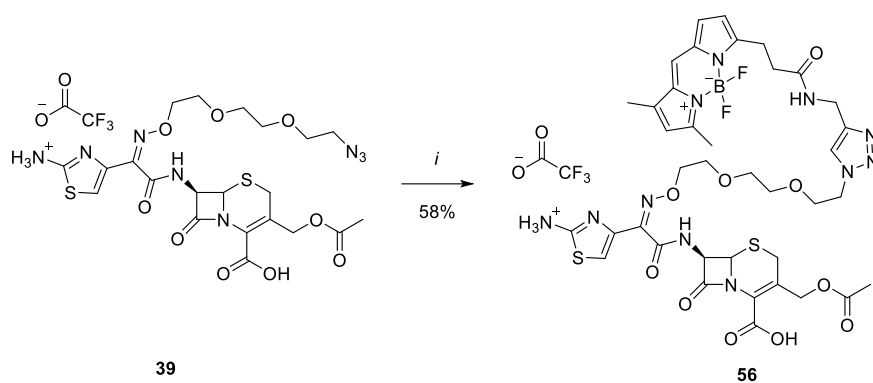
Scheme 2-18: i) CuSO₄, L-ascorbic acid, t-BuOH:DMSO, H₂O, RT, 1 h – o/n.

A catalytic amount of copper (II) sulfate and slight excess of ascorbic acid was employed to reduce oxidative homocoupling of the alkyne as reported in the literature.^{129,130} All reactions were conducted on a milligramme scale and required reagents to be added by serial dilution, prior to purification by preparative HPLC. As such, structure determination by NMR spectroscopy could not be obtained however purity analysis by LC-MS was considered sufficient, especially given parent probes, Ceph-1 **23** and Ceph-2 **39**, had both been fully characterised prior. Ceph-1 **23** and BDP-FL as the alkyne reactant partner were reacted initially to trial the methodology and to acquire a direct analogue of the BODIPY-based probe, Bocillin-FL **1**. Reaction progress was monitored by LC-MS and indicated full conversion in 2 hours. To allow for minimal product manipulation, the reaction mixture was purified directly by preparative HPLC and lyophilised to avoid exposure to heat. Following successful isolation, imaging and biological evaluation (**Table 2-3**), three further fluorescent dyes were successfully ligated: (i) 5-carboxytetramethylrhodamine (TAMRA), to allow for an analogue of the reported Cephalosporin C probe **12**, (ii) Alexa Fluor™ 647, for imaging by STORM and (iii) Cyanine5, a less established but cheaper STORM compatible fluorophore.

Entry	Fluorescent dye	Chemical structure	Product	Yield (%)
1	BDP-FL		52	45
2	TAMRA		53	98
3	Alexa Fluor™ 647 ^a		54	37
4	Cyanine5		55	77

Table 2-3: Derivatisation of Ceph-1 with fluorescent dyes. ^aPredicted structure based on molecular weight.

All reactions proceeded smoothly and generally resulted in good yields, particularly the TAMRA and Cyanine5 derivatives (**Table 2-3**, Entry 2 & 4), which may have been accounted by the additional CuSO₄ and ascorbic acid being used. The prime Alexa Fluor™ 647 target, however, did not go to completion despite successive additions of catalyst. The reaction was capricious and the final derivative more unstable compared to the rest, but nonetheless provided enough material for biological assessment. Conjugation of Atto 488, the STORM-compatible dye trialled in the post-click strategy, did not result in any reaction due to its degradation in DMSO; alternative solvents were not explored. Finally, Ceph-2 **39** was derivatised with BDP-FL to afford a final probe for evaluation.



Scheme 2-19: BDP-FL alkyne, Cu_2SO_4 , *L*-ascorbic acid, $\text{DMSO}:\text{H}_2\text{O}$, RT, 6 h.

2.3.4 Biological activity of fluorescent derivatives

All derivatives were tested against *S. aureus* SH1000 to ascertain if any activity had been lost after addition of the fluorescent dyes.

Entry	Compound	MIC ($\mu\text{g}/\text{mL}$)
1	Ceph-1 BDP 52	5
2	Ceph-1 TAMRA 53	5
3	Ceph-1 AF647 54	20 – 30
4	Ceph-1 Cy5 55	20 – 30
5	Ceph-2 BDP 56	5 – 10

Table 2-4: MICs of fluorescent Ceph-1 **23** and Ceph-2 **39** derivatives against SH1000. Assays were conducted by broth dilution procedure. Inoculation was conducted at 37 °C for 24 hours. Bacterial growth was determined by subtraction of the initial optical density (OD_{600}) of each concentration to that measured after.

Both BODIPY derivatives **52** and **56** retained biological activity compared to their parent compounds, as well as TAMRA-based Ceph-1 probe, **53**. Cyanine-based probes **54** and **55** showed a 4 – 6-fold drop compared to parent Ceph-1 **23** however, indicating the size or charge of the fluorophore may have been disrupting PBP binding in the active site. Nevertheless, it was still hoped the MIC's were within an acceptable range to gain an accurate fluorescence signal and were therefore taken further, particularly given their potential for high resolution STORM imaging capability.

2.3.5 Labelling of PBPs in *S. aureus* using a pre-click strategy

Having isolated several fluorescent antibiotic probes and confirmed their biological activity, the labelling of *S. aureus* was attempted and visualised using widefield microscopy. Ceph-1-BDP **52** was assessed first to establish viability and subsequent parameters for cell incorporation and imaging if successful.

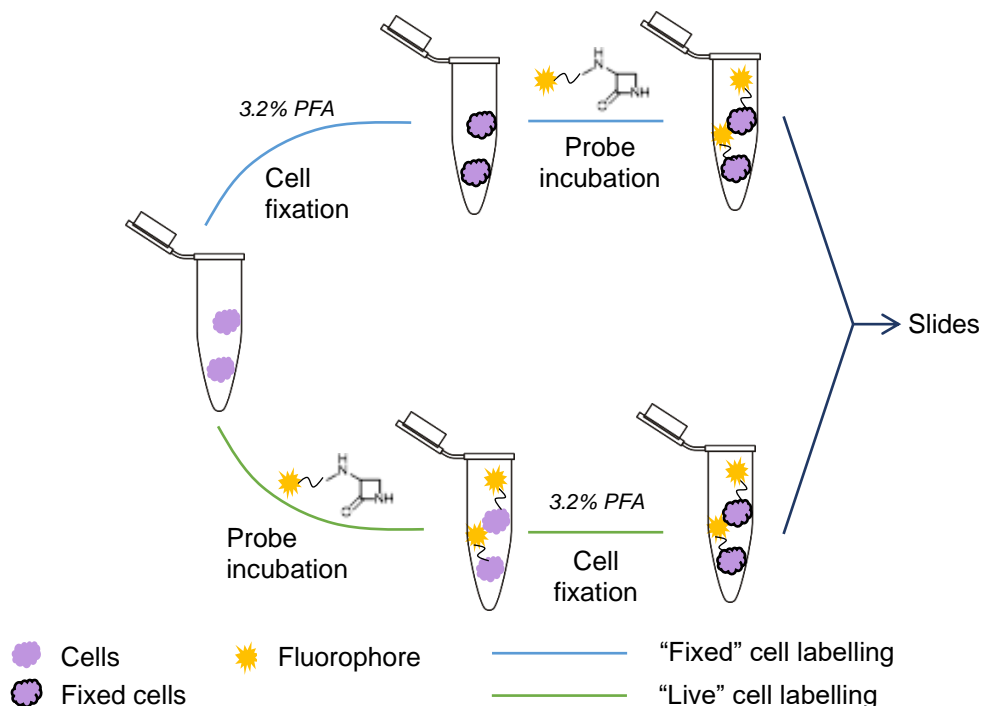


Figure 2-11: Pre-click labelling strategy. Cells were either fixed before (stationary growth phase) or after (exponential phase) probe incubation.

As per the post-click strategy, both fixed and live cells were incubated with the chemical probe to assess if live imaging of nascent PG synthesis was possible. Inoculation was carried out at the MIC and twice the MIC to determine the optimum fluorescence without extensive disturbance to cellular structure.

Ceph-1 BDP **52** successfully mapped PBPs in all conditions attempted. Cells grew as expected with strong fluorescence at the division septa showing septal rings and plates. Off-septal labelling of PBPs, even during septation, was also observed which illustrated their activity across the cell wall. This agreed with earlier studies conducted with FDAAs, that indicated that peptidoglycan biosynthesis in *S. aureus* occurred not only at the septa but also around the peripheral cell wall.^{131,132}

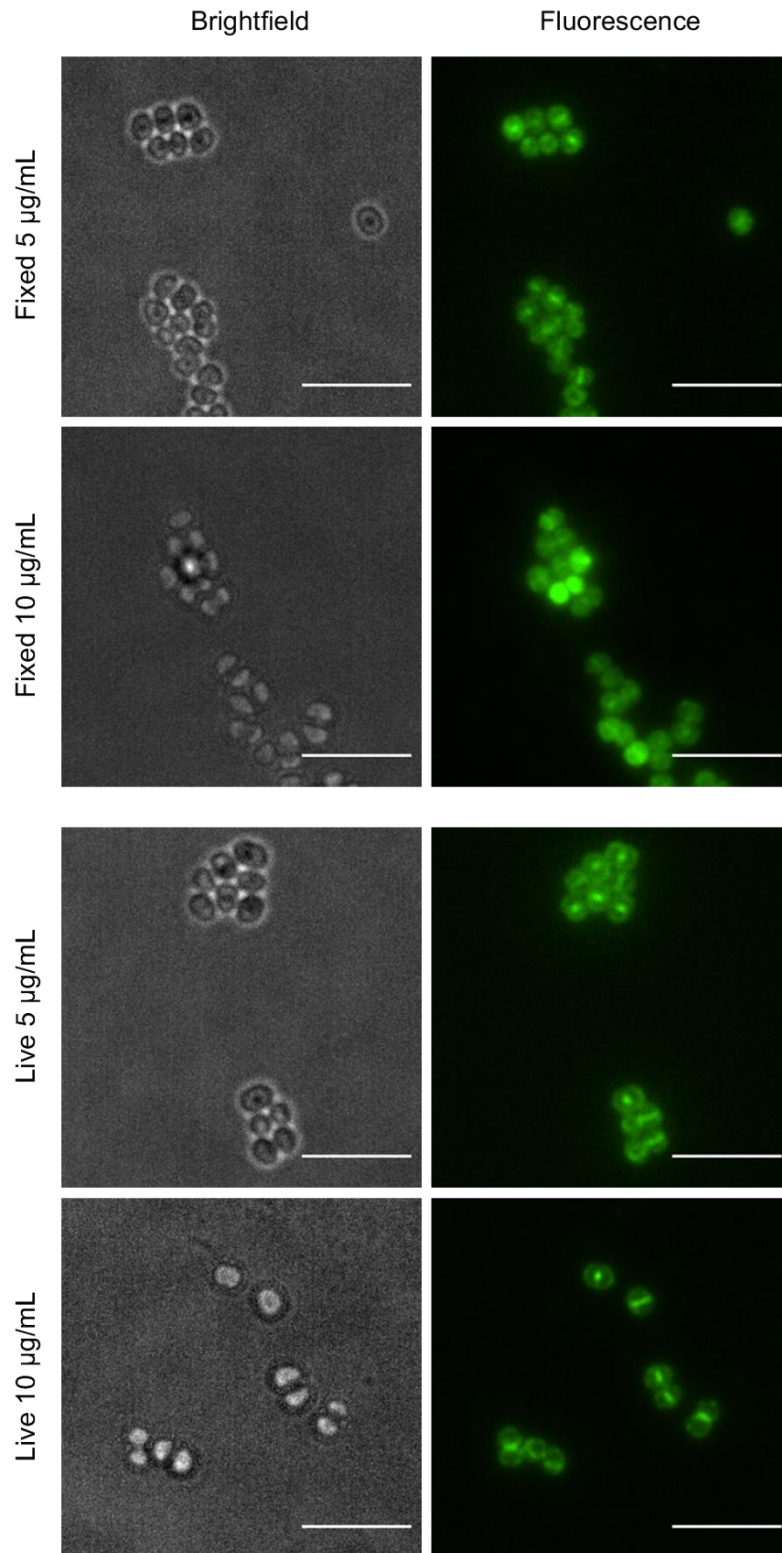
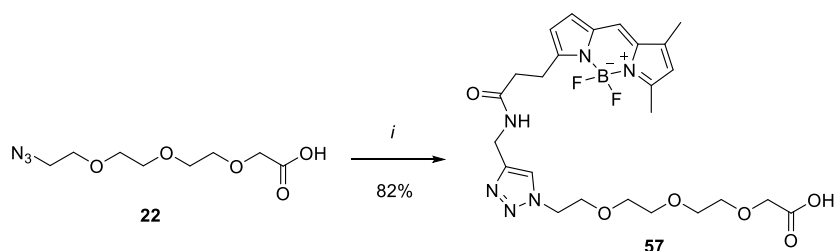


Figure 2-12: *S. aureus* labelled with Ceph-1 BDP 52. *S. aureus* SH1000 stationary (fixed) and exponential phase (live) cells were treated with Ceph-1 BDP at 5 $\mu\text{g}/\text{mL}$ (MIC) and 10 $\mu\text{g}/\text{mL}$ (2 \times MIC) for 5 min at 37 $^{\circ}\text{C}$. Fluorescence images are of a maximum intensity projection of z-stacked images. Scale bars 5 μm . Microscope setup was carried out by Kasia Wacnik.

Interestingly, live cells incorporated the probe better than fixed cells. The latter resulted in poorer image clarity which may have been owed to undesired membrane staining. Additionally, incubating the probe at $2 \times \text{MIC}$ in fixed cells resulted in some whole-cell fluorescence which suggested some damage might have occurred from the fixative; live cells showed no such discrepancy. Cells also appeared to be larger in volume when dosed at a higher concentration, an effect known to occur, however this was not confirmed quantitatively.¹³³ Perhaps the only negative found was the propensity of the fluorophore to photobleach, making it unsuitable for real-time microscopy.

To validate the labelling was occurring specifically by the antibiotic motif of the probe and not the fluorophore, a control compound was synthesised encompassing just the linker and fluorescent dye.



*Scheme 2-20: i) BDP-FL alkyne, Cu_2SO_4 , L-ascorbic acid, *t*-BuOH:DMSO, H_2O , RT, 2 h*

Precursor, carboxylic acid **22**, underwent a smooth cycloaddition with BDP-FL alkyne to give triazole **57** as the desired control compound. The MIC was tested against *S. aureus* SH1000 and no showed inhibition of bacterial growth. Further validation of its inactivity was confirmed by cell labelling experiments. Increasing the contrast significantly showed staining of the cell accounted by the background signal, rather than specific binding, and proved the antibiotic was the active recognition element of the chemical probe. This reference test was also verified using the Cy5 fluorophore to give carboxylic Cy5 analogue **58** (see appendix) which too showed no inhibition of bacterial growth.

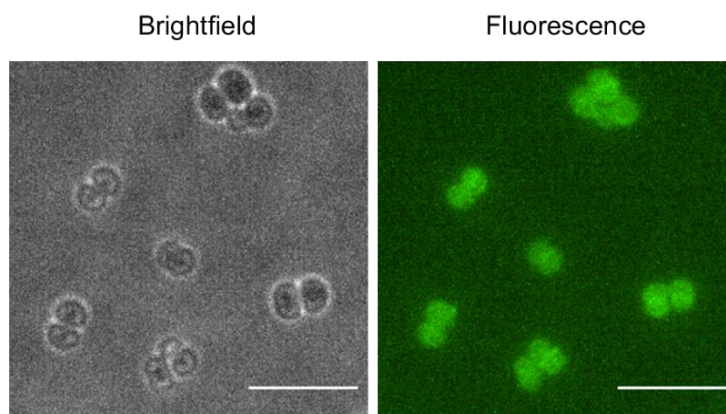


Figure 2-13: *S. aureus* labelled with compound **57**. Exponential phase cells were treated with **57** at 5 $\mu\text{g}/\text{mL}$. Fluorescence images are of a maximum intensity projection of z-stacked images. Scale bars 5 μm . Microscope setup was carried out by Kasia Wacnik.

With proof of principle of the pre click strategy now established, all other fluorescent derivatives were prosecuted to cell-labelling experiments using the optimum conditions. Ceph-1 TAMRA **53** labelled PBPs at both the MIC and $2 \times \text{MIC}$ and shared the same characteristics of localised fluorescence to that seen by Ceph-1 BDP **52**. As with all probes tested, purity was key to obtaining clear PBP binding. Labelling with an impure batch of TAMRA derivative **53** gave considerably poorer binding and largely a background signal was observed. Ceph-1 AF647 **54** was also successful and put aside any fears of larger and charged fluorescent dyes being unable to pass or approach the cytoplasmic membrane. Inoculating the bacteria at a concentration 30 $\mu\text{g}/\text{mL}$ resulted in optimum mapping of PBPs in the cell wall. Related derivative, Ceph-1 Cy5 **55**, offered slightly clearer images at both ends of the MIC range. This was likely owed to its enhanced chemical stability compared to the Alexa Fluor™ 647 analogue **54**. Pleasingly, alternative scaffold Ceph-2 BDP **56** also labelled cells using the same incubation conditions and showed that binding activity was not restricted to a simple cephalosporin motif.

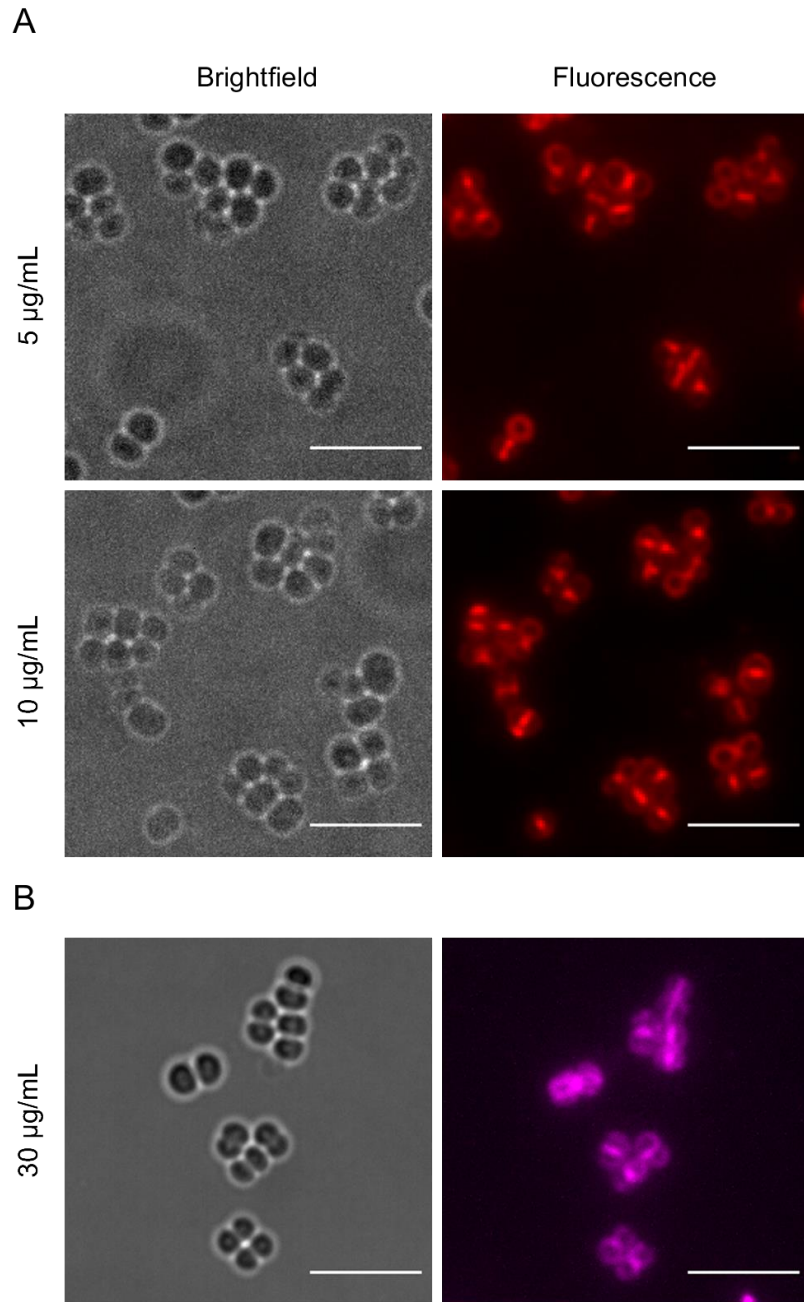


Figure 2-14: *S. aureus* labelled with fluorescent derivatives. A) Ceph-1 TAMRA 53. B) Ceph-1 AF647 54. Exponential phase (live) cells were treated at said concentrations for 5 min at 37 °C. Fluorescence images are of a maximum intensity projection of z-stacked images. Scale bars 5 μm . Microscope setup was carried out by Victoria Lund.

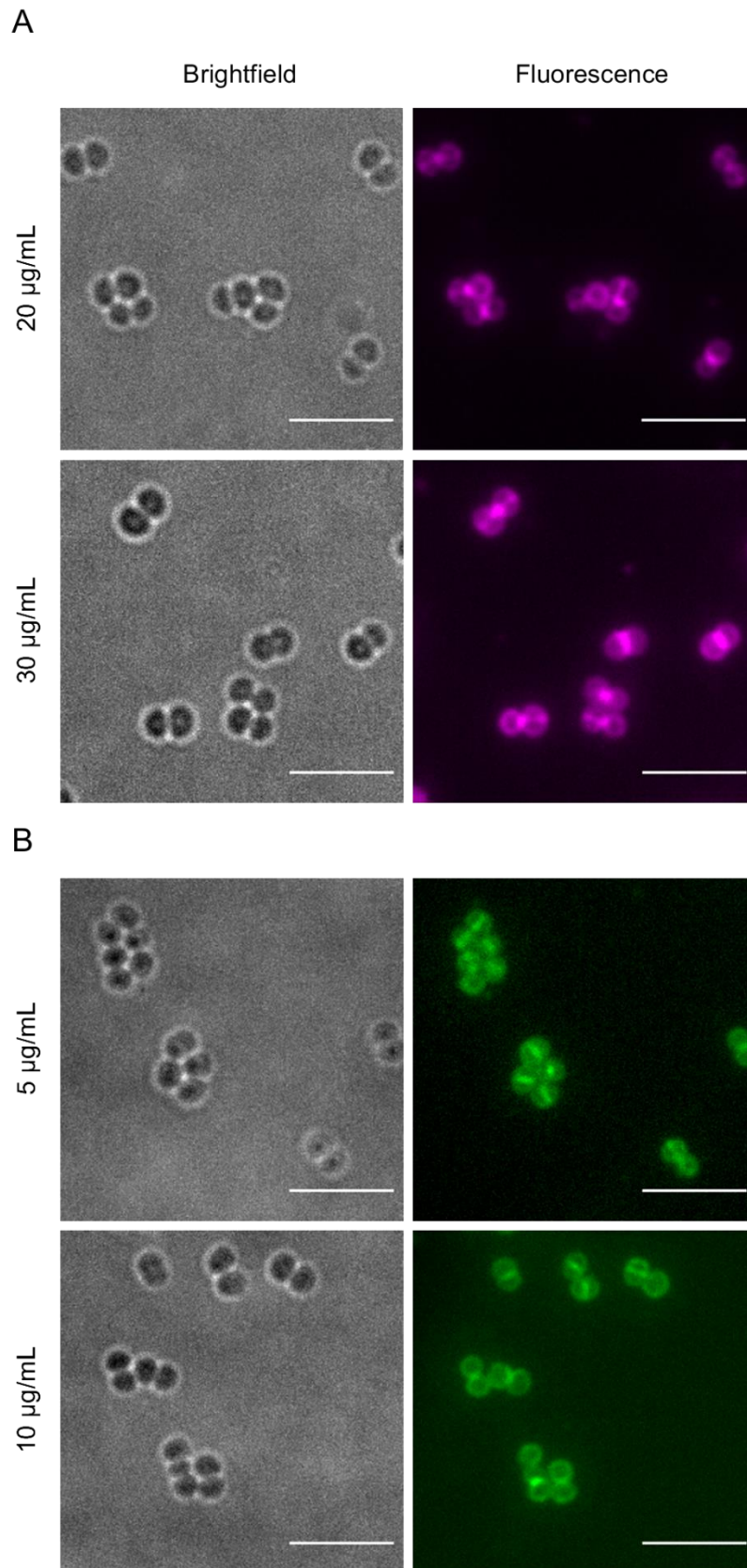
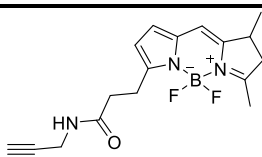
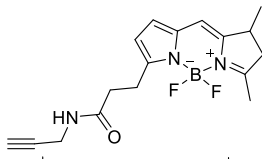
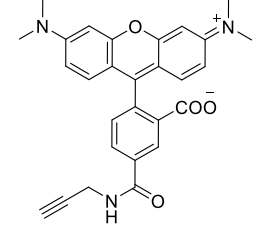
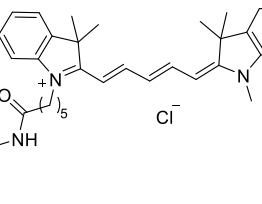
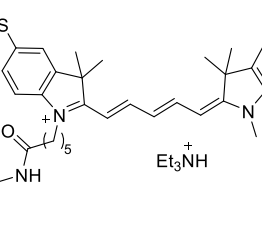


Figure 2-15: *S. aureus* labelled with fluorescent derivatives. A) Ceph-1 Cy5 55. B) Ceph-2 BDP 56. Exponential phase (live) cells were treated at said concentrations for 5 min at 37 °C. Fluorescence images are of a maximum intensity projection of z-stacked images. Scale bars 5 μm . Microscope setup was carried out by Victoria Lund.

2.3.6 Profiling of selectivity for PBPs in *S. aureus*

An important goal of this study was to develop probes with affinity for specific PBPs to better understand their individual roles in peptidoglycan biosynthesis. The antibiotic scaffold, Ceph-2 **39**, was designed for this very purpose to bind favourably to PBP2, whilst Ceph-1 **23** was seen to be more general for global PBP mapping. To assess if any selectivity had been achieved, the *in vitro* labelling of *S. aureus* by each fluorescent probe and subsequent sodium dodecyl sulfate-polyacrylamide gel electrophoresis (SDS-PAGE) and fluorography was performed. A range of concentrations was tested and the commercially available Bocillin-FL **1** used as control by virtue of its affinity to all PBPs.¹³⁴

Entry	Chemical probe	Dye structure	PBPs labelled
1	Ceph-1 BDP 52		1, 2, 3 and 4
2	Ceph-2 BDP 56		1 and 2
3	Ceph-1 TAMRA 53		1, 2 and 3
4	Ceph-1 Cy5 55		1, 2 and 3
5	Ceph-1 AF647 54		1 and 2

*Table 2-5: Selectivity profile of fluorescent probes for PBPs in *S. aureus* SH1000*

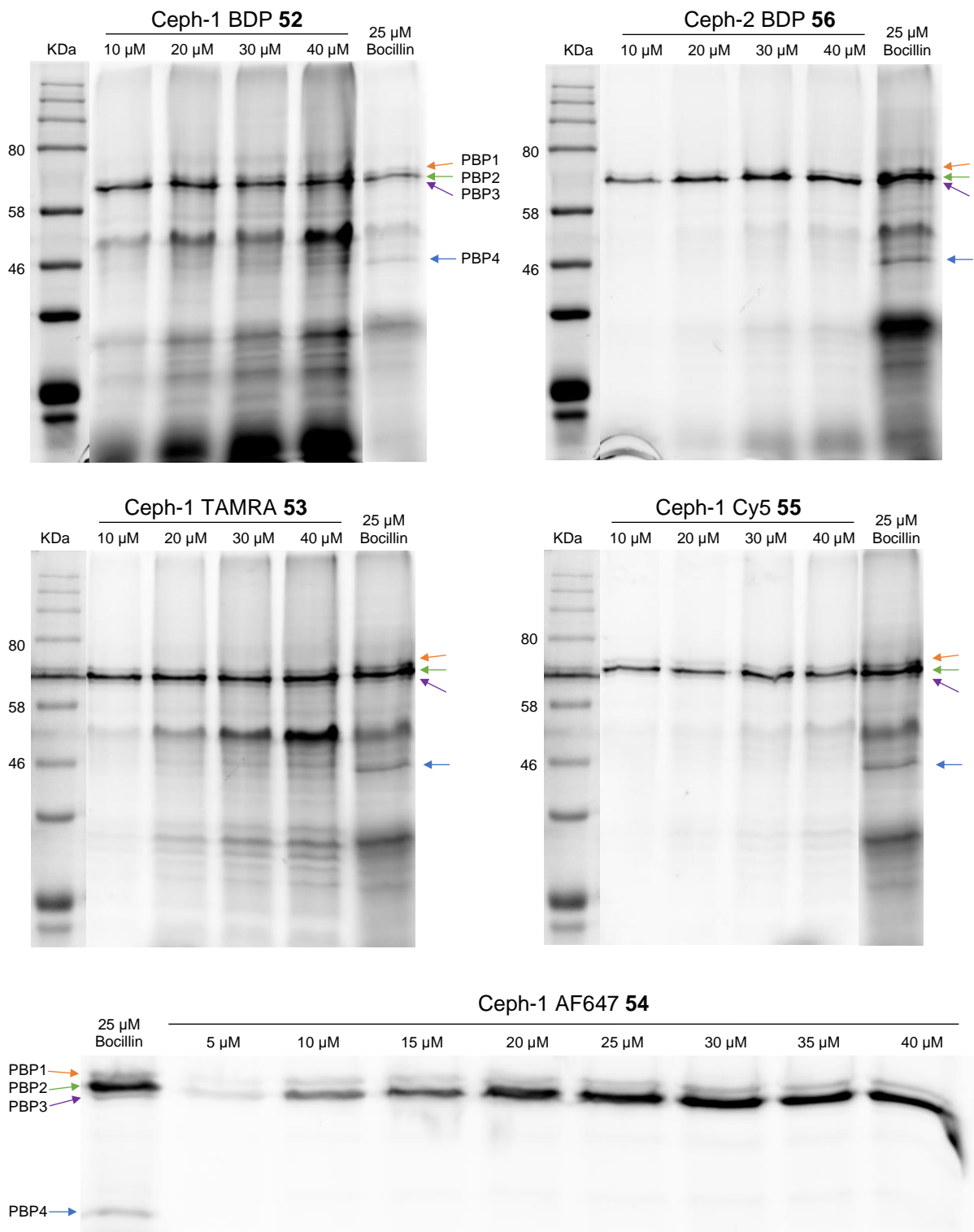


Figure 2-16: Gel based analysis of penicillin binding protein (PBP) profile in *S. aureus* SH1000 by Bocillin FL 1 and fluorescent probes. Protein membrane fractions (30 μg) were prepared and incubated with Bocillin FL 1 (25 μM) or fluorescent derivatives at said concentrations at 37 °C for 10 min. The labelled membrane fractions were resolved with 10% (w/v) SDS-PAGE. This work was carried out by Kasia Wacnik.

As expected, Ceph-1 BDP **52** labelled all PBPs much like the closely linked penicillin control, Bocillin-FL. Selectivity was indeed achieved by Ceph-2 BDP **56** and illustrated the validity of its design based upon PBP2 binding antibiotic, cefotaxime. More interestingly however, all other Ceph-1 **23** analogues also showed an affinity towards certain PBPs which indicated that the fluorescent dye was influencing their binding mode. Both Ceph-1 TAMRA **53** and Ceph-1 Cy5 **55** labelled PBPs 1, 2 and 3 which suggested that the overall size of the probes was potentially limiting access to PBP4, unlike the smaller structure of BDP analogue **52**. The result of Ceph-1 Cy5 **55** was particularly interesting given its structural similarity to AF647 analogue **54**, which only labelled PBP1 and 2. Small differences in overall probe structure and PBP affinity had been previously demonstrated by β -lactone probes developed by Sharifzadeh *et al.*, whereby even stereochemical alterations resulted in different PBPs being labelled in *S. pneumoniae*.⁸⁶ In the case here, the exact structure of Alexa Fluor™ 647 alkyne was not disclosed by the supplier but was predicted to contain sulfonate groups based on the design of Alexa dyes.¹³⁵ This would induce a difference in net overall charge compared to Cy5 and potentially differentiate access to the binding pocket of PBP3. X-ray co-crystallisation studies would be needed to confirm this, but it was clear the PBPs had a narrow tolerance for binding as illustrated by the other Ceph-1 **23** analogues tested and findings by Sharifzadeh *et al.* All fluorescent analogues bound to PBP1 and 2, both essential for minimal peptidoglycan synthesis, which showed the need for significant disparity in scaffold for their selective binding.⁴⁵ It should be noted that the additional bands on some of the gels were assumed to be degradation products from the PBPs, rather than unspecific binding to other proteins or contaminants from the samples, as these were also observed in the reference lane for Bocillin **1** when apparent.

2.3.7 Visualisation of PBPs in *S. aureus* using STORM

The small size of bacterial cells requires the need for super high-resolution microscopy to determine the structural features and machinery they possess to grow and function. Considerable understanding has been obtained in recent years by the access to such instrumentation, which has shed critical information that continues to further knowledge in the intricate processes encompassing cellular growth and division. For example, atomic force microscopy (AFM) has been used extensively to discover the architecture of peptidoglycan in *S. aureus*, illustrating its textural surface and key structural markers of cell division.^{72,136,137} Quantitative measurements and visualisation to unprecedented detail have revealed the

dynamic flexibility to which peptidoglycan allows the cell to interact with outer proteins whilst maintaining turgor and preventing lysis. The coupling of this technique with high-resolution fluorescence microscopy has furthered the understanding in cell growth, defying the conventional models previously hypothesised for cell division as well as identifying new proteins that participate in the divisome.^{138,139} What is missing still, however, is the access to such detailed information that directly map the fundamental building blocks of peptidoglycan biosynthesis, PBPs. Progress has been achieved in other bacteria, as illustrated with the probes developed by Sharifzadeh *et al*, but only GFP fusions have been used to tag PBPs in *S. aureus*.^{140,141} Consequently, visualisation has been limited to structured illumination microscopy (SIM). SIM is a high-resolution technique in its own right but does not offer the superior resolution capable of single molecular imaging such as stochastic optical reconstruction (STORM) or photoactivated localisation (PALM) microscopy.^{76,142}

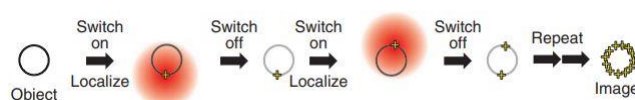


*Figure 2-17: Principle of STORM. Adapted from Dempsey et al*¹⁴³

Both of these techniques rely on fluorophores alternating between a fluorescent state (on) and a dark state (off) - a photophysical behaviour known as “blinking”. When a sample is irradiated with the required wavelength of light, only a small percentage of fluorophores are activated which allows their imaging and localisation. These are then either deactivated with another wavelength of light (STORM) or photobleached (PALM). Repeating this cycle thousands of times allows the precise mapping of each fluorophore which are then reconstructed to obtain a high-resolution image.⁷⁵ Naturally, this means only fluorescent dyes capable of “on/off” states can be used such as cyanine derivatives, hence the development of Ceph-1 AF647 **54** and Ceph-1 Cy5 **55**. Both of these dyes are capable of direct STORM (dSTORM) due to their capacity to photoswitch back and forth through the use of a single laser. A buffer is required to regulate blinking for optimum image capture and consists of: (i) a reducing agent to induce and lengthen the time in which the fluorophore exists in the “dark/off” triplet state and (ii) an oxygen scavenger to stop quenching of the triplet state by singlet oxygen and prevent photobleaching.¹⁴⁴

To that end, both Ceph-1 AF647 **54** and Ceph-1 Cy5 **55** were attempted in STORM to see if high-resolution images of PBPs in *S. aureus* could be obtained. The same incubation conditions

to those used in the widefield microscopy experiments were used for consistency. Cells were mounted using a buffer containing GLOX (oxygen scavenger) and MEA (reducing agent) and visualised using a Nikon N-STORM Ti2-E inverted microscope.

Images obtained using Ceph-1 AF647 **54** showed fluorescence of PBP localisation and proved it was possible to visualise in STORM as a proof of concept, but unfortunately the images were not of high quality to make any valid observation.

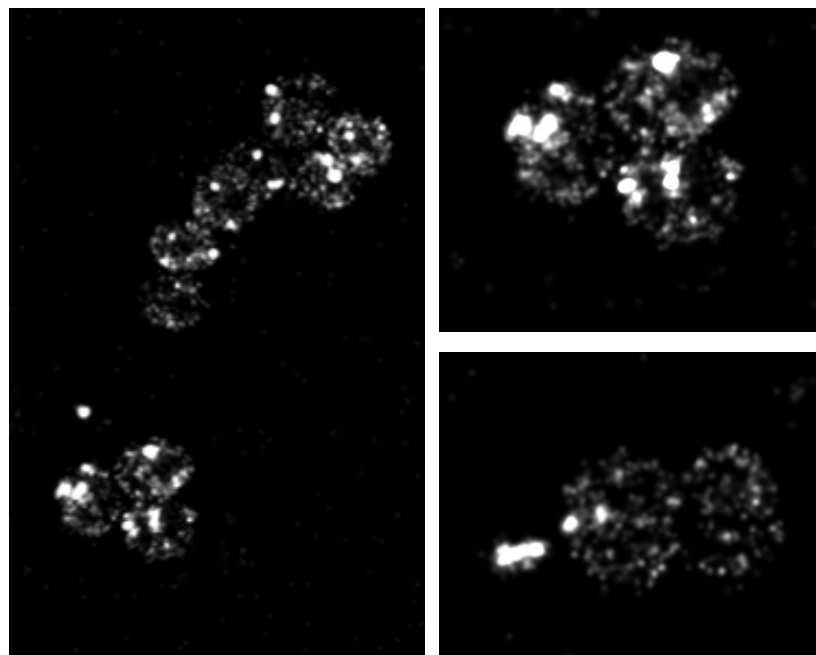


*Figure 2-18: N-STORM image of *S. aureus* labelled with Ceph-1 AF647 **54**. Exponential phase (live) cells were treated with Ceph-1 AF647 **54** (30 $\mu\text{g}/\text{ml}$) for 5 min at 37 $^{\circ}\text{C}$. Images are of a single slice. Slide preparation and images were taken by Victoria Lund.*

The same labelled cells appeared to be clearly labelled under a refraction limited, widefield microscope, but it was assumed the degradation observed of Ceph-1 AF647 **54** previously was affecting the blinking properties of the dye and therefore poor performance in STORM. Focus was switched to the more stable Ceph-1 Cy5 **55** using the same incubation and buffer conditions. Pleasingly, significantly better images were obtained which showed clear septal and off septal labelling of peptidoglycan. Whilst a thorough analysis of the images was not the goal of this project, it was interesting to note that synthesis was occurring as a zone across the septum, rather than the leading edge as long thought, and corroborated with a new model of *S. aureus* cell division recently described by Lund *et al.*¹³⁹ The activity of PBPs throughout the

cell wall, not just at the septum, was highlighted and provided the highest resolution optical images of *S. aureus* achievable to date.

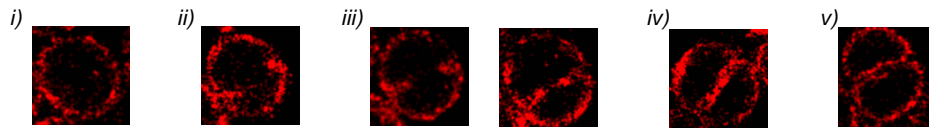


Figure 2-19: Localisation of PBPI, 2 and 3 during the cell cycle of *S. aureus* using STORM. i) Off septal labelling. ii) Localisation of PBPs at future division site. iii) Septum begins to form. iv) Synthesis is continued along the septum until uniform thickness. v) A gap is formed between two daughter cells prior to splitting.

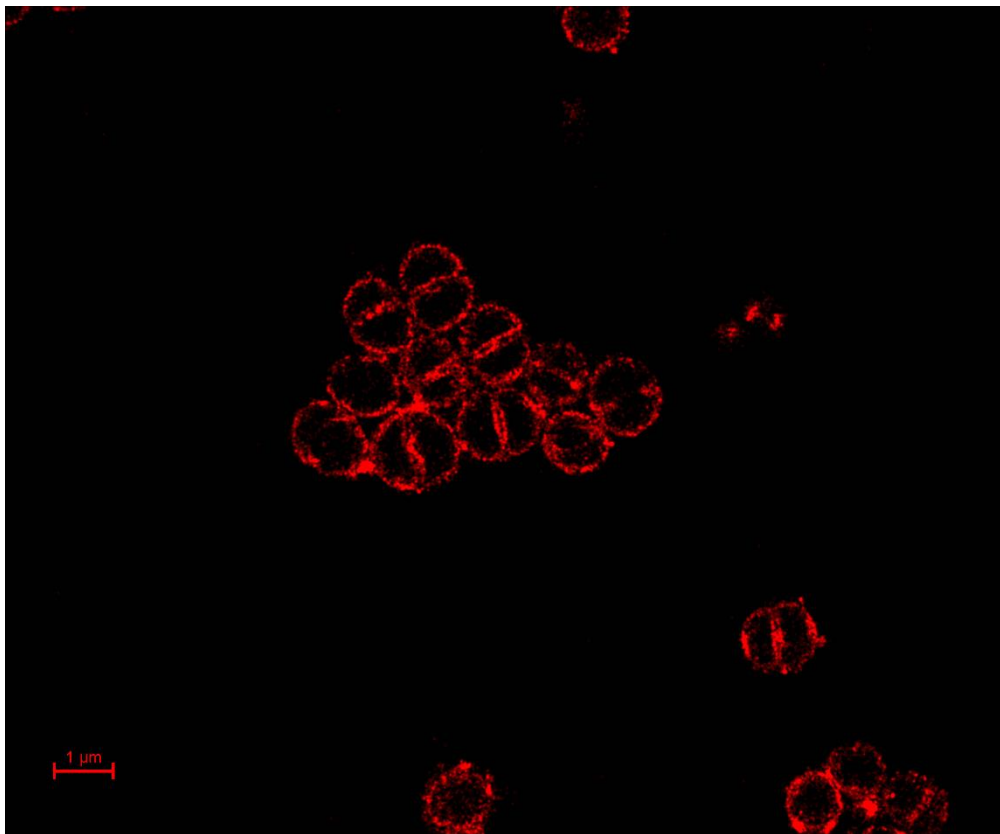


Figure 2-20: N-STORM image of *S. aureus* labelled with Ceph-1 Cy5 55. Exponential phase (live) cells were treated with Ceph-1 Cy5 55 (30 µg/ml) for 5 min at 37 °C. Images are of a single slice. Scale bars 1 µm. Slide preparation and image was taken by Christa Walther.

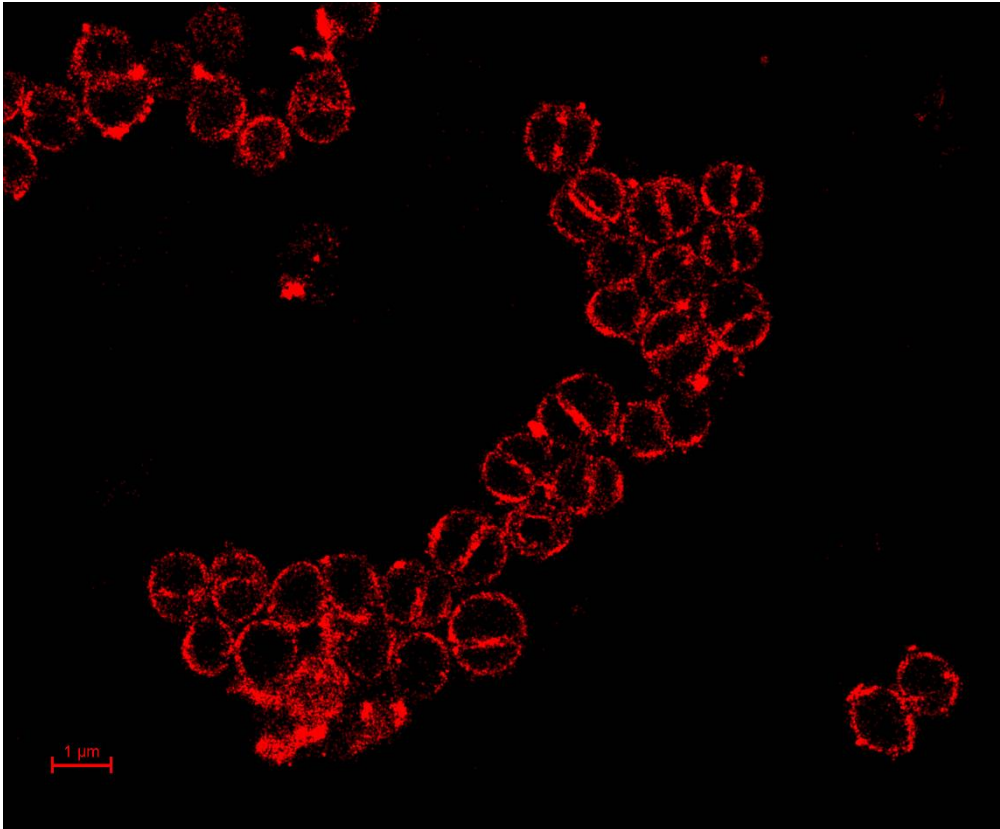


Figure 2-21: N-STORM image of S. aureus labelled with Ceph-1 Cy5 55. Exponential phase (live) cells were treated with Ceph-1 Cy5 55 (30 μg/mL) for 5 min at 37 °C. Images are of a single slice. Scale bars 1 μm. Slide preparation and image was taken by Christa Walther

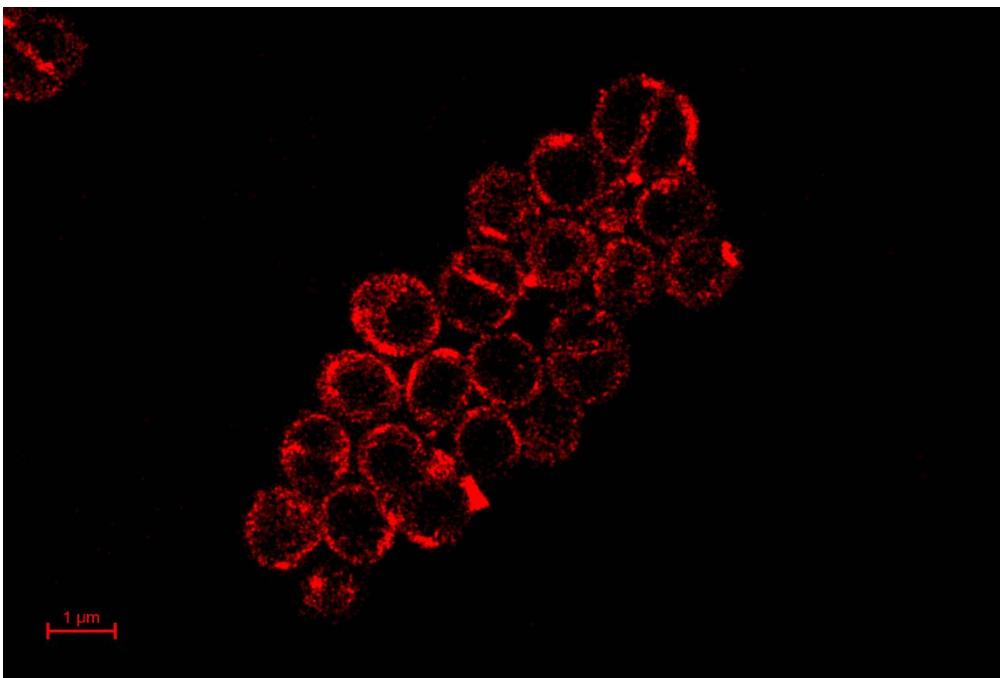


Figure 2-22: N-STORM image of S. aureus labelled with Ceph-1 Cy5 55. Exponential phase (live) cells were treated with Ceph-1 Cy5 55 (30 μg/mL) for 5 min at 37 °C. Images are of a single slice. Scale bars 1 μm. Slide preparation and image was taken by Christa Walther

2.4 Future work

The successful development of chemical probes with affinities to specific PBPs in *S. aureus* and their capacity for high-resolution fluorescence imaging has been illustrated through the Ceph-1 **23** and Ceph-2 **39** derivatives. They provide the basis for crucial studies in understanding PBP localisation and interactions with other cell wall machinery to a degree previously inaccessible. Elucidating the role of individual PBPs is of foremost interest and could be explored through:

- i) Dosing the bacteria with an antibiotic to suppress activity of a specific PBP prior to probe incubation.
- ii) Labelling mutant strains of *S. aureus* with PBP knockouts.
- iii) Dual-labelling studies through the use of two probes with fluorophores of differing wavelengths i.e. Ceph-1 TAMRA **53** and Ceph-1 Cy5 **55**.

Investigating PBP interactions with other proteins involved in the divisome also opens a myriad of studies which are critical to understanding the mechanisms of bacterial resistance. The Ceph-3 and Ceph-4 analogues offer the potential to directly map the chief PBP2a target, the cause of MRSA. Their preliminary biological and imaging evaluation is yet to be conducted, however if successful, they have the potential to give vital clues in the development of future drugs. An option also remains to test Ceph-1 and Ceph-2 chemical probes against *S. aureus* strains containing PBP2a. Although not being designed or expected to bind to PBP2a, these probes have shown that minor structural changes can have significant effects on PBP affinity. A simple gel assay of all the probes against a recombinant PBP2a protein could be a quick way of determining this.

Finally, the antibiotic scaffold approach has shown success in mapping different PBPs as shown by the PBP2 targeting Ceph-2 marker **56**. This opens the potential for further chemistry in developing other recognition markers as well as fine tuning their binding interactions through X-ray crystallography and computational methods.

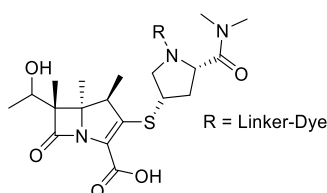


*Figure 2-23: A potential PBP1 targeting probe based on Meropenem*⁹³

3 Moenomycin scaffold

3.1 Background

Transglycosylation is a critical process in the biosynthesis of peptidoglycan whereby lipid II is polymerised to form the glycan backbone prior to transpeptidation. It therefore serves an attractive opportunity for antibiotic research and handle for chemical probe development. To date, very few inhibitors of peptidoglycan glycosyltransferases (PGTs) have been reported which has greatly hindered progress in this area. In previous research, the direct labelling and subsequent visualisation of the glycan backbone has been achieved via incorporation of a MurNAc derivative using a biorthogonal handle (**Figure 3-1**). This is an analogous approach to the use of FDAAs in labelling peptidoglycan architecture itself. In contrast, the binding and imaging of PGTs has yet to be explored. It has been shown *S. aureus*, the target organism of this study, can survive with only one of its three PGTs present, PBP2.³⁸ It therefore opens the prospect of specific PBP labelling to study localisation patterns to a significantly higher degree of detail to that observed previously, particularly with the probes targeting transpeptidase activity developed in the previous chapter.

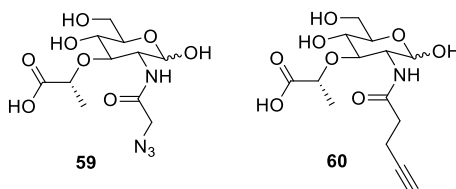


*Figure 3-1: MurNAc derivatives for direct peptidoglycan labelling*¹⁴⁵

Moenomycin A (MoeA) **61**, a natural product, has been well established as an inhibitor of transglycosylation.¹⁴⁶ It has been studied extensively in *S. aureus* and has been proven to bind to the active site of PGTs using X-ray crystallography.^{147,148} Furthermore, fluorescent derivatives of MoeA **61** have been previously synthesised for assay development and reported to retain binding affinity for PGTs, illustrating its capacity for use as a chemical tool.^{149,150} Whilst other inhibitors of simpler structures do exist, they offer significantly lower levels of potency and evidence in their profile of PGT binding.¹⁵¹

It was therefore reasoned that MoeA **61** be the most obvious candidate for chemical probe development, particularly given the chemistry for fluorescent dye derivatisation already being established by Welzel *et al.*¹⁵² Subsequent biological evaluation and attempt to label PGTs in *S. aureus* would then be interpreted using widefield microscopy in the first instance.

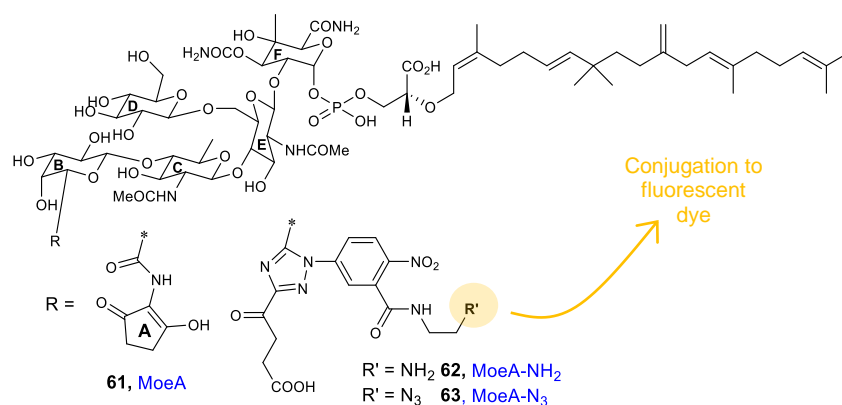
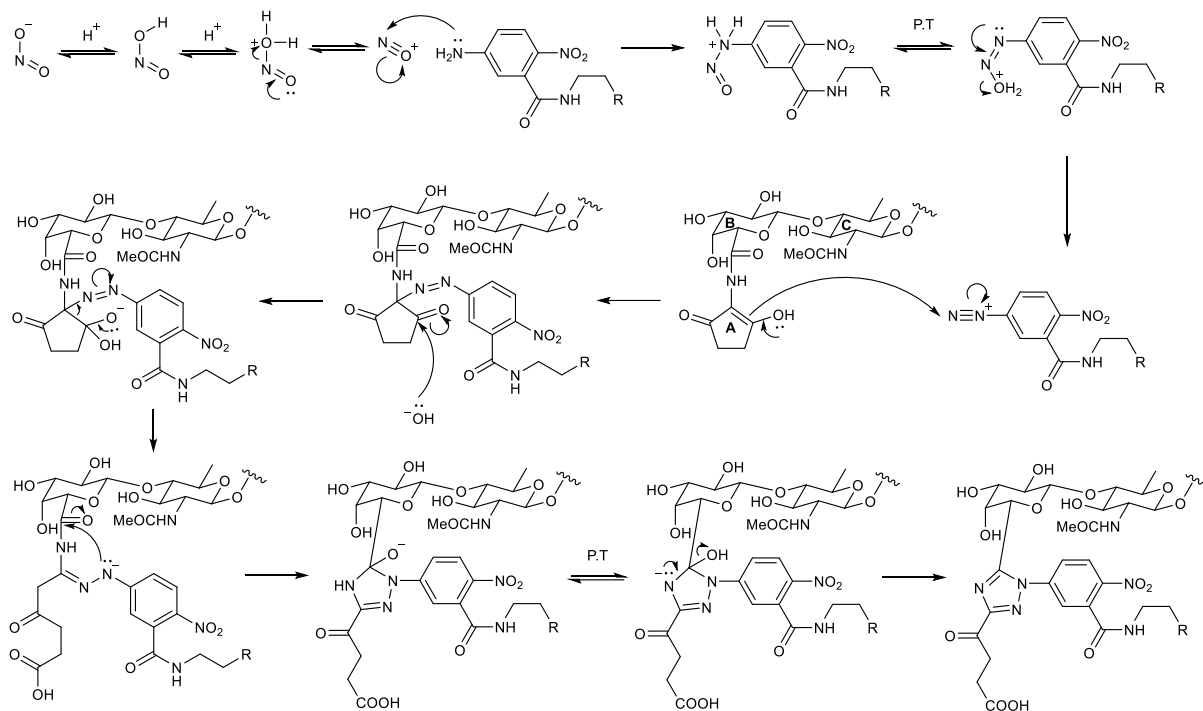


Figure 3-2: Structural basis of the Moenomycin probes

3.2 Synthesis of MoeA analogues

3.2.1 Synthesis of MoeA-NH₂ **62** and MoeA-N₃ **63**

The synthetic route described revolved around the conjugation of a fluorescent dye via an aromatic linker formed from reacting ring A of MoeA **61**. It was found that activated aryldiazonium salts could selectively react with the enolisable diketone ring and undergo a Japp-Klingemann reaction, forming an amidrazone which would then cyclise to afford a triazole bearing a handle to allow further derivatisation.¹⁵³ Highly electrophilic diazonium salts were crucial for a reaction to occur, hence the necessity of a nitro group on the aromatic linker. Following this protocol, the synthesis of amine-derivatised analogue MoeA-NH₂ **62** described by Welzel *et al.* was undertaken, as well as expanding the modular approach for inclusion of an azide analogue, MoeA-N₃ **63**, to allow an alternative handle for fluorescent dye conjugation.



Scheme 3-1: Mechanism of Japp-Klingemann reaction

Synthesis of the aromatic amine linker was first attempted by a direct coupling between 2-amino-5-nitrobenzoic acid and ethylenediamine **64** as per literature precedent, but gave primarily a dimeric mixture.¹⁵⁴ Amine **64** was consequently Boc protected prior to an amide coupling with the carboxylic acid using EDCI. This proved an insufficiently reactive activating group due to negligible product formation despite significant urea intermediate present as judged by LC-MS. HATU proved to be a far superior coupling agent despite initial attempts resulting in a surprisingly low yield of 3%. It was then realised that a near identical, but significantly more polar product was also present during purification by flash column chromatography. The ambiguous interpretation of almost indistinguishable ¹H NMR spectra between both led to the analysis by X-ray crystallography which revealed the isolates to be regioisomers of each other. An inspection of the commercially purchased 2-amino-5-nitrobenzoic acid starting material showed a small amount of the 2-nitro isomer present which accounted for a competing reaction resulting in the first product obtained, now confirmed as regioisomer **66b**.

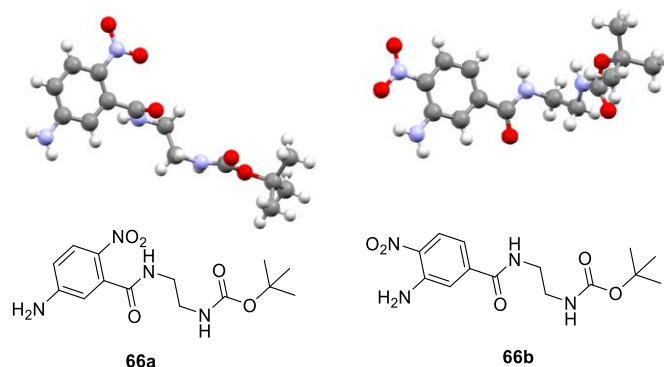
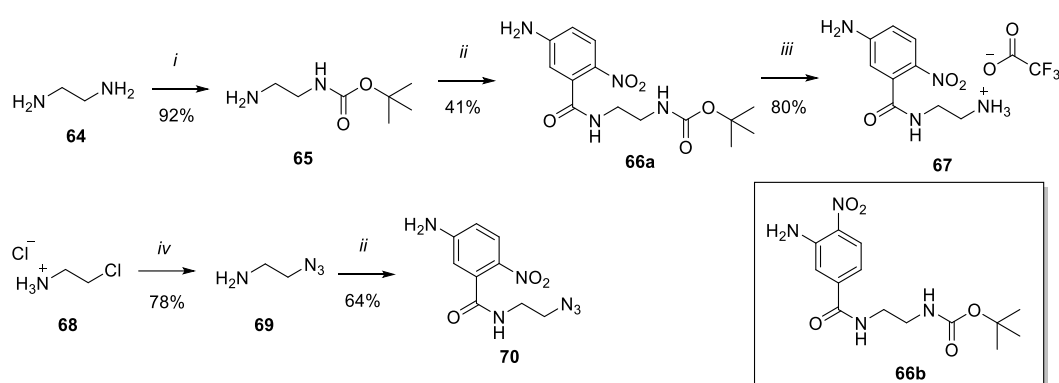


Figure 3-3: The crystal structures of nitrobenzene **66a** and 2-nitro regioisomer **66b**

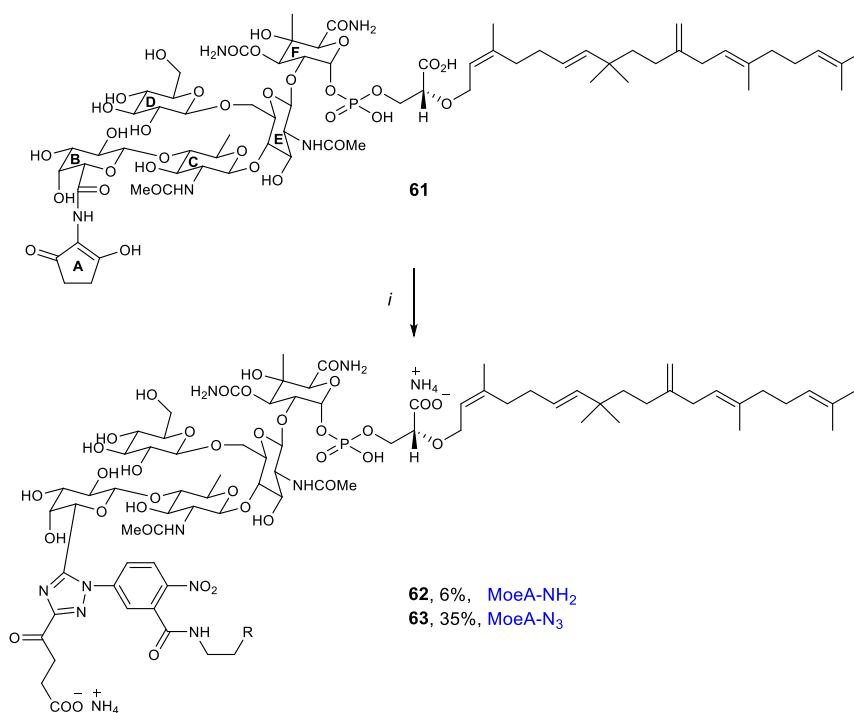
The polar and desired nitrobenzene regioisomer **66a** was obtained in a respectable yield and afforded amine **67** as a TFA salt following straightforward Boc deprotection (**Scheme 3-2**). The synthesis of azide analogue **70** was trivial in comparison, with only amino azide **69** giving difficulty due to its volatile nature.



Scheme 3-2: i) Boc_2O , CH_2Cl_2 RT, o/n. ii) 2-nitro-5-aminobenzamide, HATU, DIPEA, DMF, RT, o/n. iii) TFA, CH_2Cl_2 , RT, 15 min. iv) NaN_3 , H_2O , NaOH, 80 °C, 25 h.

Both aromatic linkers were then subjected to the key reaction step with moenomycin A (MoeA) **61**. The reactions were conducted at a milligramme scale due to a limited amount of MoeA **61** available and therefore all reagents were added by serial dilution. Reaction progress was aided by colour changes throughout, first in the diazonium salt formation whereby the solution changed from yellow to colourless, and then in the addition to MoeA **61** which gave an orange mixture, likely from the conjugated amidrazone forming. Cyclisation to the triazole required a minimum of 5 days of stirring at room temperature and was monitored by LC-MS. Increasing the reaction temperature was not tried due to the presumed sensitivity of moenomycin A. Purification, however, was far from facile and was particularly troublesome with amine

analogue **62**, presumably because of its increased amphiphilic nature. Attempts to repeat the preparative HPLC conditions described by Welzel *et al.* did not offer any retention of product with the reverse phase column available. Normal phase flash column chromatography using the highly polar eluent mixture of acetonitrile: water (1:2) described were tedious due to a very slow flow rate. Alternative HPLC conditions led to varied retention times depending on the exact pH of eluent present, as well as being highly capricious when using isocratic methods. Using trifluoroacetic acid as an ion-pairing agent offered the most consistent separation, however protic acids have been reported to cause decomposition of the glycosidic bonds in moenomycin A.¹⁵⁵ Thus, an ammonium hydroxide buffer was chosen as a compromise between separation and stability for both analogues MoeA-NH₂ **62** and MoeA-N₃ **63**, which were obtained in overall yields of 6% and 35%, respectively. It should be noted that both were assumed to be isolated as ammonium salts and that full characterisation could not be obtained due the small amount of material isolated, however were deemed pure by HPLC and mass spectrometry data.

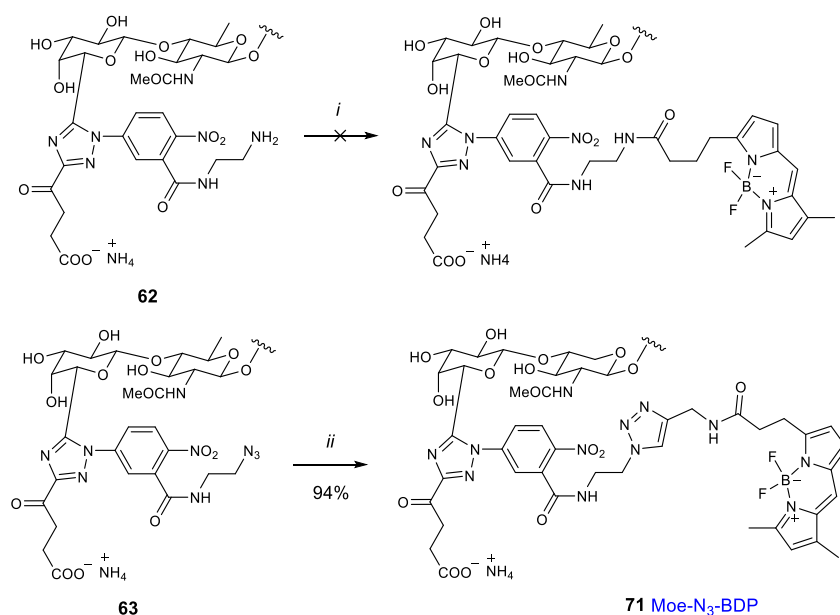


Scheme 3-3: *i)* **67** or **70**, NaNO₂, 1M HCl, 0 °C, 15 min, then moenomycin A, NaOAc, H₂O, RT, 5 – 6 days.

3.2.2 Fluorescent derivatisation of MoeA **61**

Having derivatised MoeA **61** with two different bioorthogonal handles, a BODIPY-based dye was chosen for fluorescent conjugation given its successful application in the imaging of PBPs using the previously synthesised cephalosporin probes. Moreover, it circumvented the need to further elongate the linker with diethyl squarate, as performed by Welzel *et al.*, owing to a spacer already being present.

Treating amine **61** with BODIPY-FL NHS ester in anhydrous DMSO gave negligible product, largely due to undesired hydrolysis of the fluorescent dye. Switching to a less hygroscopic solvent in DMF offered little improvement; further investigation was not conducted owing to a limited amount of material remaining. Conversely, azide analogue **62** was subjected to the click chemistry conditions established in the previous chapter using BDP-FL alkyne, which resulted in clean conversion to the desired fluorescent MoeA conjugate, Moe-N₃-BDP **71**. LC-MS analysis suggested a small amount of degradation had occurred upon isolation; however, the material was deemed pure enough for the purpose of establishing its biological and imaging evaluation.



Scheme 3-4: i) BodipyTM-FL NHS ester, Et₃N, DMSO or DMF, RT, o/n. ii) BDP-FL alkyne, Cu₅SO₄, L-ascorbic acid, DMSO:H₂O, RT, 18 h.

3.3 Biological and imaging of moenomycin derivatives

3.3.1 Biological activity of moenomycin derivatives

The MIC's of moenomycin A, precursor **63** and fluorescent probe Moe-N₃-BDP **71** were tested against *S. aureus* SH1000 to confirm bacterial activity prior to labelling cells and attempting microscopy. All compounds readily dissolved in water.

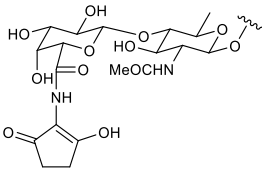
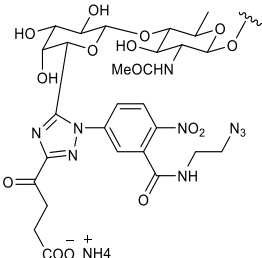
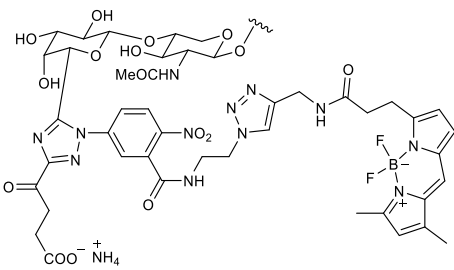
Entry	Compound	Structure	MIC (µg/mL)
1	moenomycin A 61		0.25 – 0.5
2	MoeA-N ₃ 63		1
3	Moe-N ₃ -BDP 71		20 – 30

Table 3-1: MICs of moenomycin A and derivatives against SH1000. Assays were conducted by broth dilution procedure. Inoculation was conducted at 37 °C for 24 hours. The MIC was determined to be the lowest concentration at which no bacterial growth occurred as measured by optical density (OD600).

Moenomycin A **61** showed a slightly lower MIC against SH1000 compared to other MSSA strains reported in the literature but still displayed high biological activity.^{156–158} The derivatised compound **63** retained most of this potency, however incorporating the BDP-FL dye with the linker resulted in a significant drop. It was, however, comparable to some other PGT inhibitors reported.¹⁵⁹ Furthermore, it had been well documented that minor changes to the pharmacophore of moenomycin A **61** could affect antibacterial activity, however the

minimal requirements to elicit PGT binding were that of the E ring, F ring and the lipid chain (**Scheme 3-3**).^{156,160,161} All of these were retained in fluorescent analogue Moe-N₃-BDP **71** and therefore did not cause for concern if PGT binding would be affected.

3.3.2 Labelling and imaging of PGTs in *S. aureus*

Fluorescent probe **71** was tested for its ability for labelling and imaging PGTs using widefield fluorescent microscopy. Cells were labelled at both ends of the MIC range and incubated using the same conditions to those established for the cephalosporin probes. Successful labelling was observed at both concentrations and gave the first optical images of PGTs in any organism reported to date. Fluorescence was generally poor however and required significant colour adjustment post-microscopy, particularly for cells incubated at a higher concentration which resulted in high background fluorescence, but nevertheless showed clear uptake and cell wall labelling. Specific localisation could not be discerned due to the limited resolution of the microscopy used, however a similar pattern of increased binding at the septum site, as well as off septal labelling, was seen to that of the transpeptidase targeting probes developed in the previous chapter. This was likely due to the binding of the abundant PBP2 in both cases but at different domains.

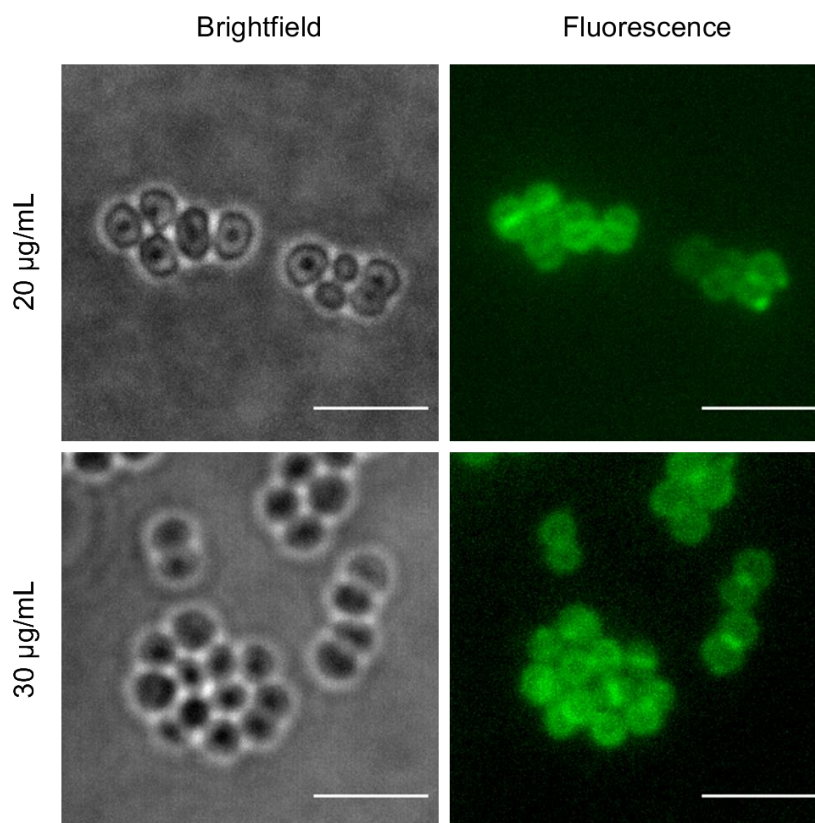


Figure 3-4: *S. aureus* labelled with Moe-N₃-BDP 71. Exponential phase (live) cells were treated at said concentrations for 5 mins at 37 °C. Fluorescence images are of a maximum intensity projection of z-stacked images. Scale bars 5 µm. Microscope setup was carried out by Victoria Lund.

3.4 Future work

The access to a fluorescent transglycosylase binder opens the opportunity to study an abundance of interactions previously unexplored. As mentioned earlier, *S. aureus* is able to survive without its monofunctional transglycosylases, MGT and SgtA, and can rely solely on the transglycosylase domain of PBP2 for normal peptidoglycan growth.³⁸ Thus, direct labelling of PBP2 could be possible using a constructed *mgt sgtA* mutant of SH1000 and labelling with fluorescent probe Moe-N₃-BDP 71.¹⁶² Furthermore, a STORM-compatible derivative could be prepared via conjugation of a compatible dye to precursor azide **63** and provide a method for localised PBP2 examination in greater detail than previously achieved. Utilising such a probe in other *S. aureus* mutations and resistant strains could also be a powerful method in furthering the understanding in cell morphology and division in general. Kahne *et al.* have reported irregularities of glycan chains and cell growth in moenomycin-resistant *S. aureus* strains, showing the importance of normal PGT function.¹⁶³ Exploring such strains using these tools will give valuable insights into their interactions with other cell wall machinery under complex

habitats and clues into future drug design, especially given the resistance exhibited by moenomycin.¹⁴⁶

4 Oxetanyl dipeptide scaffold

4.1 Background

Peptidomimetics have gained considerable interest as a means of generating small molecule drugs to act as enzyme inhibitors or receptor ligands.^{164,165} Their source of inspiration originates from Nature's most embryonic and abundant macromolecules – proteins. This approach has been harnessed to develop pseudopeptide drugs offering a high degree of selectivity for biological targets.¹⁶⁵ β -Lactam antibiotics are arguably *the* key example of this as they work by essentially mimicking the D-Ala-D-Ala terminus of the pentapeptide chain in peptidoglycan. It therefore struck us that synthesising a novel small molecule mimic of the D-Ala-D-Ala group could be a way of inhibiting PBPs and developing fluorescent derivatives of such compounds could lead to the labelling of PBPs. This approach would suitably compliment the already established field of fluorescent D-amino acids (FDAAs) for labelling peptidoglycan, with considerable progress being made in understanding cell wall dynamics.^{97,166,167} Being able to inhibit and potentially bind to PBPs locally and specifically as proposed here, would significantly further this research. As the original intention was to utilise this mimic *in vitro*, the poor ADMET properties commonly associated with peptidomimetics were not a concern. For inhibition to occur and prevent such a molecule from actively participating in peptidoglycan crosslinking, as in the case of FDAAs, a non-hydrolysable group which could effectively mimic an amide was required. Inspired by recent work of Carreira *et al.* on oxetanyl peptides, it was envisaged an oxetane group could serve this purpose well.^{168,169}

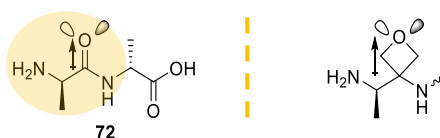


Figure 4-1: Oxetane as an amide bioisostere

Oxetanes have gained considerable interest in medicinal chemistry due to their potential as alkyl and carbonyl group isosteres, as well as being attractive for their lower ligand binding efficiency compared to larger heterocycles. Their most prominent use to date has been as *gem*-dimethyl group replacements, having shown to offer lower lipophilicity and increased overall metabolic stability for metabolically prone methylene groups, whilst maintaining

conformational constraint and thereby benefitting of the Thorpe-Ingold effect if so required.^{170,171} In addition, oxetanes have been demonstrated as carbonyl surrogates due to their likeness in polarity and hydrogen bonding basicity.^{172–174} Taxol, the chemotherapy drug, is a prime example of this capability, whereby the oxetane ring forms a key hydrogen bonding interaction within the target binding site.¹⁷⁵ This carbonyl mimicry has now been forwarded to prospective amide replacements with 3-aminooxetanes (**Figure 4-1**).^{168,169} These motifs have the same hydrogen bonding donor/acceptor resemblance structurally and, more applicable for this research, offer the possibility of being less susceptible to enzymatic cleavage such as that in peptidoglycan transpeptidation.

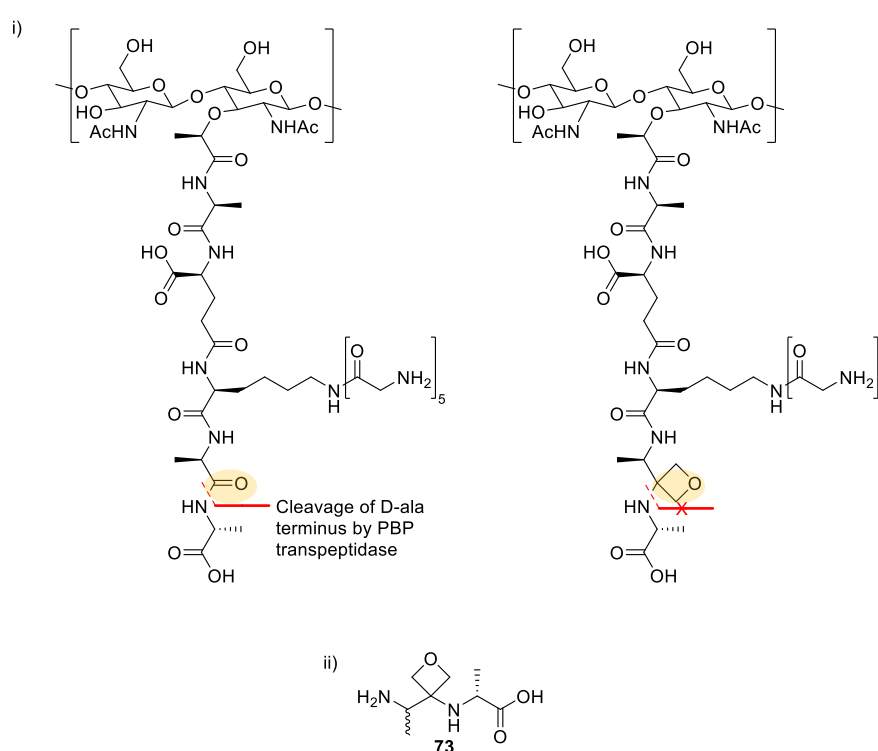


Figure 4-2: The polysaccharide backbone of peptidoglycan with natural and proposed oxetanyl D-Ala-D-Ala terminal dipeptides ii) Structure of oxetane D-Ala-D-Ala target, oxetane 73

If this process is blocked in bacteria (**Figure 4-2**), cleavage of the terminal D-Ala residue does not occur, which leads to loss of cell wall integrity resulting in apoptosis. This is evidenced by the mechanism of action of vancomycin, an antibiotic which binds to the terminal D-Ala-D-Ala dipeptide and inhibits PBP transpeptidase activity by steric means.¹⁷⁶

Encouraged by the success of Carriera *et al.* developing stable oxetane Leu-enkephalin analogues, it was proposed an oxetanyl pseudopeptide be a valid D-Ala-D-Ala mimic that could be resistant to cleavage by PBP transpeptidases.¹⁶⁹ Oxetane **73**, was chosen as the preliminary

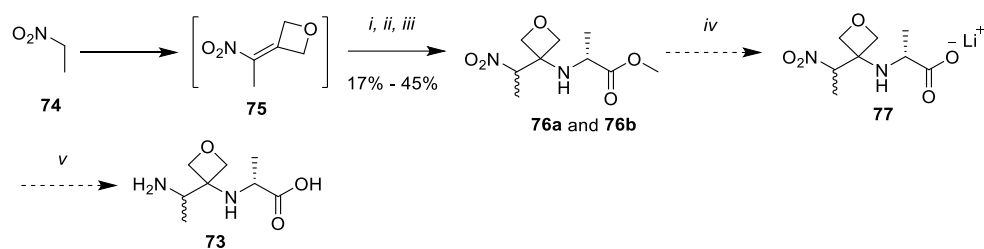
target based on the synthetic routes already established in the literature.^{168,177} If biological activity was established, installing the amino acid centre in an enantiomerically pure manner would be investigated, as well as substitution with an azide for fluorescent labelling studies.

4.2 Development of an oxetanyl dipeptide

4.2.1 Synthesis of an oxetanyl dipeptide

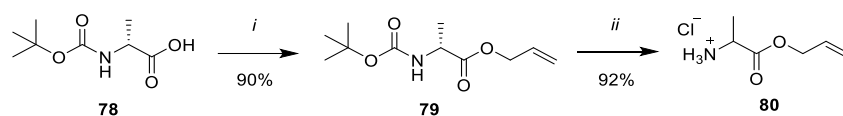
Synthesis of oxetane **73** (**Scheme 4-1**) was initiated with a one-pot nitro aldol reaction of nitroethane **74** and oxetan-3-one, prior to trapping of the resulting Michael adduct **75** with D-Ala-OMe to afford diastereomers **76a** and **76b**. The yield of this reaction was highly variable depending on the purity of oxetan-3-one, which degraded at room temperature and was highly sensitive to air. The addition of D-Ala-OMe.HCl and triethylamine in DMSO was also capricious due to insolubility of the resulting triethylammonium chloride salt. Adapting the synthetic route developed by Carriera *et al.*, by adding DCM did overcome this to some degree.¹⁶⁸ As expected, virtually no stereocontrol was achieved, with a 60:40 mixture of diastereomers being obtained.

The LiOH-mediated ester hydrolysis proved to be highly problematic and indicated the oxetane ring maybe more sensitive than anticipated. The hydrolysis reaction showed complete consumption of starting material but attempts to purify the crude material by acid/base workup indicated degradation of the oxetane ring by ¹H NMR spectroscopy. To avoid exposing the oxetane to low pH, 1 eq. of LiOH·H₂O was used and the completed reaction evaporated to dryness *in vacuo* to obtain the lithium salt of carboxylic acid **77**. ¹H NMR spectroscopy and mass spectrometry analysis of the salt showed evidence of product but in low purity. Purification was not attempted due to the high polarity of the substrate for flash column chromatography and lack of UV chromophore for subjecting to preparative HPLC. In spite of this, reduction of the nitro group of impure carboxylic acid **77** by hydrogenation was trialled but yielded material which could not be characterised. It was concluded that both acidic and basic aqueous environments were unfavourable for the oxetane substrate. Indeed, neither Carriera or Shipman *et al.* performed any hydrolysis of aminooxetane-esters in their work which furthered suspicions of instability.



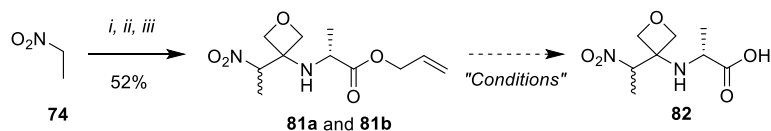
Scheme 4-1: i) oxetan-3-one, Et_3N , CH_2Cl_2 , RT, 30 mins. ii) $MsCl$, Et_3N , $-78\text{ }^\circ C$, 1 h. iii) *D-Ala-OMe.HCl*, Et_3N , $DMSO/CH_2Cl_2$, $-78\text{ }^\circ C - RT$, o/n. iv) $LiOH \cdot H_2O$, $MeOH/H_2O$ (3:1), RT, o/n. v) *Ra-Ni*, THF, H_2 , RT, o/n.

Allyl protected *D*-alanine was then synthesised to allow deprotection *via* non aqueous conditions. Facile alkylation of the Boc-*D*-Ala **78** afforded the allyl ester **79**. Boc deprotection was first conducted in MeOH however this caused partial transesterification to occur with the allyl group. Changing to EtOAc avoided any byproduct but racemised the stereogenic centre as noted by no specific rotation being observed. It was decided to proceed with the racemate **80** to assess if allyl deprotection was feasible before attempting to isolate it enantiomerically pure. The residual solvents present in amine **80** could not be removed despite attempts to form an azeotrope or triturating the product with a mixture of MeOH and Et_2O .



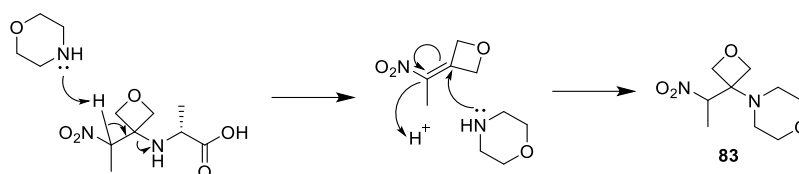
Scheme 4-2: i) allyl bromide, DIPEA, DMF, RT, o/n. ii) conc. HCl, EtOAc, RT, o/n

The formation of esters **81a** and **82b** as diastereomers proceeded in a moderate yield using a new batch of commercially available oxetan-3-one. Allyl deprotection was then tested using $Pd(PPh_3)_4$ with either potassium carbonate in MeOH or a large excess of morpholine in THF. Both conditions were found to be common for similar transformations in the literature and were based on the principle of Pd forming a π -allyl complex with the alkene and a nucleophile eliminating the carboxylate as a leaving group.



Scheme 4-3: oxetan-3-one, Et_3N , CH_2Cl_2 , RT, 2 h. ii) $MsCl$, Et_3N , $-78\text{ }^\circ C - RT$, 2h. iii) **80**, Et_3N , $DMSO/CH_2Cl_2$, RT, o/n

The outcome of utilising MeOH as the nucleophile could not be rationalised however it appeared morpholine was actively participating in both desirable and undesirable roles. The crude product of this reaction was isolated by a mild acidic aqueous work up of with 1M hydrochloric acid. Analysis of the acidic aqueous layer by mass spectrometry showed the presence of allyl morpholine, indicating cleavage of the ester had occurred. ^1H NMR spectroscopy of the crude material on the other hand, showed the oxetane to be intact but missing protons associated with the methyl group alpha to the carboxylic acid. It was postulated the desired carboxylic acid was cleaved across the pseudoamide *via* an E1cb mechanism.



Scheme 4-4: Proposed cleavage of the carboxylic acid 82 by morpholine

The reaction mechanism was examined by varying the amount of morpholine and catalyst in the reaction. Adding 1 eq. of morpholine gave a mixture of starting material and the proposed elimination adduct. No carboxylic acid was observed which suggested elimination was occurring spontaneously following cleavage of the allyl group. In the absence of $\text{Pd}(\text{PPh}_3)_4$, no reaction occurred which suggested the instability towards morpholine was intrinsic to the acid. These observations proved the hypothesis to be true and it was subsequently confirmed upon successful isolation of aminooxetane **83**. On reflection, this degradation also offered an explanation as to why impure material was retrieved when hydrolysing the methyl ester substrates **76a** and **76b**. A hydroxide ion was most likely promoting an elimination in the same fashion.

As a final effort to cleave the allyl group, an iridium based catalyst was employed to isomerise the allyl carboxylate to a labile enol group. This could then be removed by mild acid.

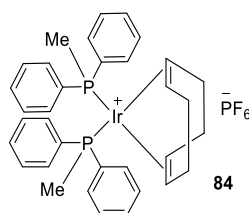
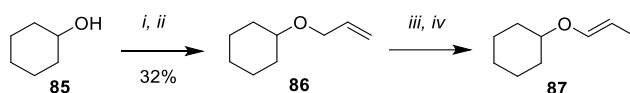


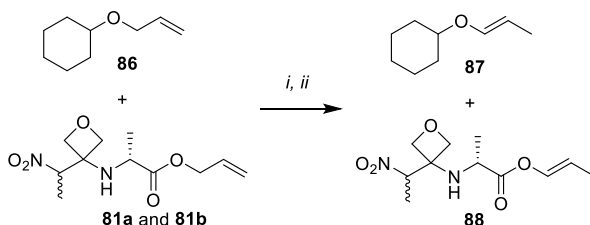
Figure 4-3: Structure of the iridium catalyst: (1,5-cyclooctadiene)bis(methylphenylphosphine)iridium(I) hexafluorophosphate 84

The conditions required no additional additive apart from hydrogen to activate the catalyst. Unfortunately, no reaction occurred when subjecting esters **81a** and **81b** to the activated catalyst. This surprising outcome could have resulted if the catalyst was not functioning and was therefore tested on a simple allyl ether.



Scheme 4-5: i) NaH, THF, 0 °C, 10 min. ii) allyl bromide, 0 °C - RT, o/n. iii) “Iridium catalyst”, H₂, 10 min, RT. iv) THF, RT, 5 h

¹H NMR spectroscopy of crude vinyl ether **87** showed consumption of allyl ether **86** and an expected peak of the new vinyl proton at 6.1 ppm, indicating isomerisation had occurred. It should be noted that **86** was highly volatile resulting in a poor yield being obtained. After proving the catalyst was effective, both allyl **86** and oxetane mixture **81a** and **81b** were subjected to the isomerisation conditions in one pot to determine if oxetanes **81a** and **81b** were affecting the reaction. Isomerisation of cyclohexanol derivative **86** still occurred which illustrated the oxetanes **81a** and **81b** were simply resistant to the iridium catalyst.



Scheme 4-6: i) “Iridium catalyst”, H₂, 10 mins, RT. ii) THF, RT, 5 h

Considerable issues with cleaving the allyl esters **81a** and **81b** led to revisiting the hydrolysis of the methyl ester diastereomers **76a** and **76b**, previously attempted *via* customary LiOH mediated conditions. Alternative conditions were sought through the use of trimethyltin hydroxide which had been well documented as a mild reagent to hydrolyse simple esters.¹⁷⁸ Reacting diastereomers **76a** and **76b** following the literature conditions resulted in poor mass recovery and an unidentifiable tin-related species *via* ¹H NMR spectroscopy, likely owing to decomposition of the oxetane substrates at elevated temperature. Neutral conditions *via* enzymatic cleavage of esters **76a** and **76b** by porcine pancreatic lipase (PPL) proved too mild as no reaction occurred and starting material was recovered.

4.2.2 Biological evaluation of oxetanyl dipeptide

The minimum inhibitory concentration (MIC) of oxetanyl dipeptide **91a** and **91b** was tested on wild-type *S. aureus* strain SH1000. Its diastereomeric nature was considered in the concentrations measured but disappointingly, no inhibition of growth was observed even at a relatively high concentration of 150 $\mu\text{g} / \text{mL}$. This likely indicated that it was not being recognised by peptidoglycan as a competitor for nascent D-Ala-D-Ala, although the possibility remained open that it was, but for the pseudoamide oxetane bond simply not being robust enough against hydrolysis. Presuming the former, it was decided to adapt oxetanes **91a** and **91b** in order to improve its chances of recognition. A closer inspection of Tipper and Strominger's theory indicated penicillin's mimick the entire acyl-D-Ala-D-Ala terminus of the pentapeptide stem, not just the dipeptide fragment.¹⁸⁰ It was therefore deduced that adding an acyl group to oxetanes **91a** and **91b** could offer biological activity. This proposal agreed with the sans acyl cephalosporin, 7-ACA **17**, which had been previously tested as inactive on SH1000. Benzyl derivative **92** was chosen as the preliminary target to allow for a direct biological comparison to a simple analogous antibiotic, penicillin G.

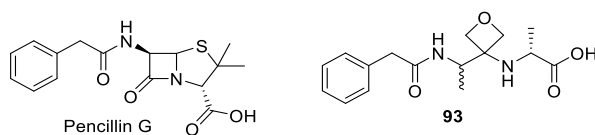
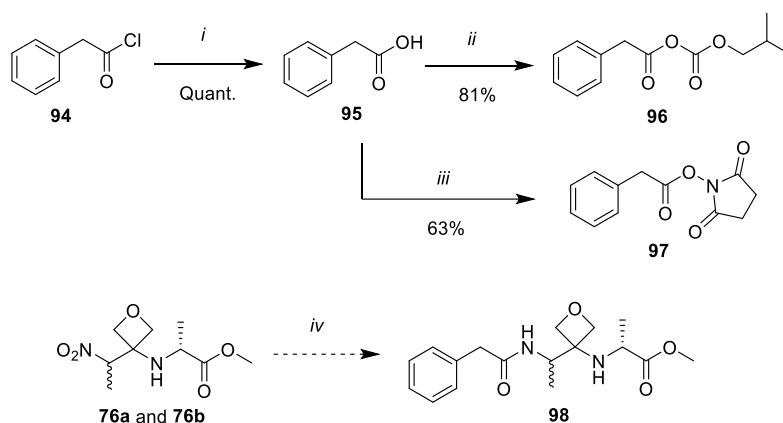


Figure 4-4: Structure of benzylated target **93**

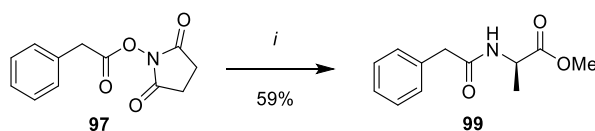
4.2.3 Synthetic approaches towards acylating an oxetanyl dipeptide

Efforts to acylate oxetane diastereomers **91a** and **91b** began by attempting to “cap” reduced oxetanes **76a** and **76b** *in situ* given the success found when using this methodology with Boc_2O . Acyl chloride **94** was first used in this instance however only the cyclised diketo product (**Scheme 4-8**) was isolated, suggesting the chloride was too reactive and likely hydrolysed *in situ* by residual water before any reaction could take place. Thus, mixed anhydride **96** was synthesised but this too appeared unstable as again, only cyclised diketo product was obtained after flash column chromatography.



Scheme 4-9: i) H_2O , $0\text{ }^\circ\text{C} - \text{RT}$, *o/n*. ii) isobutyl chloroformate, Et_3N , CH_2Cl_2 , $0\text{ }^\circ\text{C} - \text{RT}$, 17 h. iii) *N*-hydroxysuccinimide, EDCI, Et_3N , THF, RT, *o/n*. iv) **94**, **96** or **97**, *Ra-Ni*, Boc_2O , NaHCO_3 , THF, H_2 , RT, *o/n*

A final attempt sought to using NHS ester **97**. This *did* prove stable enough but participated in an undesirable reaction resulting from degradation of oxetanes **76a** and **76b**. Analysis of the major product by ^1H NMR spectroscopy indicated the NHS ester to have reacted with D-alanine methyl ester, suggesting cleavage of the oxetane **76a** and **76b** was occurring to that seen previously (**Scheme 4-4**). This was proved by reacting NHS ester **97** with commercially available D-alanine methyl ester; an identical product was obtained as judged by ^1H NMR spectroscopy.

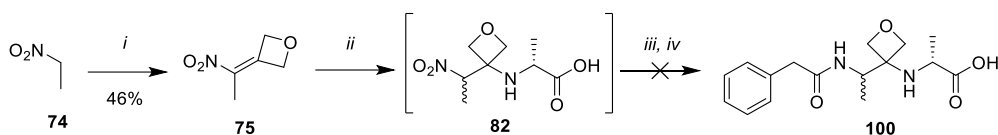


Scheme 4-10: i) *D-Ala-OMe*, Et_3N , CH_2Cl_2 , RT, *o/n*

Acidic mediated reductions were then tried to bypass any cleavage from occurring. Unfortunately, elimination was still observed when employing both indium metal in HCl or tin (II) chloride, in addition to a poor mass recovery.¹⁸¹ A final attempt using iron in acetic acid at room temperature gave complete degradation of nitro oxetanes **76a** and **76b**.

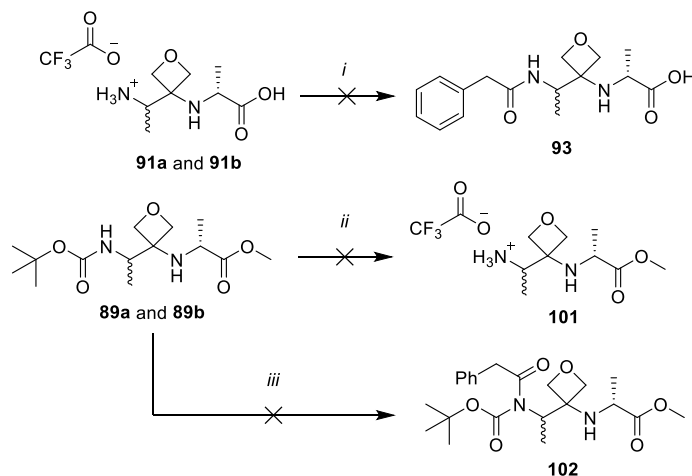
Attention was then switched to reacting vinyl oxetane **75** with D-alanine directly as an alternative means of avoiding the intramolecular transamidation involved in the nitro reduction step. Such an approach had been documented by Carreira *et al* who used either CbzCl or FmocOSu to protect the resulting amine *in situ*.¹⁶⁸ Alkene **75** was obtained in only moderate yield, likely owed to its volatile nature, prior to reacting with D-alanine under aqueous conditions. Following completion as judged by TLC, nitro acid **82** was taken directly onto the

reduction and acylating steps. Evidence of oxetane **100** was seen by LC-MS, but due to a considerable amount of impurities present, could not be isolated in sufficient purity.



Scheme 4-11: i) oxetan-3-one, Et_3N , RT, 2 h, then $MsCl$, Et_3N , CH_2Cl_2 , $-20\text{ }^\circ C$, 1 h. ii) *D*-alanine, $NaHCO_3$, $H_2O:THF$ (2:1), RT, 5 h. iii) *Ra*-Ni, THF , H_2 , RT, o/n. iv) phenylacetyl chloride, RT, o/n.

Direct acylation was attempted on oxetane mixture **91a** and **91b** using the Schotten-Baumann conditions however no reaction occurred despite some evidence of product by mass spectrometry. Final efforts switched to manipulating the stable Boc-protected precursors **89a** and **89b**. It was anticipated that deprotection would yield oxetane **101** and that the salt would inhibit cyclisation to the diketo species **92**. This appeared to be the case initially however it rapidly cyclised at the elevated temperature required to remove TFA *in vacuo* and alternative isolation methods such as trituration were unsuccessful. Acylation of precursors **89a** and **89b** also resulted in no reaction despite literature precedent for the benzoylation of Boc-protected amines.^{182–184}



Scheme 4-12: i) phenylacetyl chloride, sat. aq. $NaHCO_3$ acetone, $0\text{ }^\circ C - RT$, o/n. ii) TFA, CH_2Cl_2 , RT, 1 h. iii) phenylacetyl chloride, Et_3N , DMAP, CH_2Cl_2 , $0\text{ }^\circ C - RT$, o/n.

Due to exhaustive efforts and inherent instability of some oxetanyl substrates, further investigation of this scaffold was not conducted. It was clear that the pseudopeptide bond was not sufficiently stable under different chemical environment and therefore a similar scenario was postulated to have occurred for oxetanyl dipeptides **91a** and **91b** *in vitro*. It could well

have been recognised and incorporate into peptidoglycan, but simply for the oxetane pseudopeptide bond being susceptible to hydrolysis and transpeptidation.

4.3 Future work

The unambiguous reasoning why oxetanyl dipeptides **91a** and **91b** show no biological activity is yet to be fully established. It is not known if the lack of an acyl group is important for recognition, as initially hypothesised, or whether the pseudopeptide is too weak to resist transpeptidation. A number of tests could be done to help validate this:

- (i) A disk assay to ascertain if any inhibition of growth is occurring.
- (ii) Incubating an antibiotic with a known MIC alongside oxetanyl dipeptides **91a** and **91b** to probe if any synergistic effects exist.
- (iii) Subjecting oxetanyl dipeptides **91a** and **91b** to a MurF assay to establish if the ligase responsible for adding D-Ala-D-Ala to the UDP-N-acetylmuramic acid in peptidoglycan can recognise it directly.

A success in any of these experiments would provide a platform for separating oxetanes **91a** and **91b** as pure enantiomers, as well as synthesising an azide-derivatised analogue for labelling studies. If all tests fail, alternative amide surrogates to oxetane could be pursued and their feasibility assessed *in vitro*.

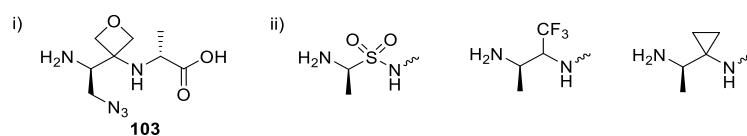


Figure 4-5: i) An azide-derivatised oxetanyl dipeptide. ii) Alternative amide bioisosteres

5 Oxetanyl phosphonates as β -lactamase inhibitors

5.1 Background

β -Lactamases are enzymes produced by bacteria to defend themselves against β -lactam drugs.¹⁸⁵ They operate by hydrolysing the β -lactam ring and thereby prevent the drugs ability to inhibit cell wall synthesis.¹⁸⁶ Their importance to bacterial survival, however, make β -lactamases an ideal target for drug development and the potential for combinatorial therapy with otherwise ineffective β -lactam drugs.

A series of ketophosphonates developed by Perumal and Pratt have been shown to offer promising activity against different classes of β -lactamase.¹⁸⁷

Class	Species	Type
A	<i>E. coli</i>	TEM
	<i>S. aureus</i>	PCI
B	<i>B. cereus</i>	
C	<i>E. cloacae</i> P99	
D	<i>E. coli</i>	OXA-1, OXA-10

Table 5-1: β -lactamase classes shown to have inhibition by ketophosphonates

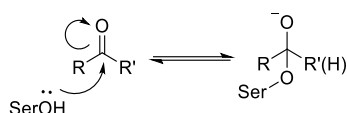
Their structural premise is based on two features: (i) an electrophilic ketone, to bind and acylate the enzyme active site, and (ii) a phosphonate moiety to enhance active site interactions. Both these characteristics have demonstrated potential for inhibitor design in previous research.¹⁸⁷⁻¹⁸⁹



Figure 5-1: Ketophosphonate inhibitor pharmacophore

Perumal and Pratt hypothesised that a more electrophilic ketone and size of the alkyl phosphonate ester would induce a change in activity. However, after various analogues were

explored, neither alteration had a significant effect on β -lactamase inhibition. Furthermore, it was proven that the tetrahedral adduct expected to form by reaction of the ketone and active site serine was not observed. This would suggest that the inhibitors were in fact acting in their carbonyl form and no acylation was occurring.



Scheme 5-1: Formation of the tetrahedral adduct from nucleophilic attack of the serine hydroxyl group

With this information in hand, it was envisioned that replacing the ketone with another functional group, for example an oxetane, could give further mechanistic insight to the inhibitor's mode of action. Oxetanes have become increasingly prevalent in drug design due to their favourable properties, such as lipophilicity and metabolic stability, compared to equivalent carbonyl-containing compounds. More interestingly in this case, they are strong H-bond acceptors, occupy different space to ketones due to their shape and can infer a different molecule orientation. Some, if not all these characteristics, may be key to improving the inhibitory activity of Perumal and Pratt's ketophosphonate series. It was therefore decided to pursue and establish the chemical methodology for synthesising a series of oxetane phosphonate analogues.

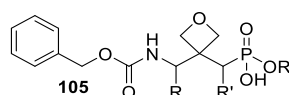
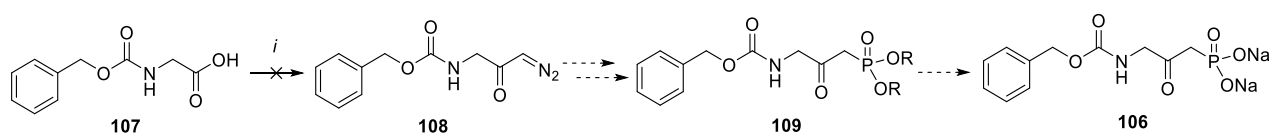


Figure 5-2: Proposed oxetane phosphonate analogue

5.2 Synthesis of ketophosphonate diesters **115** and **116**

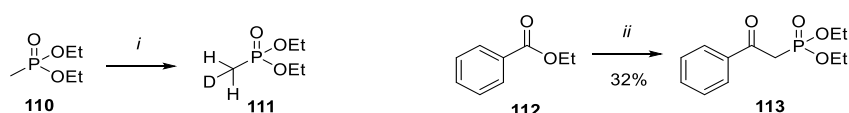
The synthesis of a diester precursor to ketophosphonate inhibitor **106** reported by Perumal and Pratt was first undertaken prior to investigating the methodology required for synthesising an analogous oxetane variant. These compounds would then be hydrolysed at a later stage to obtain inhibitor **106**, together with ketophosphonate monoesters to act as reference compounds for biological testing. Initial attempts to prepare diester derivative **109** followed the protocol described by Perumal and Pratt, but with the use of TMS-diazomethane (TMS-N₃) instead of diazomethane as a safer alternative to conduct an Arndt-Eistert reaction on carboxylic acid **107**.¹⁹⁰ Activation of the carboxylic acid with oxalyl chloride and triethylamine prior to

addition of TMS-N₃ gave no reaction in both CH₂Cl₂ and THF. Adding a sub-stoichiometric amount of DMF gave evidence of diazo compound **108** by ¹H NMR spectroscopy but resulted in a very poor recovery after workup. It was believed this may have been due to cleavage of the CBz group by excess HCl being formed from the reaction of oxalyl chloride, despite the addition of triethylamine. Milder activation conditions were then employed using either ethyl chloroformate or Ghosez's reagent to form a mixed anhydride and acid chloride, respectively, prior to addition of TMS-N₃, however both returned starting material. It was subsequently concluded that TMS-N₃ was simply not reactive enough for this substrate.^{191,192}



Scheme 5-2: i) oxalyl chloride, TMS-N₃, additive / solvent, 0 °C – RT.

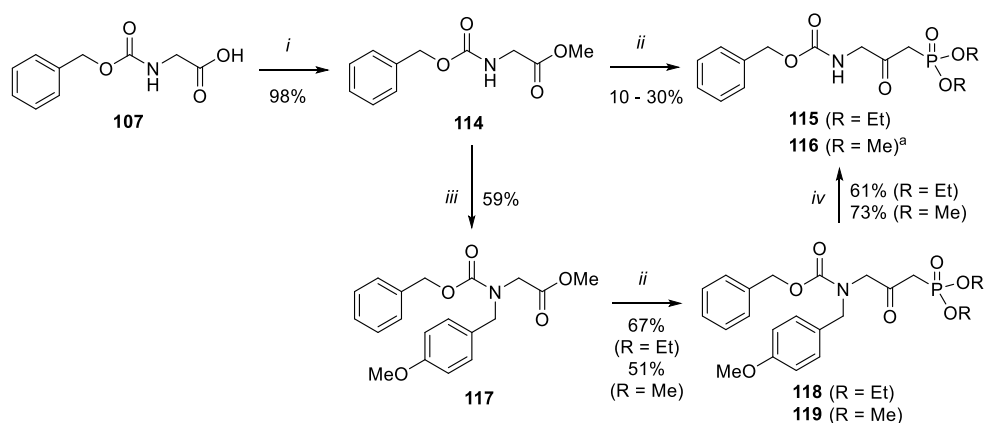
An alternative and more efficient construction of a phosphonate diester **109** was then envisaged by reacting an ester derivative of carboxylic acid **107** with a lithiated methyl phosphonate. To ensure full deprotonation of the chosen phosphonate **110** would occur, a DCl quench following treatment with *n*-BuLi was conducted; ¹H NMR spectroscopy showed complete deprotonation had taken place. Applying the conditions to model ester **112** afforded the expected ketophosphonate ester **113** and confirmed the validity of this approach.



Scheme 5-3: i) n-BuLi, THF, -78 °C, 15 min, then DCl, -78 °C – RT, 15 mins. ii) diethyl methylphosphonate, n-BuLi, THF, -78 °C – RT, 1h.

Translation to the main substrate began with straightforward esterification of carboxylic acid **107**. Treating the resulting ester **114** with lithiated diethyl methylphosphonate was highly capricious and was likely owed to the acidic amide proton present, as well as the reactive ketone forming in the product **115**. Using 1 or 2 equivalents of *n*-BuLi did not offer any trend in the yields obtained, nor did attempting to deprotonate the amide with *n*-BuLi prior to adding the lithiated methylphosphonate. This was resolved by protecting the amide **114** with a PMB group which resulted in a significantly higher yield in the alkylation. A dimethyl phosphonate derivative was also synthesised *via* the same conditions to offer an additional reference

compound for biological testing. Deprotection of the PMB protected amide **117** was attempted by conventional oxidative cleavage using dried cerium (IV) ammonium nitrate (CAN) but failed to give any reaction despite attempting with various batches of CAN.¹⁹³ The same premise was tried using DDQ but this also returned starting material. Using harsher, acidic conditions with neat TFA did cleave tertiary amides **118** and **119** and afforded the target ketophosphonate diesters **115** and **116** in moderate to good yields respectively.¹⁹⁴

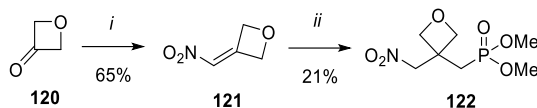


Scheme 5-4: i) SOCl_2 , MeOH, $0\text{ }^\circ\text{C} - \text{RT}$, o/n. ii) Diethyl methylphosphonate, *n*-BuLi, THF, $-78\text{ }^\circ\text{C} - \text{RT}$, o/n. iii) PMB-Cl, NaH, DMF, $0\text{ }^\circ\text{C} - \text{RT}$, o/n. iv) TFA, RT, 30 min. ^athis was obtained from **119**

5.3 Synthesis of an oxetanyl phosphonate

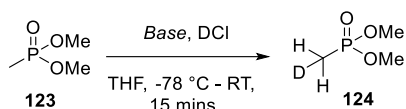
Synthesis of an oxetane analogue was sought *via* a Michael addition onto an oxetane-containing nitroolefin, similar to that used in the construction of oxetanyl peptides **91a** and **91b** in the previous chapter. No examples of additions of phosphonates onto these substrates had been reported in the literature, however it was promising to find that they were stable to a strong base such as *n*-BuLi, with precedent of aromatic halogen-lithium exchange prior to nucleophilic attack being reported by Carreira *et al.*¹⁹⁵

Contrary to the one-pot approach used towards the synthesis of oxetanyl peptides **91a** and **91b**, the intermediate nitroolefin **121** was isolated prior to attempting addition by the phosphonate ester. Early efforts were highly capricious, however it became apparent the use of pure starting material **120** and limited manipulation of the product was vital for good conversion. Thus, the reaction mixture was loaded directly onto a silica plug following completion and carefully concentrated which afforded alkene **121** in moderate yield. Treating the alkene **121** with deprotonated phosphonate ester using *n*-BuLi was indeed successful in forming oxetane **122** but only a 21% yield was obtained.



Scheme 5-5: i) oxetan-3-one, Et_3N , RT, 20 min, then MsCl , CH_2Cl_2 , $-78\text{ }^\circ\text{C}$, 30 min. ii) dimethyl methylphosphonate, $n\text{-BuLi}$, THF, $-78\text{ }^\circ\text{C}$ – RT, o/n

Alternative bases were explored by first assessing if complete deprotonation of dimethyl methyl phosphonate was occurring by quenching with DCl.

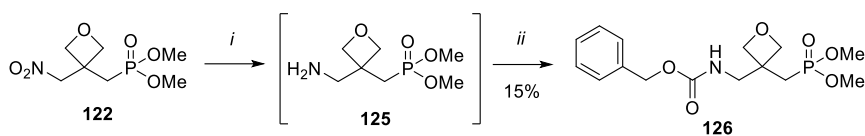


Entry	Base	Deprotonation	Reaction Yield (%)
1	$n\text{-BuLi}$	Yes	21 (16 ^a)
2	LDA	Yes	16
3	NaH	No	-
4	$\text{CH}_2=\text{CHMgBr}$	No	-
5	LiHMDS	No	-
6	KHMDS	Partial	-

Table 5-2: Deprotonation of dimethyl methyl phosphonate with various bases followed by quenching with DCl. ^aReaction was conducted in Et_2O

LDA was the only other base to give full deprotonation but offered a lower yield. Conducting the reaction in Et_2O using $n\text{-BuLi}$ also offered no improvement. The reaction was attempted *via* a one-pot approach from starting material oxetan-3-one which resulted in a 25% NMR yield; this was seen to be a comparable result and did not offer any advantage. The stability of the phosphonate ester product **122** was then examined by reacting with deprotonated phosphonate under precisely the same conditions and purification procedure. No new products formed as judged by TLC and an 80% mass recovery was obtained, illustrating its stability to further reaction. Exploration of using a more readily deprotonated nucleophile such as a diphosphonates and/or utilising ligands and Lewis acids to achieve efficient lithiation could not be undertaken due to time constraints.

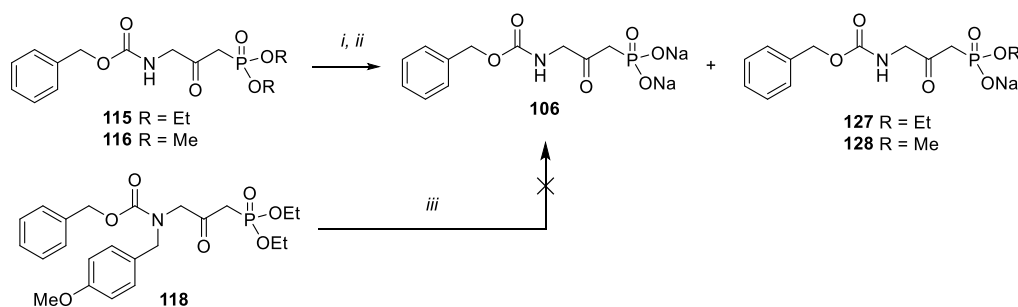
Subsequently, nitro reduction of phosphonate ester **122** using Raney-Ni prior to acylation of the resulting amine **125** with benzyl chloroformate furnished the desired oxetane phosphonate ester **126** target.



Scheme 5-6: i) *Ra-Ni*, THF, H₂, RT, o/n. ii) benzyl chloroformate, Et₃N, CH₂Cl₂, RT, o/n.

5.4 Approaches towards the hydrolysis of ketophosphonate diesters **115** and **116**

Hydrolysis of ketophosphonate diesters **115** or **116** was required to form the phosphonate inhibitor **106** reported by Perumal and Pratt, as well as monoalkylated phosphonate analogues for biological testing. Perumal and Pratt obtained inhibitor **106** by a two-step process from the analogous diphenyl phosphonate derivative, by first partially hydrolysing one of the esters using NaOH and then enzymatically cleaving the second ester using a phosphodiesterase. To avoid this, TMSBr was employed in an attempt to cleave both esters in one step.¹⁹⁶ Surprisingly however, the diethyl phosphonate ester **115** was seemingly resistant to bis-dealkylation when exposed to these conditions. Treating with 2 equivalents of TMSBr produced largely the mono-dealkylated adduct **127** and only a negligible amount of the desired bis-dealkylated product **106**. Increasing to 4 equivalents to overcome any potential silylation of the amide gave a 50:50 mixture, whilst increasing to 10 equivalents *did* achieve complete hydrolysis but also caused undesired cleavage of the CBz group. This cleavage also occurred when treating with 2 equivalents of more reactive hydrolysing agent, TMSI. An attempt at a one-pot PMB deprotection and hydrolysis from phosphonate ester **118** using TFA at elevated temperature only yielded the precursor **115**.



Scheme 5-7: i) TFA, RT, 30 min. ii) TMSBr or TMSI, DCM, RT, 3 h – o/n, then acetone, H₂O, RT, 1 h
ii) NaHCO₃, DOWEX. iii) TFA, 60 °C, o/n.

It was suspected the dimethyl phosphonate ester **116** would be more labile but when treating with 2 equivalents of TMSBr a mixture of both dealkylated products were again isolated. To

that end, it was deduced that this step *did* require enzymatic cleavage to give the phosphonate inhibitor **106** reported. Nevertheless, methodology for obtaining the monoalkylated phosphonates had been established. Purification to separate the dealkylated adducts by preparative HPLC or conducting the reaction with 1 eq of TMSBr could not be undertaken due to time constraints.

5.5 Future work

The isolation of dimethyl and diethyl mono phosphonates is still to be prosecuted, as well as synthesising the reported inhibitor **106** prior to biological testing. The conditions to obtain the latter are yet to be validated following unsuccessful efforts by traditional efforts, however the use of a phosphodiesterase, as per Perumal's and Pratt's procedure, offers an evident alternative to begin with. Hydrolysis of oxetane ketophosphonate diester **126** is still to be prosecuted as well as the optimisation towards its synthesis. The Michael addition by the phosphonate ester remains low-yielding and is yet to be fully explored, whilst alternative conditions to install the Cbz group, such as *via* an amide coupling, for example, could be employed. Once obtained, a number of compounds will be available for biological testing against β -lactamases with the scope to further develop a series of compounds as described earlier.

6 Summary and conclusion

The development of novel fluorescent chemical probes to bind to PBPs through different structural scaffolds has been pursued. By first harnessing the affinity of PBPs for β -lactam antibiotics, three cephalosporin scaffolds were developed:

Ceph-1 **23** was designed to offer a preliminary insight into the structural characteristics required for biological activity, as well as the protocol required for fluorescent imaging. Good antibacterial activity against *S. aureus* was shown, however no specific fluorescence for PBPs was observed when labelling cells first prior to conjugating a fluorophore *in situ*. Ceph-1 **23** was subsequently derivatised with four fluorescent dyes *via* a robust copper-catalysed azide–alkyne cycloaddition and each resulting compound was confirmed to retain biological activity. Labelling *S. aureus* with all compounds resulted in PBP visualisation in widefield microscopy. Derivatives **57** and **58** bearing only the fluorophore and linker showed no specific fluorescence and indicated the cephalosporin motif was actively binding to PBPs. Gel electrophoresis experiments indicated Ceph-1 BDP **52** displayed global PBP activity, like the commercially available Bocillin-FL, but TAMRA, Cy5 and Alexa Fluor™ 647 derivatives all displayed specificity. It was reasoned the overall size and charge incurred by each fluorescent probe was limiting access to the active site of some PBPs. STORM imaging of cells labelled with Ceph-1 Cy5 **55** was successful and offered the highest resolution fluorescent images to date, making it highly amenable for extensive PBP visualisation studies.

Ceph-2 **56**, based upon on PBP2 binding antibiotic cefotaxime, was synthesised in 8 steps and displayed good stability for acidic conditions throughout. Similar antibacterial activity to the parent antibiotic was demonstrated and indicated the placement of the linker was not obstructing access to the active site. Derivatisation of Ceph-2 **56** with BDP-FL and subsequent imaging of PBPs in *S. aureus* by widefield microscopy was successful. Furthermore, specific labelling to PBP1 and PBP2 was observed by gel electrophoresis experiments and showcased the viability for using antibiotics with higher affinity for specific PBPs as chemical tools.

Efforts to synthesise Ceph-3 and Ceph-4 as PBP2a binders were hampered with alkene and oxime isomerisation. The process route established by Ishikawa *et al.* was not adaptable for small-scale chemistry and purification by traditional means proved insufficient. Nonetheless, Ceph-3 **48a** and alkene Δ^2 isomer **49a** were obtained in excellent purity and sufficient amounts for full characterisation. Ceph-4 analogues **48b**, **49c** and **49d** were also obtained in excellent

purity as judged by ^1H NMR and mass spectroscopy. An alternative synthetic route would be required to obtain sufficient amounts for full characterisation.

A moneomycin-based probe targeting transglycosylase activity was prepared. Unsuccessful efforts to conjugate a fluorescent dye to the amine derivative synthesised by Welzel *et al.* led to the synthesis of azide analogue **63**, which was then reacted with BDP FL using the click chemistry conditions established previously. Moe-N₃-BDP **71** had significantly lower biological activity than the parent antibiotic moenomycin A, but nevertheless displayed specific PBP fluorescence in *S. aureus* as determined by widefield microscopy. A robust synthetic route demonstrated the potential for the conjugation of STORM-compatible fluorophores and specific visualisation of key peptidoglycan enzyme, PBP2, in mutant *S. aureus* strains.

A non-antibiotic scaffold was targeted by the synthesis of novel oxetanyl dipeptides in an attempt to mimic the D-Ala-D-Ala terminus of the pentapeptide chain in *S. aureus* peptidoglycan. Despite a revised synthetic route being successful in obtaining the target as diastereoisomers **91a** and **91b**, no biological activity was observed. The synthesis of an acyl variant to better mimic the active motif in β -lactam antibiotics was unsuccessful. To that end, it was hypothesised the oxetane functionality was labile to hydrolysis by transpeptidases and further experiments were required to ascertain if peptidoglycan recognition was occurring.

Finally, a series of oxetanyl phosphonates was pursued in an attempt to improve the biological activity of Perumal's and Pratt's ketophosphonate β -lactamase inhibitors. Synthesis of the diester precursors for both the ketophosphonate reference compound and an oxetanyl phosphonate was accomplished by novel chemical means. Hydrolysis of the precursors and biological testing could not be conducted due to time constraints.

7 Methods and materials

7.1 Growth media

Tryptic soy broth (TSB) was used for all growth media, prepared using dH₂O and autoclaved for 20 minutes at 121 °C (15 psi). For TSB agar, 1% (w/v) of bacteriological agar (VWR) was added.

Tryptic soy broth (Oxoid, 30 g/L)	30 g/L
-----------------------------------	--------

7.2 Buffers and solutions

All buffers and solutions were prepared with dH₂O, sterilised by autoclaving and stored at room temperature unless stated otherwise.

7.2.1 Phosphate buffered saline (PBS)

Phosphate Buffered Saline Tablets (Sigma)	5 tablets/L
---	-------------

7.2.2 Fixative preparation

7.2.2.1 Preparation of 16% (w/v) paraformaldehyde

Phosphate buffered saline tablets (Sigma)	5 tablets/L
---	-------------

100 mM sodium phosphate buffer (pH 7.0):

1 M Na ₂ HPO ₄	57.7 mL
--------------------------------------	---------

1 M NaH ₂ PO ₄	42.3 mL
--------------------------------------	---------

The final volume was adjusted to 1 L

16% (w/v) paraformaldehyde:

100 mM sodium phosphate buffer (pH 7.0)	50 mL
---	-------

paraformaldehyde	8.0 g
------------------	-------

Paraformaldehyde (8.0 g) was added to sodium phosphate buffer (50 mL, 100mM, pH 7.0) and the resulting mixture stirred at 60 °C. NaOH (≥ 5 M) was added dropwise until the solution cleared. The solution was allowed to cool to room temperature and stored at 4 °C up to 3 months.

7.2.2.2 Fixative

16% (w/v) paraformaldehyde	0.5 mL
PBS	2.0 mL

7.2.3 Click-iT® reaction buffer mix

Click-iT® cell reaction mixture	440µL
100mM copper (II) sulfate	10 µL
Click-iT® additive	50 µL

7.3 *Staphylococcus aureus* strain and growth conditions

Staphylococcus aureus strain SH1000 (genotype: functional rsbU+ derivative of 8325-4¹⁹⁷) was stored in Microbank storage beads (Pro-lab diagnostics) at –80 °C and grown on TSB agar plates. Plates were stored up to 2 weeks at 4 °C. Liquid culture was obtained by inoculating 10 mL of medium in 25 mL universal tube with a single colony and grown overnight at 37 °C with shaking (250 rpm). The overnight culture was used to inoculate fresh medium to an OD₆₀₀ 0.05 and grown to exponential phase (OD₆₀₀ 0.3-0.8) at 37 °C with shaking (250 rpm).

7.4 Chemicals used for microbiological work

All fluorescent dyes used in synthesis were purchased from Lumiprobe or Fisher Scientific. Stock solutions used in biological work such as bacterial cell labelling are shown below.

Stock solution	Concentration	Solvent	Storage
ADA (3-azido-D-alanine) (Iris Biotechnology)	100 mM	DMSO	–20 °C
BDP-FL (Lumiprobe)	1 mg/mL	DMSO	–20 °C (dark)
Alkyl Atto 488 (Molecular Probes)	1 mg/mL	DMSO	–20 °C (dark)

Table 7-1: Stock solutions used for microbiological work in this study

7.5 Centrifugation

Harvesting of samples was carried with two centrifuges depending on sample volume: Eppendorf microcentrifuge 5424 (Max volume 2 mL; max speed 14,468 rpm)

Sigma Centrifuge 4K15C (max volume 50 mL; 5100 rpm)

Centrifugation was carried out at room temperature unless otherwise stated.

7.6 Determination of bacterial cell density

Bacterial yields of liquid culture were obtained by spectrophotometric measurements at 600 nm (OD_{600}) using a Biochrom WPA Biowave DNA spectrophotometer. To obtain yields of fluorescent compounds absorbing at 600 nm, initial background measurements were taken and subtracted from measurements following bacterial growth. A 1:10 dilution with sterile culture media was made wherever necessary.

7.7 Determination of minimum inhibitory concentration (MIC)

Universal tubes contained either 5 or 10 mL TSB media and a serial dilution of compound dissolved in dH_2O or DMSO at different concentrations. Tubes were inoculated with *Staphylococcus aureus* overnight culture to an OD_{600} 0.05 and incubated at 37 °C with shaking (250 rpm) for 24 hours. The MIC was determined to be the lowest concentration at which no bacterial growth occurred. Tubes containing TSB media and TSB media with culture were used control for each experiment.

7.8 Cell labelling

7.8.1 Fixed cell labelling

1.0 mL aliquots of the exponential phase SH1000 culture were centrifuged and washed with PBS (1 minute, 2×) and then fixed with fixative (Section 7.2.2.2). Cells were incubated for 30 minutes at room temperature on a rotary shaker before centrifuging and washing with dH_2O (1 minute, 2×) and resuspending the pellets in 1 mL PBS. Cephalosporin derivatives were added to give a final concentration of their MIC (or 2× MIC) or 500 μ M for ADA. Samples were incubated for 5 minutes at 37 °C in the dark, before centrifuging and washing with dH_2O (1 minute, 2×) to obtain the final pellet.

7.8.2 Live cell labelling

1.0 mL aliquots of the exponential phase SH1000 culture were treated with cephalosporin derivatives to give a final concentration of their MIC (or 2× MIC) or 500 μ M for ADA. Samples were incubated at 5 minutes at 37 °C in the dark, before centrifuging and washing with PBS (1

minute, 2×). Cells were then fixed with fixative (section 7.2.2.2) and incubated for 30 minutes at room temperature on a rotary shaker in the dark, before centrifuging and washing with dH₂O (1 minute, 2×) to obtain the final pellet.

7.8.3 Click-iT® reaction for post clicking

For experiments where post-clicking of fluorophores was carried out, pellets were resuspended in the Click iT® reaction buffer mix (250 µL, as prepared in Section 7.2.3) and incubated for 30 minutes at room temperature on a rotary shaker in the dark, before centrifuging and washing with dH₂O (1 minute, 2×) to obtain the final pellet.

7.9 Microscopy imaging

7.9.1 Preparation of samples for widefield microscopy

Pellet samples were washed with PBS (1 minute, 1×) and an approximate sample dilution made with dH₂O. 5 µL of the sample was applied to a poly-L-lysine slide (Sigma) and dried with a flow of nitrogen. The slide was then washed with water and dried with nitrogen. A coverslip was mounted with 5 µL PBS or SlowFade™ Gold Antifade Mountant (Molecular Probes) and sealed with clear nail varnish.

7.9.2 Widefield fluorescence microscopy

Microscope setup was carried out by Victoria Lund or Kasia Wacnik.

Widefield microscopy was carried out using a DeltaVision microscope (Applied Precision) with appropriate filters for imaging each fluorophore (**Table 7-2**). UplanSApo 100x oil was used as the objective and images detected using a Photometrics CoolsnapHQ CCD camera. Images were deconvoluted using SoftWoRx where required. Images were processed using Fiji, ImageJ 1.52 software.

Filters	Fluorophore(s)	Excitation / nm	Emission / nm
FTIC	BDP-FL, Atto 488	492/20	528/38
RD-TR-PE/ TxRED	TAMRA	555/28	617/73
Cy5	Cyanine5 and Alexa Fluor™ 647	640/20	685/40

Table 7-2: Filters for Deltavision microscope

7.9.3 N-STORM microscopy

All preparation and microscopy for N-STORM samples were carried out by Victoria Lund and Christa Walther.

7.10 PBP analysis by SDS-PAGE

Gel electrophoresis experiments were carried out by Kasia Wacnik.¹⁶²

8 Chemical experimental

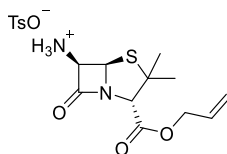
All reactions conducted with anhydrous solvents were performed under a nitrogen atmosphere using acetone-washed, flame-dried glassware with magnetic stirring and if required heated through the use of Dry SynTM blocks. Anhydrous solvents were obtained from the departmental Grubbs solvent system and stored under a positive pressure of nitrogen. All chemicals were purchased from commercial suppliers and used as received without further purification. *n*-Butyllithium was titrated with *N*-(4-phenylbenzylidene)benzylamine in anhydrous THF at 0 °C before each use to assess molarity. Reactions that were performed at 0 °C and –78 °C used water/ice baths and acetone/dry ice baths, respectively.

Analytical thin layer chromatography (TLC) was carried out utilising aluminium-backed Merck TLC plates (silica gel 60 F254) and visualised with UV light (254 nm), basic KMnO₄ or ninhydrin solution. Flash column chromatography was performed using VWR International Silica Gel 40-63µ 60Å as the stationary phase. Columns were typically packed as a slurry and equilibrated with the appropriate solvent system prior to use.

¹H, ¹³C and ³¹P NMR spectra were recorded on either Bruker AV 400, AVIIIHD 400 or AVIIIHD 500 spectrometers at 298K. Chemical shifts for ¹H NMR spectra are reported as δ in units of parts per million (ppm) downfield from SiMe₄ (δ 0.0) and relative to the signal of CHCl₃-d (δ 7.26, singlet), DMSO-d₆ (2.50, quintet), MeOH-d₄ (3.34, pentet) or H₂O-d₆ (4.79, singlet). Coupling constants (J) are given in Hertz (Hz) to the nearest 0.5 Hz and were corrected. As ¹³C NMR spectra are recorded using the JMOD or DEPT method and reported as δ in ppm downfield from SiMe₄ (δ 0.0) and relative to the signal of chloroform-d (77.0, triplet), DMSO-d₆ (39.7, quintet) or MeOH-d₄ (49.0 ppm, pentet). Mass spectra (m/z) were recorded on a 'VG'-Autospec for Electron Ionisation (EI) or a 'Waters'-LCT for Electrospray (ES). Infrared spectra were recorded on a Perkin-Elmer 1600 FT-IR using a Universal diamond ATR top-plate. Specific rotations were performed at 298K on an Optical Activity Ltd. AA-10 automatic polarimeter at 589 nm (Na D-line) and [α]_D values are given in 10⁻¹ deg cm² g⁻¹. HPLC was carried out on a Varian OD analytical system using a XBridge C₁₈ column (19 mm × 250 mm) with flow rate of 1.00 mL/min.

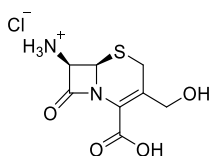
All compounds purified by HPLC were assumed to be salts of the buffer used. Melting points were measured on a Gallenkamp apparatus using a thermometer. Known compounds were compared to the literature with only the characterisation data stated. No literature data was reported for compounds that are not referenced.

(2*S*,6*R*)-3,3-Dimethyl-7-oxo-2-[(prop-2-en-1-yloxy)carbonyl]-4-thia-1-azabicyclo[3.2.0]heptan-6-aminium 4-methylbenzene-1-sulfonate **16**



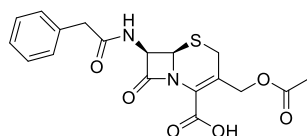
Methyl acetoacetate (500 μ L, 4.62 mmol) was added to a suspension of 6-aminopenicillanic acid (1.00 g, 4.62 mmol) and triethylamine (1.30 mL, 9.25 mmol) in anhydrous CH_2Cl_2 (30 mL) and the resulting mixture stirred at room temperature for 3 hours. The solvent was removed *in vacuo* and the residue dissolved in DMF (10 mL). Allyl bromide (450 μ L, 5.09 mmol) was added dropwise over 5 minutes and the solution stirred at room temperature overnight. The reaction was diluted with H_2O (30 mL) and extracted with $\text{Et}_2\text{O}:\text{CH}_2\text{Cl}_2$ (4:1, 3×40 mL). The combined organic extracts were washed sequentially with H_2O (50 mL) and brine (50 mL), dried over MgSO_4 , filtered and concentrated *in vacuo*. The residue was dissolved in Et_2O (20 mL), *p*-toluenesulfonic acid (monohydrate, 1.01 g, 5.78 mmol) was added and the mixture stirred at room temperature for 1 hour. Filtering the resulting precipitate under vacuum and washing with Et_2O afforded the title compound **16** as a white solid (225 mg, 11%); m.p. 150 $^\circ\text{C}$; $[\alpha]_{\text{D}}^{24} +102.0$ (*c* 1.05 in CHCl_3); ν_{max} (ATR) / cm^{-1} 2992 (C-H), 1779 (C=O), 1743 (C=O), 1632 (C=C), 1528 (C=C); δ_{H} (400 MHz, CDCl_3) 1.37 (3H, s, CH_3), 1.45 (3H, s, CH_3), 2.33 (3H, s, ArCH_3), 4.43 (1H, s, CHC), 4.61 (2H, d, *J* 6.0, OCH_2), 4.96 (1H, d, *J* 4.0, SCHCH), 5.27 (1H, dd, *J* 10.5, 1.0, CH=CHH), 5.34 (1H, dd, *J* 17.0, 1.0, CH=CHH), 5.41 (1H, d, *J* 4.0, SCHCH), 5.88 (1H, ddt, *J* 16.5, 10.5, 6.0 CH=CH_2), 7.12 (2H, app d, *J* 8.0, $2 \times \text{ArCH}$), 7.76 (2H, app d, *J* 8.0, $2 \times \text{ArCH}$); δ_{C} (101 MHz, CDCl_3) 21.5 (ArCH_3), 27.0 (CH_3), 32.2 (CH_3), 58.7 (CH), 65.4 (SCCH_3), 65.3 (CH), 66.3 (OCH_2), 70.5 (NCCO), 119.9 (CH=CH_2), 126.4 ($2 \times \text{ArCH}$), 129.1 ($2 \times \text{ArCH}$), 131.1 (CH=CH_2), 140.7 (ArC), 141.0 (ArC), 167.1 (C=O), 167.9 (C=O); *m/z* (ESI⁺) 257.0954 (1%, MH^+ , $\text{C}_{11}\text{H}_{17}\text{N}_2\text{O}_3\text{S}$ requires 257.0954), 513 (1), 468 (52), 289 (7), 279 (2), 249 (1), 231 (6), 230 (12), 229 (100). Exchangeable protons were no observed in ^1H NMR data.

(6*R*,7*R*)-2-Carboxy-3-(hydroxymethyl)-8-oxo-5-thia-1-azabicyclo[4.2.0]oct-2-en-7-aminium chloride **18**



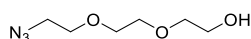
3 M Aq. NaOH (1.54 mL, 4.60 mmol) was added to a suspension of 7-aminocephalosporanic acid (500 mg, 1.84 mmol) in MeOH (4.5 mL) and H₂O (4.5 mL) at -20 °C and the mixture stirred for 30 minutes. The mixture was then acidified to pH 3 with concentrated hydrochloric acid and the resulting precipitate filtered under vacuum to afford the title compound **18** as an off-white solid that did not require further purification (258 mg, 52%); m.p. >250 °C (lit.¹ >180 °C); δ_{H} (400 MHz, d⁶-DMSO) 3.52 (2H, ABq, J_{A-B} 18.0, OCH₂), 4.20 (2H, ABq, J_{A-B} 13.5, SCH₂), 4.73 (1H, d, J 4.9, SCHCH), 4.93 (1H, d, J 4.9, SCHCH). All data were in accordance with the literature.¹⁹⁸

(6*R*,7*R*)-3-[(Acetyloxy)methyl]-8-oxo-7-(2-phenylacetamido)-5-thia-1-azabicyclo[4.2.0]oct-2-ene-2-carboxylic acid **19**



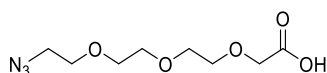
Phenylacetyl chloride (350 μ L, 427 mg, 2.76 mmol) was added to a suspension of 7-aminocephalosporanic acid (500 mg, 1.84 mmol) in sat. aq. NaHCO₃ (12 mL) and acetone (5 mL) at 0 °C and the mixture was stirred at room temperature for 17 hours. The mixture was then acidified to pH 2 with 1 M hydrochloric acid and extracted with CH₂Cl₂ (3 \times 20 mL). The combined organic extracts were washed with brine (20 mL), dried over Na₂SO₄, filtered and concentrated *in vacuo*. Trituration of the crude product with Et₂O afforded the title compound **19** as an off white solid (375 mg, 52%); m.p. 167 - 169 °C (lit.¹⁹⁹ 168 °C - 171 °C); δ_{H} (400 MHz, d⁶-DMSO) 2.03 (3H, s, O=CCH₃), 3.42 - 3.66 (4H, m, ArCH₂ + SCH₂), 4.68 (1H, d, J 13.0, OCHHC=C), 5.00 (1H, d, J 13.0, OCHHC=C), 5.07 (1H, d, J 5.0, HNCHCHS), 5.63 - 5.71 (1H, m, HNCHCHS), 7.19 - 7.34 (5H, m, 5 \times ArCH), 9.12 (1H, d, J 8.0, NH), 13.72 (1H, br s, COOH). All data were in accordance with the literature.¹⁹⁹

2-[2-(2-Azidoethoxy)ethoxy]ethanol **21**



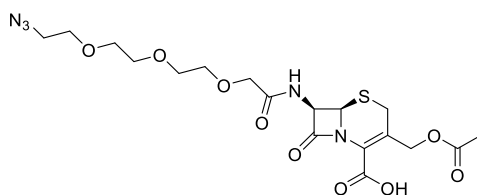
A solution of 2-[2-(2-chloroethoxy)ethoxy]ethanol (1.72 mL, 11.9 mmol), sodium azide (1.55 g, 23.8 mmol) and sodium iodide (15.9 mg, 2.3 mmol) in H₂O (40 mL) was stirred at 80 °C overnight. The reaction was cooled to room temperature and additional sodium azide (775 mg, 11.9 mmol) and sodium iodide (15.9 mg, 2.3 mmol) were added. The solution was stirred at 80 °C for a further 24 hours, cooled to room temperature and extracted with CH₂Cl₂ (4 × 50 mL). The combined organic extracts were dried over MgSO₄, filtered and concentrated *in vacuo* to afford the title compound **21** as a clear oil which did not require further purification (1.93 g, 94%); δ_H (400 MHz, CDCl₃) 2.26 (1H, br s, OH), 3.37 – 3.46 (2H, m, CH₂), 3.60 – 3.66 (2H, m, CH₂), 3.66 – 3.72 (6H, m, 3 × CH₂), 3.72 – 3.80 (2H, m, CH₂); *m/z* (ES⁺) 198.0855 (100% M+Na⁺, C₆H₁₃N₃O₃₅Na requires 198.0866), 330 (68), 319 (6), 302 (1), 242 (19), 172 (6). ¹H NMR data was reported with different multiplicity but otherwise all other data were in accordance with the literature.²⁰⁰

{2-[2-(2-Azidoethoxy)ethoxy]ethoxy}acetic acid **22**



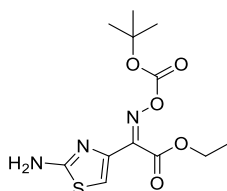
Sodium hydride (60% mineral oil, 192 mg, 22.8 mmol) in anhydrous THF (10 mL) was cooled to 0 °C and polyether **21** (1.00 g, 5.71 mmol) was added. This was stirred for 15 minutes at 0 °C prior to adding bromoacetic acid (1.19 g, 8.57 mmol) and stirring the mixture at room temperature overnight. The reaction mixture was quenched with MeOH (10 mL), concentrated *in vacuo* and the residue partitioned between CH₂Cl₂ (50 mL) and 1M HCl (30 mL). The organic layer was separated, washed with brine (30 mL), dried over MgSO₄, filtered and concentrated *in vacuo*. Purification by dry flash column chromatography using silica gel and an eluent of 0 – 100% ethyl acetate: petroleum ether 40 – 60 afforded the title compound **22** as a clear oil (700 mg, 52%); δ_H (400 MHz, CDCl₃) 3.37 – 3.44 (2H, m, CH₂), 3.65 – 3.70 (4H, m, 2 × CH₂), 3.70 – 3.74 (4H, m, CH₂), 3.75 – 3.79 (2H, m, CH₂), 4.17 (2H, s, O=CCH₂); *m/z* (ES⁺) 256.0900 (100%, M+Na⁺, C₈H₁₅N₃O₅Na requires 256.0909), 305 (100), 278 (26), 261 (9). ¹H NMR data was reported with different multiplicity and MS data was recorded as the MS⁺ ion in the literature but otherwise all data were in accordance.²⁰¹

(6*R*,7*R*)-3-[(Acetyloxy)methyl]-7-(2-{2-[2-(2-azidoethoxy)ethoxy]ethoxy}acetamido)-8-oxo-5-thia-1-azabicyclo[4.2.0]oct-2-ene-2-carboxylic acid **23**



A solution of carboxylic acid **22** (128 mg, 0.550 mmol) in anhydrous CH_2Cl_2 (4 mL) was cooled to $0\text{ }^\circ\text{C}$. Oxalyl chloride (50 μL , 0.590 mmol) and DMF (4 drops) were added and the solution stirred at room temperature for 17 hours. The mixture was concentrated *in vacuo*, dissolved in acetone (0.75 mL) and added to a suspension of 7-aminocephalosporanic acid (100 mg, 0.370 mmol) in sat. aq. NaHCO_3 (2.5 mL) and acetone (0.75 mL) at $0\text{ }^\circ\text{C}$. The resulting mixture was stirred at room temperature for 22 hours. The mixture was acidified to pH 2 with 1 M HCl and extracted with CH_2Cl_2 ($3 \times 10\text{ mL}$). The combined organic extracts were dried over Na_2SO_4 , filtered and concentrated *in vacuo*. Purification by preparative HPLC using an eluent of 30% MeCN: H_2O afforded the title compound **23** as a pale yellow oil (46 mg, 26%); $[\alpha]_{\text{D}}^{26} + 52.2$ (*c* 0.9 in CHCl_3); ν_{max} (ATR) / cm^{-1} 3304 (OH), 2915 (CH), 2879 (CH), 2103 (N=N=N), 1779 (C=O), 1731 (C=O), 1680 (C=O); δ_{H} (400 MHz, CDCl_3) 2.08 (3H, s, CH_3), 3.33 – 3.38 (2H, m, CH_2), 3.41 (1H, d, *J* 19.0, SCHH), 3.58 (1H, d, *J* 19.0, SCHH), 3.61 – 3.75 (10H, m, $5 \times \text{CH}_2$), 4.10 (2H, ABq, J_{A-B} 16.0, $\text{OCH}_2\text{C}=\text{O}$), 4.90 (1H, d, *J* 13.5, $\text{OCHHC}=\text{C}$), 5.02 (1H, d, *J* 5.0, H NCHCHS), 5.11 (1H, d, *J* 13.5, $\text{OCHHC}=\text{C}$), 5.84 (1H, dd, *J* 9.0, 5.0, H NCHCHS), 6.93 (1H, br s, COOH), 7.80 (1H, d, *J* 9.0, NH); δ_{C} (101 MHz, CDCl_3) 20.9 (CH_3), 26.6 (SCH_2), 50.8 (OCH_2), 57.5 (CH), 58.8 (CH), 63.3 (CH_2), 70.2 (CH_2), 70.3 (CH_2), 70.5 (CH_2), 70.7 (CH_2), 70.8 (CH_2), 71.4 (CH_2), 125.8 (C=C), 126.9 (C=C), 163.2 (C=O), 164.8 (C=O), 171.0 (C=O), 171.4 (C=O); *m/z* (ESI⁺) 510.1271 (69%, $\text{M}+\text{Na}^+$, $\text{C}_{18}\text{H}_{25}\text{N}_5\text{O}_9\text{SNa}$ requires 510.1265), 511 (15), 506 (22), 505 (100), 428 (66), 401 (14), 400 (73), 356 (17).

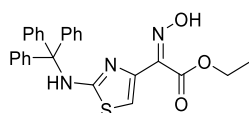
Ethyl (2*Z*)-2-(2-amino-1,3-thiazol-4-yl)-2-[[*tert*-butoxycarbonyl]oxy]imino}acetate **25**



Di-*tert*-butyl dicarbonate (319 mg, 1.46 mmol) in THF (1.4 mL) was added to a solution of ethyl 2-amino- α -(hydroxyimino)-4-thiazoleacetate (300 mg, 1.39 mmol) and 1 M aq. NaOH (2.78 mL, 2.78 mmol) and the mixture was stirred at room temperature overnight. The mixture

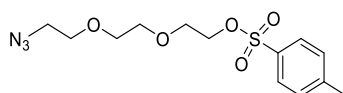
was diluted with H₂O (10 mL) and extracted with EtOAc (2 × 15 mL). The combined organic extracts were washed with sat. aq. NH₄Cl (10 mL), dried over Na₂SO₄, filtered and concentrated *in vacuo* to afford the title compound **25** as a yellow solid that did not require further purification (334 mg, 76%); m.p. 198 °C; ν_{\max} (ATR) / cm⁻¹ 3447 (N-H), 3096 (C-H), 2980, 2164, 2033, 1982, 1770 (C=O), 1743 (C=O), 1613 (C=N), 1540 (C=C); δ_{H} (400 MHz, d⁶-DMSO) 1.28 (3H, t, *J* 7.0, OCH₂CH₃), 1.47 (9H, s, 3 × CH₃), 4.37 (2H, q, *J* 7.0, OCH₂CH₃), 7.25 (1H, s, ArCH), 7.40 (2H, s, NH₂); δ_{C} (101 MHz, d⁶-DMSO) 13.9 (OCH₂CH₃); 27.2 (3 × CH₃), 62.3 (OCH₂CH₃), 84.3 [OC(CH₃)₃], 113.3 (ArCH), 139.3 (ArC), 150.1 (C=N), 152.5 (C=O), 161.0 (C=O), 169.1 (ArCNH); *m/z* (ESI⁺) 316.0969 (2%, MH⁺, C₁₂H₁₈N₃O₅S requires 316.0962), 272 (12), 217 (10), 216 (100).

Ethyl (2*Z*)-2-(*N*-Hydroxyimino)-2-{2-[(triphenylmethyl)amino]-1,3-thiazol-4-yl}acetate **26**



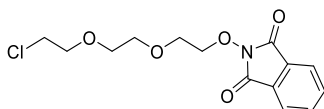
Triphenylmethyl chloride (2.77 g, 9.94 mmol) was added to a solution of ethyl 2-amino- α -(hydroxyimino)-4-thiazoleacetate (2.00 g, 9.29 mmol) in DMF (17 mL) and the mixture was stirred at room temperature overnight. H₂O (50 mL) was added and the mixture partitioned with EtOAc (70 mL). The organic layer was separated and the aqueous layer was extracted with EtOAc (2 × 70 mL). The combined organic extracts were washed sequentially with sat. aq. NH₄Cl (50 mL) and brine (50 mL), dried over Na₂SO₄, filtered and concentrated *in vacuo*. Purification by dry flash column chromatography using silica gel and an eluent of 20 – 60% ethyl acetate: petroleum ether 40 – 60 afforded the title compound **26** as a yellow solid (2.88 g, 69%); m.p. 180 – 182 °C; ν_{\max} (ATR) / cm⁻¹ 3371 (N-H), 1740 (C=O), 1732 (N=O), 1515 (C=C); δ_{H} (400 MHz, CDCl₃) 1.36 (3H, t, *J* 7.0, OCH₂CH₃), 4.39 (2H, q, *J* 7.0, OCH₂CH₃), 6.47 (1H, s, ArCH), 6.97 (1H, brs, NOH), 7.26 – 7.35 (15H, m, 15 × ArCH), 8.74 (1H, br s, NH); *m/z* (ESI⁺) 458.1548 (40%, MH⁺, C₂₆H₂₄N₃O₃S requires 458.1533), 480 (16), 244 (20), 243 (100). No melting point, infra-red or mass spectrometry data were reported in the literature; ¹H NMR data was in accordance with the literature.¹¹⁰

1-{2-[2-(2-Azidoethoxy)ethoxy]ethoxysulfonyl}-4-methylbenzene **27**



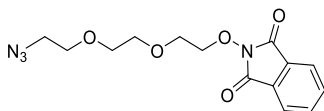
p-Toluenesulfonyl chloride (652 mg, 3.42 mmol) was added to a solution of alcohol **21** (500 mg, 2.85 mmol) and Et₃N (597 μL, 4.28 mmol) in CH₂Cl₂ (25 mL) at 0 °C and the mixture stirred for 10 minutes. The reaction mixture was allowed to warm to room temperature and the mixture was stirred overnight. The mixture was washed with sat. aq. NaHCO₃ (20 mL), H₂O (20 mL) and brine (20 mL). The organic layer was dried over MgSO₄, filtered and concentrated *in vacuo*. Purification by flash column chromatography using silica gel and an eluent of 0 – 30% ethyl acetate: petroleum ether 40 – 60 afforded the title compound **27** as a clear oil (485 mg, 52%); δ_H (400 MHz, CDCl₃) 2.45 (3H, s, ArCH₃), 3.33 – 3.39 (2H, m, CH₂), 3.60 (4H, s, 2 × CH₂), 3.62 – 3.66 (2H, m, CH₂), 3.68 – 3.72 (2H, m, CH₂), 4.14 – 4.18 (2H, m, CH₂), 7.34 (2H, *J* 8.0, ArCH₂), 7.80 (2H, *J* 8.0, CH₂). ¹H NMR data was in accordance with the literature.²⁰²

2-{2-[2-(2-Chloroethoxy)ethoxy]ethoxy}-2,3-dihydro-1*H*-isoindole-1,3-dione **29**



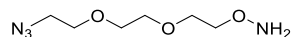
A solution of 2-[2-(2-chloroethoxy)ethoxy]ethanol (2 mL, 13.8 mmol), anhydrous THF (50 mL), PPh₃ (5.40 g, 20.7 mmol) and *N*-hydroxyphthalimide (3.37 g, 20.7 mmol) was cooled to 0 °C and DIAD (4.07 mL, 20.7 mmol) was added dropwise over 30 minutes. The reaction mixture was stirred at room temperature overnight. The mixture was concentrated *in vacuo* and filtered through a plug of silica gel using an eluent of 10 – 60% ethyl acetate: petroleum ether 40 – 60. Further purification by flash column chromatography using silica gel and an eluent of 30 – 40% ethyl acetate: petroleum ether 40 – 60 afforded the title compound **29** as a yellow oil which solidified upon standing (3.39 g, 79%); δ_H (400 MHz, CDCl₃) 3.53 – 3.58 (2H, m, CH₂), 3.59 – 3.63 (2H, m, CH₂), 3.65 – 3.70 (4H, m, 2 × CH₂), 3.85 – 3.90 (2H, m, CH₂), 4.36 – 4.40 (2H, m, CH₂), 7.73 – 7.78 (2H, m, 2 × ArCH), 7.81 – 7.87 (2H, m, 2 × ArCH). ¹H NMR data indicates the presence of diisopropyl bicarbamate (6% w/w) and but was otherwise in accordance with the literature.²⁰³

2-{2-[2-(2-Azidoethoxy)ethoxy]ethoxy}-2,3-dihydro-1*H*-isoindole-1,3-dione **30**



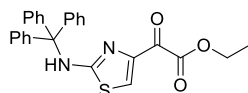
A solution of tosylate **29** (3.18 g, 10.1 mmol), sodium azide (1.97 g, 30.3 mmol) and potassium iodide (0.335 g, 2.02 mmol) in DMF (80 mL) was stirred at 80 °C for 23 hours. The reaction mixture was allowed to cool to room temperature and diluted with H₂O (100 mL). The mixture was extracted with EtOAc (4 × 100 mL) and the organic extracts were washed with brine (50 mL), dried over Na₂SO₄, filtered and concentrated *in vacuo*. Purification by flash column chromatography using silica gel and an eluent of 30 – 50% ethyl acetate: petroleum ether 40 – 60 afforded the title compound **30** as a white solid (2.23 g, 69%); m.p. 38 – 40 °C; δ_{H} (400 MHz, CDCl₃) 3.34 (2H, t, *J* 5.0, CH₂). 3.58 – 3.64 (4H, m, 2 × CH₂), 3.65 – 3.72 (2H, m, CH₂), 3.82 – 3.91 (2H, m, CH₂), 4.35 – 4.42 (2H, m, CH₂), 7.72 – 7.78 (2H, m, 2 × ArCH), 7.81 – 7.88 (2H, m, 2 × ArCH). No melting point was reported in the literature; ¹H NMR data was in accordance with the literature.²⁰³

O-{2-[2-(2-Azidoethoxy)ethoxy]ethyl}hydroxylamine **31**



Hydrazine monohydrate (64 – 65%, 380 μ L, 1.56 mmol) was added to a solution of phthalimide **30** in CH₂Cl₂ (15 mL) at 0 °C and was stirred at 0 °C for 5 minutes and then at room temperature for 1 hour. The mixture was concentrated *in vacuo* to afford the title compound **31** as a clear oil which was used without further purification (296 mg, quant.); δ_{H} (400 MHz, CDCl₃) 3.39 (2H, t, *J* 5.0, CH₂). 3.65 – 3.71 (8H, m, 4 × CH₂), 3.81 – 3.86 (2H, m, CH₂), 5.50 (2H, br s, NH₂). ¹H NMR data was in accordance with that previously reported.²⁰⁴

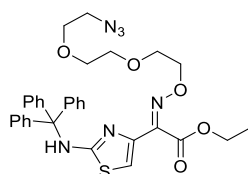
Ethyl 2-oxo-2-{2-[(triphenylmethyl)amino]-1,3-thiazol-4-yl}acetate **33**



Triphenylmethyl chloride (1.49 g, 5.35 mmol) was added to a solution of ethyl 2-amino- α -(hydroxyimino)-4-thiazoleacetate (1.00 g, 5.00 mmol) in DMF (9 mL) and the mixture was stirred at room temperature overnight. H₂O (50 mL) was added and the mixture partitioned with EtOAc (50 mL). The aqueous layer was separated and extracted with EtOAc (2 × 50 mL).

The combined organic extracts were washed with 1M HCl (40 mL), brine (40 mL), dried over Na₂SO₄, filtered and concentrated *in vacuo*. Purification by dry flash column chromatography using silica gel and an eluent of 20% ethyl acetate: petroleum ether 40 – 60 afforded the title compound **33** as a yellow solid (1.30 g, 59%); m.p. 75 – 77 °C; ν_{\max} (ATR) / cm⁻¹ 3340 (N-H), 3058 (C-H), 3026 (C-H), 2978 (C-H), 1731 (C=O), 1675 (C=O), 1530 (C=C); δ_{H} (400 MHz, CDCl₃) 1.37 (3H, t, *J* 7.0, CH₃), 4.36 (2 H, q, *J* 7.0, CH₂), 7.02 (1H, s, NH), 7.27 – 7.35 (15H, m, ArCH), 7.72 (1H, s, ArCH_{thiazole}); δ_{C} (101 MHz, d⁶-DMSO) 14.1 (OCH₂CH₃), 62.4 (OCH₂CH₃), 71.9 (TrtC), 125.1 (ArCH_{thiazole}), 127.8 (3 × ArCH), 128.4 (6 × ArCH) 129.2 (6 × ArCH), 142.9 (3 × ArC), 145.8 (NC=CS), 162.5 (N=CNH), 168.0 (C=O), 176.9 (C=O); *m/z* (ESI⁺) 465.1253 (21%, M+Na⁺, C₂₆H₂₂N₂O₃SNa requires 465.1243), 908 (12), 907 (21), 244 (100), 243 (31), 165 (1). No melting point, infra-red or mass spectrometry data were reported in the literature; ¹H NMR data shows a different shift for the NH proton but all other data was in general agreement with the literature.¹¹⁰

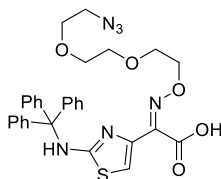
Ethyl (2*Z*)-12-azido-2-{2-[(triphenylmethyl)amino]-1,3-thiazol-4-yl}-4,7,10-trioxa-3-azadodec-2-enoate **28**



A solution of ketone **33** (279 mg, 0.631 mmol), MeOH (4 mL), hydroxylamine **31** (120 mg, 0.631 ml) and AcOH (2-3 drops) was stirred at 60 °C overnight. The reaction mixture was allowed to cool to room temperature and concentrated *in vacuo*. The residue was diluted with H₂O (10 mL) and extracted with CH₂Cl₂ (4 × 10 mL). The combined organic extracts were washed with brine (10 mL), dried over Na₂SO₄, filtered and concentrated *in vacuo*. Purification by flash column chromatography using silica gel and an eluent of 25% ethyl acetate: petroleum ether 40 – 60 afforded the title compound **28** as a yellow oil (289 mg, 75%); ν_{\max} (ATR) / cm⁻¹ 3338 (N-H), 3058 (C-H), 2930 (C-H), 2869 (C-H), 2101 (N=N=N), 1736 (C=O), 1598 (C=N), 1528 (C=C); δ_{H} (400 MHz, CDCl₃) 1.34 (3H, t, *J* 7.0, OCH₂CH₃), 3.34 – 3.41 (2H, m, CH₂), 3.59 – 3.70 (6H, m, 3 × CH₂), 3.72 – 3.79 (2H, m, CH₂), 4.31 – 4.45 (4H, m, CH₂ + OCH₂CH₃), 6.48 (1H, s, ArCH_{thiazole}), 6.97 (1H, br s, NH), 7.30 (15 H, s, 15 × ArCH); δ_{C} (101 MHz, CDCl₃) 14.2 (CH₃), 50.7 (N₃CH₂), 61.9 (OCH₂), 69.5 (CH₂), 70.0 (CH₂), 70.7 (CH₂), 70.9 (CH₂), 74.9 (TrtC), 111.5 (ArCH_{thiazole}), 127.7 (3 × ArCH), 128.3 (6 × ArCH), 129.3 (6 × ArCH), 140.8

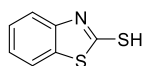
(ArC), 143.0 (3 × ArC), 147.0 (ArC), 163.0 (C=N), 168.6 (C=O); m/z (ESI⁺) 615.2404 (100%, MH⁺, C₃₂H₃₅N₆O₅S requires 615.2384), 637 (5), 392 (1), 338 (1), 243 (9), 124 (9). ¹³C NMR data reported has one less resonance than what would be predicted.

(2Z)-12-Azido-2-{2-[(triphenylmethyl)amino]-1,3-thiazol-4-yl}-4,7,10-trioxa-3-azadodec-2-enoic acid **34**



NaOH (97 mg, 2.42 mmol) was added to a mixture of ester **28** (785 mg, 1.21 mmol) in MeOH (10 ml) and water (2 mL) and the mixture was stirred at 45 °C for 3 hours. The MeOH was removed *in vacuo*, the residue diluted with H₂O (15 mL) and the solution adjusted to pH 2 with 1 M hydrochloric acid. This was extracted with CH₂Cl₂ (3 × 30 mL) and the combined organic extracts dried over Na₂SO₄, filtered and concentrated *in vacuo* to afford the title compound **34** as a yellow solid that did not require further purification (587 mg, 83%); m.p. 75 °C – 76 °C; ν_{\max} (ATR) / cm⁻¹ 2932 (C-H), 2874 (C-H), 2098 (N=N=N) 1716 (C=O), 1530 (C=C); δ_{H} (400 MHz, MeOD) 3.33 – 3.36 (2H, m, CH₂). 3.62 – 3.68 (6H, m, 3 × CH₂), 3.75 – 3.80 (2H, m, CH₂), 4.25 – 4.30 (2H, m, CH₂), 6.77 (1H, s, ArCH_{thiazole}), 7.27 – 7.37 (15H, m, 15 × ArCH); δ_{C} (101 MHz, MeOD) 51.7 (N₃CH₂), 70.4 (CH₂), 71.0 (CH₂), 71.4 (CH₂), 75.5 (TrtC), 110.4 (ArCH_{thiazole}), 128.0 (3 × ArCH), 128.7 (6 × ArCH), 129.8 (6 × ArCH), 144.4 (ArC), 145.3 (3 × ArC), 149.6 (ArC), 167.04 (C=N), 171.73 (C=O); m/z (ESI⁺) 587.2078 (100%, MH⁺, C₃₀H₃₁N₆O₅S requires 587.2071), 609 (15), 589 (1), 588 (34), 243 (12).

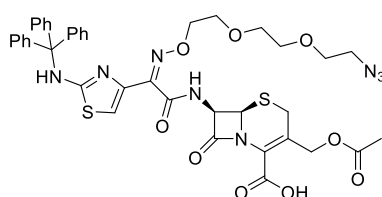
1,3-Benzothiazole-2-thiol **36**



Sodium borohydride (0.175 g, 4.63 mmol) was added to 2,2'-dithiobis(benzothiazole) (1.54 g, 4.63 mmol) in CH₂Cl₂ (12 mL) and MeOH (12 ml) and the suspension was stirred at room temperature for 30 minutes. The reaction mixture was concentrated *in vacuo* and partitioned between ethyl acetate (30 mL) and 1 M hydrochloric acid (20 mL). The aqueous layer was

separated and extracted with ethyl acetate (20 mL). The organic extracts were combined, dried over Na₂SO₄, filtered and concentrated *in vacuo* to give the title compound **36** as a yellow solid which was used without further purification (1.47 g, 95%); δ_{H} (400 MHz, CDCl₃) 7.28 – 7.42 (3H, m, 3 × ArCH). 7.48 (1H, d, *J* 8.0, ArCH), 11.13 (1H, s, SH). ¹H NMR data was in accordance with the literature.^{205,206}

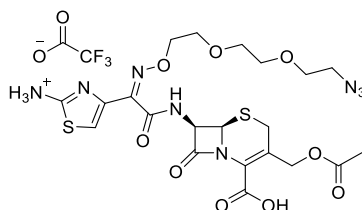
(6*R*,7*R*)-3-[(Acetyloxy)methyl]-7-[(2*Z*)-12-azido-2-{2-[(triphenylmethyl)amino]-1,3-thiazol-4-yl}-4,7,10-trioxa-3-azadodec-2-enamido]-8-oxo-5-thia-1-azabicyclo[4.2.0]oct-2-ene-2-carboxylic acid **38**



HATU (71 mg, 0.187 mmol) was added a solution of carboxylic acid **34** (100 mg, 0.710 mmol) and DIPEA (65 μ L, 0.374 mmol) in anhydrous DMF (1.7 mL) and the mixture was stirred at room temperature for 15 minutes. 7-Aminocephalosporanic acid (56 mg, 0.204 mmol) was then added and the reaction mixture was stirred overnight. The mixture was concentrated *in vacuo* and resulting residue diluted with H₂O (8 mL). This was adjusted to pH 2 with 1 M hydrochloric acid and extracted with CH₂Cl₂ (2 × 10 mL). The combined organic extracts were washed with brine (10 mL), dried over Na₂SO₄, filtered and concentrated *in vacuo*. Purification by preparative HPLC using an eluent of 50% MeCN: H₂O (0.1% TFA) afforded the title compound **38** as a white solid (38 mg, 27%); m.p. 92 °C – 94 °C; ν_{max} (ATR) / cm⁻¹ 3205 (N-H), 2933 (C-H), 2106 (N=N=N), 1776 (C=O), 1733 (C=O), 1668 (C=N), 1533 (C=C); δ_{H} (400 MHz, CDCl₃) 2.08 (3H, s, CH₃). 3.25 (2H, t, *J* 5.0, CH₂), 3.34 (1H, d, *J* 19.0, SCHH), 3.54 (1H, d, *J* 19.0, SCHH), 3.57 – 3.69 (6H, m, 3 × CH₂), 3.73 – 3.84 (2H, m, CH₂), 4.38 (2H, t, *J* 4.5, CH₂N₃), 4.86 (1H, ABq, *J*_{A-B} 13.0, OCHHC=O), 5.01 – 5.13 (2H, m, HNCHCHS + OCHHC=O), 5.77 – 5.83 (1H, m, HNCHCHS), 6.77 (1H, s, ArCH_{thiazole}), 7.27 – 7.37 (15H, m, 15 × ArCH), 7.79 (1H, s, NHC=O); δ_{C} (101 MHz, MeOD) 20.6 (CH₃), 27.3 (SCH₂), 51.8 (OCH₂), 54.8 (CH₂), 58.8 (HNCHCHS), 60.4 (HNCHCHS), 64.3 (CH₂), 70.3 (CH₂), 71.1 (CH₂), 71.5 (CH₂), 71.7 (CH₂), 76.4 (TrtC), 111.8 (ArCH_{thiazole}), 127.2 (C=C), 127.6 (C=C), 128.0 (3 × ArCH), 128.7 (6 × ArCH), 129.8 (6 × ArCH), 145.4 (3 × ArC), 145.9 (ArC) 148.8

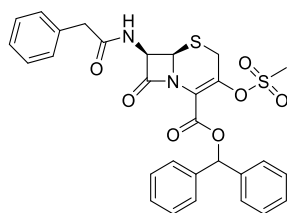
(ArC), 163.1 (C=N), 164.4 (C=O), 165.1 (C=O), 172.2 (C=O), 172.4 (C=O); m/z (ESI⁺) 841.2431 (32%, MH⁺, C₄₀H₄₁N₈O₉S₂ requires 841.2432), 803 (1), 283 (8), 243 (100).

4-[(1Z)-1-[[[(6R,7R)-3-[(Acetyloxy)methyl]-2-carboxy-8-oxo-5-thia-1-azabicyclo[4.2.0]oct-2-en-7-yl]carbamoyl]-11-azido-3,6,9-trioxa-2-azaundec-1-en-1-yl]-1,3-thiazol-2-aminium trifluoroacetate **39**



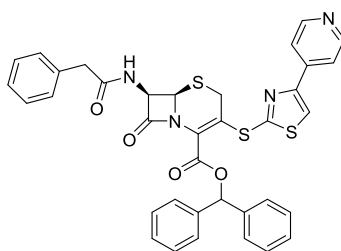
Trifluoroacetic acid (1 mL) was added to Boc-protected azide **38** (27 mg, 0.0321 mmol) in CH₂Cl₂ (3 mL) and solution was stirred at room temperature for 1 hour. The mixture was concentrated *in vacuo* and the resulting residue triturated with Et₂O (3 × 5 mL) to give a crude pink solid (25 mg). This was combined with previously synthesised crude material (14 mg) and purified by preparative HPLC using an eluent of 10% MeCN: H₂O (0.1% TFA) to give the title compound **39** as a white solid (12 mg, 28%); ν_{\max} (ATR) / cm⁻¹ 3250 (N-H), 2951 (O-H), 2878 (N-H), 2115 (N=N=N), 1782 (C=O), 1678 (C=O), 1538 (C=C); δ_{H} (400 MHz, MeOD) 2.07 (3H, s, CH₃). 3.33 – 3.38 (2H, m, CH₂), 3.52 (1H, d, J 19.0, SCHH), 3.63 – 3.68 (6H, m, 3 × CH₂), 3.71 (2H, d, J 19.0, SCHH), 3.82 – 3.87 (2H, m, CH₂), 4.39 – 4.45 (2H, m, CH₂), 4.85 (1H, d, J 13.0, OCHHC=O), 5.12 (1H, d, J 13.0, OCHHC=O), 5.19 (1H, d, J 5.0, HNCHCHS), 5.90 (1H, d, J 5.0, HNCHCHS), 7.09 (1H, s, ArCH_{thiazole}); δ_{C} (126 MHz, MeOD) 20.6 (CH₃). 27.3 (SCH₂), 51.8 (OCH₂), 58.8 (HNCHCHS), 60.4 (HNCHCHS), 64.3 (CH₂), 70.2 (CH₂), 71.1 (CH₂), 71.5 (CH₂), 71.7 (CH₂), 76.5 (CH₂), 111.8 (SC=CN), 127.2 (C=C), 127.61 (C=C), 142.9 (ArC) 145.6 (ArC), 162.9 (C=N), 164.8 (C=O), 165.14 (C=O), 172.3 (C=O), 172.4 (C=O), 175.2 (CF₃C=O); m/z (ESI⁺) 599.1342 (100%, MH⁺, C₂₁H₂₇N₈O₉S₂ requires 599.1337), 601 (14), 600 (33). 539 (1), 467 (1), 270 (1), 202 (1), 125 (1). Melting point could not be measured due to the hygroscopic nature of the salt.

Diphenylmethyl (6R,7R)-3-(methanesulfonyloxy)-8-oxo-7-(2-phenylacetamido)-5-thia-1-azabicyclo[4.2.0]oct-2-ene-2-carboxylate **42**



Methanesulfonyl chloride (0.363 mL, 4.69 mmol) was added to a solution of (6*R*,7*R*)-benzhydryl 3-hydroxy-8-oxo-7-(2-phenylacetamido)-5-thia-1-azabicyclo[4.2.0]oct-2-ene-2-carboxylate (1.02 g, 4.69 mmol) and K₂CO₃ (0.395 g, 2.86 mmol) in anhydrous DMF (5 mL) at -40 °C and the mixture was stirred for 90 mins. The reaction mixture was poured onto EtOAc (50 mL) and partitioned with H₂O (50 mL). The organic layer was separated, washed with brine (3 × 50 mL), dried over MgSO₄, filtered and concentrated *in vacuo*. Trituration with Et₂O (40 mL) gave the title compound **42** as a yellow solid which was used without further purification (1.13 g, 94%). A small amount of this was purified with silica gel flash column chromatography for characterisation purposes; δ_H (400 MHz, CDCl₃) 2.79 (3H, s, CH₃), 3.53 (1H, d, *J* 18.5, SCHH), 3.62 (1H, d, *J* 16.0, ArCHH), 3.68 (1H, d, *J* 16.0, ArCHH), 3.81 (1H, d, *J* 18.5, SCHH), 5.04 (1H, d, *J* 5.0, NH), 5.88 (1H, dd, *J* 9.0, 5.0, HNCHCHS), 6.00 (1H, d, *J* 9.0, HNCHCHS), 6.93 (1H, s, OCHAr), 7.27 – 7.41 (15H, m, 15 × ArCH); δ_C (101 MHz, CDCl₃) 27.4 (SCH₂), 38.7 (CH₃), 43.4 (ArCH₂), 57.6 (CH), 58.9 (CH), 80.0 (Ar₂CH), 127.5 (2 × ArCH), 127.8 (2 × ArCH), 128.0 (ArCH), 128.4 (ArCH), 128.5 (ArCH), 128.7 (2 × ArCH), 128.7 (2 × ArCH), 129.4 (2 × ArCH), 129.6 (2 × ArCH), 133.7 (OC=CN) 138.9 (ArC), 139.0 (ArC), 140.6 (OC=CN), 158.8 (C=O), 165.3 (C=O), 171.2 (C=O). No ¹³C NMR data was reported in the literature; ¹H NMR data was reported with different multiplicity couplings but was otherwise in accordance with the literature.²⁰⁷

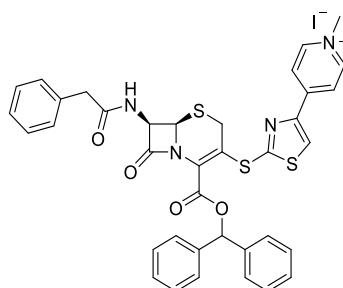
Diphenylmethyl (6*R*,7*R*)-8-oxo-7-(2-phenylacetamido)-3-[[4-(pyridin-4-yl)-1,3-thiazol-2-yl]sulfanyl]-5-thia-1-azabicyclo[4.2.0]oct-2-ene-2-carboxylate **43a**



A suspension of 4-(4-pyridinyl)thiazole-2-thiol (58 mg, 0.301 mmol), anhydrous THF (1.5 mL) and NaOMe (30% in MeOH, 60 μL, 0.301 mmol) was stirred at room temperature for 1 hour.

The resulting solution was added dropwise over 1 minute to a suspension of mesylate **42** (152 mg, 0.262 mmol) in anhydrous THF (1.5 mL) at -5 °C and the mixture was stirred for 2 hours. Stirring was continued at room temperature overnight. The reaction mixture was diluted with MeOH (4 mL) and H₂O (2 mL), adjusted to pH 5 – 6 with AcOH and then concentrated *in vacuo*. The mixture was diluted with H₂O (5 mL) and extracted with EtOAc (2 × 10 mL), before the organic extracts were dried over Na₂SO₄, filtered and concentrated *in vacuo*. Purification by flash column chromatography using silica gel and an eluent of 50 – 100% ethyl acetate: hexane afforded the title compound **43a** as an off-white solid (108 mg, 55%); δ_{H} (400 MHz, CDCl₃) 3.47 (1H, d, *J* 18.0, SCHH), 3.63 (1H, d, *J* 16.0, ArCHH), 3.67 (1H, d, *J* 16.0, ArCHH), 3.70 (1H, d, *J* 18.0, SCHH), 5.04 (1H, d, *J* 5.0, NH), 5.89 (1H, dd, *J* 9.0, 5.0, HNCHCHS), 6.04 (1H, d, *J* 9.0, HNCHCHS), 6.98 (1H, s, OCHAr), 7.24 – 7.42 (15H, m, 15 × ArCH), 7.72 (2H, m, 2 × ArCH_{pyridine}), 7.74 (1H, s, ArCH_{thiazole}), 8.69 (2H, m, 2 × ArCH_{pyridine}). ¹H NMR data was reported with different multiplicity couplings but was otherwise in accordance with the literature.¹¹³

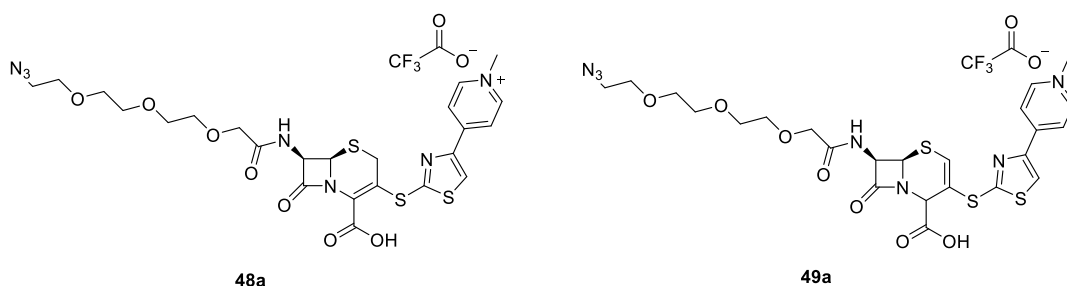
4-(2-[[[(6*R*,7*R*)-2-[(Diphenylmethoxy)carbonyl]-8-oxo-7-(2-phenylacetamido)-5-thia-1-azabicyclo[4.2.0]oct-2-en-3-yl]sulfanyl]-1,3-thiazol-4-yl]-1-methylpyridin-1-ium iodide **44**



Methyl iodide (0.30 mL, 4.70 mmol) was added dropwise to a solution of thiazole **43a** (0.636 mg, 0.940 mmol) in DMF (5 mL) and the mixture was stirred at room temperature overnight. The reaction mixture was concentrated *in vacuo*, dissolved in the minimal amount of MeCN (5 mL) and Et₂O (50 mL) was added. The resulting precipitate was filtered under vacuum and washed with Et₂O (20 mL) to afford the title compound **44** as an orange solid (625 mg, 71%); δ_{H} (400 MHz, DMSO) 3.51 (1H, d, *J* 14.0, ArCHH), 3.57 (1H, d, *J* 14.0, ArCHH), 3.72 (1H, d, *J* 18.0, SCHH), 4.00 (1H, d, *J* 18.0, SCHH), 4.32 (3H, s, CH₃), 5.32 (1H, d, *J* 5.0, HNCHCHS), 5.89 (1H, dd, *J* 8.0, 5.0, HNCHCHS), 6.98 (1H, s, OCHAr), 7.17 – 7.38 (15H, m, 15 × ArCH), 8.53 (2H, m, 2 × ArCH_{pyridine}), 8.95 – 9.02 (3H, m, 2 × ArCH_{pyridine} and

ArCH_{thiazole}), 9.32 (1H, d, *J* 8.5, NH); *m/z* (ESI⁺) 691.1514 (100%, MH⁺, C₃₇H₃₂N₄O₄S₃ requires 691.1502), 694 (6), 693 (23), 692 (43). Mass spectrometry data was not reported in the literature; ¹H NMR data was reported with different multiplicity couplings but was in otherwise accordance with the literature.¹¹³

4-(2-{{[(6*R*,7*R*)-7-(2-{2-[2-(2-Azidoethoxy)ethoxy]ethoxy}acetamido)-2-carboxy-8-oxo-5-thia-1-azabicyclo[4.2.0]oct-2-en-3-yl]sulfanyl}-1,3-thiazol-4-yl)-1-methylpyridin-1-ium trifluoroacetate **48a** and 4-(2-{{[(6*R*,7*R*)-7-(2-{2-[2-azidoethoxy]ethoxy}acetamido)-2-carboxy-8-oxo-5-thia-1-azabicyclo[4.2.0]oct-3-en-3-yl]sulfanyl}-1,3-thiazol-4-yl)-1-methylpyridin-1-ium trifluoroacetate **49a**



Pyridine (60 μL, 0.732 mmol) was added to a suspension of iodide salt **44** (200 mg, 0.244 mmol) and PCl₅ (150 mg, 0.732 mmol) in CH₂Cl₂ (2 mL) at 0 °C and the mixture was stirred for 1 hour. The reaction mixture was cooled to -10 °C, MeOH (4 mL) was added and the mixture stirred at room temperature overnight. The mixture was evaporated to dryness *in vacuo* and triturated with Et₂O (10 mL) and MeCN (10 mL) to afford the amine intermediate **45** as a yellow solid which was used in the next step without further purification (130 mg, 76%); selected ¹H NMR data; δ_H (400 MHz, DMSO) 3.86 (1H, d, *J* 17.5, SCHH), 3.98 (1H, d, *J* 17.5, SCHH), 4.32 (3H, s, CH₃), 5.32 (1H, d, *J* 5.0, HNCHCHS), 5.41 (1H, d, *J* 5.0, HNCHCHS), 6.99 (1H, s, OCHAr), 7.18 – 7.41 (10H, m, 10 × ArCH), 8.55 (2H, d, *J* 7.0, 2 × ArCH_{pyridine}), 9.02 (2H, d, *J* 7.0, 2 × ArCH_{pyridine}), 9.07 (1H, s, ArCH_{thiazole}). A small amount of this was used in the next step.

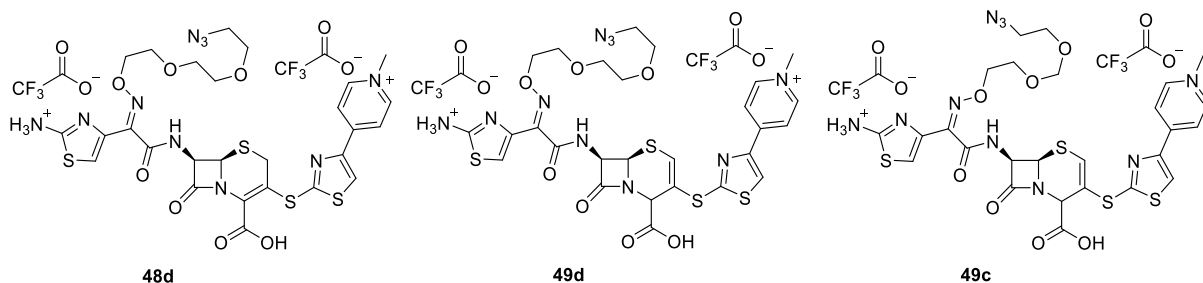
HATU (35 mg, 0.0873 mmol) was added to a solution of carboxylic acid **22** (20 mg, 0.0794 mmol) and diisopropylethylamine (0.058 mL, 0.334 mmol) in anhydrous DMF (0.3 mL) and the mixture was stirred at room temperature for 15 minutes. Amine intermediate **45** (62 mg, 0.0953 mmol) in anhydrous DMF (0.8 mL) was then added and the reaction mixture was stirred overnight. The reaction mixture was concentrated *in vacuo* and dissolved in dichloromethane (1

mL). Anisole (0.150 mL) and TFA (0.300 mL) were added and the reaction mixture stirred for 2 hours. The reaction mixture was concentrated *in vacuo* and the resulting crude residue was purified by preparative HPLC using an eluent of 5% - 95% MeCN: H₂O (0.1% TFA) to give Ceph-3 **48a** as a yellow solid which became an oil upon exposure to air (2 mg, 4%); ν_{\max} (ATR) / cm⁻¹ 3272 (N-H), 3080 (C-H), 2921 (C-H), 2881 (C-H). 2106 (N=N=N), 1771 (C=O), 1674 (C=O), 1638 (C=O); δ_{H} (400 MHz, D₂O) 3.43 – 3.48 (2H, m, CH₂). 3.54, 3.92 (2H, ABq, *J*_{A-B} 17.5, SCH₂), 3.65 – 3.79 (10H, m, 5 × CH₂), 4.18 (2H, s, CH₂), 4.32 (3H, s, CH₃), 5.28 (1H, d, *J* 5.0, HNCHCHS), 5.74 (1H, d, *J* 5.0, HNCHCHS), 8.32 (2H, d, *J* 7.0, 2 × ArCH_{pyridine}), 8.50 (1H, s, ArCH_{thiazole}), 8.72 (2H, d, *J* 7.0, 2 × ArCH_{pyridine}); δ_{C} (101 MHz, D₂O) 29.0 (SCH₂), 47.3 (CH₃), 50.1 (CH₂C=O), 57.7 (HNCHCHS), 59.2 (HNCHCHS), 69.2 (CH₂), 69.3 (CH₂), 69.5 (2 × CH₂), 69.6 (CH₂), 70.4 (CH₂), 106.7 (SC=CN) 123.5 (2 × ArCH_{pyridine}), 127.0 (ArCH_{thiazole}), 139.3 (SC=CN), 145.27 (2 × ArCH_{pyridine}), 147.5 (ArC), 149.3 (ArC), 163.7 (C=O), 167.5 (C=O), 167.7 (SC=N), 173.4 (C=O); *m/z* (ESI⁺) 622.1223 (100%, MH⁺, C₂₄H₂₉N₇O₇S₃ requires 622.1207), 1243 (9), 640 (14), 632 (1), 624 (75), 623 (91), 610 (6), 298 (9). Carbon NMR data was assigned by HMBC and HSQC correlations.

Also obtained was the Δ^2 isomer **49a** as a yellow solid which became an oil upon exposure to air (8.5 mg, 16%); $[\alpha]_{\text{D}}^{23} + 190$ (*c* 1.00 in MeOH); ν_{\max} (ATR) / cm⁻¹ 3250 (N-H), 3050 (C-H), 2922 (C-H), 2105 (N=N=N), 1765 (C=O), 1674 (C=O), 1637 (C=O); δ_{H} (400 MHz, D₂O) 3.33 – 3.38 (2H, m, CH₂). 3.57 – 3.77 (10 H, m, 5 × CH₂), 4.07 – 4.18 (2H, app d, CH₂), 4.26 (3H, s, CH₃), 5.09 (1H, d, *J* 1.0, SCCHN), 5.35 (1H, d, *J* 4.0, HNCHCHS), 5.38 (1H, d, *J* 4.0, HNCHCHS), 7.24 (1H, d, *J* 1.0, SCH=S), 8.30 (2H, d, *J* 7.0, 2 × ArCH_{pyridine}), 8.41 (1H, s, ArCH_{thiazole}), 8.65 (2H, d, *J* 7.0, 2 × ArCH_{pyridine}). δ_{C} (126 MHz, D₂O) 47.4 (CH₃), 50.1 (CH₂C=O), 52.9 (CH), 55.1 (HNCHCHS), 59.8 (HNCHCHS), 69.2 (CH₂), 69.4 (CH₂), 69.5 (2 × CH₂), 69.6 (CH₂), 70.6 (CH₂), 113.8 (C=CH), 123.7 (2 × ArCH_{pyridine}), 126.1 (ArCH_{thiazole}), 134.3 (SC=CN), 145.3 (2 × ArCH_{pyridine}), 147.6 (ArC), 149.3 (ArC), 165.3, 169.2, 171.7 (C=O), 173.3 (C=O); *m/z* (ESI⁺) 622.1225 (100%, MH⁺, C₂₄H₂₉N₇O₇S₃ requires 622.1207), 624 (19), 623 (31), 600 (9), 615 (1), 612 (1), 354 (5).

4-(2-[[[(6*R*,7*R*)-7-[(2*Z*)-2-(2-Azaniumyl-1,3-thiazol-4-yl)-11-azido-4,7,9-trioxa-3-azaundec-2-enamido]-2-carboxy-8-oxo-5-thia-1-azabicyclo[4.2.0]oct-3-en-3-yl]sulfanyl]-1,3-thiazol-4-yl)-1-methylpyridin-1-ium ditrifluoroacetate **48d**, 4-(2-[[[(6*R*,7*R*)-7-[(2*E*)-2-(2-Azaniumyl-1,3-thiazol-4-yl)-12-azido-4,7,10-trioxa-3-azadodec-2-enamido]-2-carboxy-8-oxo-5-thia-1-

azabicyclo[4.2.0]oct-3-en-3-yl)sulfanyl}-1,3-thiazol-4-yl)-1-methylpyridin-1-ium ditrifluoroacetate **49d** and 4-(2-{{(6*R*,7*R*)-7-[(2*E*)-2-(2-Azaniumyl-1,3-thiazol-4-yl)-12-azido-4,7,10-trioxa-3-azadodec-2-enamido]-2-carboxy-8-oxo-5-thia-1-azabicyclo[4.2.0]oct-2-en-3-yl)sulfanyl}-1,3-thiazol-4-yl)-1-methylpyridin-1-ium ditrifluoroacetate **49c**

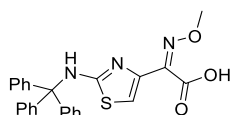


HATU (21 mg, 0.0554 mmol) was added to a solution of carboxylic acid **22** (30 mg, 0.0504 mmol) and DIPEA (0.37 mL, 0.212 mmol) in anhydrous DMF (0.5 mL) and the mixture was stirred at room temperature for 15 minutes. Amine intermediate **45** (39 mg, 0.0605 mmol) in anhydrous DMF (0.5 mL) was then added and the reaction mixture was stirred overnight. The reaction mixture was concentrated *in vacuo* and dissolved in CH₂Cl₂ (1 mL). Anisole (0.150 mL) and TFA (0.30 mL) were added and the reaction mixture stirred overnight. The reaction mixture was concentrated *in vacuo* and the resulting crude residue was purified by preparative HPLC using an eluent of 10% - 35% MeCN: H₂O (0.1% TFA) to give **48d** an off-white solid which became an oil upon exposure to air (2.5 mg, 5%); δ_{H} (400 MHz, D₂O) 3.36 (2H, t, *J* 5.0, CH₂), 3.52 (2H, d, *J* 17.5, SCHH), 3.61 (2H, t, *J* 5.0, CH₂), 3.62 – 3.69 (4H, m, 2 × CH₂), 3.85 – 3.95 (3H, m, CH₂ + SCHH), 4.29 (3H, s, CH₃), 4.52 – 4.58 (2H, m, CH₂), 5.31 (1H, d, *J* 5.0, HNCHCHS), 5.79 (1H, d, *J* 5.0, HNCHCHS), 7.74 (1H, s, ArCH_{aminothiazole}), 8.30 (2H, d, *J* 7.0, 2 × ArCH_{pyridine}), 8.48 (1H, s, ArCH_{thiazole}), 8.69 (2H, d, *J* 7.0, 2 × ArCH_{pyridine}); *m/z* (ESI⁺) 733.1087 (5%, MH⁺, C₂₇H₂₉N₁₀O₇S₄ requires 733.1098), 368 (26), 367 (100), 245 (18), 231 (42), 209 (21), 113 (29).

Also obtained was E oxime of Δ^2 isomer **49d** as an off-white solid which became an oil upon exposure to air (2.2 mg, 5%); δ_{H} (400 MHz, D₂O) 3.36 (2H, t, *J* 5.0, CH₂), 3.60 (2H, t, *J* 5.0, CH₂), 3.62 – 3.70 (4H, m, 2 × CH₂), 3.84 – 3.89 (2H, m, CH₂), 4.28 (3H, s, CH₃), 4.50 – 4.56 (2H, m, CH₂), 5.01 (1H, s, SCCHN), 5.41 (1H, d, *J* 4.0, HNCHCHS), 5.48 (1H, d, *J* 4.0, HNCHCHS), 7.24 (1H, s, SCH=S), 7.69 (1H, s, ArCH_{aminothiazole}), 8.33 (2H, d, *J* 7.0, 2 × ArCH_{pyridine}), 8.43 (1H, s, ArCH_{thiazole}), 8.66 (2H, d, *J* 7.0, 2 × ArCH_{pyridine}); *m/z* (ESI⁺) 733.1085 (13%, MH⁺, C₂₇H₂₉N₁₀O₇S₄ requires 733.1098), 405 (18), 368 (65), 367 (100), 363 (22), 359 (36), 346 (20), 208 (22).

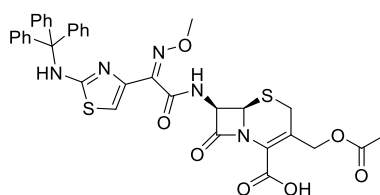
Also obtained was Z oxime of Δ^2 isomer **49c** as an off-white solid which became an oil upon exposure to air (2.5 mg, 5%); δ_{H} (400 MHz, D_2O) 3.36 (2H, t, J 5.0, CH_2), 3.59 (2H, t, J 5.0, CH_2) 3.60 – 3.70 (4H, m, $2 \times \text{CH}_2$), 3.79 – 3.88 (2H, m, CH_2), 4.27 (3H, s, CH_3), 4.36 – 4.45 (2H, m, CH_2), 5.02 (1H, s, SCCHN), 5.43 (1H, d, J 4.0, HNCHCHS), 5.50 (1H, d, J 4.0, HNCHCHS), 7.13 (1H, s, $\text{SCH}=\text{S}$), 7.26 (1H, s, $\text{ArCH}_{\text{aminothiazole}}$), 8.32 (2H, d, J 7.0, $2 \times \text{ArCH}_{\text{pyridine}}$), 8.42 (1H, s, $\text{ArCH}_{\text{thiazole}}$), 8.65 (1 H, d, J 7.0, $2 \times \text{ArCH}_{\text{pyridine}}$). m/z (ESI⁺) 733.1095 (21%, MH^+ , $\text{C}_{27}\text{H}_{29}\text{N}_{10}\text{O}_7\text{S}_4$ requires 733.1098), 734 (9), 378 (13), 368 (72), 367 (100), 364 (27), 347 (6), 346 (28), 208 (13).

(2Z)-2-(Methoxyimino)-2-{2-[(triphenylmethyl)amino]-1,3-thiazol-4-yl}acetic acid **S1**



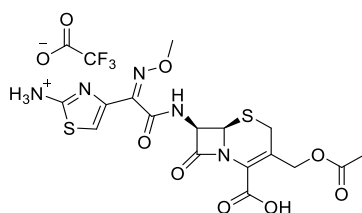
Triphenyl chloride (1.52 g, 5.47 mmol) was added to a suspension of 2-amino- α -(methoxyimino)-4-thiazoleacetic acid, predominantly syn (1.00 g, 4.97 mmol) and Et_3N (1.52 mL, 10.93 mmol) in CHCl_3 : DMF (25 mL, 2:1) and the mixture was stirred at room temperature overnight. The reaction mixture was quenched 1 M hydrochloric acid (25 mL) and the organic phase separated. The organic phase was washed with brine (2×20 mL), dried over MgSO_4 , filtered and concentrated *in vacuo*. Purification by flash column chromatography using silica and an eluent of 10% methanol: dichloromethane afforded the title compound **S1** as an off white solid (805 mg, 37%); ν_{max} (ATR) / cm^{-1} 3058 (C-H), 3024 (C-H), 298 (C-H), 1707 (C=O), 1532 (C=C); δ_{H} (400 MHz, CDCl_3) 3.94 (3H, s, CH_3), 4.68 (1H, br s, OH), 6.59 (1H, s, $\text{ArCH}_{\text{thiazole}}$), 7.26 – 7.37 (15H, m, $15 \times \text{ArCH}$), 9.86 (1H, s, NH). Infra-red data was not reported in the literature; ^1H NMR data was in general accordance with the literature.²⁰⁸

(6R,7R)-3-[(Acetyloxy)methyl]-7-[(2Z)-2-(methoxyimino)-2-{2-[(triphenylmethyl)amino]-1,3-thiazol-4-yl}acetamido]-8-oxo-5-thia-1-azabicyclo[4.2.0]oct-2-ene-2-carboxylic acid **S2**



HATU (356 mg, 0.937 mmol) was added a solution of carboxylic acid **S1** (378 mg, 0.852 mmol) and DIPEA (330 μ L, 1.87 mmol) in anhydrous DMF (8 mL) and the mixture was stirred at room temperature for 15 minutes. 7-Aminocephalosporanic acid (349 mg, 1.28 mmol) was then added and the reaction mixture was stirred overnight. H₂O (30 mL) was added and the mixture extracted with EtOAc (50 mL). The organic extract was washed with brine (2 \times 20 mL), water (20 mL), Na₂SO₄, filtered and concentrated *in vacuo*. Purification by flash column chromatography using silica gel and an eluent of 90: 10: 1 dichloromethane: methanol: acetic acid gave the title compound **S2** as a brown solid (472 mg, 79%); ν_{\max} (ATR) / cm⁻¹ 3363 (N-H), 3055 (C-H), 3029 (C-H), 3237 (C-H), 1780 (C=O), 1738 (C=O), 1730 (C=O), 1675 (C=N), 1525 (C=C); δ_{H} (400 MHz, CDCl₃) 2.03 (3H, s, CH₃). 3.31 (1H, d, *J* 18.5, SCHH), 3.53 (1H, d, *J* 18.5, SCHH), 4.04 (3H, s, OCH₃), 4.85 (1H, d, *J* 13.5, OCHHC=O), 5.02 (1H, d, *J* 5.0, HNCHCHS), 5.07 (1H, d, *J* 13.5, OCHHC=O), 5.79 (1H, dd, *J* 8.0, 5.0, HNCHCHS), 6.76 (1H, s, ArCH_{thiazole}), 7.28 – 7.36 (15H, m, 15 \times ArCH), 7.58 (1H, d, *J* 7.5, NH). 9.20 (1H, br s, COOH); *m/z* (ESI⁺) 698.1762 (100%, MH⁺, C₃₅H₃₂N₅O₇S₂ requires 698.1738), 1395 (1), 699 (51), 638 (1), 494 (1), 243 (54).

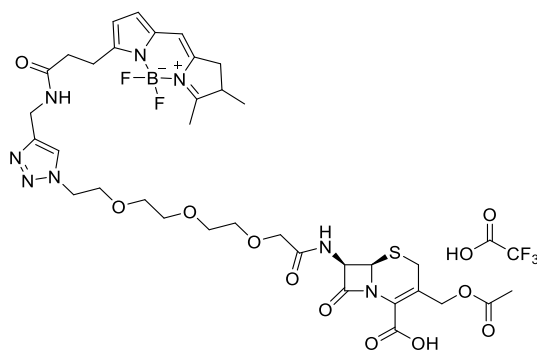
(6*R*,7*R*)-3-[(Acetyloxy)methyl]-7-[(2*Z*)-2-(2-amino-1,3-thiazol-4-yl)-2-(methoxyimino)acetamido]-8-oxo-5-thia-1-azabicyclo[4.2.0]oct-2-ene-2-carboxylic acid; trifluoroacetic acid **51**



Trifluoroacetic acid (0.6 mL) was added to Boc-protected aminothiazole **S2** (145 mg, 0.208 mmol) in CH₂Cl₂ (2 mL) and the solution was stirred at room temperature for 16 hours. No reaction was observed. The CH₂Cl₂ was removed in *in vacuo* and MeOH (2 mL) and trifluoroacetic acid (0.6 mL) were added. The reaction mixture was stirred at 35 °C for 1 hour and then at 50 °C for a further 2 hours. The mixture was then concentrated *in vacuo* and the resulting residue triturated with Et₂O (3 \times 5 mL) and filtered. Purification by preparative HPLC using an eluent of 13% MeCN: H₂O (0.1% TFA) gave the title compound **51** as a white solid (52 mg, 49%); δ_{H} (400 MHz, MeOD) 2.07 (3H, s, CH₃). 3.51 (1H, d, *J* 18.0, SCHH), 3.71 (1H, d, *J* 18.0, SCHH), 4.05 (3H, s, OCH₃), 4.85 (1H, d, *J* 13.5, OCHHC=O), 5.13 (1H, d, *J* 13.5,

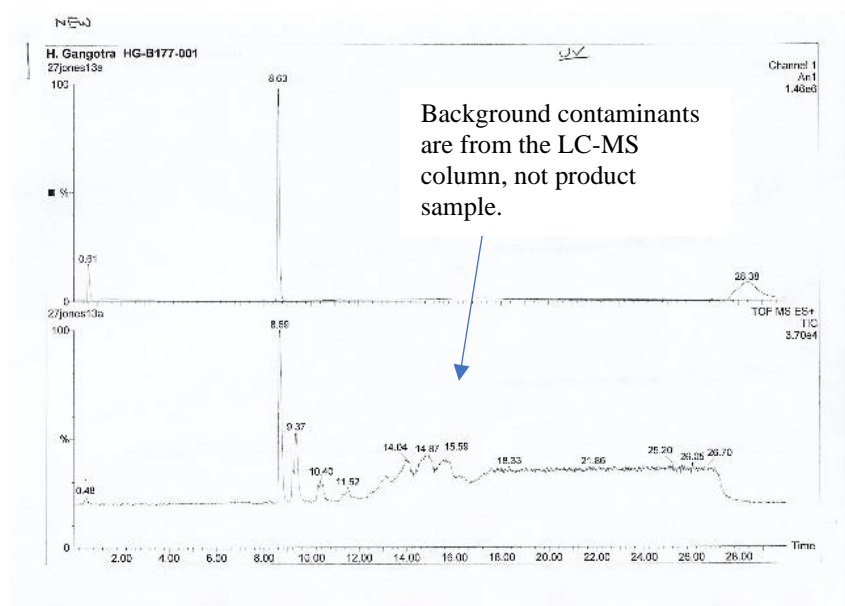
OCHHC=O), 5.18 (1H, d, *J* 5.0, HNCHCHS), 5.88 (1 H, d, *J* 5.0, HNCHCHS), 7.03 (1H, s, *J* 5.0, ArCH_{thiazole}); *m/z* (ESI⁺) 456.0641 (100%, MH⁺, C₁₆H₁₈N₅O₇S₂ requires 456.0642), 458 (15), 457 (59), 447 (1), 425 (10).

4-[2-({[1-(2-{2-[2-({[(6*R*,7*R*)-3-[(Acetyloxy)methyl]-2-carboxy-8-oxo-5-thia-1-azabicyclo[4.2.0]oct-2-en-7-yl]carbamoyl}methoxy)ethoxy]ethoxy}ethyl)-1*H*-1,2,3-triazol-4-yl)methyl}carbamoyl)ethyl]-2,2-difluoro-1,1,2-dimethyl-1*λ*⁵,3-diaza-2-boratricyclo[7.3.0.0^{3,7}]dodeca-1(12),4,6,8-tetraen-1-ylum-2-uide; trifluoroacetic acid **52**

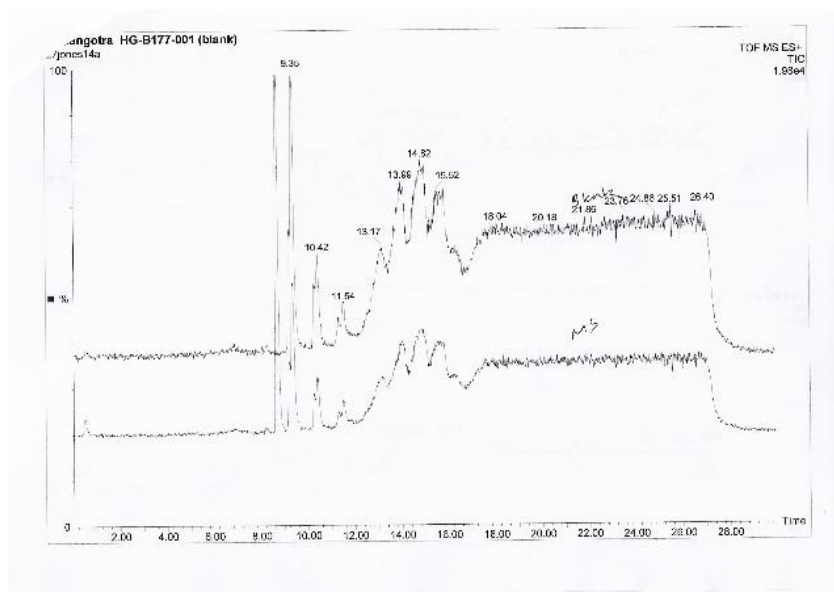


Ascorbic acid (0.350 mg, 0.00197 mmol) in H₂O (20 μ L) was added to a solution of azide **23** (1.20 mg, 0.00246 mmol) and BDP-FL alkyne (0.80 mg, 0.00246 mmol) in DMSO (100 μ L) and *t*-BuOH (100 μ L). This mixture was stirred for 2 minutes and then CuSO₄ (0.160 mg, 0.000984 mmol) in H₂O (20 μ L) was added and the reaction mixture stirred for 2 hours. The reaction mixture was then purified directly by preparative HPLC using an eluent of 35% MeCN: H₂O (0.1% TFA) to afford the title compound **52** as an orange solid (0.9 mg, 45%); λ_{max} (MeOH)/nm 503 ($\epsilon/\text{dm}^3 \text{ mol}^{-1} \text{ cm}^{-1}$ 68 023); *m/z* (ESI⁺) 817.2927 (59%, MH⁺, C₃₅H₄₄¹¹BF₂N₈O₁₀S, requires 817.2957), 224 (82), 179 (37), 106 (100); LC-MS data demonstrating purity below (UV₅₀₀).

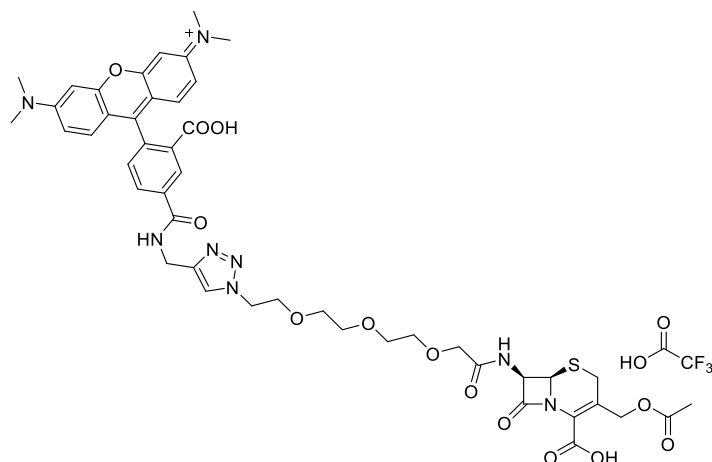
Sample:



Blank (illustrated to highlight contaminants on the LC-MS column):

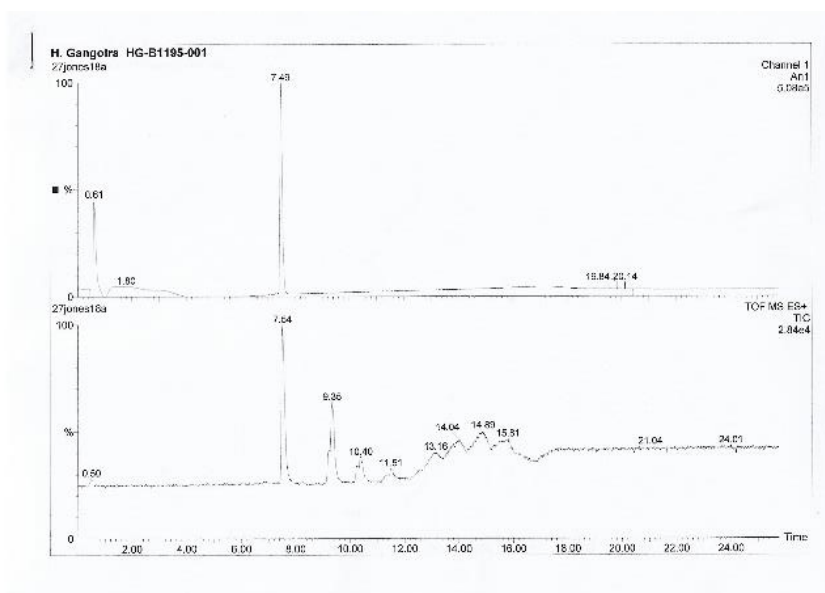


9-[4-({[1-(2-{2-[2-({[(6R,7R)-3-[(Acetyloxy)methyl]-2-carboxy-8-oxo-5-thia-1-azabicyclo[4.2.0]oct-2-en-7-yl]carbamoyl}methoxy)ethoxy]ethoxy}ethyl)-1H-1,2,3-triazol-4-yl]methyl}carbamoyl)-2-carboxyphenyl]-6-(dimethylamino)-N,N-dimethyl-3H-xanthen-3-iminium; trifluoroacetic acid **53**

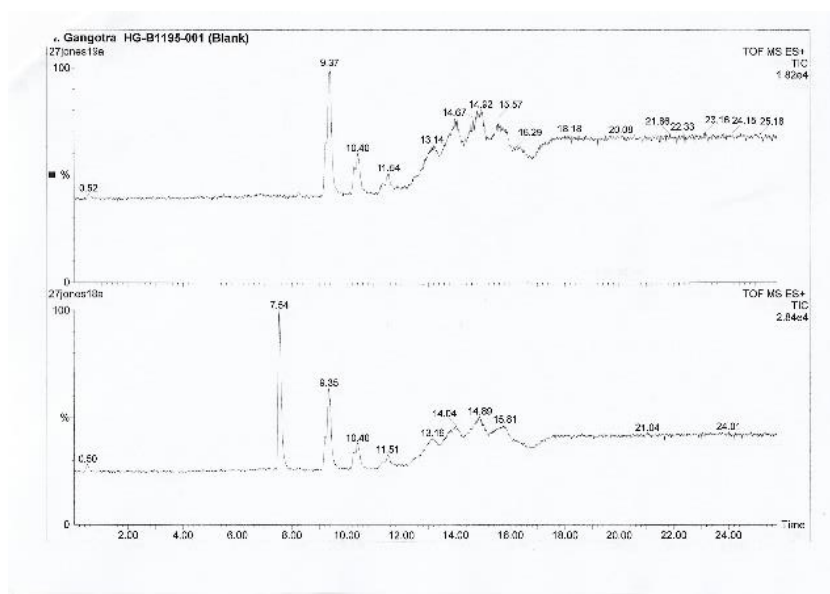


Ascorbic acid (0.301 mg, 0.00171 mmol) in H₂O (20 μL) was added to a solution of azide **23** (0.52 mg, 0.00107 mmol) and TAMRA alkyne, 5-isomer (0.50 mg, 0.00107 mmol) in DMSO (200 μL). This was stirred for 2 minutes and then CuSO₄ (0.137 mg, 0.000856 mmol) in H₂O (20 μL) was added and the reaction mixture stirred for 16 hours. The reaction mixture was then purified directly by preparative HPLC using an eluent of 5 – 95% MeCN: H₂O (0.1% TFA) over 20 minutes to afford the title compound **53** as a pink solid (1.0 mg, 98%); λ_{max}(MeCN)/nm 204 (ε/dm³ mol⁻¹ cm⁻¹ 28 802); *m/z* (ESI⁺) 955.3255 (39%, MH⁺, C₄₆H₅₁N₈O₁₃S requires 955.3291), 479 (55); 478 (100); LC-MS data demonstrating purity below (UV₅₄₀).

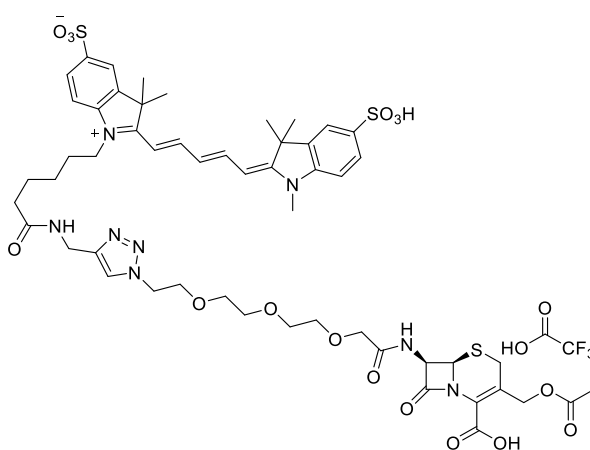
Sample:



Blank:



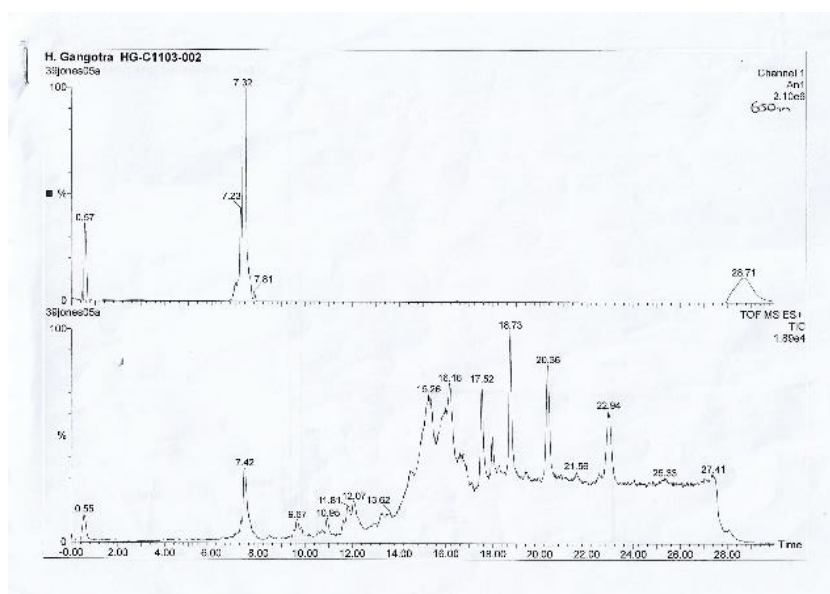
1-[5-({[1-(2-{2-[2-({[(6*R*,7*R*)-3-[(Acetyloxy)methyl]-2-carboxy-8-oxo-5-thia-1-azabicyclo[4.2.0]oct-2-en-7-yl]carbamoyl}methoxy)ethoxy}ethoxy}ethyl)-1*H*-1,2,3-triazol-4-yl]methyl]carbamoyl)pentyl]-3,3-dimethyl-2-[(1*E*,3*E*)-5-[(2*E*)-1,3,3-trimethyl-5-sulfo-2,3-dihydro-1*H*-indol-2-ylidene]penta-1,3-dien-1-yl]-3*H*-indol-1-ium-5-sulfonate; trifluoroacetic acid **54**



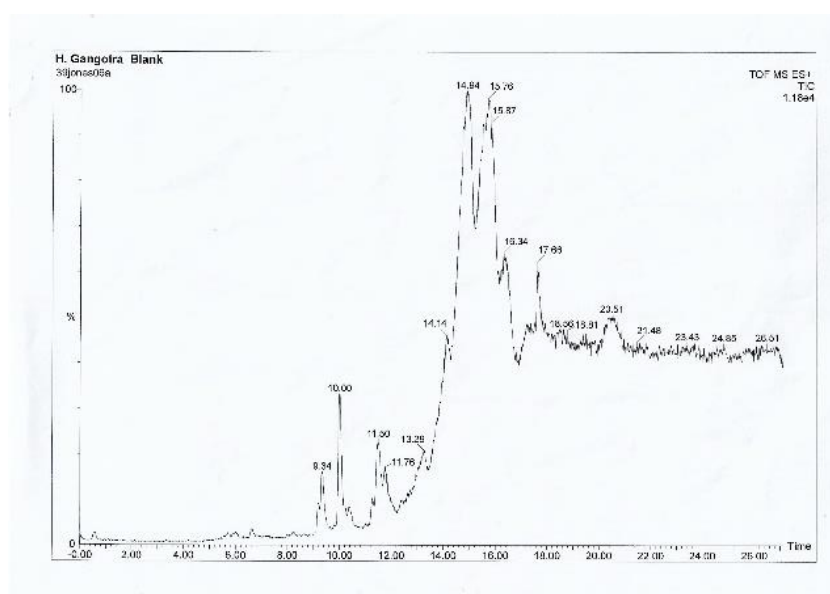
Ascorbic acid (0.176 mg, 0.00100 mmol) in H₂O (20 μ L) was added to a solution of **23** (0.340 mg, 0.000688 mmol) and Alexa Fluor™ 647 Alkyne, triethylammonium salt (0.500 mg, 0.000625 mmol) in DMSO (150 μ L). This was stirred for 2 minutes and then CuSO₄ (0.080 mg, 0.000500 mmol) in H₂O (20 μ L) was added and the reaction mixture stirred for 15 hours. Further additions of ascorbic acid (0.176 mg, 0.00100 mmol) in H₂O (20 μ L) and CuSO₄ (0.080

mg, 0.000500 mmol) were added and stirring continued for 6 hours. The reaction mixture then was purified directly by preparative HPLC using an eluent of 23% MeCN: H₂O (0.1% TFA) to afford the title compound **54** as a blue solid (0.3 mg, 37%); $\lambda_{\text{max}}(\text{MeCN})/\text{nm}$ 658 ($\epsilon/\text{dm}^3 \text{ mol}^{-1} \text{ cm}^{-1}$ 42 712); m/z (ESI⁺) 1167.3846 (52%, MH⁺, C₅₃H₆₇N₈O₁₆S₃ requires 1167.3832), 581 (59), 581 (45), 370 (82), 325 (90), 309 (56), 292 (36), 242 (65), 112 (100); LC-MS data demonstrating purity below (UV₆₅₀). N.B. The chemical structure and corresponding IUPAC name has been predicted based on molecular formula.

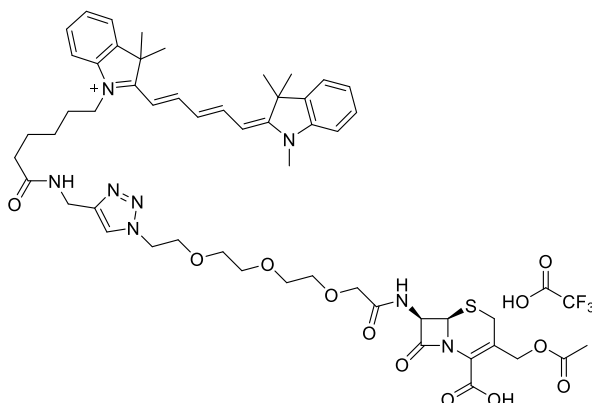
Sample:



Blank:

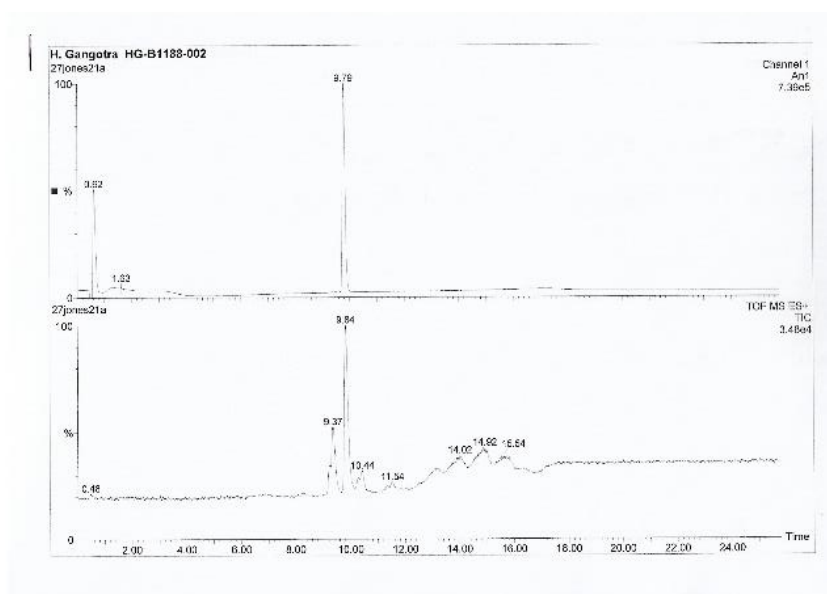


1-[5-({[1-(2-{2-[2-({[(6*R*,7*R*)-3-[(Acetyloxy)methyl]-2-carboxy-8-oxo-5-thia-1-azabicyclo[4.2.0]oct-2-en-7-yl]carbamoyl}methoxy)ethoxy]ethoxy}ethyl)-1*H*-1,2,3-triazol-4-yl)methyl}carbamoyl)pentyl]-3,3-dimethyl-2-[(1*E*,3*E*)-5-[(2*E*)-1,3,3-trimethyl-2,3-dihydro-1*H*-indol-2-ylidene]penta-1,3-dien-1-yl]-3*H*-indol-1-ium; trifluoroacetic acid **55**

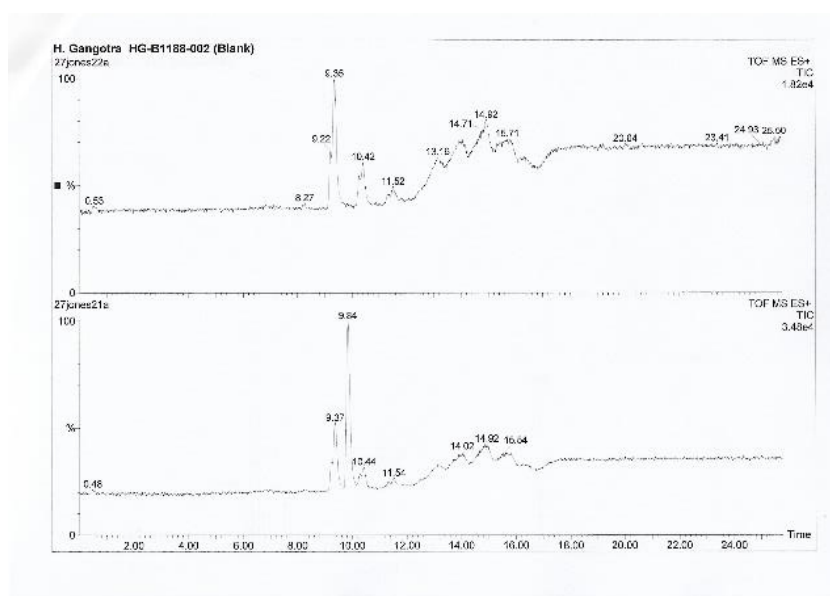


Ascorbic acid (0.510 mg, 0.00288 mmol) in H₂O (20 μ L) was added to a solution of azide **22** (0.92 mg, 0.00180 mmol) and Cyanine5 alkyne (1.00 mg, 0.00180 mmol) in DMSO (200 μ L). This was stirred for 2 minutes and then CuSO₄ (0.230 mg, 0.00144 mmol) in H₂O (20 μ L) was added and the reaction mixture stirred for 17 hours. The reaction mixture was then purified directly by preparative HPLC using an eluent of 50% MeCN: H₂O (0.1% TFA) to afford the title compound **55** as a blue solid (1.4 mg, 77%); λ_{max} (MeCN)/nm 641 ($\epsilon/\text{dm}^3 \text{ mol}^{-1} \text{ cm}^{-1}$ 11 686); m/z (ESI⁺) 1007.4681 (41%, MH⁺, C₅₃H₆₇N₈O₁₀S requires 1007.4695), 948 (6), 504 (100), 474 (4); LC-MS data demonstrating purity below (UV₆₅₀).

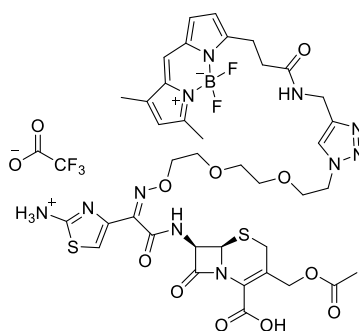
Sample:



Blank:



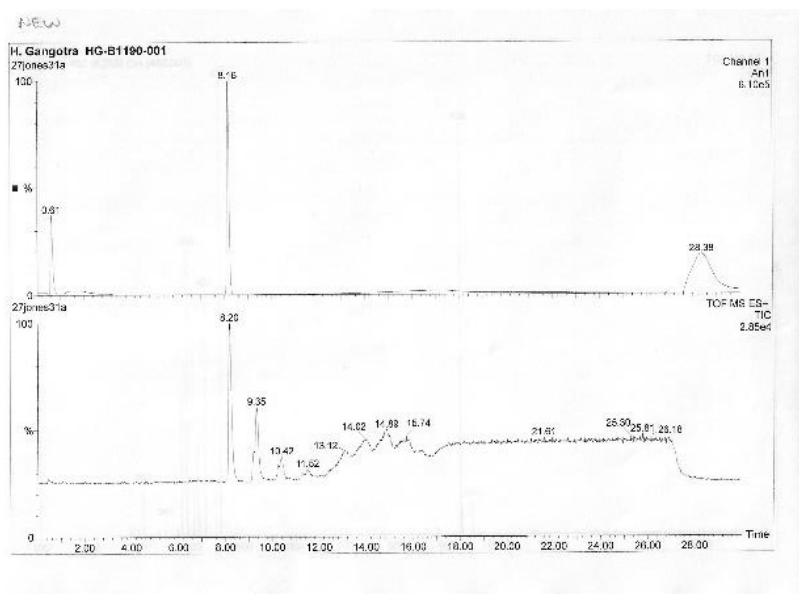
4-{2-[(1-[(1Z)-1-[(6R,7R)-3-[(Acetyloxy)methyl]-2-carboxy-8-oxo-5-thia-1-azabicyclo[4.2.0]oct-2-en-7-yl]carbamoyl}-1-(2-azaniumyl-1,3-thiazol-4-yl)-3,6,9-trioxa-2-azaundec-1-en-11-yl]-1H-1,2,3-triazol-4-yl)methyl]carbamoyl]ethyl}-2,2-difluoro-10,11-dimethyl-1λ⁵,3-diaza-2-boratricyclo[7.3.0.0^{3,7}]dodeca-1(12),4,6,8-tetraen-1-ylum-2-uide trifluoroacetate **56**



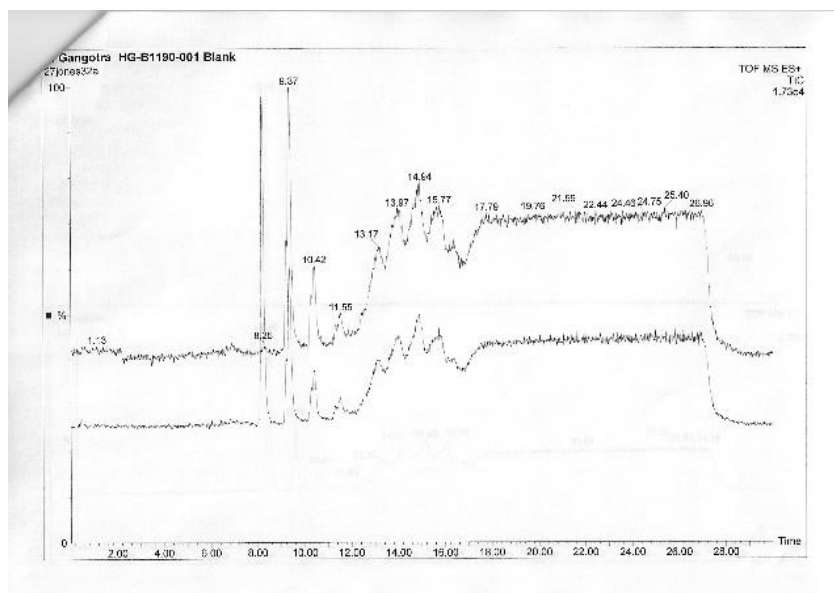
Ascorbic acid (0.416 mg, 0.00236 mmol) in H₂O (20 μL) was added to a solution of azide **39** (2.8 mg, 0.00295 mmol) and BDP-FL alkyne (0.97 mg, 0.00295 mmol) in DMSO (300 μL). This was stirred for 2 minutes and then CuSO₄ (0.188 mg, 0.000118 mmol) in H₂O (20 μL) was added and the reaction mixture stirred for 20 hours. Further additions of ascorbic acid (0.416 mg, 0.00236 mmol) and CuSO₄ (0.470 mg, 0.000295 mmol) were added and stirring continued for 2 hours. The reaction mixture was then purified directly by preparative HPLC using an eluent of 33% MeCN: H₂O (0.1% TFA) to afford the title compound **56** as an orange

solid (1.8 mg, 58%); $\lambda_{\text{max}}(\text{MeCN})/\text{nm}$ 503 ($\epsilon/\text{dm}^3 \text{ mol}^{-1} \text{ cm}^{-1}$ 28,944); m/z (ESI⁺) 928.2871 (35%, MH⁺, C₃₈H₄₅¹¹BF₂N₁₁O₁₀S₂ requires 928.2848), 309 (49), 224 (53), 130 (46), 114 (41), 106 (96), 102 (74), 101 (100); LC-MS data demonstrating purity below (UV₅₀₀).

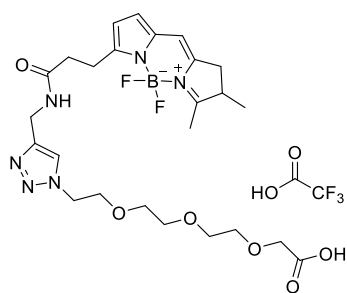
Sample:



Blank:

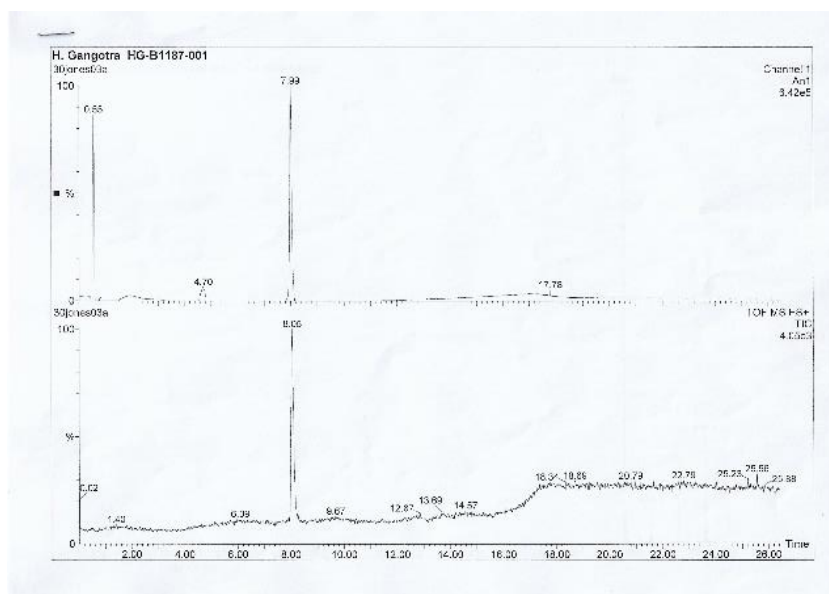


4-[2-([1-(2-[2-(2-(Carboxymethoxy)ethoxy]ethoxy)ethyl)-1H-1,2,3-triazol-4-yl]methyl)carbamoyl)ethyl]-2,2-difluoro-11,12-dimethyl-1 λ^5 ,3-diaza-2-boratricyclo[7.3.0.0^{3,7}]dodeca-1(12),4,6,8-tetraen-1-ylum-2-uide; trifluoroacetic acid **57**

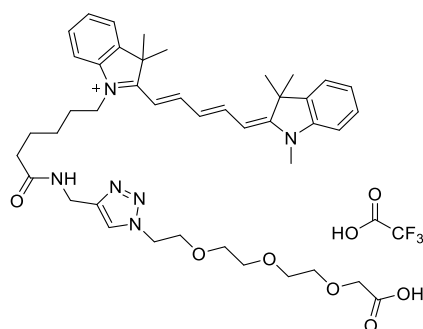


Ascorbic acid (0.600 mg, 0.00343 mmol) in H₂O (20 μ L) was added to a solution of azide **22** (1.00 mg, 0.00429 mmol) and BDP-FL alkyne (1.40 mg, 0.00429 mmol) in DMSO (100 μ L) and ^tBuOH (100 μ L). This was stirred for 2 minutes and then CuSO₄ (0.270 mg, 0.00172 mmol) in H₂O (20 μ L) was added and the reaction mixture stirred for 2 hours. The reaction mixture was then purified directly by preparative HPLC using an eluent of 35% MeCN: H₂O (0.1% TFA) to afford the title compound **57** as an orange solid (2.0 mg, 82%); λ_{max} (MeCN)/nm 503 ($\epsilon/\text{dm}^3 \text{ mol}^{-1} \text{ cm}^{-1}$ 43 315); m/z (ESI⁺) 563.2575 (9%, MH⁺, C₂₅H₃₄¹¹BF₂N₆O₆ requires 563.2595), 607 (24), 585 (11), 545 (100); LC-MS data demonstrating purity below (UV₅₀₀).

Sample:

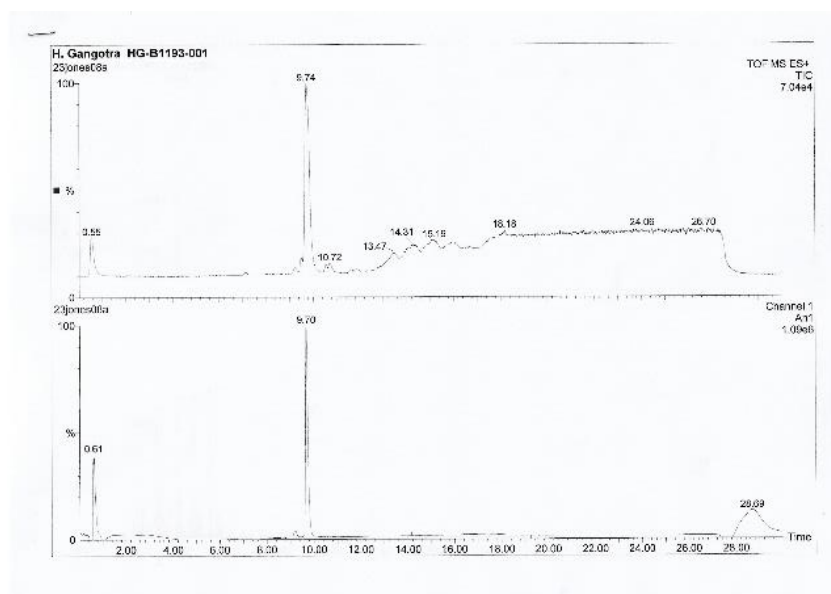


1-[5-({[1-(2-{2-[2-(Carboxymethoxy)ethoxy]ethoxy}ethyl)-1H-1,2,3-triazol-4-yl]methyl}carbamoyl)pentyl]-3,3-dimethyl-2-[(1E,3E)-5-[(2E)-1,3,3-trimethyl-2,3-dihydro-1H-indol-2-ylidene]penta-1,3-dien-1-yl]-3H-indol-1-ium; trifluoroacetic acid **58**

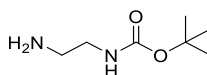


Ascorbic acid (0.507 mg, 0.00288 mmol) in H₂O (20 μL) was added to a solution of azide **22** (0.42 mg, 0.00180 mmol) and Cyanine5 alkyne (1.00 mg, 0.00180 mmol) in DMSO (200 μL). This was stirred for 2 minutes and then CuSO₄ (0.230 mg, 0.00144 mmol) in H₂O (20 μL) was added and the reaction mixture stirred for 16 hours. The reaction mixture was then purified directly by preparative HPLC using an eluent of 50% MeCN: H₂O (0.1% TFA) to afford the title compound **58** as a blue solid (1.4 mg, 77%); λ_{max}(MeCN)/nm 641 (ε/dm³ mol⁻¹ cm⁻¹ 58 320); *m/z* (ESI⁺) 753.4317 (100%, MH⁺, C₄₆H₅₇N₆O₆ requires 753.4334), 377 (100), 354 (6), 330 (25); LC-MS data demonstrating purity below (UV₆₅₀).

Sample:

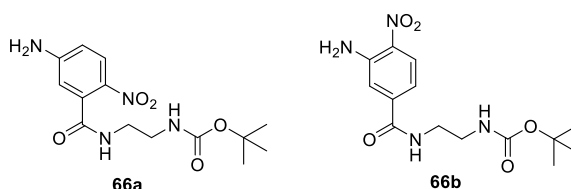


tert-Butyl *N*-(2-aminoethyl)carbamate **65**



Di-*tert*-butyl dicarbonate (1.09 g, 4.99 mmol) in DCM (50 mL) was added to a stirring solution of ethylenediamine (29.92 mmol, 2 mL) in DCM (50 mL) over 30 minutes and then stirred at room temperature overnight. The mixture was concentrated *in vacuo* and the residue partitioned between EtOAc (100 mL) and 1 M NaOH (50 mL). The organic extract was separated and the aqueous layer extracted with EtOAc (2 × 50 mL). The combined organic extracts were dried over Na₂SO₄, filtered and evaporated to dryness *in vacuo* to afford the title compound **65** as a clear oil (732 mg, 92%) that was used without further purification; δ_H (400 MHz, CDCl₃) 1.47 (9H, s, 3 × CH₃), 2.82 (2H, t, *J* 6.0, CH₂), 3.23 – 3.15 (2H, m, CH₂), 4.87 (1H, s, NH). ¹H NMR data was in accordance with the literature.²⁰⁹

tert-Butyl *N*-{2-[(5-amino-2-nitrophenyl)formamido]ethyl}carbamate **66a** and *tert*-butyl *N*-{2-[(3-amino-4-nitrophenyl)formamido]ethyl}carbamate **66b**

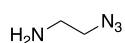


HATU (460 mg, 1.21 mmol) was added to a solution of 5-amino-2-nitrobenzoic acid (200 mg, 1.10 mmol), Boc protected amine **65** (352 mg, 2.20 mmol), DIPEA (420 μL, 2.42 mmol) in anhydrous DMF (10 L) and the mixture was stirred at room temperature overnight. The mixture was diluted with EtOAc (30 mL) and partitioned with H₂O (20 mL). The aqueous layer was separated and extracted with EtOAc (4 × 15 mL). The combined organic extracts were washed sequentially with sat. aq. NaHCO₃ (20 mL) and brine (20 mL) and then dried over Na₂SO₄, filtered and concentrated *in vacuo*. Purification by flash column chromatography using silica gel and an eluent of 70% ethyl acetate: petroleum ether 40 – 60 afforded the title compound **66a** as a yellow solid (147 mg, 41%); m.p. 85 – 86 °C; ν_{max} (ATR) / cm⁻¹ 3336 (N-H), 3230 (N-H), 2981 (C-H), 2930 (C-H), 1637 (C=O), 1584 (C=O), 1531 (N-O) 1503 (N-O); δ_H (400 MHz, MeOD) 1.47 (9H, s, 3 × CH₃). 3.27 – 3.32 (2H, m, CH₂), 3.40 – 3.47 (2H, m, CH₂), 6.56 – 6.51 (1H, m, ArCH), 6.66 – 6.71 (1H, m, ArCH), 7.99 (1H, app d, *J* 1.5, ArCH); δ_C (101 MHz, MeOD) 28.7 (3 × CH₃), 40.6 (CH₂), 40.9 (CH₂), 80.2 (CCH₃), 113.2 (ArCH), 114.1 (ArCH), 128.7 (ArCH), 134.9 (ArC), 137.5 (ArC), 156.2 (ArC), 158.5 (C=O), 171.5 (C=O); *m/z* (ESI⁺) 347.134 (100%, M+Na⁺, C₁₄H₂₀N₄O₅Na requires 347.1326), 409.1 (4), 344 (4), 225 (38), 175 (7), 153 (16), 132 (11).

Also isolated was isomer **66b** as a yellow solid (9 mg, 3%); m.p. 80 – 82 °C; ν_{\max} (ATR) / cm^{-1} 3641 (N-H), 3570 (N-H), 3468 (N-H), 3390 (N-H), 3315 (C-H), 1667 (C=O), 1628 (C=O), 1577 (N-O), 1516 (N-O); δ_{H} (400 MHz, MeOD) 1.45 (9H, s, $3 \times \text{CH}_3$), 3.26 – 3.31 (2H, m, CH_2), 3.43 – 3.49 (2H, m, CH_2), 6.99 (1H, d, J 9.0, ArCH), 7.42 (1H, s, ArCH), 8.12 (1H, d, J 9.0, ArCH); δ_{C} (126 MHz, MeOD) 28.7 ($3 \times \text{CH}_3$), 40.7 (CH_2), 41.5 (CH_2), 80.2 (CCH_3), 114.6 (ArCH), 119.7 (ArCH), 127.2 (ArCH), 133.7 (ArC), 142.1 (ArC), 147.1 (ArC), 158.8 (C=O), 169.0 (C=O); m/z (ESI⁺) 347.1326 (79%, $\text{M}+\text{Na}^+$, $\text{C}_{14}\text{H}_{20}\text{N}_4\text{O}_5\text{Na}$ requires 347.1236), 671 (33), 363 (6), 348 (14), 269 (24), 258 (4), 226 (10), 225 (100), 208 (9). 5-amino-2-nitrobenzoic acid was contaminated with 3-amino-4-nitrobenzoic acid which gave resulted in the formation of this isomer.

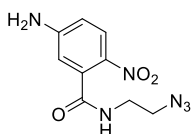
X-Ray crystallography data shown in the appendix.

2-Azidoethanamine **69**



Sodium azide (2.80 g, 43.1 mmol) was added to a solution of 2-chloroethylamine hydrochloride (2.5 g, 21.6 mmol) in water (75 mL) and the mixture was stirred at 80 °C for 25 hours. The mixture was allowed to cool to RT, basified to pH 9 with NaOH (864 mg, 21.6 mmol) and extracted with DCM (4×50 mL). The combined organic extracts were dried over Na_2SO_4 , filtered and concentrated (volatile!) *in vacuo* to give the title compound **69** as a clear oil (1.45 g, 78%) which was used without further purification; δ_{H} (400 MHz, CDCl_3) 2.87 (2H, t, J 5.5, H_2NCH_2), 3.36 (2H, t, J 5.5, N_3CH_2). ^1H NMR data was in accordance with the literature.²¹⁰ Product is extremely hazardous and presents a high explosion risk. The use of a blast shield, avoid heating and minimal purification should be followed if repeating this procedure.

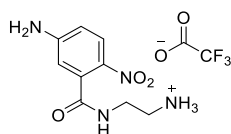
5-Amino-*N*-(2-azidoethyl)-2-nitrobenzamide **70**



HATU (460 mg, 1.21 mmol) was added to a solution of 5-amino-2-nitrobenzoic acid (200 mg, 1.10 mmol), amine **69** (264 mg, 1.65 mmol), DIPEA, (420 μL , 2.42 mmol) in anhydrous DMF

(5 ml) and the mixture was stirred at room temperature overnight. The mixture was concentrated *in vacuo* and partitioned between EtOAc (30 mL) and H₂O (20 ml). The aqueous layer was separated and extracted with EtOAc (4 × 15 mL). The combined organic extracts were washed sequentially with sat. aq. NaHCO₃ (30 mL) and brine (30 mL) and then dried over Na₂SO₄, filtered and concentrated *in vacuo*. Purification by flash column chromatography using silica gel and an eluent of 30% ethyl acetate: petroleum ether 40 – 60 afforded the title compound **70** a yellow solid (175 mg, 64%); m.p. 108 – 110 °C; ν_{\max} (ATR) / cm⁻¹ 3469 (N-H), 3335 (N-H), 3304 (N-H), 2110 (N=N=N), 1625 (C=O), 1548 (N-O); δ_{H} (400 MHz, MeOD) 3.60 – 3.41 (4H, m, 2 × CH₂). 6.56 (1H, d, *J* 2.5, ArCH), 6.66 (1 H, dd, *J* 9.0, 2.5, ArCH), 7.98 (1 H, d, *J* 9.0, ArCH); δ_{C} (101 MHz, MeOD) 40.4 (CH₂), 51.2 (CH₂), 113.1 (ArCH), 114.1 (ArCH), 128.7 (ArCH), 134.9 (ArC), 137.4 (ArC), 156.2 (ArC), 171.5 (C=O); *m/z* (ESI⁺) 273.0718 (100%, MH⁺, C₂₆H₂₄N₃O₃S requires 273.0707), 335 (4), 289 (14), 274 (10), 251 (13), 165 (16), 131 (11).

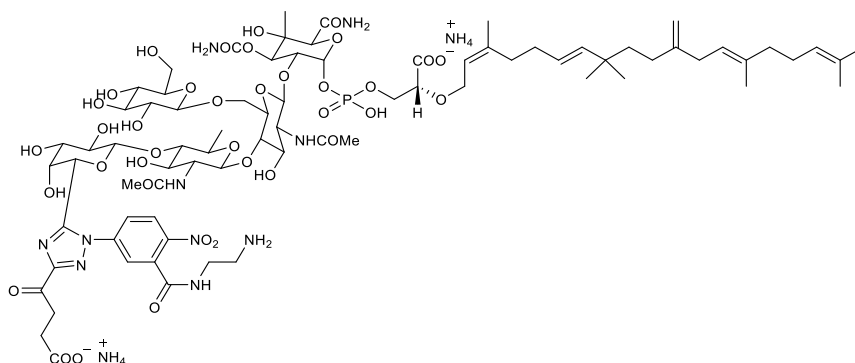
5-Amino-*N*-(2-azaniumylethyl)-2-nitrobenzamide trifluoroacetate **67**



TFA (0.2 mL) was added to a solution of Boc-protected amine **66a** (35 mg, 0.108 mmol) in CH₂Cl₂ (1 mL) and the mixture was stirred at room temperature for 15 minutes. The mixture was evaporated to dryness *in vacuo* and triturated with Et₂O:DCM (1:1, 3 × 5 mL) to afford the title compound **67** as a yellow solid (29 mg, 80%); m.p. 194 – 196 °C; ν_{\max} (ATR) / cm⁻¹ 3429 (N-H), 3331 (N-H), 3222 (N-H), 1655 (C=O), 1523 (N-O); δ_{H} (400 MHz, MeOD) 3.48 – 3.5 (4H, m, 2 × CH₂). 6.55 (1H, d, *J* 2.5, ArCH), 6.66 (1H, dd, *J* 9.0, 2.5, ArCH), 7.98 (1H, d, *J* 9.0, ArCH); δ_{C} (101 MHz, MeOD) 38.5 (CH₂), 40.5 (CH₂), 112.9 (ArCH), 114.3 (ArCH), 128.9 (ArCH), 134.7 (ArC), 136.9 (ArC), 156.5 (ArC), 172.3 (C=O); *m/z* (ESI⁺) 225.0993 (100%, MH⁺, C₉H₁₄N₄O₃ requires 225.0982), 471 (11), 305 (5), 261 (20), 247 (11), 190 (94), 169 (43), 153 (93), 124 (16). The TFA salt of this compound was not reported in the literature.

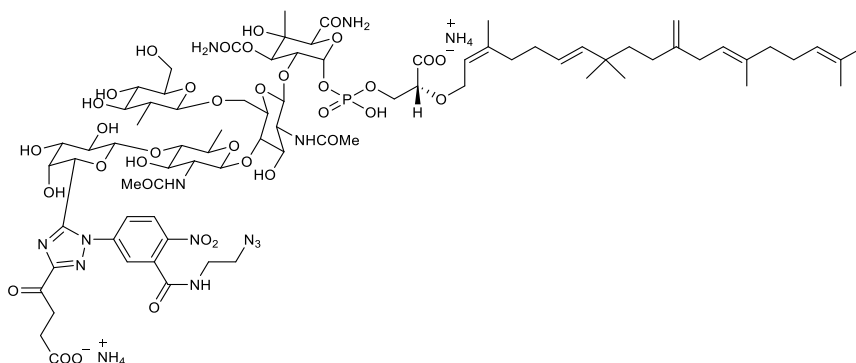
Diammonium 4-(1-{3-[(2-aminoethyl)carbamoyl]-4-nitrophenyl}-5-[6-({6-([6-carbamoyl-4-(carbamoyloxy)-2-([(2*R*)-2-carboxylato-2-([(2*Z*,6*E*,13*E*)-3,8,8,14,18-

pentamethyl-11-methylidenonadeca-2,6,13,17-tetraen-1-yl]oxy}ethoxy](hydroxy)phosphoryl}oxy)-5-hydroxy-5-methyloxan-3-yl]oxy}-5-acetamido-4-hydroxy-2-([3,4,5-trihydroxy-6-(hydroxymethyl)oxan-2-yl]oxy}methyl)oxan-3-yl)oxy]-5-acetamido-4-hydroxy-2-methyloxan-3-yl]oxy)-3,4,5-trihydroxyoxan-2-yl]-1H-1,2,4-triazol-3-yl)-4-oxobutanoate **62**



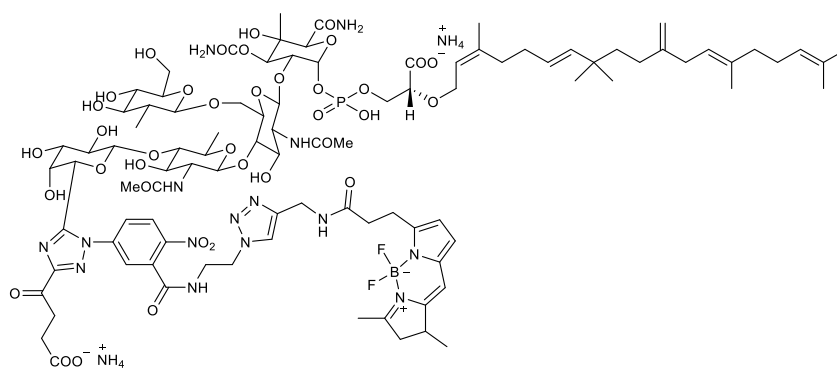
A solution of sodium nitrite (0.4 mg, 0.00520 mmol) in H₂O (1 mL) was added to a solution amine salt **67** (1.6 mg, 0.00472 mmol) in 1 M hydrochloric acid (140 μ L) at 0 °C and the mixture was stirred for 15 minutes. The mixture was added to a solution of moenomycin A (6.2 mg, 0.00392 mmol) and NaOAc (170 mg) in H₂O (6 mL) and stirred at room temperature for 5 days. The mixture was lyophilised and purified by preparative HPLC using an eluent of 5 – 30% MeCN: H₂O (0.1% NH₄OH) to afford the title compound **62** as an off-white fluffy solid (0.5 mg, 6%); *m/z* (ESI⁻) 1815.7215 (13%, MH⁻, C₇₈H₁₁₆N₁₀O₃₇P requires 1815.7246), 908 (22), 907 (42), 279 (100), 249 (13), 165 (22), 97 (18). Mass spectrometry data was in accordance with the literature.²¹¹

Diammonium 4-(1-{3-[(2-azidoethyl)carbamoyl]-4-nitrophenyl}-5-[6-({6-[(6-[[6-carbamoyl]-4-(carbamoyloxy)-2-({[(2*R*)-2-carboxylato-2-{{[(2*Z*,6*E*,13*E*)-3,8,8,14,18-pentamethyl-11-methylidenonadeca-2,6,13,17-tetraen-1-yl]oxy}ethoxy](hydroxy)phosphoryl}oxy)-5-hydroxy-5-methyloxan-3-yl]oxy}-2-({[4,5-dihydroxy-6-(hydroxymethyl)-3-methyloxan-2-yl]oxy}methyl)-5-acetamido-4-hydroxyoxan-3-yl)oxy]-5-acetamido-4-hydroxy-2-methyloxan-3-yl]oxy)-3,4,5-trihydroxyoxan-2-yl]-1H-1,2,4-triazol-3-yl)-4-oxobutanoate **63**



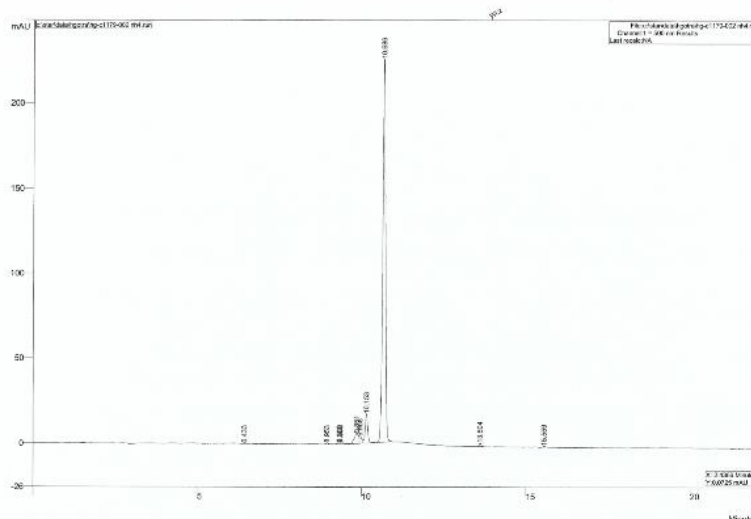
A solution of sodium nitrite (0.23 mg, 0.00336 mmol) in H₂O (0.5 mL) was added to a solution azide **70** (0.76 mg, 0.00305 mmol) in 1 M hydrochloric acid (125 μ L) at 0 °C and the mixture was stirred for 15 minutes. The mixture was added to a solution of moenomycin A (4 mg, 0.00253 mmol) and NaOAc (140 mg) in H₂O (4 mL) and stirred at room temperature for 6 days. The mixture was lyophilised and purified by preparative HPLC using an eluent of 5 – 50% MeCN: H₂O (0.1% NH₄OH) to afford the title compound **63** as a yellow solid (2.0 mg, 35%); *m/z* (ESI⁻) 1841.7173 (8%, MH⁻, C₇₈H₁₁₄N₁₂O₃₇P requires 1841.7151), 922 (19), 921 (93), 920 (100), 113 (10).

Diammonium 4-(2-([(1-{2-[(5-{5-[6-({6-[(6-{[6-carbamoyl-4-(carbamoyloxy)-2-([(2*R*)-2-carboxylato-2-[(2*Z*,6*E*,13*E*)-3,8,8,14,18-pentamethyl-11-methylidenonadeca-2,6,13,17-tetraen-1-yl]oxy}ethoxy](hydroxy)phosphoryl)oxy)-5-hydroxy-5-methyloxan-3-yl]oxy}-2-([4,5-dihydroxy-6-(hydroxymethyl)-3-methyloxan-2-yl]oxy)methyl)-5-acetamido-4-hydroxyoxan-3-yl]oxy]-5-acetamido-4-hydroxy-2-methyloxan-3-yl]oxy)-3,4,5-trihydroxyoxan-2-yl]-3-(3-carboxylatopropanoyl)-1*H*-1,2,4-triazol-1-yl]-2-nitrophenyl]formamido]ethyl)-1*H*-1,2,3-triazol-4-yl)methyl]carbamoyl]ethyl)-2,2-difluoro-10,12-dimethyl-1 λ^5 ,3-diaza-2-boratricyclo[7.3.0.0^{3,7}]dodeca-1(12),4,6,8-tetraen-1-ylum-2-uide **71**

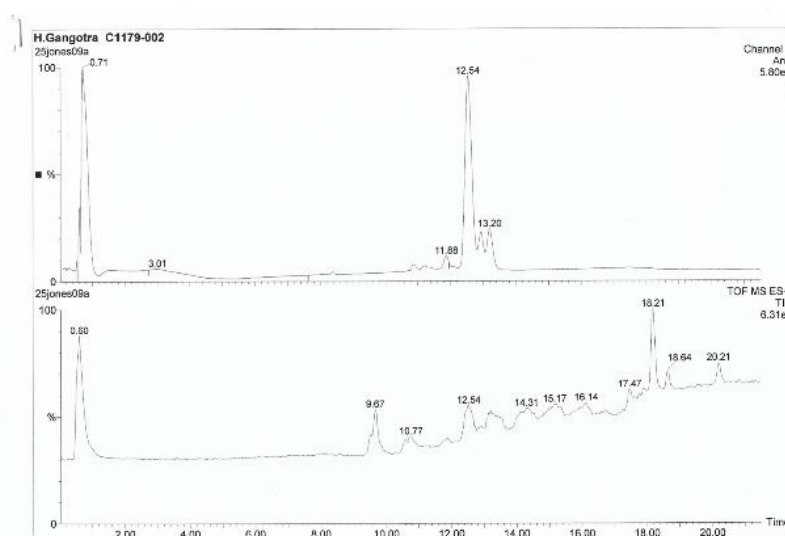


Ascorbic acid (0.160 mg, 0.000868 mmol) in H₂O (15 μL) was added to a solution of azide **63** (0.8 mg, 0.000434 mmol) and BDP-FL alkyne (0.15 mg, 0.000434 mmol) in DMSO (200 μL). This was stirred for 2 minutes and then CuSO₄ (0.07 mg, 0.000434 mmol) in H₂O (15 μL) was added and the reaction mixture stirred for 18 hours. The reaction mixture then was purified directly by preparative HPLC using an eluent of 5 – 95% MeCN: H₂O (0.1% NH₄OH) to afford the title compound **71** as an orange solid (0.9 mg, 94%); *m/z* (ESI⁺) 2173.8776 (13%, MH⁺, C₉₅H₁₃₄¹¹BF₂N₁₅O₃₈P requires 2173.8886), 1832 (18), 1647 (2), 1415 (7), 1087 (18), 907 (100), 814 (67), 468 (5), 341 (35). LC-MS data demonstrating purity below (UV₅₀₀).

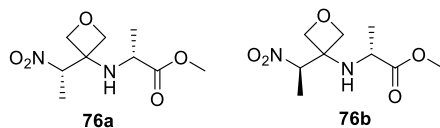
Sample (LC only):



Sample (LC-MS):

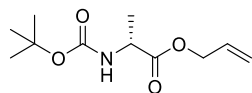


Methyl (2*R*)-2-({3-[(1*S*)-1-nitroethyl]oxetan-3-yl}amino)propanoate **76a** and Methyl (2*R*)-2-({3-[(1*R*)-1-nitroethyl]oxetan-3-yl}amino)propanoate **76b**



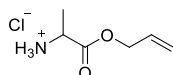
A mixture of oxetan-3-one (515 mg, 7.15 mmol), nitroethane (720 μ L, 10.0 mmol) and Et₃N (0.2 mL, 1.43 mmol) was stirred at room temperature for 30 minutes. The mixture was diluted with anhydrous CH₂Cl₂ (20 mL) and cooled to -78 °C. Et₃N (1.99 mL, 14.3 mmol) and methanesulfonyl chloride (550 mL, 7.15 mmol) were added and the reaction mixture stirred at -78 °C for 1 hour. In a separate flask, a suspension of D-ala-OMe.HCl (2.00 g, 14.3 mmol) and Et₃N (2.00 mL, 14.3 mmol) in CH₂Cl₂ (20 mL) was stirred at room temperature for 15 minutes. This was then added to the oxetane solution at -78 °C dropwise over 10 minutes and the resulting mixture was stirred at room temperature overnight. The reaction mixture was quenched with sat. aq NH₄Cl (40 mL) and the organic layer separated. The aqueous layer was extracted further with CH₂Cl₂ (3 \times 40 mL) prior to washing the combined organic extracts with brine (40 mL), drying over Na₂SO₄, filtering and concentrating *in vacuo*. Purification by flash column chromatography using silica gel and an eluent 10 – 30% ethyl acetate: petroleum ether 40 – 60 afforded the title compounds **76a** and **76b** as a yellow oil in a 60:40 mixture of diastereoisomers (755 mg, 45%); $[\alpha]_D^{24} + 28.0$ (*c* 1.00 in CHCl₃); ν_{\max} (ATR) / cm⁻¹ 3336 (N-H), 2954 (C-H), 2884 (C-H), 1733 (C=O), 1550 (N-O); δ_H (400 MHz, CDCl₃) 1.30 (3H, d, *J* 7.0, CH₃major), 1.33 (3H, d, *J* 7.0, CH₃minor), 1.71 (3H, d, *J* 7.0, CH₃minor), 1.75 (3H, d, *J* 7.0, CH₃major), 2.21 (1H, br d, NHCH_{major}) 2.40 (1H, br s, NHCH_{minor}), 3.63 – 3.77 (2H, m, NH_{major} & minor), 3.74 (6H, s, OCH₃major & minor), 4.46 (1H, d, *J* 8.0, CHH_{minor}) 4.53 (1H, s, CHH), 4.58 (3H, s, 3 \times CHH_{major} & minor), 4.71 (1H, d, *J* 8.0, CHH_{major}), 4.97 (2H, dq, *J* 20.0, 7.0, CH₃CH_{major} & minor); δ_C (101 MHz, CDCl₃) 13.7 (CH₃major), 14.1 (CH₃minor), 20.7 (CH₃major), 21.2 (CH₃minor), 51.0 (OCH₃major), 51.3 (OCH₃minor), 52.5 (CH₃CHC_{major}), 52.5 (CH₃CHC_{minor}), 62.1 (NHC_{minor}), 62.4 (NHC_{major}), 77.0 (CH₂minor), 77.8 (CH₂minor), 77.8 (CH₂major), 78.1 (CH₂major), 84.9 (NHCH_{major}), 86.5 (NHCH_{minor}), 176.5 (C=O_{minor}), 176.6 (C=O_{major}); *m/z* (ESI⁺) 233.1134 (100%, MH⁺, C₉H₁₇N₂O₅ requires 233.1132), 174 (48), 114 (35).

Prop-2-en-1-yl (2*R*)-2-[(tert-butoxycarbonyl)amino]propanoate **79**



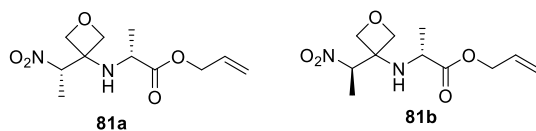
Allyl bromide (3.00 ml, 34.3 mmol) was added dropwise over 2 minutes to a solution of Boc-D-alanine (5.00 g, 26.4 mmol) and DIPEA (5.80 ml, 32.3 mmol) in DMF (50 mL) at 0 °C and then stirred at room temperature overnight. The mixture was diluted with EtOAc (150 mL) and washed with H₂O (2 × 50 mL) and brine (50 mL). The organic was dried over Na₂SO₄, filtered and the solvent removed *in vacuo* to afford the title compound **79** as a yellow oil which was used without further purification (5.58 g, 90%); $[\alpha]_D^{22} + 10.0$ (*c* 1.00 in CHCl₃); ν_{\max} (ATR) / cm⁻¹ 3371 (N-H), 2981 (C-H), 1744 (C=O), 1715 (C=O); δ_H (400 MHz, CDCl₃) 1.39 (3H, d, *J* 7.0, CH₃), 1.44 (9H, s, 3 × CH₃), 4.27 – 4.39 (1H, m, NHCH), 4.55 – 4.70 (2H, m, OCH₂), 5.04 (1H, s, NH), 5.25 (1H, dd, *J* 10.5, 1.0, CH=CHH), 5.33 (1H, dd, *J* 17.0, 1.0, CH=CHH), 5.90 (1H, ddt, *J* 17.0, 10.5, 5.5, CH=CHH); δ_C (101 MHz, CDCl₃): 18.7 (CH₃), 28.4 (3 × CH₃), 49.3 (CH), 65.9 (OCH₂), 79.9 (CCH₃), 118.7 (CH=CH₂), 131.8 (CH=CH₂), 155.2 (C=O), 173.2 (C=O); *m/z* (ESI⁺) 252.1215 (100%, M+Na⁺, C₁₁H₁₉NO₄Na requires 252.1206), 543 (11), 481 (18), 364 (20), 313 (7), 214 (5), 149 (9), 139 (80).

(±)-Prop-2-en-1-yl 2-aminopropanoate hydrochloride **80**



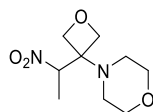
12 M hydrochloric acid (10 mL) was added to a solution of Boc protected amine **79** (5.00 g, 21.8 mmol) in EtOAc (150 mL) and the mixture was stirred at room temperature overnight. Concentration of the mixture *in vacuo* afforded the title compound **80** as a brown oil (3.63 g, 92%) which was used without further purification; ν_{\max} (ATR) / cm⁻¹ 3401 (N-H), 2888 (C-H), 1741 (C=O), 1596 (C=C); δ_H (400 MHz, MeOD) 1.56 (3H, d, *J* 7.0, CH₃), 4.14 (1H, q, *J* 7.0, NCH), 4.75 (2H, m, OCH₂), 5.30 (1H, dd, *J* 10.5, 1.5, CH=CHH), 5.39 (1 H, dd, *J* 17.0, 1.5, CH=CHH), 5.99 (1 H, ddt, *J* 17.0, 10.5, 6.0, CH=CHH); δ_C (101 MHz, MeOD) 16.2 (CH₃), 49.9 (CH), 67.8 (OCH₂), 119.6 (CH=CH₂), 132.7 (CH=CH₂), 170.7 (C=O); *m/z* (ESI⁺) 130.0865 (100%, MH⁺, C₆H₁₂NO₂ requires 130.0863), 459 (1), 236 (1), 131 (7).

Prop-2-en-1-yl (2*R*)-2-({3-[(1*S*)-1-nitroethyl]oxetan-3-yl}amino)propanoate **81a** and prop-2-en-1-yl (2*R*)-2-({3-[(1*R*)-1-nitroethyl]oxetan-3-yl}amino)propanoate **81b**



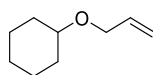
A mixture of nitroethane (370 μL , 5.20 mmol), oxetan-3-one (500 μL , 7.80 mmol) and Et_3N (180 μL , 1.30 mmol) was stirred at room temperature for 2 hours. The mixture was diluted with anhydrous CH_2Cl_2 (20 mL) and cooled to -78°C . Methanesulfonyl chloride (440 μL , 5.72 mmol) and Et_3N (940 μL , 6.76 mmol) were added and the reaction mixture was stirred at -78°C for 30 minutes and then at 0°C for 2 hours. The mixture was diluted with CH_2Cl_2 (30 mL) and washed with H_2O (20 mL). The aqueous layer was separated, extracted with EtOAc (40 mL) and the combined organic extracts dried over Na_2SO_4 and filtered. Removal of the solvent *in vacuo* afforded the crude Michael adduct. In a separate flask, Et_3N (2.20 mL, 15.6 mmol) was added to a solution of amine **80** (1.90 g, 10.4 mmol) in DMSO (9 mL) and CH_2Cl_2 (5 mL) and the mixture was stirred at room temperature for 10 minutes. The crude Michael adduct was dissolved in DMSO (18 mL), added to the stirring mixture and the resulting mixture was stirred at room temperature overnight. The mixture was diluted with EtOAc (130 mL), washed with H_2O (100 mL) and the organic extract dried over Na_2SO_4 and filtered. Removal of the solvent *in vacuo* and purification of the crude material by flash column chromatography using silica gel and an eluent of 20% ethyl acetate: petroleum ether 40 – 60 afforded the title compounds **81a** and **81b** as a yellow oil in a 60:40 mixture of diastereoisomers (700 mg, 52%); $[\alpha]_{\text{D}}^{24} + 23.5$ (c 0.98 in CHCl_3); ν_{max} (ATR) / cm^{-1} 3340 (N-H), 2982 (C-H), 2888 (C-H), 1731 (C=O), 1550 (N-O); δ_{H} (400 MHz, CDCl_3) 1.34 (3H, d, J 7.0, CH_3 major), 1.37 (3H, d, J 7.0 CH_3 minor), 1.73 (3H, d, J 7.0, CH_3 minor), 1.77 (3H, d, J 7.0, CH_3 major), 2.22 (2H, br s, NH major & minor), 3.72 (1H, q, J 7.0, CH_3CHCO major), 3.79 (1H, q, J 7.0, CH_3CHCO minor), 4.49 (1H, d, J 8.0, CHH minor), 4.52 – 4.68 (10H, m, $5 \times \text{CH}_2$ major & minor), 4.72 (1H, d, J 8.0, CHH major), 5.01 (2H, dq, J 17.0, 7.0 CH_3CHNO major & minor) 5.27 – 5.33 (2H, m, $\text{CH}=\text{CHH}$ major & minor), 5.34 – 5.42 (2H, m, $\text{CH}=\text{CHH}$ major & minor), 5.87 – 6.00 (2H, ddt, J 19.0, 10.5, 6.0 $\text{CH}=\text{CHH}$ major & minor); δ_{C} (101 MHz, CDCl_3) 13.8 (CH_3 major), 14.1 (CH_3 minor), 20.8 (CH_3 major), 21.3 (CH_3 minor), 51.8 (CH_3CH major), 51.4 (CH_3CH minor), 66.6 (NHCCH_3 major), 66.4 (NHCCH_3 minor), 77.0 (CH_2 minor), 77.6 (CH_2 major), 77.9 (CH_2 minor), 78.20 (CH_2 major), 84.9 (NHCH major), 86.7 (NHCH minor), 119.3 ($\text{CH}=\text{CH}_2$ minor), 119.3 ($\text{CH}=\text{CH}_2$ major), 131.6 ($\text{CH}=\text{CH}_2$ major), 131.6 ($\text{CH}=\text{CH}_2$ minor), 175.9 (C=Omajor & minor); m/z (ESI⁺) 259.1296 (100%, MH^+ , $\text{C}_{11}\text{H}_{19}\text{N}_2\text{O}_5$ requires 259.1288), 477 (1), 329 (1), 229 (65), 200 (30).

4-[3-[(±)-1-Nitroethyl]oxetan-3-yl]morpholine **83**



A solution of **81a** and **81b** (50 mg, 0.194 mmol) in degassed THF (10 mL) was purged with nitrogen. Pd(Ph₄)₃ (2.2 mg, 0.00194 mmol) and morpholine (170 μL, 1.94 mmol) were added and the reaction mixture stirred at room temperature overnight. The mixture was concentrated *in vacuo* and the residue partitioned between CH₂Cl₂ (20 ml) and 1 M hydrochloric acid (10 mL). The organic extract was separated, dried over Na₂SO₄, filtered and concentrated *in vacuo*. Purification by flash column chromatography using silica gel and an eluent of 50% ethyl acetate: petroleum ether 40 – 60 afforded the title compound **83** as a white solid (17 mg, 41%); m.p. 85 °C - 87 °C; ν_{\max} (ATR) / cm⁻¹ 2959 (C-H), 2920 (C-H), 2896 (C-H), 2862 (C-H), 2821 (C-H), 1545 (N-O); δ_{H} (400 MHz, CDCl₃) 1.87 (3H, d, *J* 7.0, CH₃), 2.52 – 2.63 (2H, m, CH₂morpholine), 2.70 – 2.81 (2H, m, CH₂morpholine), 3.66 – 3.74 (4H, m, 2 × CH₂morpholine), 4.35 (1H, d, *J* 7.0, CH), 4.78 (1H, d, *J* 7.0, CH_{oxetane}), 4.84 – 4.91 (2H, m, 2 × CH_{oxetane}), 5.00 (1H, q, *J* 7.0, CH_{oxetane}); δ_{C} (101 MHz, CDCl₃) 15.5 (CH₃), 46.6 (2 × NCH₂morpholine), 65.9 (C), 67.4 (2 × OCH₂morpholine), 72.5 (CH₂), 73.7 (CH₂), 82.8 (CH₃CH); *m/z* 217.1185 (MH⁺, C₉H₁₇N₂O₄ requires 217.1183). Infrared spectrum contains impurities.

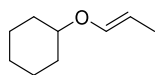
(Prop-2-en-1-yloxy)cyclohexane **86**



Sodium hydride (60% mineral oil, 110 mg, 2.74 mmol) was washed with heptane (3 × 5 mL) and suspended in anhydrous THF (1 mL). Cyclohexanol (211 mg, 2.11 mmol) in anhydrous THF (2 ml) was then added and the mixture stirred at 0 °C. After 10 minutes, allyl bromide (240 μL, 2.74 mmol) was added dropwise over 1 minute and the mixture stirred at 70 °C for 4 hours. The reaction mixture was allowed to cool to room temperature, quenched with sat. aq. NH₄Cl (3 mL) and extracted with Et₂O (3 x 5 mL). The combined organics were washed H₂O (10 mL), brine (10 mL) and dried over Na₂SO₄ and filtered. Removal of the solvent *in vacuo* prior to purification by flash column chromatography using silica gel and an eluent of 0 – 2% ethyl acetate: petroleum ether 40 – 60 afforded the title compound **86** as a clear oil. (95 mg, 32%). δ_{H} (400 MHz, CDCl₃) 1.10 – 1.38 (5H, m, 5 × CHH), 1.44 – 1.63 (1H, m, CHH), 1.63

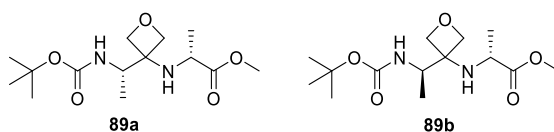
– 1.80 (2H, m, 2 × CHH), 1.80 – 2.01 (2H, m, 2 × CHH), 3.18 – 3.39 (1H, m, OCH), 3.98 – 4.14 (2H, m, OCH₂), 5.08 – 5.21 (1H, m, CH=CHH), 5.21 – 5.37 (1 H, m, CH=CHH), 5.87 – 6.04 (1H, m, CH=CHH). ¹H NMR data was in general accordance with the literature.²¹²

[(1*E*)-Prop-1-en-1-yloxy]cyclohexane **87**



A mixture of 1,5-cyclooctadienebis(methyldiphenylphosphine)iridium(I) hexafluorophosphate (15 mg, 0.0178 mmol) in anhydrous THF (1.5 mL) was purged and evacuated with nitrogen three times and the mixture was stirred under a hydrogen atmosphere for 10 minutes. The solution was purged and evacuated with nitrogen three times and alkene **86** (49.9 mg, 0.356 mmol) in anhydrous THF (1.5 mL) was added. The reaction mixture was stirred for 5 hours and then concentrated *in vacuo* affording the title compound **87** as a crude mixture (29 mg); selected peaks showing isomerisation has occurred δ_{H} (400 MHz, CDCl₃) 1.56 (3H, dd, *J* 7.0, 1.5), 4.91 (1H, dq, *J* 13.5, 7.0), 6.12 (1H, dd, *J* 13.5, 1.5).

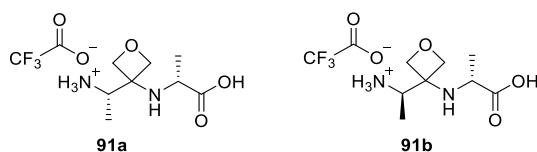
Methyl (2*R*)-2-({3-[(1*S*)-1-[(tert-butoxy)carbonyl]amino]ethyl}oxetan-3-yl)amino)propanoate **89a** and methyl (2*R*)-2-({3-[(1*R*)-1-[(tert-butoxy)carbonyl]amino]ethyl}oxetan-3-yl)amino)propanoate **89b**



A mixture of nitrooxetane diastereoisomers **76a** and **76b** (1.27 mmol, 295 mg), Boc₂O (1.52 mmol, 330 mg), NaHCO₃ (2.54 mmol, 215 mg) and Raney nickel (50% slurry in water, 0.5 mL) in anhydrous THF (15 mL) was purged and evacuated with nitrogen three times and then stirred under a hydrogen atmosphere (1 ATM) at room temperature overnight. The reaction vessel was purged and evacuated with nitrogen three times and the mixture filtered through Celite with CH₂Cl₂ (20 mL). The filtrate was concentrated *in vacuo* and the resulting oil purified by flash column chromatography using silica gel and an eluent of 30% ethyl acetate: petroleum ether 40 – 60 to afford the title compounds **89a** and **89b** as a clear oil in a 55:45 mixture of diastereoisomers (168 mg, 44%); ν_{max} (ATR) / cm⁻¹ 3341 (N-H), 2978 (C-H), 2879

(C-H), 1736 (C=O), 1710 (C=O); $f\delta_{\text{H}}$ (400 MHz, CDCl_3) 1.15 (3H, d, J 7.0, $\text{CH}_{3\text{major}}$), 1.17 (3H, d, J 7.0, $\text{CH}_{3\text{minor}}$), 1.34 (3H, d, J 7.0, $\text{CH}_{3\text{major \& minor}}$), 1.45 (18H, s, $3 \times \text{C}(\text{CH}_3)_{3\text{major \& minor}}$), 3.69 (1H, q, J 7.0, $\text{CH}_3\text{CH}_{\text{major}}$), 3.74 (3H, s, $\text{OCH}_{3\text{major}}$), 3.75 (3H, s, $\text{OCH}_{3\text{minor}}$), 3.82 (1H, q, J 7.0, $\text{CH}_3\text{CH}_{\text{minor}}$), 4.18 – 4.02 (2H, m, $\text{CH}_3\text{CH}_{\text{major \& minor}}$), 4.50 – 4.31 (8H, m, $2 \times \text{CH}_2_{\text{major \& minor}}$), 4.92 (1H, br s, NH_{minor}), 5.03 z(1H, br s, NH_{major}); $f\delta_{\text{C}}$ (101 MHz, CDCl_3) 14.6 ($\text{CH}_{3\text{major}}$), 15.0 ($\text{CH}_{3\text{minor}}$), 20.9 ($\text{CH}_{3\text{minor}}$), 21.4 ($\text{CH}_{3\text{major}}$), 28.4 ($3 \times \text{C}(\text{CH}_3)_{\text{major \& minor}}$), 50.7 ($\text{CH}_{\text{major \& minor}}$), 51.34 ($\text{CH}_{\text{major \& minor}}$), 52.4 ($\text{OCH}_{3\text{minor}}$), 52.4 ($\text{OCH}_{3\text{major}}$), 62.5 (C_{major}), 62.6 (C_{minor}), 74.1 ($\text{C}(\text{CH}_3)_{\text{major \& minor}}$), 77.8 ($\text{CH}_2_{\text{major}}$), 78.6 ($\text{CH}_2_{\text{minor}}$), 78.8 ($\text{CH}_2_{\text{major \& minor}}$), 155.7 ($\text{C}=\text{O}_{\text{major}}$), 155.9 ($\text{C}=\text{O}_{\text{minor}}$), 177.0 ($\text{C}=\text{O}_{\text{major}}$), 177.4 ($\text{C}=\text{O}_{\text{minor}}$); m/z (ESI^+) 303.1927 (100%, MH^+ , $\text{C}_{14}\text{H}_{27}\text{N}_2\text{O}_5$ requires 303.1914), 297 (1), 247 (39).

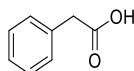
(1*S*)-1-(3-[[*(1R)*-1-Carboxyethyl]amino]oxetan-3-yl)ethan-1-aminium trifluoroacetate **91a** and (*1R*)-1-(3-[[*(1R)*-1-carboxyethyl]amino]oxetan-3-yl)ethan-1-aminium trifluoroacetate **91b**



$\text{LiOH}\cdot\text{H}_2\text{O}$ (34 mg, 0.813 mmol) was added to a solution of esters **89a** and **89b** (164 mg, 0.542 mmol) in THF (3.3 mL) and water (1.7 mL) and the mixture was stirred at room temperature overnight. The THF was removed *in vacuo* and the remaining aqueous acidified to pH 5 with 1 M hydrochloric acid. This was extracted with CHCl_3 :IPA (4:1, 3×10 mL) and the organic extracts then dried over Na_2SO_4 , filtered and concentrated *in vacuo* to afford crude carboxylic acid **90** (118 mg); selected data (m/z (ESI^+) 289.1764 (100%, MH^+ , $\text{C}_{13}\text{H}_{25}\text{N}_2\text{O}_5$ requires 289.1758), 290 (14), 233 (24), 187 (1). A small amount of this was taken on the next step below TFA (0.4 mL) was added dropwise to a solution of Boc protected amine **90** in CH_2Cl_2 (1.3 mL) and the mixture was stirred at room temperature for 2 hours. The mixture was concentrated *in vacuo* and the resulting residue triturated with Et_2O (3×5 mL) to afford the title compounds **91a** and **91b** as a pink solid in a 52:48 mixture of diastereoisomers (28 mg, 74%); ν_{max} (ATR) / cm^{-1} 3241 (N-H), 2988 (C-H), 1668 (C=O); δ_{H} (400 MHz, D_2O) 1.40 (3H, d, J 7.0, CH_3), 1.57 (6H, d, J 7.0, CH_3), 1.61 (6H, d, J 7.0, CH_3), 4.03 (1H, q, J 7.0, $\text{NH}_3\text{CH}_{\text{minor}}$), 4.16 (1H, q, J 7.0, $\text{NH}_3\text{CH}_{\text{major}}$), 4.20 – 4.29 (2H, m, $\text{NHCH}_{\text{major \& minor}}$), 4.83 – 4.98 (8H, m, $2 \times \text{CH}_2_{\text{major \& minor}}$); δ_{C} (101 MHz, D_2O) 13.7 ($\text{CH}_{3\text{major}}$), 14.3 ($\text{CH}_{3\text{minor}}$), 14.4 ($\text{CH}_{3\text{major}}$), 15.8 ($\text{CH}_{3\text{minor}}$), 48.6

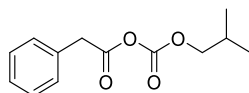
(CH_{major}), 49.3 (CH_{minor}), 49.7 (CH_{major}), 50.1 (CH_{minor}), 58.5 (NHC_{minor}), 58.6 (NHC_{major}), 71.9 (CH_{2major}), 74.2 (CH_{2major}), 74.3 (CH_{2minor}), 76.9 (CH_{2minor}), 167.8 (C=O_{minor}), 168.1 (C=O_{major}); δ_F (400 Mhz, D₂O) 75.80; m/z (ESI⁺) 189.1237 (51%, MH⁺, C₈H₁₈N₂O₃ requires 189.1234), 363 (8), 193 (34), 172 (16), 171 (100), 143 (27).

2-Phenylacetic acid **95**



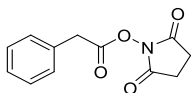
Phenyl acetyl chloride (0.6 mL, 4.53 mmol) was added to H₂O (20 mL) at 0 °C and then stirred at room temperature overnight. The mixture was extracted with CH₂Cl₂ (3 × 40 mL) and the combined organic extracts were washed with brine (40 mL), dried over Na₂SO₄, filtered and evaporated to dryness *in vacuo* to afford the title compound **95** as a white solid (616 mg, quant.) which was used without further purification; δ_H (400 MHz, CDCl₃) 3.66 (2H, s, CH₂), 7.28 – 7.37 (5H, m, 5 x ArCH). ¹H NMR data was in accordance with the literature.^{213,214}

1-[[2-(2-Methylpropoxy)carbonyl]oxy]-2-phenylethan-1-one **96**



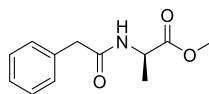
Isobutyl chloroformate (140 μ L, 1.07 mmol) was added dropwise to a solution of **95** (166 mg, 1.07 mmol) and Et₃N (150 μ L, 1.07 mmol) in anhydrous CH₂Cl₂ at 0 °C. The reaction mixture was then stirred at room temperature for 17 hours. The mixture was concentrated *in vacuo* to afford the title compound **96** as a clear oil which was used without further purification (205 mg, 81%); selected data showing formation δ_H (400 MHz, CDCl₃) 0.89 (6H, d, *J* 6.5, 2 × CH₃), 1.91 (1H, dp, *J* 13.5, 6.5, CH), 3.63 (2H, s, CH₂), 3.88 (2H, d, *J* 6.5, OCH₂), 7.27 – 7.36 (5H, m, 5 × ArCH). ¹H NMR data shows presence of a small impurity at 3.7 ppm.

2,5-Dioxopyrrolidin-1-yl 2-phenylacetate **97**



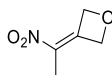
EDCI (415 mg, 2.17 mmol) was added to a suspension of carboxylic acid **95** (227 mg, 1.67 mmol), *N*-hydroxysuccinimide (250 mg, 2.17 mmol), Et₃N (535 μ L, 3.84 mmol) and anhydrous THF (10 mL). CH₂Cl₂ (5 mL) was added to aid solubility and the reaction mixture was stirred at room temperature overnight. The reaction mixture was diluted with CH₂Cl₂ (20 mL) and washed sequentially with 1 M hydrochloric acid (20 mL) and sat. aq. NaHCO₃ (20 mL). The organic layer was dried over Na₂SO₄, filtered and concentrated *in vacuo*. Purification by flash column chromatography using silica gel and an eluent 30% ethyl acetate: petroleum ether 40 – 60 afforded the title compound **97** as a white solid (245 mg, 63%); δ_{H} (400 MHz, CDCl₃) 2.83 (4H, s, 2 \times CH₂pyr), 3.94 (2H, s, CH₂), 7.28 – 7.40 (5H, m, 5 \times ArCH). ¹H NMR data was in accordance with the literature.²¹¹

Methyl (2*R*)-2-(2-phenylacetamido)propanoate **99**



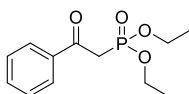
H-D-Ala-OMe (0.319 mmol, 45 mg) was added to a solution of NHS ester **97** (0.266 mmol, 62 mg) and Et₃N (0.702 mmol, 71 μ L) in CH₂Cl₂ (3 mL) and the mixture was stirred at room temperature overnight. The mixture was diluted with CH₂Cl₂ (10 mL) and washed sequentially with 1 M hydrochloric acid (10 mL), H₂O (10 mL) and brine (10 mL). The organic layer was dried over Na₂SO₄, filtered and evaporated to dryness *in vacuo* to afford the title compound **99** as a white solid (35 mg, 59%) which did not require further purification; m.p. 40 °C; $[\alpha]_{\text{D}}^{23} + 40.0$ (*c* 0.50 in MeOH); ν_{max} (ATR) / cm⁻¹ 3342 (N-H), 1742 (C=O), 1646 (C=O); δ_{H} (400 MHz, CDCl₃) 1.36 (3H, d, *J* 7.0, CH₃), 3.61 (2H, s, CH₂), 3.73 (3H, s, OCH₃), 4.60 (1H, p, *J* 7.0, CH), 6.05 (1H, br d, *J* 4.0, NH), 7.19 – 7.50 (5H, m, ArCH); δ_{C} (101 MHz, CDCl₃) 18.3 (OCH₃), 43.6 (CH₂), 48.1 (CH₃CH), 52.5 (CH₃CH), 127.4 (ArCH), 129.0 (ArCH), 129.4 (ArCH), 134.5 (ArC), 170.5 (C=O), 173.4 (C=O); *m/z* (ESI⁺) 222.1126 (100%, MH⁺, C₁₂H₁₆NO₃ requires 222.1125), 244 (27), 223 (17), 190 (7), 159 (3), 131 (1). Melting point, optical rotation, ¹³C NMR or mass spectrometry was not previously reported in the literature; ¹H NMR data is in general accordance with the literature.²¹⁵

3-(1-Nitroethylidene)oxetane **75**



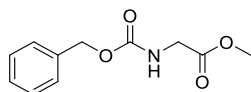
Et₃N (0.275 mL, 1.98 mmol) was added to nitroethane (0.650 mL, 9.00 mmol) and oxetan-3-one (713 mg, 9.89 mmol) and the mixture stirred neat at room temperature for 2 hours. The mixture was cooled to $-78\text{ }^{\circ}\text{C}$, diluted with CH₂Cl₂ (70 mL) and Et₃N (2.50 mL, 18 mmol) and methanesulfonyl chloride (0.765 mL, 9.89 mmol) were added. The reaction mixture was stirred at $-20\text{ }^{\circ}\text{C}$ for 1 hour, quenched with 1 M hydrochloric acid (30 mL) and the organic layer separated. The aqueous layer was extracted further with CH₂Cl₂ (2 \times 30 mL) and the combined organic extracts were dried over Na₂SO₄, filtered and concentrating (volatile!) *in vacuo*. Purification by flash column chromatography using silica gel and an eluent 20 – 30% ethyl acetate: petroleum ether 40 – 60 afforded the title compound **75** as a yellow oil (530 mg, 46%); δ_{H} (400 MHz, CDCl₃) 2.03 (3H, p, *J* 2.0, CH₃), 5.29 – 5.34 (2H, m, CH₂), 5.51 – 5.61 (2H, m, CH₂). ¹H NMR data was in accordance with the literature.²¹⁶

Diethyl (2-oxo-2-phenylethyl)phosphonate **113**



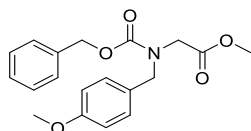
A solution of diethyl methylphosphonate (0.22 mL, 1.52 mmol) in anhydrous THF (10 mL) was cooled to $-78\text{ }^{\circ}\text{C}$ and treated dropwise with *n*-BuLi (2M in hexanes, 0.80 mL, 1.59 mmol) over 2 minutes before stirring for 15 minutes. Ethyl benzoate (0.20 mL, 1.39 mmol) was added dropwise and the resulting solution was gradually allowed to warm to room temperature and the mixture was stirred for 1 hour (after of which TLC showed no starting material remained). The reaction mixture was quenched with sat. aq. NH₄Cl (5 mL) and diluted with H₂O (5 mL). The mixture was extracted with EtOAc (2 \times 20 mL) before drying the combined organic extracts with MgSO₄, filtering and concentration *in vacuo*. Purification by flash column chromatography using silica gel and an eluent of ethyl acetate afforded the title compound **113** as a clear oil (114 mg, 32%); δ_{H} (400 MHz, CDCl₃) 1.28 (6H, t, *J* 7.0, 2 \times CH₃), 3.63 (2H, d, *J* 23.0, CH₂), 4.07 – 4.21 (4H, m, 2 \times CH₂), 7.44 – 7.54 (2H, m, 2 \times ArCH), 7.55 – 7.64 (1H, m, ArCH), 7.95 – 8.09 (2H, m, 2 \times ArCH); *m/z* (ESI⁺) 257.0948 (44%, MH⁺, C₁₂H₁₇O₄P requires 257.0937), 535 (86), 279 (100), 169 (18). Mass spectrometry data was in accordance with the literature; ¹H NMR data was reported with different multiplicity but was otherwise in accordance with literature.²¹⁷

Methyl 2-[[[(benzyloxy)carbonyl]amino]acetate **114**



Thionyl Chloride (1.60 mL, 21.6 mmol) was added dropwise over 1 minute to a solution of Z-Gly-OH (3 g, 14.4) in MeOH (50 mL) at 0 °C before gradually allowed to warm to room temperature and stirring overnight. Concentration of the mixture *in vacuo* afforded prior to purification by flash column chromatography using silica gel and an eluent of 20% ethyl acetate: hexane afforded the title compound **114** (3.16 g, 98%); δ_{H} (400 MHz, CDCl_3) 3.76 (3H, s, CH_3), 3.99 (2H, d, J 5.5, CH_2), 5.13 (2H, s, OCH_2), 5.26 (1H, br s, NH), 7.29 – 7.40 (5H, m, $5 \times \text{ArCH}$); m/z (ESI^+) 246.0746 (44%, $\text{M}+\text{Na}^+$, $\text{C}_{11}\text{H}_{13}\text{NO}_4\text{Na}$ requires 246.0737), 355 (26), 180 (43), 91 (21). Mass spectrometry data was reported as the Na ion but was otherwise in accordance with literature; ^1H NMR data was in accordance with the literature.²¹⁷

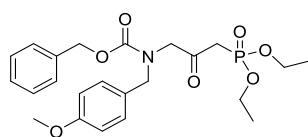
Methyl 2-[[[(benzyloxy)carbonyl][(4-methoxyphenyl)methyl]amino]acetate **117**



A solution of amide **114** (1.08 g, 4.84 mmol) in anhydrous DMF (10 mL) was added to a stirring suspension of NaH (60% in mineral oil, 230 mg, 5.81 mmol) in anhydrous DMF (10 mL) at 0 °C. The mixture was stirred for 30 minutes before adding dropwise 4-methoxybenzyl chloride (0.72 mL, 5.32 mmol) over 1 minute and stirring the reaction mixture at room temperature overnight. The reaction mixture was quenched with MeOH (10 mL) and extracted with EtOAc (3×50 mL). The organic extracts were washed with H_2O (2×50 mL), brine (2×50 mL), dried over Na_2SO_4 , filtered and concentrated *in vacuo*. Purification by flash column chromatography using silica gel and eluent of 20% ethyl acetate: hexane afforded the title compound **117** as a clear oil (979 mg, 59%); ν_{max} (ATR) / cm^{-1} 2958 (C-H), 1752 (C=O), 1704 (C=O); δ_{H} (400 MHz, CDCl_3) (mixture of rotamers) 3.63 (1.5H, s, $\text{OCH}_{3\text{rotA}}$), 3.71 (1.5H, s, $\text{OCH}_{3\text{rotB}}$), 3.79 (3H, s, ArOCH_3), 3.87 (1H, s, $\text{NCH}_{2\text{rotA}}$), 3.95 (1H, s, $\text{NCH}_{2\text{rotB}}$), 4.53 (1H, s, $\text{PMBCH}_{2\text{rotA}}$), 4.55 (1H, s, $\text{PMBCH}_{2\text{rotB}}$), 5.19 (1H, s, $\text{OCH}_{2\text{rotA}}$), 5.22 (1H, s, $\text{OCH}_{2\text{rotB}}$), 6.77 – 6.92 (2H, m, $2 \times \text{ArCH}$), 7.11 (1H, app d, J 8.5, ArCH), 7.19 (1H, app d, J 8.5, ArCH), 7.26 – 7.40 (5H, m,

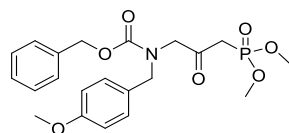
5 × ArCH); δ_C (101 MHz, CDCl₃) (mixture of rotamers) δ 47.3 (CH_{2rotA}), 47.6 (CH_{2rotB}), 50.7 (CH_{2rotA}), 51.1 (CH_{2rotB}), 52.1 (CH_{3rotA}), 52.2 (CH_{3rotB}), 55.4 (CH₃), 67.7 (OCH_{2rotA}), 67.9 (OCH_{2rotB}), 114.1 (2 × ArCH), 127.9, 128.0, 128.1, 128.2, 128.8 (ArC_{rotA}), 128.8 (ArC_{rotB}), 129.3, 129.8, 136.5 (ArC_{rotA}), 136.6 (ArC_{rotB}), 156.4, 156.6, 159.3, 170.2 (C=O); m/z (ESI⁺) 366.1327 (44%, M+Na⁺, C₁₉H₂₁NO₅ requires 366.1312), 709 (4), 534 (5), 428 (5), 367 (33), 336 (9), 289 (5), 248 (4), 121 (18).

Benzyl *N*-[3-(diethoxyphosphoryl)-2-oxopropyl]-*N*-[(4-methoxyphenyl)methyl]carbamate
118



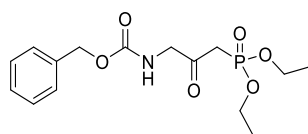
A solution of diethyl methylphosphonate (0.45 mL, 3.08 mmol) in anhydrous THF (10 mL) was cooled to -78 °C and treated dropwise with *n*-BuLi (2.5M in hexanes, 1.30 mL, 3.21 mmol) over 2 minutes before stirring for 15 minutes. Ester **117** (880 mg, 2.57 mmol) in anhydrous THF (10 mL) was added dropwise over 5 minutes and the resulting solution was gradually allowed to warm to room temperature and the mixture was stirred overnight. The reaction mixture was quenched with MeOH (10 mL) and concentrated *in vacuo*. Purification by flash column chromatography using silica gel and an eluent of ethyl acetate afforded the title compound **118** as a clear oil (796 mg, 67%); ν_{\max} (ATR) / cm⁻¹ 2984 (C-H), 1702 (C=O); δ_H (400 MHz, CDCl₃) (mixture of rotamers) 1.24 (3H, t, *J* 7.0, CH_{3rotA}), 1.29 (3H, t, *J* 7.0, CH_{3rotB}), 2.92 (1H, d, *J* 22.5, PCH_{2rotA}), 3.04 (1H, d, *J* 22.5, PCH_{2rotB}), 3.77 (3H, s, OCH₃), 3.98 – 4.20 (6H, m, 2 × OCH₂ and NCH₂), 4.46 (1H, s, PMBCH_{2rotA}), 4.48 (1H, s, PMBCH_{2rotB}), 5.13 (1H, s, OCH_{2rotA}), 5.19 (1H, s, OCH_{2rotB}), 6.79 – 6.86 (2H, m, 2 × ArCH), 7.10 (1H, app d, *J*=8.5, ArCH), 7.19 (1H, app d, *J* 8.5, ArCH), 7.27 – 7.37 (5H, m, 5 × ArCH); δ_C (101 MHz, CDCl₃) (mixture of rotamers) 16.3, 16.4, 39.0, 39.2, 40.3, 40.5, 50.7, 51.0, 55.3, 55.7, 56.2, 62.8, 62.9, 67.7, 67.8, 114.1, 128.0, 128.2, 128.6, 128.9, 129.3, 129.8, 136.4, 136.5, 156.4, 156.5, 159.2, 159.3, 197.1, 197.2, 197.3, 197.4. δ_P (162 MHz, CDCl₃) (mixture of rotamers) 18.9, 19.1; m/z (ESI⁺) 464.1848 (45%, MH⁺, C₂₃H₃₁NO₇P requires 464.1833), 949 (36), 486 (100), 251 (21).

Benzyl *N*-[3-(dimethoxyphosphoryl)-2-oxopropyl]-*N*-[(4-methoxyphenyl)methyl]carbamate
119



A solution of dimethyl methylphosphonate (0.078 mL, 0.716 mmol) in anhydrous THF (3 mL) was cooled to $-78\text{ }^{\circ}\text{C}$ and treated dropwise with *n*-BuLi (1.6M in hexanes, 0.5 mL, 0.746 mmol) over 2 minutes before stirring for 15 minutes. Ester **117** (205 mg, 0.597 mmol) in anhydrous THF (3 mL) was added dropwise over 2 minutes and the resulting solution was gradually allowed to warm to room temperature and the mixture was stirred overnight. The reaction mixture was quenched with MeOH (5 mL) and concentrated *in vacuo*. Purification by flash column chromatography using silica gel and an eluent of ethyl acetate afforded the title compound **119** as a pale yellow oil (132 mg, 51%); ν_{max} (ATR) / cm^{-1} 2957 (C-H), 1701 (C=O); δ_{H} (400 MHz, CDCl_3) 2.93 (1H, d, J 22.5, PCH_2), 3.05 (1H, d, J 22.5, PCH_2), 3.66 (3H, d, J 11.0, OCH_3), 3.76 (3H, d, J 11.0, OCH_3), 3.78 (3H, s, ArOCH_3), 4.09 (1H, s, NCH_2), 4.15 (1H, s, NCH_2), 4.46 (1H, s, PMBCH_2), 4.49 (1H, s, PMBCH_2), 5.14 (1H, s, OCH_2), 5.20 (1H, s, OCH_2), 6.78 – 6.89 (2H, m, $2 \times \text{ArCH}$), 7.07 – 7.13 (1H, d, J , 8.5, ArCH), 7.19 (1H, d, J 8.5, ArCH), 7.28 – 7.38 (5H, m, $5 \times \text{ArCH}$); δ_{C} (101 MHz, CDCl_3) (mixture of rotamers) 37.9, 38.1, 39.2, 39.4, 50.8, 51.1, 53.2, 53.2, 53.3, 53.3, 55.4, 55.8, 56.2, 67.8, 67.9, 114.1, 128.0, 128.0, 128.2, 128.6, 128.8, 128.9, 129.4, 129.9, 136.4, 136.5, 156.3, 156.6, 159.3, 159.3, 197.0, 197.1, 197.3, 197.3; δ_{P} (162 MHz, CDCl_3) (mixture of rotamers) 21.6, 21.8; m/z (ESI⁺) 436.1534 (31%, MH^+ , $\text{C}_{21}\text{H}_{27}\text{NO}_7\text{P}$ requires 436.1520), 893 (36), 458 (100).

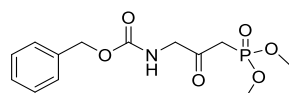
Benzyl *N*-[3-(diethoxyphosphoryl)-2-oxopropyl]carbamate **115**



TFA (1 mL) was added to a solution of tertiary amide **118** (49 mg, 0.120 mmol) and the mixture was stirred at room temperature for 30 minutes. The mixture concentrated *in vacuo* and purified by flash column chromatography using silica gel and eluent of ethyl acetate to afford the title compound **115** as a clear oil (25 mg, 61%); ν_{max} (ATR) / cm^{-1} 2982 (C-H), 1718 (C=O); δ_{H} (400 MHz, CDCl_3) 1.34 (6H, t, J 7.0, $2 \times \text{CH}_3$), 3.12 (2H, d, J 23.0, PCH_2), 4.09 – 4.21 (4H, m, $2 \times \text{CH}_2\text{CH}_3$), 4.23 (2H, d, J 5.0, NCH_2), 5.54 (1H, br s, NH), 7.29 – 7.41 (5H, m, $5 \times \text{ArCH}$); δ_{C} (101 MHz, CDCl_3) 16.3 (d, $J_{\text{C-P}}$ 10, $2 \times \text{CH}_3$), 39.8 (d, $J_{\text{C-P}}$ 128.0 PCH_2), 51.5

(NCH₂), 63.0 (d, J_{C-P} 6.5, 2 × CH₂CH₃), 67.1 (d, J_{C-P} 6.0, OCH₂), 127.9 (2 × ArCH), 128.1 (ArCH), 128.6 (2 × ArCH), 136.2 (ArC), 156.2 (C=O), 197.6 (d, J_{C-P} 7.0, C=O); m/z (ESI⁺) 344.1270 (34%, MH⁺, C₁₅H₂₃NO₆P requires 344.1258), 366 (100), 192 (7). Infrared spectrum shows broad peak ~3200 (N-H) but was not peak picked during sample analysis. Sample contains minor impurities.

Benzyl *N*-[3-(dimethoxyphosphoryl)-2-oxopropyl]carbamate **116**



TFA (2 mL) was added to a solution of tertiary amide **119** (127 mg, 0.292 mmol) and the mixture was stirred at room temperature for 30 minutes. The mixture was diluted with CH₂Cl₂ (5 mL) and Et₂O (10 mL) and concentrated *in vacuo*. Purification by flash column chromatography using silica gel and eluent of ethyl acetate afforded the title compound **116** as a pale yellow oil (67 mg, 73%); ν_{\max} (ATR) / cm⁻¹ 3298 (N-H), 2959 (C-H), 1716 (C=O); δ_{H} (400 MHz, CDCl₃) 3.13 (2H, d, J 23.0, PCH₂), 3.79 (6H, d, J 11.5, 2 × CH₃), 4.22 (2H, d, J 5.5, NCH₂), 5.12 (2H, s, OCH₂), 5.53 (1H, br s, NH), 7.28 – 7.42 (5H, m, 5 × ArCH); δ_{C} (101 MHz, CDCl₃) 38.7 (d, J_{C-P} 129.0, PCH₂), 51.6 (NCH₂), 53.4 (d, J_{C-P} 7.0, 2 × CH₃), 67.2 (OCH₂), 128.2 (2 × ArCH), 128.3 (ArCH), 128.6 (2 × ArCH), 136.3 (ArC), 156.36 (C=O), 197.55 (d, J_{C-P} 6.5, C=O); δ_{P} (162 MHz, CDCl₃) 21.5; m/z (ESI⁺) 338.0779 (31%, M+Na⁺, C₁₃H₁₈NO₆PNa requires 338.0764), 316 (18), 273 (9), 178 (11), 91 (7).

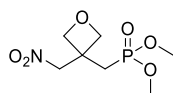
3-(Nitromethylidene)oxetane **121**



A mixture of oxetan-3-one (325 mg, 4.50 mmol), nitromethane (4 mL) and Et₃N (6 drops) was stirred for 20 minutes. The mixture was concentrated *in vacuo*, diluted with anhydrous CH₂Cl₂ (10 mL) and cooled to -78 °C. Methanesulfonyl chloride (1 mL, 13.5 mmol) was added dropwise over 10 minutes and the reaction mixture was stirred for 20 minutes at -78 °C. The reaction mixture was loaded directly onto a silica plug and eluted with 50% diethyl ether: pentane to afford the title compound **121** as a white solid (340 mg, 65%); δ_{H} (400 MHz, CDCl₃)

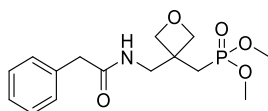
5.34 – 5.45 (2H, m, CH₂), 5.62 – 5.74 (2H, m, CH₂), 6.86 – 7.02 (1H, m, CH). ¹H NMR data was in accordance with the literature.¹⁹⁵

Dimethyl {[3-(nitromethyl)oxetan-3-yl]methyl}phosphonate **122**



A solution of dimethyl methylphosphonate (0.130 mL, 1.15 mmol) in anhydrous THF (5 mL) was cooled to $-78\text{ }^{\circ}\text{C}$ and treated dropwise with *n*-BuLi (2.3M in hexanes, 0.5 mL, 1.20 mmol) before stirring for 15 minutes. Alkene **121** (110 mg, 0.956 mmol) in anhydrous THF (5 mL) was added dropwise and the resulting solution was gradually allowed to warm to room temperature and the mixture was stirred overnight. The reaction mixture was quenched with MeOH (5 mL) and concentrated *in vacuo*. Purification by flash column chromatography using silica gel and an eluent of ethyl acetate afforded the title compound **122** as a pale yellow oil (47 mg, 21%); ν_{max} (ATR) / cm^{-1} 3469, 2958 (C-H), 2886 (C-H), 1551 (N-O); δ_{H} (400 MHz, CDCl₃) 2.44 (2H, d, *J* 18.5, PCH₂), 3.72 (6H, d, *J* 11.0, 2 × CH₃), 4.54 (2H, app dd, *J* 7.0, 2.0, 2 × CHH), 4.63 (2H, d, *J* 7.0, 2 × CHH), 4.99 (2H, s, NCH₂); δ_{C} (101 MHz, CDCl₃) 29.7 (d, *J*_{C-P} 139.0, PCH₂), 39.4 (d, *J*_{C-P} 6.0, CCH₂), 52.7 (d, *J*_{C-P} 7.0, 2 × CH₃), 78.4 (d, *J*_{C-P} 2.0, 2 × CH₂), 79.4 (d, *J*_{C-P} 14.0, NCH₂); δ_{P} (162 MHz, CDCl₃) 28.9; *m/z* (ESI⁺) 240.0637 (37%, MH⁺, C₇H₁₅NO₆P requires 240.0632), 501 (18), 324 (13), 262 (100), 160 (23).

Dimethyl ({3-[(2-phenylacetamido)methyl]oxetan-3-yl}methyl)phosphonate **126**



A mixture of oxetane **122** (96 mg, 0.401 mmol), THF (4 mL) and Raney nickel (50% slurry in water, 1 mL) was purged and evacuated with nitrogen three times and the mixture was stirred under hydrogen at room temperature overnight. The reaction vessel was purged and evacuated with nitrogen three times before filtering the mixture through Celite with CH₂Cl₂ and concentrating *in vacuo* to afford the crude amine intermediate **125** as a pale yellow oil. The amine intermediate was dissolved in anhydrous CH₂Cl₂ (4 mL) before adding Et₃N (0.110 mL, 0.802 mmol) and benzyl chloroformate (0.070 mL, 0.481 mmol) and stirring the reaction

mixture at room temperature overnight. The reaction mixture was diluted with CH₂Cl₂ (10 mL) and washed sequentially with 1 M hydrochloric acid (5 mL), H₂O (5 mL), brine (5 mL) and dried over Na₂SO₄, filtered and concentrated *in vacuo*. Purification by flash column chromatography using silica gel and an eluent of ethyl acetate affording the title compound **126** as a clear oil (21 mg, 15%); ν_{\max} (ATR) / cm⁻¹ 3291 (N-H), 2955 (C-H), 1717 (C=O); δ_{H} (400 MHz, CDCl₃) 2.22 (2H, d, *J* 19.0, PCH₂), 3.63 – 3.75 (8H, m, 2 × CH₃ and NCH₂), 4.47 (2H, d, *J* 6.5, 2 × CHH), 4.54 (2H, d, *J* 6.5, 2 × CHH), 5.10 (2H, s, OCH₂), 5.67 (1H, br s, NH), 7.30 – 7.44 (5H, m, 5 × ArCH); δ_{C} (101 MHz, CDCl₃) 30.6 (d, *J*_{C-P} 138.5, PCH₂), 41.1 (d, *J*_{C-P} 5.0, CCH₂), 46.4 (NCH₂), 52.6 (d, *J*_{C-P} 7.0, 2 × CH₃), 67.0 (OCH₂), 80.2 (d, *J*_{C-P} 14.0, 2 × CH₂), 128.3 (3 × ArCH), 128.7 (2 × ArCH), 136.5 (ArC), 157.1 (C=O); δ_{P} (162 MHz, CDCl₃) 30.9; *m/z* (ESI⁺) 344.1265 (28%, MH⁺, C₁₅H₂₃NO₆P requires 344.1258), 366 (100), 212 (9), 91 (9).

9 References

- 1 Jim O’Neill, *Tackling Drug-Resistant Infections Globally: final report and recommendations*, 2016.
- 2 WHO | World Health Organization.
- 3 D. Lyddiard, G. L. Jones and B. W. Greatrex, *FEMS Microbiol. Lett.*, 2016, **363**, 4.
- 4 K. Lewis, *Nat. Rev. Drug Discov.*, 2013, **12**, 371–387.
- 5 L. L. Ling, T. Schneider, A. J. Peoples, A. L. Spoering, I. Engels, B. P. Conlon, A. Mueller, T. F. Schäberle, D. E. Hughes, S. Epstein, M. Jones, L. Lazarides, V. A. Steadman, D. R. Cohen, C. R. Felix, K. A. Fetterman, W. P. Millett, A. G. Nitti, A. M. Zullo, C. Chen and K. Lewis, *Nature*, 2015, **520**, 388–388.
- 6 H. F. L. Wertheim, D. C. Melles, M. C. Vos, W. Van Leeuwen, A. Van Belkum, H. A. Verbrugh and J. L. Nouwen, *Lancet Infect. Dis.*, 2005, **5**, 751–762.
- 7 J. Kluytmans, A. Van Belkum and H. Verbrugh, *Clin. Microbiol. Rev.*, 1997, **10**, 505–520.
- 8 A. Mackley, C. Baker and A. Bate, *Parliament: House of Commons*, 2018, 1–23.
- 9 A. F. Monegro, V. Muppidi and H. Regunath, *Hospital Acquired Infections*, StatPearls Publishing, 2020.
- 10 Public Health England, *Annual epidemiological commentary: bacteraemia, MSSA bacteraemia and C . difficile infections, up to and including financial year April 2018 to March 2019*, 2019.
- 11 R. J. Gordon and F. D. Lowy, *Clin. Infect. Dis.*, 2008, **46**, 350–359.
- 12 G. L. Archer, *Clin. Infect. Dis.*, 1998, **26**, 1179–1181.
- 13 S. J. Peacock, C. E. Moore, A. Justice, M. Kantzanou, L. Story, K. Mackie, G. O’Neill and N. P. J. Day, *Infect. Immun.*, 2002, **70**, 4987–4996.
- 14 N. Malachowa and F. R. Deleo, *Cell. Mol. Life Sci.*, 2010, **67**, 3057–3071.
- 15 M. P. Jevons, *Br. Med. J.*, 1961, **1**, 124–125.

- 16 T. J. Silhavy, D. Kahne and S. Walker, *Cold Spring Harb. Perspect. Biol.*, 2010, **2**(5), a000414.
- 17 F. D. Lowy, *N. Engl. J. Med.*, 1998, **339**, 520–532.
- 18 L. Brown, J. M. Wolf, R. Prados-Rosales and A. Casadevall, *Nat. Rev. Microbiol.*, 2015, **13**, 620–630.
- 19 K. H. Schleifer and O. Kandler, *Bacteriol. Rev.*, 1972, **36**, 407–477.
- 20 M. Ge, Z. Chen, H. R. Onishi, J. Kohler, L. L. Silver, R. Kerns, S. Fukuzawa, C. Thompson and D. Kahne, *Science*, 1999, **284**, 507–511.
- 21 L. J. Wu and J. Errington, *Nat. Rev. Microbiol.*, 2012, **10**, 8–12.
- 22 V. R. Steele, A. L. Bottomley, J. Garcia-Lara, J. Kasturiarachchi and S. J. Foster, *Mol. Microbiol.*, 2011, **80**, 542–555.
- 23 J. Errington, R. A. Daniel and D.-J. Scheffers, *Microbiol. Mol. Biol. Rev.*, 2003, **67**, 52–65.
- 24 W. Vollmer, B. Joris, P. Charlier and S. Foster, *FEMS Microbiol. Rev.*, 2008, **32**, 259–286.
- 25 V. A. Lund, University of Sheffield, March 2016.
- 26 A. L. Bottomley, University of Sheffield, June 2011.
- 27 K. H. Schleifer and O. Kandler, *Microbiol. Mol. Biol. Rev.*, 1972, **36**, 407–417.
- 28 W. Vollmer, D. Blanot and M. A. De Pedro, *FEMS Microbiol. Rev.*, 2008, **32**, 149–167.
- 29 H. Barreteau, A. Kovač, A. Boniface, M. Sova, S. Gobec and D. Blanot, *FEMS Microbiol. Rev.*, 2008, **32**, 168–207.
- 30 M. G. Pinho, M. Kjos and J.-W. Veening, *Nat. Rev. Microbiol.*, 2013, **11**, 601–614
- 31 E. Sauvage, F. Kerff, M. Terrak, J. A. Ayala and P. Charlier, *FEMS Microbiol. Rev.*, 2008, **32**, 234–258.
- 32 T. P. T. Cushnie, N. H. O’Driscoll and A. J. Lamb, *Cell. Mol. Life Sci.*, 2016, **73**, 4471–4492.

- 33 P. Macheboeuf, C. Contreras-Martel, V. Job, O. Dideberg and A. Dessen, *FEMS Microbiol. Rev.*, 2006, **30**, 673–691.
- 34 A. Zapun, C. Contreras-Martel and T. Vernet, *FEMS Microbiol. Rev.*, 2008, **32**, 361–385.
- 35 E. Sauvage and M. Terrak, *Antibiotics*, 2016, **5**, 12.
- 36 B. G. Spratt, J. Zhou, M. Taylor and M. J. Merrick, *Mol. Microbiol.*, 1996, **19**, 639–640.
- 37 A. J. Meeske, E. P. Riley, W. P. Robins, T. Uehara, J. J. Mekalanos, D. Kahne, S. Walker, A. C. Kruse, T. G. Bernhardt and D. Z. Rudner, *Nature*, 2016, **537**, 634–638.
- 38 P. Reed, H. Veiga, A. M. Jorge, M. Terrak and M. G. Pinho, *J. Bacteriol.*, 2011, **193**, 2549–2556.
- 39 N. T. Reichmann, A. C. Tavares, B. M. Saraiva, A. Jousselin, P. Reed, A. R. Pereira, J. M. Monteiro, R. G. Sobral, M. S. VanNieuwenhze, F. Fernandes and M. G. Pinho, *Nat. Microbiol.*, 2019, **4**, 1368–1377.
- 40 S. F. F. Pereira, A. O. Henriques, M. G. Pinho, H. De Lencastre and A. Tomasz, *Mol. Microbiol.*, 2009, **72**, 895–904.
- 41 T. A. Łęski and A. Tomasz, *J. Bacteriol.*, 2005, **187**, 1815–1824.
- 42 M. G. Pinho, H. De Lencastre and A. Tomasz, *J. Bacteriol.*, 2000, **182**, 1074–1079.
- 43 N. A. C. Curtis, M. V. Hayes, A. W. Wyke and J. B. Ward, *FEMS Microbiol. Lett.*, 1980, **9**, 263–266.
- 44 M. G. Pinho and J. Errington, *Mol. Microbiol.*, 2005, **55**, 799–807.
- 45 P. Reed, M. L. Atilano, R. Alves, E. Hoicznyk, X. Sher, N. T. Reichmann, P. M. Pereira, T. Roemer, S. R. Filipe, J. B. Pereira-Leal, P. Ligoxygakis and M. G. Pinho, *PLoS Pathog.*, 2015, **11**(5), e1004891.
- 46 R. R. Yocum, J. R. Rasmussen and J. L. Strominger, *J. Biol. Chem.*, 1980, **255**, 3977–3986.
- 47 P. Giesbrecht, T. Kersten, H. Maidhof and J. Wecke, *Microbiol. Mol. Biol. Rev.*, 1998, **62**, 1371–1414.

- 48 C. Y. Huang, H. W. Shih, L. Y. Lin, Y. W. Tien, T. J. R. Cheng, W. C. Cheng, C. H. Wong and C. Ma, *Proc. Natl. Acad. Sci. U. S. A.*, 2012, **109**, 6496–6501.
- 49 Y. Yuan, S. Fuse, B. Ostash, P. Sliz, D. Kahne and S. Walker, *ACS Chem. Biol.*, 2008, **3**, 429–436.
- 50 A. L. Lovering, L. H. De Castro, D. Lim and N. C. J. Strynadka, *Science (80-.)*, 2007, **315**, 1402–1405.
- 51 J. Halliday, D. McKeveney, C. Muldoon, P. Rajaratnam and W. Meutermans, *Biochem. Pharmacol.*, 2006, **71**, 957–967.
- 52 P. E. Reynolds, *Eur. J. Clin. Microbiol. Infect. Dis.*, 1989, **8**, 943–950.
- 53 H. R. Perkins, *Biochem. J.*, 1969, **111**, 195–205.
- 54 B. Périchon and P. Courvalin, *Antimicrob. Agents Chemother.*, 2009, **53**, 4580–4587.
- 55 J. Eirich, R. Orth and S. A. Sieber, *J. Am. Chem. Soc.*, 2011, **133**, 12144–12153.
- 56 B. Ostash and S. Walker, *Nat. Prod. Rep.*, 2010, **27**, 1594–1617.
- 57 E. P. Abraham and E. Chain, *Rev. Infect. Dis.*, 1940, **10**, 677–678.
- 58 J. C. Sheehan, 1960, 216–223.
- 59 N. Choices, Staphylococcal infections - NHS Choices, <http://www.nhs.uk/>, (accessed 30 January 2017).
- 60 B. L. M. De Jonge, Y. S. Chang, D. Gage and A. Tomasz, *J. Biol. Chem.*, 1992, **267**, 11248–11254.
- 61 C. Fuda, M. Suvorov, S. B. Vakulenko and S. Mobashery, *J. Biol. Chem.*, 2004, **279**, 40802–40806.
- 62 K. V. Mahasenan, R. Molina, R. Bouley, M. T. Batuecas, J. F. Fisher, J. A. Hermoso, M. Chang and S. Mobashery, *J. Am. Chem. Soc.*, 2017, **139**, 2102–2110
- 63 L. H. Otero, A. Rojas-Altuve, L. I. Llarrull, C. Carrasco-López, M. Kumarasiri, E. Lastochkin, J. Fishovitz, M. Dawley, D. Heseck, M. Lee, J. W. Johnson, J. F. Fisher, M. Chang, S. Mobashery and J. A. Hermoso, *Proc. Natl. Acad. Sci. U. S. A.*, 2013, **110**, 16808–13.

- 64 I. Acebrón, M. Chang, S. Mobashery and J. A. Hermoso, *Curr. Med. Chem.*, 2015, **22**, 1678–86.
- 65 S. W. Long, R. J. Olsen, S. C. Mehta, T. Palzkill, P. L. Cernoch, K. K. Perez, W. L. Musick, A. E. Rosato and J. M. Musser, *Antimicrob. Agents Chemother.*, 2014, **58**, 6668–6674.
- 66 R. Banerjee, M. Gretes, C. Harlem, L. Basuino and H. F. Chambers, *Antimicrob. Agents Chemother.*, 2010, **54**, 4900–4902.
- 67 G. Memmi, S. R. Filipe, M. G. Pinho, Z. Fu and A. Cheung, *Antimicrob. Agents Chemother.*, 2008, **52**, 3955–3966.
- 68 R. Banerjee, M. Gretes, L. Basuino, N. Strynadka and H. F. Chambers, *Antimicrob. Agents Chemother.*, 2008, **52**, 2089–2096.
- 69 L. C. Chan, A. Gilbert, L. Basuino, T. M. Da Costa, S. M. Hamilton, K. R. Dos Santos, H. F. Chambers and S. S. Chatterjee, *Antimicrob. Agents Chemother.*, 2016, **60**, 3934–3941.
- 70 R. M. Corrigan, J. C. Abbott, H. Burhenne, V. Kaefer and A. Gründling, *PLoS Pathog.*, 2011, **7(9)**, e1002217.
- 71 T. A. Łęski and A. Tomasz, *J. Bacteriol.*, 2005, **187**, 1815–1824.
- 72 R. D. Turner, W. Vollmer and S. J. Foster, *Mol. Microbiol.*, 2014, **91**, 862–874.
- 73 L. Shapiro et al., *Science*, 2009, **326**, 1255–1228.
- 74 J. Lippincott-Schwartz, E. Snapp and A. Kemvorthy, *Nat. Rev. Mol. Cell Biol.*, 2001, **2**, 444–456.
- 75 B. Huang, H. Babcock and X. Zhuang, *Cell*, 2010, **143**, 1047–1058.
- 76 M. J. Rust, M. Bates and X. Zhuang, *Nat. Methods*, 2006, **3**, 793–795.
- 77 D. M. Livermore, *J. Antimicrob. Chemother.*, 1987, **19**, 733–742.
- 78 D. A. Preston, C. Y. E. Wu, L. C. Blaszczak, D. E. Seitz and N. G. Halligan, *Antimicrob. Agents Chemother.*, 1990, **34**, 718–721.
- 79 W. Margolin, *J. Bacteriol.*, 2012, **194**, 6369–6371.

- 80 R. Carballido-López, *Microbiol. Mol. Biol. Rev.*, 2006, **70**, 888–909.
- 81 M. J. Evans and B. F. Cravatt, *Chem. Rev.*, 2006, **106**, 3279–3301.
- 82 B. F. Cravatt, A. T. Wright and J. W. Kozarich, *Annu. Rev. Biochem.*, 2008, **77**, 383–414.
- 83 K. R. Gee, H. C. Kang, T. I. Meier, G. Zhao and L. C. Blaszcak, *Electrophoresis*, 2001, **22**, 960–965.
- 84 I. Staub and S. A. Sieber, *J. Am. Chem. Soc.*, 2008, **130**, 13400–13409.
- 85 O. Kocaoglu, R. A. Calvo, L.-T. Sham, L. M. Cozy, B. R. Lanning, S. Francis, M. E. Winkler, D. B. Kearns and E. E. Carlson, *ACS Chem. Biol.*, 2012, **7**, 1746–1753.
- 86 S. Sharifzadeh, M. J. Boersma, O. Kocaoglu, A. Shokri, C. L. Brown, J. D. Shirley, M. E. Winkler and E. E. Carlson, *ACS Chem. Biol.*, 2017, **12**, 2849–2857.
- 87 A. Nangia, K. Biradha and G. R. Desiraju, *J. Chem. Soc., Perkin Trans. 2*, 1996, 943–953.
- 88 R. B. Woodward, *Phil. Trans. R. Soc. Lond. B*, 1980, **289**, 239–250.
- 89 A. D. Deshpande, K. G. Baheti and N. R. Chatterjee, *Curr. Sci.*, 2004, **87**, 1684–1695.
- 90 P. M. Dewick, *Medicinal Natural Products: A Biosynthetic Approach: Third Edition*, John Wiley & Sons, 2009, New York, USA.
- 91 G. L. Dunn, *J. Antimicrob. Chemother.*, 1982, **10**, 1–10.
- 92 S. D. Lahiri and R. A. Alm, *J. Antimicrob. Chemother.*, 2016, **71**, 34–40.
- 93 A. D. Berti, G. Sakoulas, V. Nizet, R. Tewhey and W. E. Rose, *Antimicrob. Agents Chemother.*, 2013, **57**, 5005–5012.
- 94 H. Moisan, M. Pruneau and F. Malouin, *J. Antimicrob. Chemother.*, 2010, **65**, 713–716.
- 95 O. Dumitrescu, P. Choudhury, S. Boisset, C. Badiou, M. Bes, Y. Benito, C. Wolz, F. Vandenesch, J. Etienne, A. L. Cheung, M. G. Bowden and G. Lina, *Antimicrob. Agents Chemother.*, 2011, **55**, 3261–71.
- 96 H. C. Kolb and K. B. Sharpless, *Drug Discov. Today*, 2003, **8**, 1128–1137.

- 97 K. E. Beatty, J. C. Liu, F. Xie, D. C. Dieterich, E. M. Schuman, Q. Wang and D. A. Tirrell, *Angew. Chem. Int. Ed.*, 2006, **45**, 7364–7367.
- 98 A. Raulf, C. K. Spahn, P. J. M. Zessin, K. Finan, S. Bernhardt, A. Heckel and M. Heilemann, *RSC Adv.*, 2014, **4**, 30462–30466.
- 99 E. Kuru, H. V. Hughes, P. J. Brown, E. Hall, S. Tekkam, F. Cava, M. A. De Pedro, Y. V. Brun and M. S. Vannieuwenhze, *Angew. Chem. Int. Ed.*, 2012, **51**, 12519–12523.
- 100 Polyethylene Glycol (PEG) and Pegylation of Proteins,
<https://www.thermofisher.com/uk/en/home/life-science/protein-biology/protein-biology-learning-center/protein-biology-resource-library/pierce-protein-methods/polyethylene-glycol-peg-pegylation-proteins.html>, (accessed 16 June 2017).
- 101 RCSB PDB - 3ZG0: Crystal structure of ceftaroline acyl-PBP2a from MRSA with non-covalently bound ceftaroline and muramic acid at allosteric site obtained by cocrystallization, <https://www.rcsb.org/structure/3zg0>, (accessed 31 March 2020).
- 102 RCSB PDB - 3HUM: Crystal structure of Penicillin binding protein 4 from *Staphylococcus aureus* COL in complex with Cefotaxime,
<https://www.rcsb.org/structure/3HUM>, (accessed 31 March 2020).
- 103 RCSB PDB - 3VSL: Crystal structure of penicillin-binding protein 3 (PBP3) from methicillin-resistant *Staphylococcus aureus* in the cefotaxime bound form.,
<http://www.rcsb.org/structure/3VSL>, (accessed 31 March 2020).
- 104 G. G. Zhanel, G. Sniezek, F. Schweizer, S. Zelenitsky, P. R. S. Lagacé-Wiens, E. Rubinstein, A. S. Gin, D. J. Hoban and J. A. Karlowsky, *Drugs*, 2009, **69**, 809–831.
- 105 A. Bruggink, Ed., *Synthesis of β -Lactam Antibiotics*, Springer Netherlands, Dordrecht, 2001.
- 106 J. H. C. Nayler, *Trends Biochem. Sci.*, 1991, **16**, 195–197.
- 107 M. A. Schwartz, *J. Pharm. Sci.*, 1965, **54**, 472–473.
- 108 M. González, Z. Rodríguez, B. Tolón, J. C. Rodríguez, H. Velez, B. Valdés, M. A. López and A. Fini, *Farmaco*, 2003, **58**, 409–418.
- 109 R. Keltjens, S. Vadivel, E. de Vroom, A. ?H. Klunder and B. Zwanenburg, *Eur. J. Org. Chem.*, 2001, **2001**, 2529–2534.

- 110 H.-G. Fu, X.-X. Hu, C.-R. Li, Y.-H. Li, Y.-X. Wang, J.-D. Jiang, C.-W. Bi, S. Tang, X.-F. You and D.-Q. Song, *Eur. J. Med. Chem.*, 2016, **110**, 151–163.
- 111 D. L. Hughes, *Org. Process Res. Dev.*, 2017, **21**, 800–815
- 112 E. Valeur and M. Bradley, *Chem. Soc. Rev.*, 2009, **38**, 606–631.
- 113 T. Ishikawa, N. Matsunaga, H. Tawada, N. Kuroda, Y. Nakayama, Y. Ishibashi, M. Tomimoto, Y. Ikeda, Y. Tagawa, Y. Iizawa, K. Okonogi, S. Hashiguchi and A. Miyake, *Bioorg. Med. Chem.*, 2003, **11**, 2427–2437.
- 114 US 7419,973 B2, 2008.
- 115 G. F. H. Green, J. E. Page and S. E. Staniforth, *J. Chem. Soc.*, 1965, 1595–1605.
- 116 Y. Sendo, M. Yoshioka and W. Nagata, *Heterocycles*, 1982, **17**, 231–234.
- 117 M. Miyauch, K. Sasahar, K. Fujimoto, I. Kawamot, J. Idi and H. Nakao, *Chem. Pharm. Bull.*, 1989, **37**, 2369–2374.
- 118 R. R. Chauvette and E. H. Flynn, *J. Med. Chem.*, 1966, **9**, 741–745.
- 119 J. D. Cocker, S. Eardley, G. I. Gregory, M. E. Hall and A. G. Long, *J. Chem. Soc.*, 1966.
- 120 V. Farina, S. R. Baker and S. I. Hauck, *J. Org. Chem.*, 1989, **54**, 4962–4966.
- 121 Y. Okamoto, K. Kiriya, Y. Namiki, J. Matsushita, M. Fujioka and T. Yasuda, *J. Pharm. Sci.*, 1996, **85**, 976–983.
- 122 J. Wang, D. Ruan and W. Shan, *J. Liq. Chromatogr. Relat. Technol.*, 2013, **36**, 2125–2141.
- 123 R. Rajadurai, B. Sivakumar, R. Murugan, S. Anantham and P. Y. Naidu, *ACAIJ*, 2010, **9**, 265–269.
- 124 W. Scholar, E. Pratt, *The antimicrobial drugs. Second Edition.*, Oxford University Press, 2000.
- 125 V. B. Arumugham and M. Cascella, *Third Generation Cephalosporins*, StatPearls Publishing, 2020.
- 126 A. Forsgren, *Acta Pathol. Microbiol. Scand. Sect. B Microbiol.*, 1981, **89 B**, 221–225.

- 127 B. Cotterell, *Novel Probes to Map Cell Wall Biosynthesis in Staphylococcus aureus at the Nanoscale*, 2017.
- 128 Click-iT™ Cell Reaction Buffer Kit,
<https://www.thermofisher.com/order/catalog/product/C10269#/C10269>, (accessed 22 June 2020).
- 129 F. Himo, T. Lovell, R. Hilgraf, V. V. Rostovtsev, L. Noodleman, K. B. Sharpless and V. V. Fokin, *J. Am. Chem. Soc.*, 2005, **127**, 210–216.
- 130 C. D. Hein, X. M. Liu and D. Wang, *Pharm. Res.*, 2008, **25**, 2216–2230.
- 131 J. M. Monteiro, P. B. Fernandes, F. Vaz, A. R. Pereira, A. C. Tavares, M. T. Ferreira, P. M. Pereira, H. Veiga, E. Kuru, M. S. Vannieuwenhze, Y. V. Brun, S. R. Filipe and M. G. Pinho, *Nat. Commun.*, 2015, **6**, 1–12.
- 132 X. Zhou, D. K. Halladin, E. R. Rojas, E. F. Koslover, T. K. Lee, K. C. Huang and J. A. Theriot, *Science (80-.)*, 2015, **348**, 574–578.
- 133 M. von und zur Mühlen, University of Sheffield, September 2019.
- 134 G. Zhao, T. I. Meier, S. D. Kahl, K. R. Gee and L. C. Blaszcak, *Antimicrob. Agents Chemother.*, 1999, **43**, 1124–1128.
- 135 N. Panchuk-Voloshina, R. P. Haugland, J. Bishop-Stewart, M. K. Bhalgat, P. J. Millard, F. Mao, W. Y. Leung and R. P. Haugland, *J. Histochem. Cytochem.*, 1999, **47**, 1179–1188.
- 136 R. D. Turner, E. C. Ratcliffe, R. Wheeler, R. Golestanian, J. K. Hobbs and S. J. Foster, *Nat. Commun.*, 2010, **1**, 1–9.
- 137 L. Pasquina-Lemonche, J. Burns, R. D. Turner, S. Kumar, R. Tank, N. Mullin, J. S. Wilson, B. Chakrabarti, P. A. Bullough, S. J. Foster and J. K. Hobbs, *Nature*, 2020, **582**, 294–297.
- 138 M. S. Bojer, K. Wacnik, P. Kjølgaard, C. Gallay, A. L. Bottomley, M. T. Cohn, G. Lindahl, D. Frees, J. W. Veening, S. J. Foster and H. Ingmer, *Mol. Microbiol.*, 2019, **112**, 1116–1130.
- 139 V. A. Lund, K. Wacnik, R. D. Turner, B. E. Cotterell, C. G. Walther, S. J. Fenn, F. Grein, A. J. M. Wollman, M. C. Leake, N. Olivier, A. Cadby, S. Mesnage, S. Jones

- and S. J. Foster, *Elife*, 2018, **7**, e32057
- 140 P. M. Pereira, H. Veiga, A. M. Jorge and M. G. Pinho, *Appl. Environ. Microbiol.*, 2010, **76**, 4346–4353.
- 141 M. G. Pinho and J. Errington, *Mol. Microbiol.*, 2005, **55**, 799–807.
- 142 S. T. Hess, T. P. K. Girirajan and M. D. Mason, *Biophys. J.*, 2006, **91**, 4258–4272.
- 143 G. T. Dempsey, J. C. Vaughan, K. H. Chen, M. Bates and X. Zhuang, *Nat. Methods*, 2011, **8**, 1027–1040.
- 144 A. Renn, J. Seelig and V. Sandoghdar, *Mol. Phys.*, 2006, **104**, 409–414.
- 145 H. Liang, K. E. DeMeester, C. W. Hou, M. A. Parent, J. L. Caplan and C. L. Grimes, *Nat. Commun.*, 2017, **8**.
- 146 B. Ostash and S. Walker, *Nat. Prod. Rep.*, 2010, **27**, 1594–1617.
- 147 S. Fuse, H. Tsukamoto, Y. Yuan, T. S. A. Wang, Y. Zhang, M. Bolla, S. Walker, P. Sliz and D. Kahne, *ACS Chem. Biol.*, 2010, **5**, 701–711.
- 148 Y. Yuan, S. Fuse, B. Ostash, P. Sliz, D. Kahne and S. Walker, *ACS Chem. Biol.*, 2008, **3**, 429–436.
- 149 T. J. R. Cheng, M. T. Sung, H. Y. Liao, Y. F. Chang, C. W. Chen, C. Y. Huang, L. Y. Chou, Y. Da Wu, Y. H. Chen, Y. S. E. Cheng, C. H. Wong, C. Ma and W. C. Cheng, *Proc. Natl. Acad. Sci. U. S. A.*, 2008, **105**, 431–436.
- 150 C. M. Gampe, H. Tsukamoto, E. H. Doud, S. Walker and D. Kahne, *J. Am. Chem. Soc.*, 2013, **135**, 3776–3779.
- 151 N. F. Galley, A. M. O'Reilly and D. I. Roper, *Bioorg. Chem.*, 2014, **55**, 16–26.
- 152 A. Buchynskyy, U. Kempin, S. Vogel, L. Hennig, M. Findeisen, D. Müller, S. Giesa, H. Knoll and P. Welzel, *European J. Org. Chem.*, 2002, **2002**, 1149–1162.
- 153 U. Kempin, L. Hennig, D. Knoll, P. Welzel, D. Müller, A. Markus and J. Van Heijenoort, *Tetrahedron*, 1997, **53**, 17669–17690.
- 154 E. W. Kovacs, J. M. Hooker, D. W. Romanini, P. G. Holder, K. E. Berry and M. B. Francis, *Bioconj. Chem.*, 2007, **18**, 1140–1147.

- 155 M. Adachi, Y. Zhang, C. Leimkuhler, B. Sun, J. V. LaTour and D. E. Kahne, *J. Am. Chem. Soc.*, 2006, **128**, 14012–14013.
- 156 P. Welzel, F. Kunisch, F. Kruggel, H. Stein, J. Scherckenbeck, A. Hiltmann, H. Duddeck, D. Müller, J. E. Maggio, H. W. Fehlhaber, G. Seibert, Y. van Heijenoort and J. van Heijenoort, *Tetrahedron*, 1987, **43**, 585–598.
- 157 J. Scherckenbeck, A. Hiltmann, K. Hobert, W. Bankova, T. Siegels, M. Kaiser, D. Müller, H. J. Veith, H. W. Fehlhaber, G. Seiberg, A. Markus, M. Limbert, G. Huber, D. Böttger, A. Stärk, S. Takahashi, Y. van Heijenoort, J. van Heijenoort and P. Welzel, *Tetrahedron*, 1993, **49**, 3091–3100.
- 158 M. J. Sofia, N. Allanson, N. T. Hatzenbuehler, R. Jain, R. Kakarla, N. Kogan, R. Liang, D. Liu, D. J. Silva, H. Wang, D. Gange, J. Anderson, A. Chen, F. Chi, R. Dulina, B. Huang, M. Kamau, C. Wang, E. Baizman, A. Branstrom, N. Bristol, R. Goldman, K. Han, C. Longley, S. Midha and H. R. Axelrod, *J. Med. Chem.*, 1999, **42**, 3193–3198.
- 159 X. Chen, C. H. Wong and C. Ma, *ACS Infect. Dis.*, 2019, **5**, 1493–1504.
- 160 N. El-Abadla, M. Lampilas, L. Hennig, M. Findeisen, P. Welzel, D. Müller, A. Markus and J. Van Heijenoort, *Tetrahedron*, 1999, **55**, 699–722.
- 161 Y. Yuan, S. Fuse, B. Ostash, P. Sliz, D. Kahne and S. Walker, *ACS Chem. Biol.*, 2008, **3**, 429–436.
- 162 K. Wacnik, University of Sheffield, April 2016.
- 163 Y. Rebets, T. Lupoli, Y. Qiao, K. Schirner, R. Villet, D. Hooper, D. Kahne and S. Walker, *ACS Chem. Biol.*, 2014, **9**, 459–467.
- 164 H. J. L. G. L. Amidon, *Annu. Rev. Pharmacol. Toxicol.*, 1994, **34**, 321–341.
- 165 D. J. Craik, D. P. Fairlie, S. Liras and D. Price, *Chem. Biol. Drug Des.*, 2013, **81**, 136–147.
- 166 M. S. Siegrist, S. Whiteside, J. C. Jewett, A. Aditham, F. Cava and C. R. Bertozzi, *ACS Chem. Biol.*, 2013, **8**, 500–505.
- 167 G. W. Liechti, E. Kuru, E. Hall, A. Kalinda, Y. V. Brun, M. Vannieuwenhze and A. T. Maurelli, *Nature*, 2014, **506**, 507–510.
- 168 M. McLaughlin, R. Yazaki, T. C. Fessard and E. M. Carreira, *Org. Lett.*, 2014, **16**,

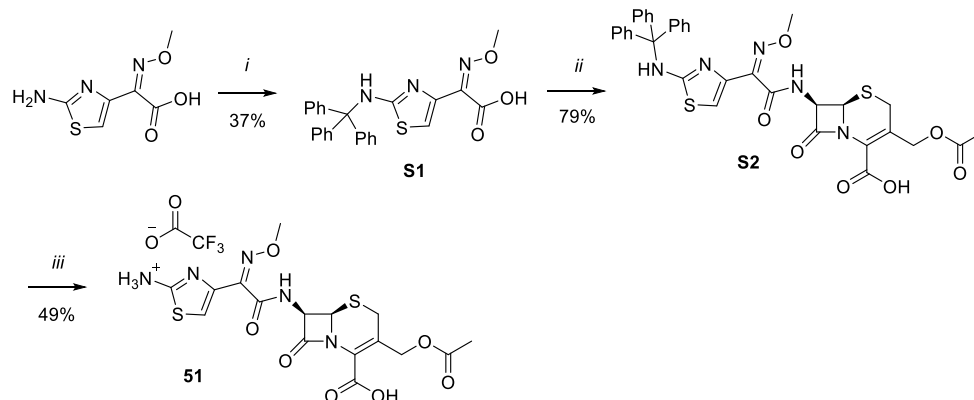
- 4070–4073.
- 169 G. P. Möller, S. Müller, B. T. Wolfstädter, S. Wolfrum, D. Schepmann, B. Wünsch and E. M. Carreira, *Org. Lett.*, 2017, **19**, 2510–2513.
- 170 G. Wuitschik, M. Rogers-Evans, K. Müller, H. Fischer, B. Wagner, F. Schuler, L. Polonchuk and E. M. Carreira, *Angew. Chem. Int. Ed.*, 2006, **45**, 7736–7739.
- 171 N. A. Meanwell, *J. Med. Chem.*, 2011, **54**, 2529–2591.
- 172 F. Besseau, M. Luçon, C. Laurence and M. Berthelot, *J. Chem. Soc. Perkin Trans. 2*, 1998, **2**, 101–107.
- 173 M. Berthelot, F. Besseau and C. Laurence, *European J. Org. Chem.*, 1998, **1998**, 925–931.
- 174 J. A. Burkhard, G. Wuitschik, M. Rogers-Evans, K. Müller and E. M. Carreira, *Angew. Chem. Int. Ed.*, 2010, **49**, 9052–9067.
- 175 M. Wang, B. Cornett, J. Nettles, D. C. Liotta and J. P. Snyder, *J. Org. Chem.*, 2000, **65**, 1059–1068.
- 176 J. C. J. Barna and D. H. Williams, *Annu. Rev. Microbiol.*, 1984, **38**, 339–357.
- 177 N. H. Powell, G. J. Clarkson, R. Notman, P. Raubo, N. G. Martin and M. Shipman, *Chem. Commun.*, 2014, **50**, 8797–8800.
- 178 K. C. Nicolaou, A. A. Estrada, M. Zak, S. H. Lee and B. S. Safina, *Angew. Chem. Int. Ed.*, 2005, **44**, 1378–1382.
- 179 J. D. Beadle, N. H. Powell, P. Raubo, G. J. Clarkson and M. Shipman, *Synlett*, 2016, **27**, 169–172.
- 180 Y. Yang, W. Wang, S. Xiong, Y. Song and C. Du, *Pharm. Care Res.*, 2014, **14**, 462–464.
- 181 M. R. Pitts, J. R. Harrison and C. J. Moody, *J. Chem. Soc. Perkin 1*, 2001, 955–977.
- 182 S. Shi, G. Meng and M. Szostak, *Angew. Chem. Int. Ed.*, 2016, **55**, 6959–6963.
- 183 G. Meng and M. Szostak, *Org. Lett.*, 2016, **18**, 796–799.
- 184 S. Ni, W. Zhang, H. Mei, J. Han and Y. Pan, *Org. Lett.*, 2017, **19**, 2536–2539.

- 185 S. M. Drawz and R. A. Bonomo, *Clin. Microbiol. Rev.*, 2010, **23**, 160–201.
- 186 K. Bush and P. A. Bradford, *Nat. Rev. Microbiol.*, 2019, **17**, 295–306.
- 187 S. K. Perumal and R. F. Pratt, *J. Org. Chem.*, 2006, **71**, 4778–4785.
- 188 N. Li and R. F. Pratt, *J. Am. Chem. Soc.*, 1998, **120**, 4264–4268.
- 189 D. Leung, G. Abbenante and D. P. Fairlie, *J. Med. Chem.*, 2000, **43**, 305–341.
- 190 T. Aoyama and T. Shioiri, *Chem. Pharm. Bull.*, 1981, **29**, 3249–3255.
- 191 J. Cesar and M. Sollner Dolenc, *Tetrahedron Lett.*, 2001, **42**, 7099–7102.
- 192 A. Devos, J. Remion, A. M. Frisque-Hesbain, A. Colens and L. Ghosez, *J. Chem. Soc. Chem. Commun.*, 1979, 1180–1181.
- 193 M. Yamaura, T. Suzuki, H. Hashimoto, J. Yoshimura, T. Okamoto and C. Shin, *Bull. Chem. Soc. Jpn.*, 1985, **58**, 1413–1420.
- 194 P. G. M. Wuts and T. W. Greene, *Greene's Protective Groups in Organic Synthesis*, John Wiley & Sons, Inc., Hoboken, NJ, USA, 2006.
- 195 G. Wuitschik, E. M. Carreira, B. Wagner, H. Fischer, I. Parrilla, F. Schuler, M. Rogers-Evans and K. Müller, *J. Med. Chem.*, 2010, **53**, 3227–3246.
- 196 C. E. McKenna and J. Schmidhuser, *J. Chem. Soc. Chem. Commun.*, 1979, **870**, 739.
- 197 M. J. Horsburgh, J. L. Aish, I. J. White, L. Shaw, J. K. Lithgow and S. J. Foster, *J. Bacteriol.*, 2002, **184**, 5457–5467.
- 198 J. A. Jiang, J. J. Zhai, X. H. Yu, X. Teng and Y. F. Ji, *Synthesis*, **2012**, 207–214.
- 199 L. D. Patterson and M. J. Miller, *J. Org. Chem.*, 2010, **75**, 1289–1292.
- 200 W. Shi, S. Dolai, S. Averick, S. S. Fernando, J. A. Saltos, W. L'Amoreaux, P. Banerjee and K. Raja, *Bioconjug. Chem.*, 2009, **20**, 1595–1601.
- 201 G. R. Newkome, K. K. Kotta, A. Mishra and C. N. Moorefield, *Macromolecules*, 2004, **37**, 8262–8268.
- 202 S. Eising, F. Lelivelt and K. M. Bongers, *Angew. Chem. Int. Ed.*, 2016, **55**, 12243–12247.
- 203 T. J. Styslinger, N. Zhang, V. S. Bhatt, N. Pettit, A. F. Palmer and P. G. Wang, *J. Am.*

- Chem. Soc.*, 2012, **134**, 7507–7515.
- 204 Z. Zhao, University of Sheffield, August 2017.
- 205 F. Wang, S. Cai, Z. Wang and C. Xi, *Org. Lett.*, 2011, **13**, 3202–3205.
- 206 W. Tan, C. Wang and X. Jiang, *Org. Chem. Front.*, 2018, **5**, 2390–2394.
- 207 Y. Yoshida, K. Matsuda, H. Sasaki, Y. Matsumoto, S. Matsumoto, S. Tawara and H. Takasugi, *Bioorg. Med. Chem.*, 2000, **8**, 2317–2335.
- 208 M. I. Montañez, C. Mayorga, M. J. Torres, A. Ariza, M. Blanca and E. Perez-Inestrosa, *Chem. Res. Toxicol.*, 2011, **24**, 706–717.
- 209 M. Keller, D. Erdmann, N. Pop, N. Pluym, S. Teng, G. Bernhardt and A. Buschauer, *Bioorg. Med. Chem.*, 2011, **19**, 2859–2878.
- 210 M. S. Manna and S. Mukherjee, *J. Am. Chem. Soc.*, 2015, **137**, 130–133.
- 211 K. Stembera, A. Buchynskyy, S. Vogel, D. Knoll, A. A. Osman, J. A. Ayala and P. Welzel, *ChemBioChem*, 2002, **3**, 332–340.
- 212 D. S. Hemming, E. P. Talbot and P. G. Steel, *Tetrahedron Lett.*, 2017, **58**, 17–20.
- 213 S. Bazzi, E. Schulz and M. Mellah, *Org. Lett.*, 2019, **21**, 10033–10037.
- 214 G. Bin Zhou, P. F. Zhang and Y. J. Pan, *Tetrahedron*, 2005, **61**, 5671–5677.
- 215 C. Carboni, P. J. L. M. Quaedflieg, Q. B. Broxterman, P. Linda and L. Gardossi, *Tetrahedron Lett.*, 2004, **45**, 9649–9652.
- 216 J. P. Phelan, E. J. Patel and J. A. Ellman, *Angew. Chem. Int. Ed.*, 2014, **53**, 11329–11332.
- 217 R. R. Milburn, K. McRae, J. Chan, J. Tedrow, R. Larsen and M. Faul, *Tetrahedron Lett.*, 2009, **50**, 870–872.

10 Appendix

Synthesis of cefotaxime **51** reference as a TFA salt.



Scheme 10-1: i) Trityl chloride, Et₃N, CHCl₃:DMF (2:1), RT, o/n. ii) HATU, DIPEA, DMF, RT, 15 mins then 7-ACA, RT, o/n. ii) TFA, CH₂Cl₂, RT – 50 °C, 3 h.

Cells labelled with dye, des probe, which indicate whole cell fluorescence and no specificity.

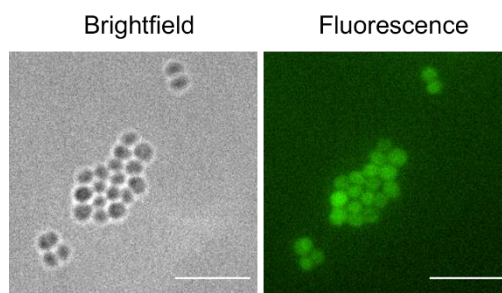
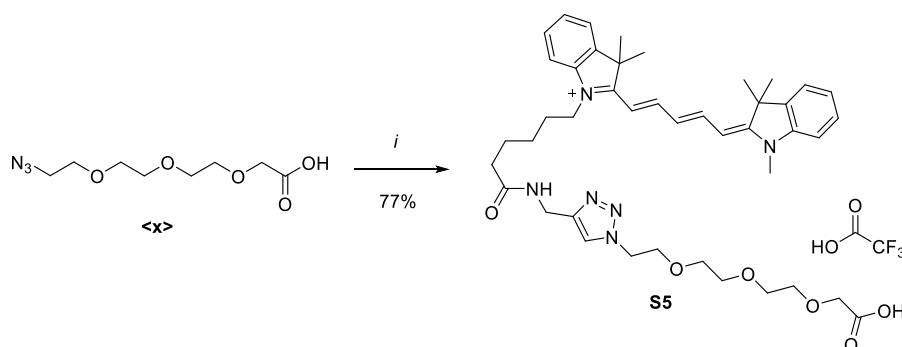


Figure 10-1: SH1000 cells labelled with dye and no probe

Synthesis of Cy5 control compound.



Scheme 10-2: i) Cyanine5 alkyne, Cu₅SO₄, L-ascorbic acid, DMSO, H₂O, RT, 16 h

X-ray data for amide <x>

Table 1 Crystal data and structure refinement for OSJ240k_0m.

Identification code	OSJ240k_0m
Empirical formula	C ₁₅ H ₂₂ Cl ₂ N ₄ O ₅
Formula weight	409.26
Temperature/K	100
Crystal system	monoclinic
Space group	P2 ₁ /c
a/Å	12.534(5)
b/Å	9.483(4)
c/Å	16.727(7)
α/°	90
β/°	94.418(9)
γ/°	90
Volume/Å ³	1982.4(14)
Z	4
ρ _{calc} /cm ³	1.371
μ/mm ⁻¹	0.360
F(000)	856.0
Crystal size/mm ³	0.14 × 0.07 × 0.05
Radiation	MoKα (λ = 0.71073)
2θ range for data collection/°	3.26 to 55.338
Index ranges	-16 ≤ h ≤ 15, -12 ≤ k ≤ 12, -21 ≤ l ≤ 21
Reflections collected	21943
Independent reflections	4575 [R _{int} = 0.1284, R _{sigma} = 0.1217]
Data/restraints/parameters	4575/0/264
Goodness-of-fit on F ²	1.019
Final R indexes [I ≥ 2σ (I)]	R ₁ = 0.0768, wR ₂ = 0.1705
Final R indexes [all data]	R ₁ = 0.1696, wR ₂ = 0.2092
Largest diff. peak/hole / e Å ⁻³	0.47/-0.65

Table 2 Fractional Atomic Coordinates (×10⁴) and Equivalent Isotropic Displacement Parameters (Å²×10³) for OSJ240k_0m. U_{eq} is defined as 1/3 of the trace of the orthogonalised U_{ij} tensor.

Atom	x	y	z	U(eq)
C11	1316.4(15)	2608.7(15)	7135.1(9)	62.3(5)
Cl2A	1262(2)	5629(2)	6925(3)	44.7(9)
Cl2B	989(11)	5495(9)	6413(16)	68(6)
O1	1637(2)	9121(3)	6976.6(17)	26.7(7)

O2	223(2)	9212(3)	6164.4(19)	36.1(8)
O3	3597(2)	7463(3)	6979.1(15)	18.0(6)
O4	6014(2)	7406(3)	9037.5(15)	19.2(7)
O5	6882(2)	9238(3)	9686.1(16)	20.8(7)
N1	1194(3)	9044(3)	6299(2)	20.9(8)
N2	3646(4)	8079(4)	3710(2)	25.9(9)
N3	3993(3)	9761(3)	6815.6(19)	15.2(7)
N4	6157(3)	9570(4)	8469(2)	19.7(8)
C1	1832(3)	8735(4)	5632(2)	15.8(9)
C1S	501(4)	4098(5)	6927(4)	47.7(14)
C2	2938(3)	8572(4)	5762(2)	13.5(8)
C3	3521(3)	8352(4)	5116(2)	16.5(9)
C4	3034(3)	8282(4)	4333(2)	16.8(9)
C5	1913(3)	8441(4)	4218(2)	20.1(9)
C6	1325(4)	8673(4)	4865(2)	21.0(9)
C7	3519(3)	8561(4)	6581(2)	14.1(8)
C8	4526(3)	9928(4)	7607(2)	14.5(9)
C9	5621(3)	9243(4)	7697(2)	18.9(9)
C10	6330(3)	8639(4)	9059(2)	17.0(9)
C11	7381(4)	8408(4)	10356(2)	20.3(9)
C12	8209(4)	7427(5)	10042(3)	37.8(13)
C13	6555(4)	7609(5)	10795(3)	31.4(11)
C14	7920(4)	9548(5)	10885(3)	28.0(11)

Table 3 Anisotropic Displacement Parameters ($\text{\AA}^2 \times 10^3$) for OSJ240k_0m. The Anisotropic displacement factor exponent takes the form: - $2\pi^2[h^2a^*^2U_{11}+2hka^*b^*U_{12}+\dots]$.

Atom	U ₁₁	U ₂₂	U ₃₃	U ₂₃	U ₁₃	U ₁₂
C11	101.3(14)	43.1(8)	43.4(8)	11.8(6)	11.2(8)	11.1(8)
C12A	53.8(14)	33.8(10)	47(2)	7.2(10)	5.8(12)	-4.3(9)
C12B	60(6)	46(4)	104(15)	16(5)	37(8)	10(4)
O1	24.3(18)	39.4(18)	16.2(15)	-4.3(13)	-0.3(13)	4.7(14)
O2	15.8(18)	58(2)	34.3(19)	-1.0(16)	2.1(15)	6.0(17)
O3	28.3(17)	10.5(13)	14.6(13)	3.2(11)	-2.7(12)	-0.1(12)
O4	31.3(18)	9.7(13)	16.1(14)	-2.0(11)	-0.8(12)	-2.3(12)
O5	31.1(18)	11.0(13)	18.1(14)	0.6(11)	-13.1(13)	-1.0(13)
N1	18(2)	18.5(17)	26(2)	-2.2(15)	1.9(16)	4.1(15)
N2	30(3)	33(2)	14(2)	-4.4(16)	1.5(19)	-2.1(19)
N3	22(2)	10.1(15)	12.2(16)	1.9(13)	-6.4(14)	-1.4(14)
N4	28(2)	12.1(17)	17.7(18)	1.1(14)	-9.6(16)	-2.1(15)

C1	18(2)	16.3(19)	13.7(19)	2.0(15)	3.0(17)	2.8(16)
C1S	39(3)	50(3)	55(4)	7(3)	10(3)	-6(3)
C2	21(2)	6.9(17)	12.4(18)	2.9(14)	-3.7(17)	1.8(16)
C3	16(2)	14.4(19)	19(2)	-0.7(16)	-1.6(17)	0.9(16)
C4	26(2)	13.3(19)	10.9(19)	0.4(15)	-0.8(17)	-3.4(17)
C5	24(3)	23(2)	12.5(19)	0.6(16)	-6.8(18)	-4.3(19)
C6	18(2)	21(2)	23(2)	4.8(17)	-5.2(19)	0.4(18)
C7	18(2)	11.1(17)	13.0(19)	-0.4(15)	0.6(16)	2.8(16)
C8	22(2)	9.3(17)	11.5(18)	-1.1(14)	-4.8(17)	-1.8(16)
C9	23(2)	16.7(19)	15(2)	-0.8(16)	-7.0(18)	-2.5(18)
C10	21(2)	13.7(19)	15.4(19)	-1.5(16)	-4.0(18)	2.1(17)
C11	31(3)	17(2)	12.6(19)	1.2(16)	-3.5(18)	0.9(18)
C12	44(3)	35(3)	33(3)	-3(2)	-6(2)	20(2)
C13	39(3)	35(3)	20(2)	0(2)	-1(2)	-12(2)
C14	31(3)	31(2)	21(2)	-1.7(19)	-8(2)	-6(2)

Table 4 Bond Lengths for OSJ240k_0m.

Atom	Atom	Length/Å	Atom	Atom	Length/Å
C11	C1S	1.762(6)	N4	C9	1.444(5)
C12A	C1S	1.737(6)	N4	C10	1.329(5)
C12B	C1S	1.717(10)	C1	C2	1.396(6)
O1	N1	1.225(4)	C1	C6	1.390(5)
O2	N1	1.230(4)	C2	C3	1.366(5)
O3	C7	1.236(4)	C2	C7	1.501(5)
O4	C10	1.234(4)	C3	C4	1.402(5)
O5	C10	1.338(5)	C4	C5	1.412(6)
O5	C11	1.469(5)	C5	C6	1.372(6)
N1	C1	1.452(5)	C8	C9	1.515(6)
N2	C4	1.354(5)	C11	C12	1.518(6)
N3	C7	1.329(5)	C11	C13	1.517(6)
N3	C8	1.445(5)	C11	C14	1.522(6)

Table 5 Bond Angles for OSJ240k_0m.

Atom	Atom	Atom	Angle/°	Atom	Atom	Atom	Angle/°
C10	O5	C11	122.3(3)	C3	C4	C5	118.6(4)
O1	N1	O2	122.2(3)	C6	C5	C4	120.0(4)
O1	N1	C1	119.0(3)	C5	C6	C1	120.0(4)
O2	N1	C1	118.7(3)	O3	C7	N3	123.1(3)

C7	N3	C8	122.0(3)	O3	C7	C2	120.7(3)
C10	N4	C9	124.0(3)	N3	C7	C2	116.0(3)
C2	C1	N1	120.2(3)	N3	C8	C9	113.2(3)
C6	C1	N1	118.6(4)	N4	C9	C8	110.6(3)
C6	C1	C2	121.1(4)	O4	C10	O5	124.8(3)
Cl2A	C1S	Cl1	111.1(3)	O4	C10	N4	125.0(4)
Cl2B	C1S	Cl1	119.6(4)	N4	C10	O5	110.2(3)
C1	C2	C7	123.3(3)	O5	C11	C12	109.1(3)
C3	C2	C1	118.6(3)	O5	C11	C13	111.8(4)
C3	C2	C7	118.0(4)	O5	C11	C14	101.9(3)
C2	C3	C4	121.7(4)	C12	C11	C14	110.6(4)
N2	C4	C3	119.6(4)	C13	C11	C12	111.8(4)
N2	C4	C5	121.8(4)	C13	C11	C14	111.2(3)

Table 6 Hydrogen Atom Coordinates ($\text{\AA}\times 10^4$) and Isotropic Displacement Parameters ($\text{\AA}^2\times 10^3$) for OSJ240k_0m.

Atom	x	y	z	U(eq)
H2A	4320(40)	7960(40)	3810(30)	14(12)
H2B	3330(40)	7980(50)	3300(30)	33(15)
H1SA	101	3981	6398	57
H1SB	-25	4179	7337	57
H1SC	-160	3770	6621	57
H1SD	288	4463	7446	57
H3A	4275	8243	5199	20
H5	1566	8388	3694	24
H6	571	8790	4787	25
H8A	4073	9511	8005	17
H8B	4603	10946	7727	17
H9A	5543	8208	7640	23
H9B	6057	9584	7267	23
H12A	7851	6728	9683	57
H12B	8598	6943	10493	57
H12C	8714	7975	9748	57
H13A	5960	8239	10894	47
H13B	6886	7262	11308	47
H13C	6287	6809	10468	47
H14A	8407	10094	10574	42
H14B	8325	9109	11344	42
H14C	7375	10176	11078	42
H4	6400(40)	10370(50)	8540(30)	30(13)

H3	3920(40)	10480(50)	6480(30)	38(14)
----	----------	-----------	----------	--------

Table 7 Atomic Occupancy for OSJ240k_0m.

Atom	Occupancy	Atom	Occupancy	Atom	Occupancy
Cl2A	0.767(14)	Cl2B	0.233(14)	H1SA	0.767(14)
H1SB	0.767(14)	H1SC	0.233(14)	H1SD	0.233(14)

Crystal structure determination of OSJ240k_0m

Crystal Data for C₁₅H₂₂Cl₂N₄O₅ ($M = 409.26$ g/mol): monoclinic, space group P2₁/c (no. 14), $a = 12.534(5)$ Å, $b = 9.483(4)$ Å, $c = 16.727(7)$ Å, $\beta = 94.418(9)^\circ$, $V = 1982.4(14)$ Å³, $Z = 4$, $T = 100$ K, $\mu(\text{MoK}\alpha) = 0.360$ mm⁻¹, $D_{\text{calc}} = 1.371$ g/cm³, 21943 reflections measured ($3.26^\circ \leq 2\theta \leq 55.338^\circ$), 4575 unique ($R_{\text{int}} = 0.1284$, $R_{\text{sigma}} = 0.1217$) which were used in all calculations. The final R_1 was 0.0768 ($I > 2\sigma(I)$) and wR_2 was 0.2092 (all data).

X-ray data for 2-nitro regioisomer <x>

Table 1 Crystal data and structure refinement for OIC307v_data_0m.

Identification code	OIC307v_data_0m
Empirical formula	C ₁₄ H ₂₀ N ₄ O ₅
Formula weight	324.34
Temperature/K	100
Crystal system	monoclinic
Space group	P2 ₁ /n
$a/\text{\AA}$	17.210(6)
$b/\text{\AA}$	5.3665(19)
$c/\text{\AA}$	17.899(6)
$\alpha/^\circ$	90
$\beta/^\circ$	110.487(4)
$\gamma/^\circ$	90
Volume/Å ³	1548.5(9)
Z	4
$\rho_{\text{calc}}/\text{g/cm}^3$	1.391
μ/mm^{-1}	0.107
F(000)	688.0
Crystal size/mm ³	0.5 × 0.1 × 0.09
Radiation	MoK α ($\lambda = 0.71073$)
2 θ range for data collection/°	4.072 to 54.668
Index ranges	-22 ≤ h ≤ 22, -6 ≤ k ≤ 6, -23 ≤ l ≤ 23
Reflections collected	28372
Independent reflections	3475 [$R_{\text{int}} = 0.0725$, $R_{\text{sigma}} = 0.0408$]

Data/restraints/parameters	3475/0/211
Goodness-of-fit on F^2	1.126
Final R indexes [$I \geq 2\sigma(I)$]	$R_1 = 0.0529$, $wR_2 = 0.1358$
Final R indexes [all data]	$R_1 = 0.0668$, $wR_2 = 0.1435$
Largest diff. peak/hole / $e \text{ \AA}^{-3}$	0.39/-0.32

Table 2 Fractional Atomic Coordinates ($\times 10^4$) and Equivalent Isotropic Displacement Parameters ($\text{\AA}^2 \times 10^3$) for OIC307v_data_0m. U_{eq} is defined as 1/3 of of the trace of the orthogonalised U_{ij} tensor.

Atom	x	y	z	U(eq)
O1	6810.6(9)	-2219(3)	7479.0(10)	21.8(4)
O2	5852.4(10)	-4601(3)	7613.7(10)	23.3(4)
O3	3732.9(9)	4040(3)	4483.4(9)	16.4(3)
O4	1630.9(10)	9434(3)	5404.6(9)	17.1(3)
O5	1226.3(11)	6470(3)	6108.7(10)	20.9(4)
N1	6067.7(11)	-2853(4)	7287.1(10)	16.0(4)
N2	6416.7(11)	1572(4)	6464.4(11)	16.6(4)
N3	2727.9(11)	1948(4)	4756.7(10)	13.1(4)
N4	1577.4(12)	5339(4)	5088.2(11)	17.2(4)
C1	5448.6(13)	-1475(4)	6679.2(12)	13.1(4)
C2	5652.0(13)	654(4)	6319.2(12)	13.2(4)
C3	4974.1(13)	1870(4)	5738.9(12)	13.5(4)
C4	4172.1(13)	1025(4)	5525.3(12)	12.9(4)
C5	3993.0(13)	-1129(4)	5886.1(12)	14.1(4)
C6	4626.3(13)	-2341(4)	6454.4(12)	14.4(4)
C7	3525.1(13)	2470(4)	4877.9(12)	12.8(4)
C8	2056.1(12)	3165(4)	4130.2(12)	13.5(4)
C9	1831.5(14)	5656(4)	4394.4(12)	15.3(4)
C10	1485.7(13)	7272(4)	5524.2(13)	14.5(4)
C11	963.0(14)	8234(4)	6609.6(13)	17.1(5)
C12	708.2(19)	6480(5)	7147.3(16)	28.7(6)
C13	231.8(14)	9766(5)	6091.4(14)	22.1(5)
C14	1684.3(15)	9859(5)	7092.9(14)	23.1(5)

Table 3 Anisotropic Displacement Parameters ($\text{\AA}^2 \times 10^3$) for OIC307v_data_0m. The Anisotropic displacement factor exponent takes the form: - $2\pi^2[h^2a^{*2}U_{11}+2hka^*b^*U_{12}+...]$.

Atom	U ₁₁	U ₂₂	U ₃₃	U ₂₃	U ₁₃	U ₁₂
O1	12.4(7)	25.7(9)	23.9(8)	4.3(7)	2.1(6)	-0.1(7)
O2	21.0(8)	25.4(9)	23.2(8)	11.8(7)	7.4(7)	1.2(7)
O3	12.5(7)	17.6(8)	18.9(7)	4.0(6)	5.3(6)	-1.7(6)
O4	17.9(8)	14.0(8)	23.6(8)	1.9(6)	12.4(6)	-0.8(6)
O5	31.1(9)	14.1(8)	26.7(8)	-1.4(7)	21.7(7)	-0.6(7)
N1	15.7(9)	18.7(10)	14.7(8)	0.9(7)	6.5(7)	1.3(8)
N2	9.7(8)	17.8(10)	20.9(9)	4.8(8)	3.6(7)	-1.1(7)
N3	10.2(8)	15.5(9)	14.8(8)	2.5(7)	5.9(7)	-0.8(7)
N4	21.3(10)	13.7(9)	21.5(9)	0.2(8)	13.6(8)	-1.7(8)
C1	13.4(10)	13.9(11)	12.6(9)	-0.5(8)	5.3(8)	1.5(8)
C2	11.7(10)	15.3(11)	13.4(9)	-2.5(8)	5.4(8)	0.4(8)
C3	13.0(10)	13.9(10)	15.0(9)	-0.1(8)	6.7(8)	-1.5(8)
C4	12.7(10)	12.7(10)	14.9(9)	-1.9(8)	6.7(8)	0.5(8)
C5	10.8(9)	16.2(11)	16.1(9)	-0.9(8)	5.6(8)	-0.9(8)
C6	15.9(10)	14.3(11)	14.9(9)	0.1(8)	7.9(8)	-1.4(9)
C7	11.3(9)	13.2(10)	15.1(9)	-2.8(8)	6.2(8)	-1.0(8)
C8	9.1(9)	17.8(11)	13.4(9)	0.3(8)	3.8(7)	-0.4(8)
C9	14.7(10)	16.5(11)	16.5(10)	2.7(8)	7.7(8)	1.2(9)
C10	9.8(9)	17.3(11)	17.9(10)	0.9(8)	6.8(8)	0.4(8)
C11	21.8(11)	14.1(11)	20.0(10)	-1.4(9)	13.0(9)	1.5(9)
C12	47.1(16)	18.8(13)	33.9(13)	0.9(11)	31.1(13)	1.4(12)
C13	14.2(11)	31.3(14)	22.4(11)	-0.8(10)	8.3(9)	1.7(10)
C14	20.8(11)	24.0(13)	22.3(11)	-2.2(10)	4.8(9)	1.6(10)

Table 4 Bond Lengths for OIC307v_data_0m.

Atom	Atom	Length/Å	Atom	Atom	Length/Å
O1	N1	1.249(2)	C1	C2	1.414(3)
O2	N1	1.229(3)	C1	C6	1.408(3)
O3	C7	1.230(3)	C2	C3	1.420(3)
O4	C10	1.222(3)	C3	C4	1.374(3)
O5	C10	1.344(3)	C4	C5	1.410(3)
O5	C11	1.480(3)	C4	C7	1.510(3)
N1	C1	1.433(3)	C5	C6	1.367(3)
N2	C2	1.343(3)	C8	C9	1.513(3)
N3	C7	1.341(3)	C11	C12	1.516(3)
N3	C8	1.454(3)	C11	C13	1.517(3)
N4	C9	1.464(3)	C11	C14	1.516(3)
N4	C10	1.340(3)			

Table 5 Bond Angles for OIC307v_data_0m.

Atom	Atom	Atom	Angle/°	Atom	Atom	Atom	Angle/°
C10	O5	C11	121.51(18)	C6	C5	C4	119.1(2)
O1	N1	C1	119.04(18)	C5	C6	C1	121.0(2)
O2	N1	O1	121.80(18)	O3	C7	N3	122.45(19)
O2	N1	C1	119.15(18)	O3	C7	C4	120.51(18)
C7	N3	C8	121.55(18)	N3	C7	C4	117.04(18)
C10	N4	C9	122.36(19)	N3	C8	C9	112.15(17)
C2	C1	N1	121.72(19)	N4	C9	C8	110.32(18)
C6	C1	N1	116.90(19)	O4	C10	O5	125.8(2)
C6	C1	C2	121.38(19)	O4	C10	N4	124.1(2)
N2	C2	C1	126.2(2)	N4	C10	O5	110.16(19)
N2	C2	C3	118.1(2)	O5	C11	C12	101.85(18)
C1	C2	C3	115.68(19)	O5	C11	C13	109.91(18)
C4	C3	C2	122.7(2)	O5	C11	C14	110.52(18)
C3	C4	C5	120.2(2)	C12	C11	C13	111.2(2)
C3	C4	C7	116.31(19)	C14	C11	C12	110.8(2)
C5	C4	C7	123.49(19)	C14	C11	C13	112.0(2)

Table 6 Hydrogen Atom Coordinates ($\text{\AA} \times 10^4$) and Isotropic Displacement Parameters ($\text{\AA}^2 \times 10^3$) for OIC307v_data_0m.

Atom	x	y	z	U(eq)
H2A	6849	833	6813	20
H2B	6486	2913	6211	20
H3	2609	843	5064	16
H4	1481	3825	5224	21
H3A	5080	3327	5488	16
H5	3440	-1729	5737	17
H6	4510	-3790	6701	17
H8A	1562	2069	3969	16
H8B	2223	3414	3659	16
H9A	2316	6788	4532	18
H9B	1373	6420	3952	18
H12A	274	5353	6820	43
H12B	496	7450	7499	43
H12C	1190	5505	7470	43
H13A	423	10973	5782	33
H13B	-17	10654	6430	33

H13C	-182	8661	5727	33
H14A	2170	8811	7355	35
H14B	1534	10769	7498	35
H14C	1815	11049	6739	35

Crystal Data for C₁₄H₂₀N₄O₅ ($M = 324.34$ g/mol): monoclinic, space group P2₁/n (no. 14), $a = 17.210(6)$ Å, $b = 5.3665(19)$ Å, $c = 17.899(6)$ Å, $\beta = 110.487(4)^\circ$, $V = 1548.5(9)$ Å³, $Z = 4$, $T = 100$ K, $\mu(\text{MoK}\alpha) = 0.107$ mm⁻¹, $D_{\text{calc}} = 1.391$ g/cm³, 28372 reflections measured ($4.072^\circ \leq 2\Theta \leq 54.668^\circ$), 3475 unique ($R_{\text{int}} = 0.0725$, $R_{\text{sigma}} = 0.0408$) which were used in all calculations. The final R_1 was 0.0529 ($I > 2\sigma(I)$) and wR_2 was 0.1435 (all data).